Optimisation de structures composites d'épaisseur variable. Application à la pale de CROR.

Alexis Lasseigne

N° d'ordre NNT : 2016LYSEM006

THESE de DOCTORAT DE L'UNIVERSITE DE LYON

opérée au sein de

l'Ecole des Mines de Saint-Etienne

Ecole Doctorale n° 488

Sciences, Ingénierie, Santé

Spécialité de doctorat : Mécanique et Ingénierie

Soutenue publiquement le 26/04/2016, par :

Alexis Lasseigne

OPTIMIZATION OF VARIABLE-THICKNESS COMPOSITE STRUCTURES. APPLICATION TO A CROR BLADE.

Devant le jury composé de :

M. BES Christian	Professeur	Université P. Sabatier	Président
M. MORLIER Joseph	Enseignant/chercheur, HDR	ISAE	Rapporteur
M. DESMORAT Boris	Maître de conferences, HDR	Université P. et M. Curie	Rapporteur
M. PARK Chung Hae	Professeur	Mines de Douai	Examinateur
M. LE RICHE Rodolphe	Directeur de Recherche	EMSE	Dir. de thèse
M. DELATTRE Grégory	Ingénieur de Recherche	ONERA	Examinateur
M. IRISARRI F.-Xavier	Ingénieur de Recherche	ONERA	Examinateur

Spécialités doctorales	Responsables :	Spécialités doctorales	Responsables
SCIENCES ET GENIE DES MATERIAUX	K. Wolski Directeur de recherche	MATHEMATIQUES APPLIQUEES	O. Roustant, Maître-assistant
MECANIQUE ET INGENIERIE	S. Drapier, professeur	INFORMATIQUE	O. Boissier, Professeur
GENIE DES PROCEDES	F. Gruy, Maître de recherche	IMAGE, VISION, SIGNAL	J.C. Pinoli, Professeur
SCIENCES DE LA TERR	B. Guy, Directeur de recherche	GENIE INDUSTRIEL	X. Delorme, Maître assistant
SCIENCES ET GENIE DE L'ENVIRONNEMENT	D. Graillot, Directeur de recherche	MICROELECTRONIQUE	Ph. Lalevée, Professeur

EMSE : Enseignants-chercheurs et chercheurs autorisés à diriger des thèses de doctorat (titulaires d'un doctorat d'État ou d'une HDR)

ABSI	Nabil	CR	Génie industriel	CMP
AUGUSTO	Vincent	CR	Image, Vision, Signal	CIS
AVRIL	Stéphane	PR2	Mécanique et ingénierie	CIS
BADEL	Pierre	MA(MDC)	Mécanique et ingénierie	CIS
BALBO	Flavien	PR2	Informatique	FAYOL
BASSEREAU	Jean-François	PR	Sciences et génie des matériaux	SMS
BATTON-HUBERT	Mireille	PR2	Sciences et génie de l'environnement	FAYOL
BEIGBEDER	Michel	MA(MDC)	Informatique	FAYOL
BLAYAC	Sylvain	MA(MDC)	Microélectronique	CMP
BOISSIER	Olivier	PR1	Informatique	FAYOL
BONNEFOY	Olivier	MA(MDC)	Génie des Procédés	SPIN
BORBELY	Andras	MR(DR2)	Sciences et génie des matériaux	SMS
BOUCHER	Xavier	PR2	Génie Industriel	FAYOL
BRODHAG	Christian	DR	Sciences et génie de l'environnement	FAYOL
BRUCHON	Julien	MA(MDC)	Mécanique et ingénierie	SMS
BURLAT	Patrick	PR1	Génie Industriel	FAYOL
CHRISTIEN	Frédéric	PR	Science et génie des matériaux	SMS
DAUZERE-PERES	Stéphane	PR1	Génie Industriel	CMP
DEBAYLE	Johan	CR	Image Vision Signal	CIS
DELAFOSSE	David	PR0	Sciences et génie des matériaux	SMS
DELORME	Xavier	MA(MDC)	Génie industriel	FAYOL
DESRAYAUD	Christophe	PR1	Mécanique et ingénierie	SMS
DJENIZIAN	Thierry	PR	Science et génie des matériaux	CMP
DOUCE	Sandrine	PR2	Sciences de gestion	FAYOL
DRAPIER	Sylvain	PR1	Mécanique et ingénierie	SMS
FAVERGEON	Loïc	CR	Génie des Procédés	SPIN
FEILLET	Dominique	PR1	Génie Industriel	CMP
FOREST	Valérie	MA(MDC)	Génie des Procédés	CIS
FOURNIER	Jacques	Ingénieur chercheur CEA	Microélectronique	CMP
FRACZKIEWICZ	Anna	DR	Sciences et génie des matériaux	SMS
GARCIA	Daniel	MR(DR2)	Génie des Procédés	SPIN
GAVET	Yann	MA(MDC)	Image Vision Signal	CIS
GERINGER	Jean	MA(MDC)	Sciences et génie des matériaux	CIS
GOEURIOT	Dominique	DR	Sciences et génie des matériaux	SMS
GONDRAN	Natacha	MA(MDC)	Sciences et génie de l'environnement	FAYOL
GRAILLOT	Didier	DR	Sciences et génie de l'environnement	SPIN
GROSSEAU	Philippe	DR	Génie des Procédés	SPIN
GRUY	Frédéric	PR1	Génie des Procédés	SPIN
GUY	Bernard	DR	Sciences de la Terre	SPIN
HAN	Woo-Suck	MR	Mécanique et ingénierie	SMS
HERRI	Jean Michel	PR1	Génie des Procédés	SPIN
KERMOUCHE	Guillaume	PR2	Mécanique et Ingénierie	SMS
KLOCKER	Helmut	DR	Sciences et génie des matériaux	SMS
LAFOREST	Valérie	MR(DR2)	Sciences et génie de l'environnement	FAYOL
LERICHE	Rodolphe	CR	Mécanique et ingénierie	FAYOL
MALLIARAS	Georges	PR1	Microélectronique	CMP
MOLIMARD	Jérôme	PR2	Mécanique et ingénierie	CIS
MOUTTE	Jacques	CR	Génie des Procédés	SPIN
NIKOLOVSKI	Jean-Pierre	Ingénieur de recherche	Mécanique et ingénierie	CMP
NORTIER	Patrice	PR1	SPIN	
OWENS	Rosin	MA(MDC)	Microélectronique	CMP
PERES	Véronique	MR	Génie des Procédés	SPIN
PICARD	Gauthier	MA(MDC)	Informatique	FAYOL
PIJOLAT	Christophe	PR0	Génie des Procédés	SPIN
PIJOLAT	Michèle	PR1	Génie des Procédés	SPIN
PINOLI	Jean Charles	PR0	Image Vision Signal	CIS
POURCHEZ	Jérémy	MR	Génie des Procédés	CIS
ROBISSON	Bruno	Ingénieur de recherche	Microélectronique	CMP
ROUSSY	Agnès	MA(MDC)	Génie industriel	CMP
ROUSTANT	Olivier	MA(MDC)	Mathématiques appliquées	FAYOL
STOLARZ	Jacques	CR	Sciences et génie des matériaux	SMS
TRIA	Assia	Ingénieur de recherche	Microélectronique	CMP
VALDIVIESO	François	PR2	Sciences et génie des matériaux	SMS
VIRICELLE	Jean Paul	DR	Génie des Procédés	SPIN
WOLSKI	Krzystof	DR	Sciences et génie des matériaux	SMS
XIE	Xiaolan	PR1	Génie industriel	CIS
YUGMA	Gallian	CR	Génie industriel	CMP

ACKNOWLEDGMENTS

This thesis was an opportunity for me to challenge, to grow and to develop myself, both scientifically and humanly. All this wouldn't have been possible without the help of the people who surrounded me during these years.

Firstly, I would like to thank the members of the jury, for having accepted evaluating my research. Thanks go to Pr Christian Bes (University Paul Sabatier) and Pr Chung Hae Park (Ecole des Mines de Douai) for their interest and fruitful questions. I also would like to thank Dr Joseph Morlier (Institut Supérieur de l'Aéronautique et de l'Espace) and Dr Boris Desmorat (University Pierre and Marie Curie) for the time they spent in reading this thesis and their highly valuable feedbacks.

I would like to thank my thesis supervisor, Dr Rodolphe Le Riche (Ecole des Mines de Saint-Etienne), for his availability, his patience and his pedagogy when dealing with applied mathematics during our several meetings and calls. I am also grateful to Dr Grégory Delattre of the Department of Applied Aerodynamics at Onera Meudon who introduced me to the science of applied aerodynamics, and guided me to overcome scientific and computational issues when dealing with the aerodynamic behavior of blades. Many thanks go to my supervisor François-Xavier Irisarri of the Department of Composite Systems and Materials (DMSC) at Onera Châtillon, for his patience, his strong commitment and support, day-to-day, during all these years. I keep from him a model of humility, rigor and perseverance that surely will be an inspiration throughout my career.

I would also like to acknowledge Myriam Kaminski, Christian Fagiano, Cédric Huchette and Frédéric Laurin of the DMSC for their help during my time at Onera, even until my very last training for the defense of this thesis. I am gratefully indebted to them for their very valuable comments on my presentation. I would like to thank Jean-François Maire, director of the DMSC, for having me involved in several industrial partnerships of the department, as well as Cédric Julien and François-Henry Leroy, for their invaluable support in bringing my researches to a whole new technical level. I would like to thank the PhD students of the DMSC, old and new, especially Azalia Moradi, Gaël Grail, Elen Hémon, Emilie Trousset, Carole Rakotoarisoa, Thomas Vandellos et Jean-Michel Roche for enlightening me with their advice and for sharing with me their valuable experience. I have a special thought for my buddies Antoine Hurmane, Adrien Elias and Camélia Ben Ramedane for their involvement in the excellent working atmosphere of the office we shared, despite the intrusions, yet precious, of our respective supervisors, our mood swings and my bad jokes. I wish them all the best things in their life and career.

Finally, I would like to express my sincere gratitude to my closest friends, to my parents and to my partner for bringing me their unconditional support and continuous encouragement throughout my years of study and through the whole process of researching and writing this thesis.

To the memory of Alice B.
To the memory of Romain S.

CONTENTS

LIST OF TABLES

LIST OF FIGURES

RÉSUMÉ DE SYNTHÈSE

La protection de l'environnement est devenue un enjeu majeur à l'échelle mondiale, débattu annuellement depuis 1995 à l'occasion des Conférences des Parties (COP). Il apparait que l'aviation est responsable de près de 2% des émissions globales de CO_2. Cette proportion devrait progresser avec la croissance du trafic aérien et la réduction potentielle des émissions des autres secteurs. L'ACARE, pour Advisory Council for Aviation Research in Europe, a été créée en 2001 pour aider le secteur de l'aviation à atteindre les objectifs détaillés dans le rapport « European Aeronautics : A vision for 2020 ». Un des principaux objectifs visés pour 2020 consiste à réduire la consommation de carburant de 50%. En 2011, l'initiative de l'ACARE a été réitérée pour 2050, en marge de la publication du rapport « New Vision, Flightpath 2050 », relevant les objectifs de réduction des émissions de CO_2 à 75%, des émissions de NO_X à 90% et du bruit perçu de 65%. Deux voies importantes pour atteindre ces objectifs consistent en (i) la réduction de la masse des aéronefs et en (ii) l'amélioration du rendement des moteurs. Les matériaux innovants, notamment les matériaux composites, peuvent résoudre une partie du problème. En effet, la plupart des matériaux composites ont des propriétés spécifiques élevées intéressantes pour l'allégement de certaines structures. De plus, les matériaux composites thermo-structurés conçus pour les applications à haute température peuvent contribuer à augmenter la température de combustion au sein des moteurs et ainsi améliorer leur rendement. Enfin, de nouveaux concepts de motorisation sont également étudiés, tel que les *open-rotors* contrarotatifs (CROR).

Cette thèse traite majoritairement de la conception optimale de structures en composites stratifiés et dans une moindre mesure de la conception de pale de CROR. Les travaux présentés ont été effectués dans le cadre d'une collaboration entre le Département Matériaux et Structures Composites (DMSC) et le Département d'Aérodynamique Appliquée (DAAP) de l'Onera. Le but de cette étude est double. D'une part, l'étude vise à développer un algorithme d'optimisation, dédié spécifiquement aux composites stratifiés à épaisseur variable, et destiné à la conception optimale de petites structures composites en tant qu'outil de conception rapide. D'autre part, l'étude vise à estimer le potentiel des composites stratifiés dans la maîtrise des performances aérodynamiques d'une pale de CROR à échelle réduite destinée aux essais en soufflerie.

Le premier axe de l'étude traite de l'optimisation des matériaux composites stratifiés. Ce sujet intéresse la communauté scientifique depuis les années 1970, au regard du potentiel offert par les composites stratifiés pour l'optimisation des structures et de la complexité potentielle de la conception pour atteindre ce potentiel. Une large littérature traitant de l'optimisation des composites existe. Des revues de littérature récentes sur ce sujet sont disponibles dans (Ghiasi et al., 2009) et (Ghiasi et al., 2010). L'optimisation de structures en composites stratifiés repose sur l'optimisation du nombre de plis, de leur orientation et de leur ordre au sein du stratifié. Les propriétés spécifiques des matériaux composites, mais également leur anisotropie, sont exploitées. Si le nombre de plis est directement lié à l'épaisseur de la structure (une variable classique de l'optimisation de structure), l'orientation des plis et l'ordre des plis sont de nouvelles variables de conception par rapport aux structures métalliques. Le but de l'optimisation de structure composite réside dans l'organisation du matériau composite dans la structure afin de minimiser la masse tout en satisfaisant des contraintes liées à la raideur ou à la résistance de la structure.

Le nombre de plis est une variable discrète, tandis que l'ordre des plis est une variable combinatoire. L'orientation des plis est quant à elle parfois choisie parmi des valeurs continues ou, plus souvent pour des raisons de fabrication, quelques valeurs discrètes. Le problème d'optimisation composite peut ainsi être approché comme un problème combinatoire à variables mixtes. De plus, les variables de design, tel que l'orientation des fibres, et les multiples règles de conception dans les problèmes de conception composite, vallonnent l'espace de design de nombreux optima locaux. Ce type de problème peut se résoudre soit par une approche directe, soit par une approche à deux niveaux. Cette dernière consiste à trouver dans un premier temps les propriétés mécaniques locales optimales de la structure puis dans un second temps de trouver les empilements dont les propriétés s'en rapprochent le plus (Herencia et al., 2008; IJsselmuiden et al., 2009; Liu et al., 2011; Montemurro et al., 2012). Dans les deux cas, la résolution du problème combinatoire visant à optimiser les variables d'empilement, est inévitable.

Pour trouver les designs composites les plus intéressants, de nombreux auteurs recourent aux algorithmes d'optimisation stochastiques, parmi lesquels figurent notamment les Algorithmes Evolutionnaires, et plus spécifiquement les Algorithmes Génétiques. Ceux-ci sont en effet particulièrement bien adaptés à l'optimisation composite (Le Riche and Haftka, 1993), et trouvent plusieurs applications comme répertoriées dans (Venkataraman and Haftka, 2004). D'autres métaheuristiques ont prouvé leur efficacité quant à l'optimisation composite, telle que la méthode *fractal branch-and-bound* (Matsuzaki and Todoroki, 2007), les colonies de fourmis (Aymerich and Serra, 2008; Koide et al., 2013; Sebaey et al., 2011; Wang et al., 2010), le recuit simulé (Erdal and Sonmez, 2005), la recherche tabou (Pai et al., 2003) ou la méthode des essaims particulaires (Chang, 2010). Un comparatif entre algorithme génétique, colonies de fourmis et essaims particulaires a été effectué dans (Bloomfield et al., 2010). Les algorithmes d'optimisation stochastique présentent trois principaux avantages pour résoudre les problèmes d'optimisation composite. Premièrement, ce sont des algorithmes globaux, autrement dit capables d'échapper aux optima locaux. Deuxièmement, ces algorithmes ne requièrent aucune information de gradient, et sont donc aptes à gérer des critères non linéaires ou des outils de conception utilisés comme boîte noire. Troisièmement, ils peuvent être facilement adaptés aux spécificités de certains problèmes d'optimisation, ce qui permet d'améliorer significativement leurs performances sur la famille de problèmes considérée et de prendre en compte des règles de conception spécifiques. En effet, le caractère multi-échelle des composites étant intrinsèquement lié à leur procédé de fabrication, leur conception repose sur de nombreuses variables, augmentant drastiquement le nombre de problèmes possibles. Mais diverses connaissances mécaniques peuvent aider la conception optimale de structures composites.

Dans cette étude, il sera question de résoudre les problèmes d'optimisation des structure en composites stratifiés d'épaisseur variable. Pour cela, une méthode d'optimisation adaptée permettant de gérer les tables de drapage est proposée. Ceci requiert la spécialisation de l'algorithme proposé initialement dans (Irisarri et al., 2009), et permet *de facto* d'introduire des connaissances métiers quant au problème à résoudre.

Il sera également question d'améliorer l'aspect algorithmique de la méthode proposée et d'étudier le réglage de cette méthode. Une étude du paramétrage de l'algorithme est effectuée en marge de l'implémentation d'une technique de guidage. Ce guidage est effectué via l'estimation des densités de probabilités d'un espace auxiliaire, renfermant davantage de connaissance sur la physique du

problème. Cette technique, issue de l'Algorithme d'Optimisation à Double Distribution (DDOA) proposé dans (Grosset et al., 2006), est améliorée et implémentée dans l'AE proposé précédemment afin d'en accroître l'efficacité.

Le deuxième axe de cette étude vise à exploiter l'algorithme proposé dans un processus de conception de pales composites pour CROR (catégorie des moteurs dits « propfans »). Ce concept de moteur, connu depuis les années 1980 et remis au goût du jour à travers l'initiative européenne CleanSky, est plus économe par rapport aux technologies conventionnelles (catégories des moteurs dits « turbofans » et « turbopropulseurs »). Le rendement de ce type de moteur en est amélioré grâce à son excellent taux de dilution, au prix d'émissions acoustiques trop importantes pour envisager une mise en service immédiate.

Afin de parvenir aux objectifs de l'ACARE, le dimensionnement des CROR est effectué en partie en recourant aux méthodes d'optimisation aérodynamique et acoustique des doublets d'hélices. Basées sur la seule évaluation des performances aérodynamiques via la résolution d'équations de type Reynolds-Averaged Navier Stockes (RANS), ces méthodes permettent d'établir les formes optimales des pales, ou *formes à chaud*, pour chaque point de fonctionnement du moteur, sans connaître la forme initiale de la pale, ou *forme à froid*. Or, l'envergure et l'élancement caractéristiques des pales de CROR impliquent des efforts inertiels et aérodynamiques relativement importants, qui se traduisent par des déformations substantielles en fonctionnement. Celles-ci remettent en question les hypothèses classiques issues du dimensionnement des aubes fans métalliques quant aux petites perturbations observées par la pale et posent également la question de l'intégrité des pales de CROR. Une des solutions envisagées pour garantir l'intégrité de la pale et minimiser les déformations consiste à recourir aux matériaux composites. Une solution de pale CROR en composites stratifiés est envisagée dans le cadre de cette étude. Enfin, la faisabilité de la pale en fabrication dépend directement de la correspondance des formes à froid aux différents points de fonctionnement. Il est donc nécessaire de trouver les structures composites permettant à la forme à froid de se rapprocher des formes à chaud optimisées pour chaque point de fonctionnement.

Dans le but de déterminer si la structure peut contribuer à l'optimisation du rendement aérodynamique d'une hélice de CROR en différents points de fonctionnement (ou phases de vol), il est essentiel, dans un premier temps, de connaitre la forme à froid de la pale CROR pour en déduire l'état des contraintes dans la forme à chaud. Ceci requiert le développement de processus de *mise à froid* et de *mise à chaud* de la forme de la pale. Ces méthodes itératives reposent sur l'évaluation successive des efforts aérodynamiques induits par la forme de la pale et des déformations qui en résultent. Dans un second temps, il s'agira d'intégrer la gestion des variations spatiales des propriétés mécaniques locales de la structure de la pale CROR dans son processus de conception. La méthode d'optimisation des structures composites à épaisseur variable, proposée dans la première partie, est donc exploitée pour maximiser le rendement propulsif de l'hélice amont du CROR, au décollage et en croisière.

Synthèse du manuscrit

Le premier chapitre de ce manuscrit traite la problématique de l'optimisation de structures stratifiées d'épaisseur variable. Au sein d'une pièce en composite stratifié, les variations d'épaisseur sont obtenues par arrêt ou reprise de plis. La technique de *blending* (Adams et al.,

2004)permet d'assurer la continuité des empilements entre zones adjacentes pour assurer la continuité structurale de la pièce. Cette technique est difficilement applicable lorsque des contraintes doivent être introduites pour lier des optimisations d'empilement indépendantes entre zones. Une alternative consiste à optimiser toutes les zones de la pièce en une seule fois. Pour cela, l'utilisation de la technique de *guide-based blending* est préconisée. L'empilement le plus épais est optimisé en premier avant de déduire les autres zones par suppression des plis de cet empilement. Usuellement, la suppression des plis s'effectue par l'extérieur (*outer blending*) ou par l'intérieur (*inner blending*) du stratifié, comme illustré en Figure 1. Cette technique ne permet cependant pas d'optimiser l'ordre des empilements. Une solution possible pour optimiser l'ordre des empilements consiste à optimiser directement la table de drapage de la structure.

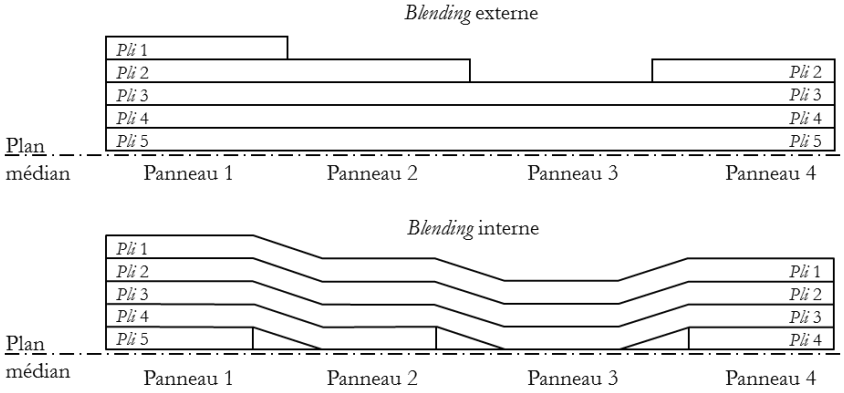

Figure 1. *Blending* externe et interne pour un panneau à 4 régions (traduit d'après [Adams 2004]).

La table de drapage permet de décrire l'organisation des séquences des reprises de plis (ou arrêts de plis) entre des zones d'épaisseur différentes au sein d'une pièce, comme illustré en Figure 2. La table de drapage permet initialement d'évaluer un ensemble de règles métier relatives à la conception et à la fabrication des composites stratifiés. Ces règles métiers intègrent les bonnes pratiques de conception issues des retours d'expérience, empêchant certains phénomènes (par exemple : rupture, délaminage ou propagation de fissures) dont la description échappe aux modèles de pré-dimensionnement utilisés pour l'optimisation.

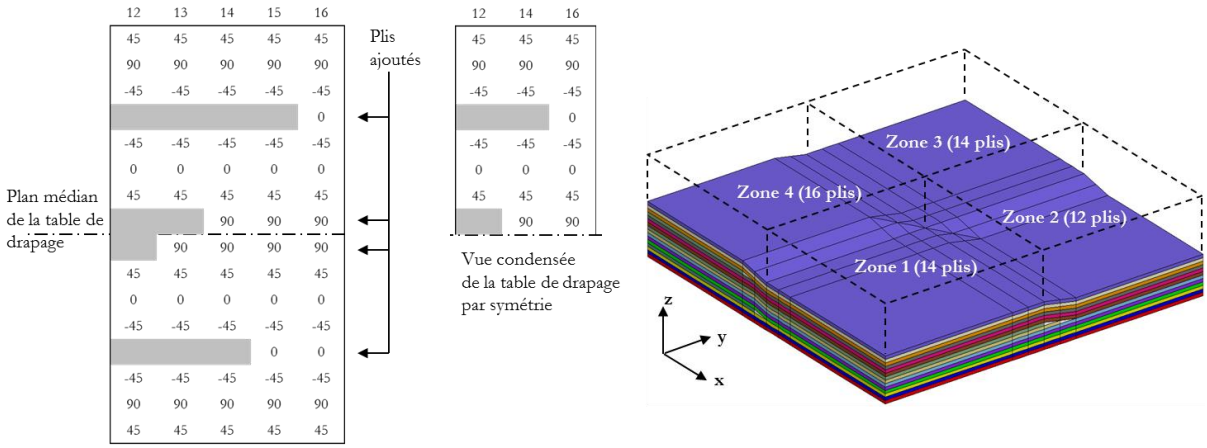

Figure 2. Panneau à 4 régions avec variations d'épaisseur (à droite) et table de drapage correspondante avec 4 reprises de plis (à gauche). Le nombre de plis du stratifié concerné est indiqué au-dessus de sa colonne (n_{min}= 12 and n_{max}= 16).

Les règles sont ainsi distinctes des autres contraintes telles que le flambement, et sont incorporées à l'algorithme d'optimisation directement à partir d'opérateurs sans passer par la fonction coût.

Ainsi, dans cette étude, ces règles sont prises en compte dans l'optimisation afin de produire des solutions faisables techniquement en termes de fabrication. Pour cela, le développement d'un Algorithme Evolutionnaire dédié à l'optimisation des tables de drapage est envisagé. En partant d'un AE existant à l'Onera et dédié à l'optimisation d'empilements et dont la structure initiale sera conservée, un nouvel algorithme spécialisé pour les tables de drapage est créé. La spécialisation de l'algorithme, illustrée en Figure 3, implique de (i) proposer une représentation efficace de la table de drapage et de (ii) développer des opérateurs de variation spécifiques.

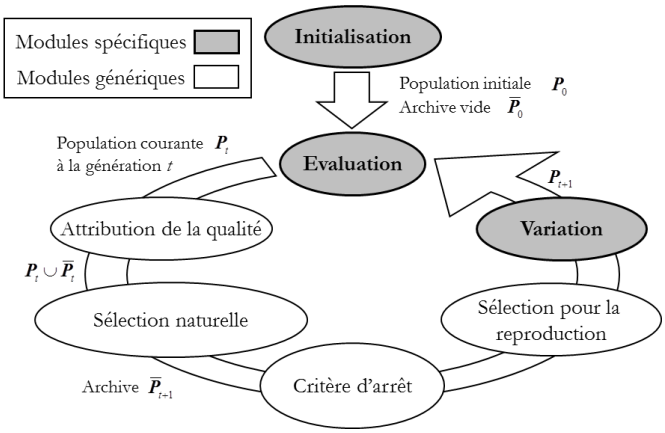

Figure 3. Diagramme de l'algorithme évolutionnaire. Les modules spécifiques étant dépendants du problème traité, ceux-ci ont été développés pour l'optimisation de tables de drapage.

L'encodage de la table de drapage consiste en trois chromosomes, dont un dédié à la description de l'empilement de base, un deuxième dédié à l'ordre des reprises de plis, et un troisième dédié à la distribution du nombre de plis dans la structure. Ces trois chromosomes constituent le

"génotype" de la solution encodée. Ces trois chromosomes sont traduits en une table de drapage qui, accompagnée de la distribution des nombres de plis dans la structure, permet d'évaluer la performance (masse, tenue au flambement, ...) qui constitue le "phénotype" de la solution. Le processus d'optimisation génère des solutions telles que les valeurs contenues dans le chromosome des distributions des nombres de plis ne couvrent que partiellement la table générée par les chromosomes de l'empilement de base et de l'ordre d'insertion des plis. Une partie du génotype est donc non codant. Les solutions sont créées via le générateur de l'algorithme et les opérateurs de variation. Ceux-ci construisent les stratifiés symétriques pli par pli depuis leur surface jusqu'à leur plan médian. Les orientations de pli faisables au regard des règles métier sont ensuite énumérées. Enfin, un choix aléatoire de tout ou partie de l'ensemble des orientations de plis admissibles est ensuite effectué. La construction des tables de drapage proposée ici s'effectue donc par insertion de plis à partir d'un empilement fin, au lieu de supprimer les plis à partir du plus épais. En procédant par suppression, l'opération aboutit fréquemment à des impasses vis-à-vis des règles d'empilement et d'arrêts de plis.

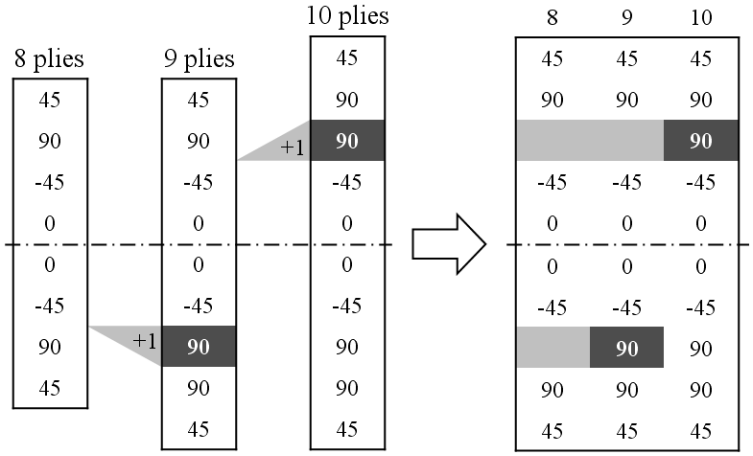

Figure 4. Création d'une table de drapage. Les plis sont ajoutés un par un pour créer la table à droite de la figure. L'orientation du premier pli inséré est choisi parmi l'ensemble $\{\mathbf{0°}, \mathbf{\pm 45°}, \mathbf{90°}\}$. $\mathbf{0°}$ et $\mathbf{+45°}$ sont interdites par la règle de désorientation. Un pli de $\mathbf{90°}$ est retiré de l'ensemble des valeurs admissibles restantes. Un second pli de $\mathbf{90°}$ est ensuite inséré pour retrouver la symétrie.

L'algorithme proposé est appliqué, en mono-objectif (minimiser la masse totale de la structure) et en multi-objectif (minimiser la masse totale de la structure et maximiser la résistance au flambement), à un problème-type issu de la littérature avec des résultats convaincants. L'AE montre une vitesse de convergence satisfaisante par rapport aux résultats de la littérature et une bonne reproductibilité des résultats. Les concepts les plus légers obtenus sont à peine plus massifs que les solutions publiées jusqu'à présent, tout en satisfaisant beaucoup plus de règles de conception. Notamment, les résultats donnés dans cette étude montrent que les règles relatives à la résistance de la structure peuvent être imposées sans pénaliser outre mesure le comportement en rigidité et *de facto* la masse de la structure. Enfin, une pièce composite conçue par l'entreprise MECANO I&D, et destinée à équiper une antenne de satellite, est optimisée via cette méthode avec des résultats intéressants. Un problème multiobjectif est formulé à partir du cahier des charges de la pièce. Les évaluations des solutions générées sont effectuées via solveur éléments

finis en conséquence de la géométrie complexe de la pièce. Le problème d'optimisation est résolu pour le drapage de tissus 2D carbone/époxy et le drapage de plis UD carbone/époxy afin d'explorer des espaces de design différents et de fournir des alternatives améliorant la solution de référence en alliage de titane.

L'algorithme proposé est relativement versatile à l'instar des autres algorithmes évolutionnaires et permet de traiter une large gamme de problèmes. Il est ainsi pertinent aussi bien (i) dans le cadre d'une approche directe, dans laquelle les solutions sont évaluées par un modèle paramétré utilisé en boîte noire, ce qui autorise à traiter n'importe quel type de réponse mécanique, même non-linéaire ; que (ii) dans une approche bi-niveau pour restituer les empilements permettant de s'approcher au mieux d'une distribution de rigidité souhaitée. Néanmoins, comme pour tout AE, cette versatilité n'est possible qu'au prix de milliers voire de dizaines ou centaines de milliers d'évaluations. Dans le cadre de l'approche directe, avec des modèles mécaniques pouvant eux-mêmes réclamer de quelques minutes à quelques heures, le temps total devient rapidement prohibitif. Or, en optimisation de structure, un budget de calcul limité est souvent imparti. Il est donc intéressant de travailler à l'amélioration de l'efficacité de l'algorithme afin de pouvoir aborder des problèmes de plus en plus exigeants en termes de qualité des modèles et de coût de calcul unitaire.

Le deuxième chapitre aborde l'amélioration de l'efficacité de l'algorithme par deux aspects, (i) l'étude du réglage de ses paramètres et (ii) l'ajout d'un mécanisme additionnel de guidage vers les solutions les plus prometteuses. Pour étudier le réglage de l'algorithme, on revient à un problème composite simple, la maximisation de la force critique de premier flambement d'une plaque rectangulaire simplement appuyée sur ses 4 bords et sollicitée en compression uniaxiale. On optimise un empilement à nombre de plis fixé, sans se soucier de règles de conception. Le problème est également résolu avec un algorithme à distribution marginale univariée (UMDA), en comparaison avec l'AE, afin de mieux comprendre la gestion du compromis entre exploration de l'espace de design et intensification de la recherche autour des meilleures solutions. UMDA a l'avantage de la simplicité et ses réglages sont relativement intuitifs. L'AE reste plus performant sur les problèmes traités, mais les tendances sont moins évidentes en matière de réglages. Le réglage de ces algorithmes dépend du problème, rendant indispensable l'expertise de l'utilisateur comme prévu dans les théories *No Free Lunch* (Wolpert and Macready, 1997) ; et ce même si des réglages génériques permettant un comportement généralement acceptable sont proposés dans la thèse.

En matière d'amélioration algorithmique, une technique de guidage dans un espace de recherche auxiliaire est intégrée dans l'AE étudié précédemment. Cette technique provient de l'Algorithme d'Optimisation à Double Distribution (DDOA) (Grosset et al., 2006), lui-même conçu comme une évolution d'UMDA pour l'optimisation composite. DDOA hérite de la simplicité d'UMDA mais également de l'introduction de l'estimation par noyaux à densité (KDE) dans l'espace des variables auxiliaires lui-même. Ici, les variables auxiliaires sont les paramètres de stratification issus de la théorie classique des stratifiés (Tsai and Hahn, 1980; Gürdal et al., 1999) et permettant de représenter la rigidité macroscopique d'un stratifié avec 12 paramètres continus et adimensionnés. Ceci requiert une connaissance avancée du problème et de l'algorithme concerné. Dans cette étude, les noyaux ont été réglés d'après les domaines de variation connus des paramètres de stratification. Cette étude propose une implémentation de ce mécanisme de

guidage à l'AE dans le but de profiter de son efficacité, mise en lumière par la comparaison avec UMDA et DDOA, et ce tout en conservant les avantages de l'AE en matière de gestion des règles de conception. Les performances et la fiabilité comparées de l'AE et de DDEA sont illustrées en Figure 5.

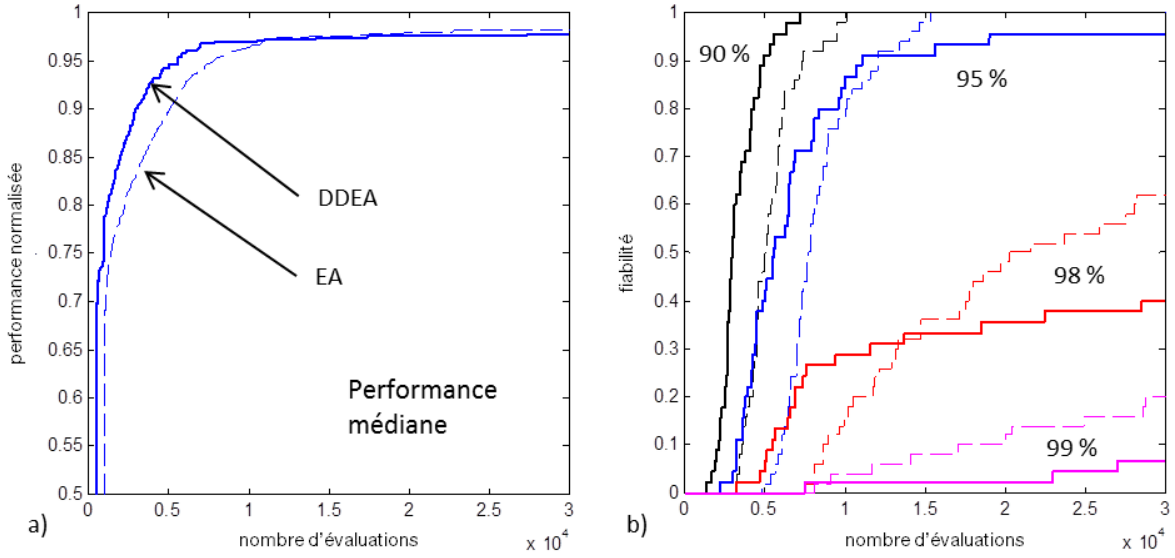

Figure 5. Comparaison de l'AE et de DDEA sur le problème de panneau en U. Toutes les règles de conception sont imposées. a) Courbes des performances médianes. b) Courbes des fiabilités.

Dans le troisième chapitre de ce manuscrit, l'approche par table de drapage est appliquée à la conception de pales de propulseur. Le but de cette application est d'intégrer la structure dans le processus de conception de la pale, par opposition à la démarche usuelle reposant sur des optimisations de forme en fonctionnement. En effet, cette démarche ne permet pas de travailler directement à partir de la forme au repos de la pale, ou forme à froid, qui est pourtant celle qui est fabriquée. L'étude se base sur le modèle de la pale HTC5, créé à l'Onera et destiné aux études aérodynamiques sur CROR (Bousquet et al., 1991). Les paramètres géométriques de la pale sont présentés avant de justifier la construction d'un modèle simplifié pour le calcul de ligne portante courbe (LPC2), et d'un modèle éléments finis pour le calcul de structure (ABAQUS). Dans cette étude, la pale est décrite avec un jeu réduit de paramètres géométriques (i.e. l'angle d'incidence, le vrillage, la flèche, le dièdre et la hauteur des profils constituant la pale) qui sont utilisés pour paramétrer et chaîner les modèles. Des méthodes de mise à froid et de mise à chaud, basées sur ces deux modèles, sont proposées (voir Figure 6). La mise à froid permet d'estimer la forme de la pale au repos, appelée forme à froid, depuis sa forme à chaud définie en un point de fonctionnement particulier (ex : décollage ou croisière). La mise à chaud réfère au processus opposé.

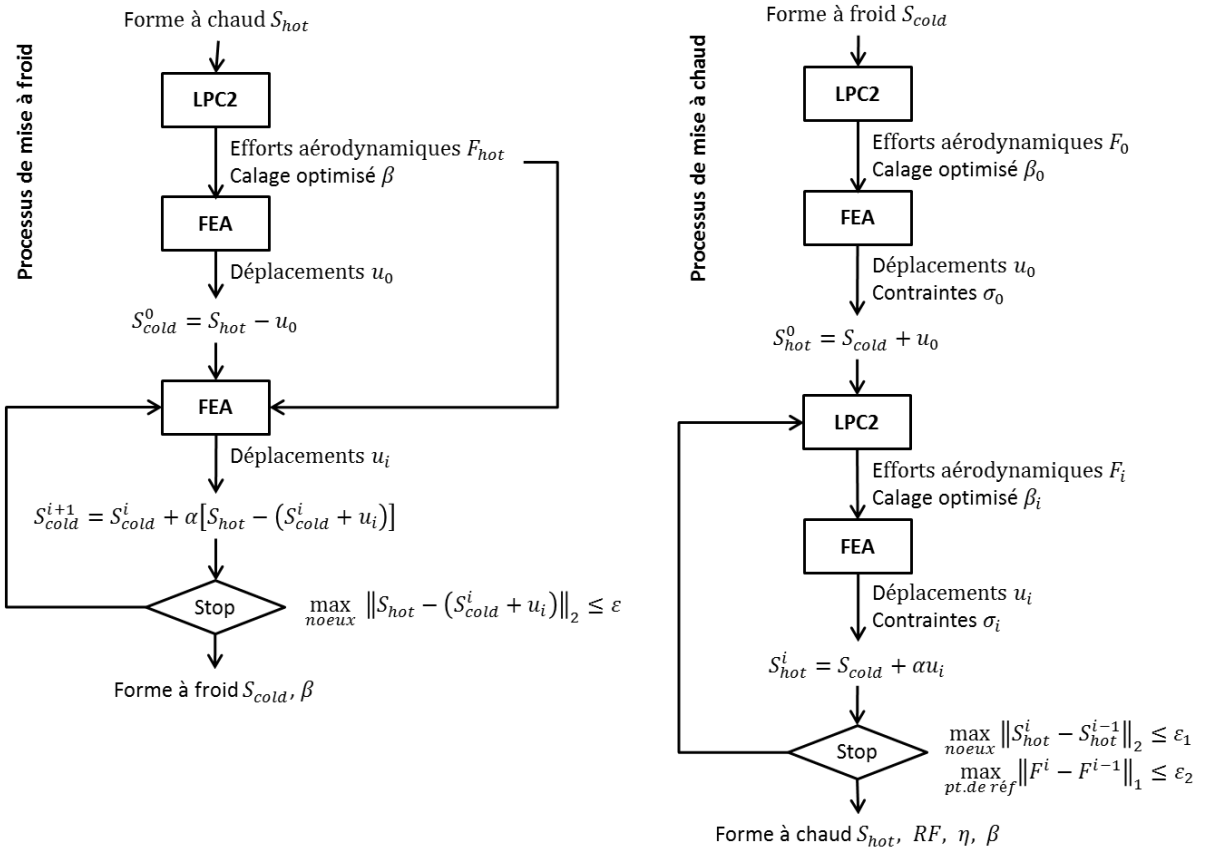

Figure 6. Processus itératifs de mise à froid (à gauche) et de mise à chaud (à droite).

La difficulté majeure dans le chaînage des modèles réside dans le transfert du chargement aérodynamique. En effet, le code de ligne portante LPC2 (Gardarein, 2013), qui est un outil de pré-design basse fidélité, fournit une description approchée du chargement aérodynamique, réduit à des résultantes de densité d'efforts exprimées au quart de corde de quelques profils répartis le long de l'envergure de la pale. Deux méthodes ont été implémentées et comparées afin d'appliquer le chargement aérodynamique au modèle éléments finis de la pale. La première méthode étant la plus cohérente vis-à-vis des hypothèses induites par LPC2 : les résultantes des efforts aérodynamiques sont introduites aux points de référence correspondant au quart de corde du profil correspondant supposé rigide. Cependant, cette méthode génère de nombreuses surcontraintes à proximité des profils rigides et rend le champ de contrainte inexploitable pour estimer la rupture de la pale à l'aide d'un critère de première rupture de pli appliqué en post-traitement de l'analyse élastique. La seconde méthode est basée sur des distributions de pression types, déterminées à partir de calculs RANS sous le solveur CFD 3D elsA (Cambier and Veuillot, 2008) qui sont interpolées sur le maillage du modèle structure et paramétrées comme fonctions des sorties de calcul LPC2. Cette méthode résulte en une meilleure description de l'état des contraintes internes de la pale, illustré en Figure 7, et est donc privilégiée par la suite. De plus, décrire le chargement aérodynamique via un champ de pression permettrait de remplacer à terme le calcul sous LPC2 par une analyse aérodynamique plus précise sous solveur CFD 3D.

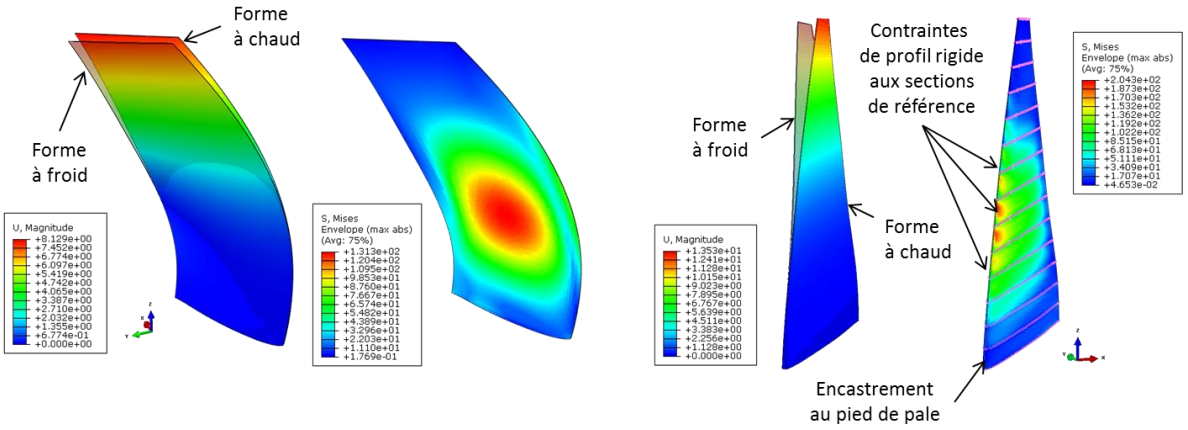

Figure 7. Formes à froid de la pale HTC5 en alliage d'aluminiuum et états des contraintes de Von Mises à la surface de la pale via la méthode des pressions (à gauche) et de la ligne portante courbe (à droite).

Le processus de mise à froid est appliqué à une pale en aluminium afin d'estimer une forme à froid de référence. Il est montré que l'analyse éléments finis en déplacement non linéaire est nécessaire pour intégrer la réorientation des axes matériaux, en particulier pour des composites anisotropes, puisque la pale subit des déformations importantes. Cette condition de non-linéarité des déplacements participe également à l'amélioration de la convergence du solveur structure.

En partant de la forme à froid obtenue pour la pale en aluminium, le processus de mise à chaud est appliqué à des pales de matériaux différents. Les résultats de calcul montrent que le matériau de la pale peut être utilisé pour maîtriser la forme à chaud. Cependant, les variations des rendements de l'hélice calculés via LPC2 sont inférieures à 1% au décollage, ce qui est largement en dessous des variations attendues. Deux optimisations bi-objectif sont effectuées pour maximiser la résistance de la pale et le rendement total de l'hélice, l'une pour le décollage et l'autre pour la croisière. Les deux optimisations confirment que les variations de rendements obtenues en modifiant la structure de la pale sont minimes. Deux sortes de structures composites sont considérées, avec des conclusions similaires : les pales monolithiques et sandwich. On observe donc que des structures internes différentes aboutissent à des formes à froid potentiellement très différentes en partant de la même forme à chaud. En partant de la forme à froid, quelle que soit la structure interne, les formes à chaud restent similaires, tout comme les performances aérodynamiques. Ceci est probablement dû au fait que la description du chargement aérodynamique est trop grossière pour permettre de capter l'essentiel des moments de torsion au sein de la pale. La contribution des efforts centrifuges s'en trouve largement prédominante sur le comportement de la pale.

Ces résultats peuvent s'expliquer par la façon dont les efforts aérodynamiques sont calculés et transférés au modèle structure. En effet, l'évaluation du chargement aérodynamique reste grossière. Les moments de torsion dus aux chargements aérodynamiques – qui ont une influence majeure sur le rendement de la pale et donc de l'hélice – pourraient être sous-estimés ou mal décris. Le modèle éléments finis reste également relativement grossier, et peut être trop rigide à cause de la densité trop faible du maillage. Ces approximations ne sont cependant pas la

principale raison pour que la structure de la pale n'autorise que peu de variations en termes de rendement. En effet, il s'avère que l'hélice HTC5 fonctionne sous des forces centrifuges prédominantes sur les efforts aérodynamiques. Ces efforts sont sous-estimés par l'interpolation sur le maillage structure, ce dernier étant trop grossier par rapport au gradient de pression en bord d'attaque. Puisque la vitesse de rotation reste la même pour tous les points de fonctionnement envisagés, toutes les formes à chaud sont similaires malgré les différences notables en termes de matériaux. D'autres concepts d'hélice, avec des vitesses de rotation plus faibles et variables d'un point de fonctionnement à un autre, devraient résulter en différentes contributions entre les chargements centrifuges et aérodynamiques, et amener des conclusions différentes. Dans les travaux présentés, cependant, il s'avère que modifier la structure de la pale (sans changement de masse) ne permet pas de modifier significativement son rendement en un point de fonctionnement. Seules de petites variations des formes à chaud sont possibles. Néanmoins, la structure influence la forme à froid de la pale – qui est montrée comme substantiellement différente de la forme à chaud – et de la résistance de la pale. Ici, des marges importantes sont obtenues pour des pales à échelle réduite en tenant compte de la rupture. Cependant, puisque les chargements varient en fonction du carré du facteur d'échelle, la résistance pourrait être un problème en grandeur nature. Pour pallier à ces limites et améliorer sa résistance, sachant que la mise à l'échelle des structures composites restant un problème ouvert, la pale à taille réelle est envisagée en tissus 3D. Ceci impose une modélisation de structure et un codage des solutions différents.

GENERAL INTRODUCTION

The protection of the environment is nowadays a major challenge at global scale, debated each year since 1995 at a political level during Conference of the Parties (COP). It is estimated that aviation is currently responsible for about 2% of the global emissions of carbon dioxide. Nevertheless, this proportion is expected to increase with the air traffic growth and the potential reduction of emissions that other sectors could achieve. The Advisory Council for Aviation Research in Europe (ACARE) has been launched in 2001 to help achieve the goals detailed in the "European Aeronautics: A vision for 2020" report[1]. One of the objectives set for 2020 consists in a 50% cut of fuel consumption. In 2011, the reflection has been extended to 2050 and the "New Vision, Flightpath 2050" report[2] raises the objective up to a 75% cut of CO_2 emission, 90% NO_X emissions and 65% perceived noise reduction relative to the year 2000. Two important paths to achieve this goal are (i) the reduction of the mass of the airliners and (ii) the increase of the engine efficiency. Innovative materials and especially composite materials can bring part of the answer. Indeed, most composite materials have high specific properties, i.e. stiffness-to-weight ratio and strength-to-weight ratio, which makes them well suited for lightweight design applications. Additionally thermo-structural composite materials designed for high temperature applications can help increasing the combustion temperature inside the engines and thus improve their efficiency. New engine concepts are also investigated, such as the Counter-Rotating Open Rotor (CROR)[3].

This thesis deals with the optimal design of laminated composite structures in general and of a CROR blade in particular. The present work has been performed in collaboration between the Composite Materials and Structures Department (DMSC) and the Department of Applied AeroDynamics (DAAP) of ONERA. The purpose of the study is twofold. First, the study aims at developing an efficient optimization algorithm for variable-thickness composite laminates, to be used as a rapid design tool for the optimal design of small composite structures. Second, the potential of composite laminates to tailor the aerodynamic performances of a CROR blade is investigated. The study considers a scaled blade designed for wind tunnel testing.

Optimization of laminated composite structures

Most composites used for aeronautical structures are laminates assembled from a base composite ply. The base ply is usually a unidirectional ply made of continuous carbon fibers and an organic matrix. Carbon Fiber reinforced Plastics (CFRP) have been used for aeronautical secondary structures for decades and have been introduced into load carrying primary structures in the last year, with the Airbus A380, A350 and the Boeing B787. The first applications of composite laminates in aeronautical structures were mostly taking advantage of the superior specific properties of the material with respect to metallic alloys. However, the design of composite structures suffers from very conservative design practices related to the inherent complexity of

[1] http://www.acare4europe.org/sites/acare4europe.org/files/document/Vision%202020_0.pdf
[2] http://www.acare4europe.org/sites/acare4europe.org/files/attachment/SRIA%20Executive%20Summary.pdf
[3] http://www.cleansky.eu/content/interview/counter-rotative-open-rotor-cror

their damage and failure mechanisms and the lack of robust, predictive and computationally efficient models. Thus, the so-called "black aluminum" design practice consisting in replacing metallic materials by quasi-isotropic laminates only brings mass savings that have to be put into perspective with the complexity related to the manufacturing process of the composite part. Additionally, composite solutions have to compete with highly optimized metallic designs. Hence optimization of the composite structures is required to allow the emergence of innovative and competitive composite designs.

Composite structure optimization in the industry is still limited nowadays for two main reasons. First, composite materials are very often used to replace light alloys into existing parts, without really redesigning the structure. Thus, the shape of the part and its connection to the surrounding structures are only slightly modified – if modified at all – when designing the composite solution. Nevertheless, the optimal metallic shape is often far from the optimal shape of the composite structure. The resulting mass savings can be significantly sub-optimal. Finding the optimal shape of a composite structure is currently an open field of research. Second, the certification process of composite structures relies heavily on experiments, which lead to a major shrinking of the design space, reduced to a few tested laminates. Nonetheless, both design methods and certification requirements are evolving and composite structures are increasingly optimized in the aeronautical industry.

The scientific community has understood since the 70's the potential offered by the composite laminates for structural optimization and a large literature about composite optimization is available. A simple search with the keywords "composite" and "optimization" on the ScienceDirect database returns 90,053 references among which 1,648 references published in 2000, 4,339 references published in 2010 and 9,671 references published in 2015[4]. Recent reviews on the topic can be found in (Ghiasi et al., 2009, 2010). Optimization of laminated composite structures deals with the optimization of the number of plies, the ply orientations and the ply order within the laminate. If the number of plies is directly related to the thickness of the structure which is a classical variable in the field of structural optimization, the ply orientations and ply order are new design variables compared to metallic structures. The aim of composite structure optimization is to tailor the composite material in the structure to minimize its mass while satisfying stiffness-related or strength-related specifications.

The number of plies is a discrete variable. The ply order is a combinatorial variable. The ply orientations are usually chosen from a continuous or, for manufacturing reasons, from a discrete set of allowed values. Thus, the composite optimization problem can be seen as a mixed-variable and combinatorial problem. More, design variables (i.e. fiber orientations) and design guidelines in excess in composite design problems create many locally optimal arrangements. Many authors have investigated discrete stochastic optimizers to find interesting composite designs. Generally speaking, there is a consensus to say that Evolutionary Algorithms (EAs) – and among them Genetic Algorithms (GAs) – are well-suited for composite optimization, see for instance (Le Riche and Haftka, 1993). Numerous examples of EAs applied to composite optimization problems can be found in (Park et al., 2003; Venkataraman and Haftka, 2004). Nevertheless other metaheuristics have also been successfully applied to composite optimization such as the fractal branch-and-bound method (Matsuzaki and Todoroki, 2007), the Ant Colony Optimization

[4] Retrieved from http://www.sciencedirect.com/ on the 02 December 2015.

(ACO) algorithm (Aymerich and Serra, 2008; Koide et al., 2013; Sebaey et al., 2011; Wang et al., 2010), the simulated annealing (Erdal and Sonmez, 2005), the tabu search (Pai et al., 2003) or the Particle Swarm Optimization (PSO) method (Chang, 2010). A benchmark between GA, ACO and PSO can be found in (Bloomfield et al., 2010). Discrete stochastic optimizers present three main advantages for composite optimization. First, they are global optimizers which are able to escape local optima. Second, they do not require gradient information which enables to handle any kind of non-linear criteria or black-box design tools. Third, they can be easily adapted to the optimization problem which enables significant improvement of their efficiency on the considered family of problems and enables to take into account specific design guidelines.

The main limitation of discrete optimization methods is related to the number of required evaluations of the mechanical models and the resulting computational cost. For instance, in the case of EA, thousands of evaluations or more can be required before having sufficiently sampled the volume of the design space to find high-performance solutions, or to simply avoid premature convergence. If each solution evaluation corresponds to a Finite Element Analysis (FEA), the total computational cost can be prohibitive. One way of controlling and keeping the number of required evaluations reasonably low is to replace the costly FEA by a response surface. Response surface methods consist in approximating the output of a detailed and costly physical model by a fast mathematical model. The development of response surface methods is in itself a rich field of research and many methods are available in the literature (Bishop, 2006; Forrester and Keane, 2009; Queipo et al., 2005; Timothy Simpson et al., 2008). In the field of composite optimization, most published work investigate the choice of the response surface method and the way to apply it rather than developing new methods, even if some works have been led for the development of surrogate models specialized for multimodal response such as buckling (Bettebghor et al., 2011; Leroy et al., 2013; Bettebghor and Leroy, 2014). (Lanzi and Giavotto, 2006) compares Neural Networks, Radial Basis Functions and Kriging approximation for the buckling and post-buckling maximization of composite stiffened panel using an EA. (F.-X. Irisarri et al., 2011) uses Radial Basis Functions under Tension (RBFT) for a similar design problem. (Todoroki and Ishikawa, 2004) shows that lamination parameters form a very convenient set of variables to learn accurate response surfaces with a limited design of experiments.

Lamination parameters come from the classical plate lamination theory (Tsai and Hahn, 1980; Gürdal et al., 1999) and are a convenient way to represent the macroscopic stiffness of a laminate with 12 continuous and non-dimensional parameters. Numerous authors have chosen to formulate the composite optimization problem as a continuous optimization problem using the lamination parameters as design variables (IJsselmuiden et al., 2010; Liu and Toropov, 2013; Miki, 1985). An alternative approach consists in using the polar description of the macroscopic stiffness tensors (Jibawy et al., 2011). Both methods enable gradient-based optimizers to be used for all usual linear elastic rapid sizing criteria such as buckling, eigen frequencies, stiffness, nodal displacements and strength, since lamination parameters and polar descriptions lead naturally to continuous variables. The variables of the optimization are the spatial distributions of the laminate macroscopic stiffness and thickness over the structure. The problem can be solved using gradient-based structural optimization method. For instance (Wu et al., 2015) uses the Method of Moving Asymptotes (MMA) (Svanberg, 1987) for the buckling optimization of a Variable Angle Tow (VAT) plate. Commercial software such as MSC NASTRAN and ALTAIR OPTISTRUCT can also be used. A specialized optimization method is proposed in (IJsselmuiden et al., 2010) for

composite structure manufactured by Automated Fiber Placement (AFP) process. Compared with the discrete approach, the continuous formulation of the composite optimization problem allows handling very large number of design variables with the greatest computational efficiency. Problems are often solved within a few dozens of evaluations. Nevertheless, the continuous approach suffers from two main limitations. First, the lamination parameters feasible domain is difficult to describe, especially for coupled problem between membrane and bending behaviors (Bloomfield et al., 2009; Setoodeh et al., 2006; Vannucci, 2013). Second, gradient-based methods are prone to be trapped by local optima. Third, the stacking sequences are not known. Thus, the description of strength at macroscopic level is limited (Catapano and Montemurro, 2014; IJsselmuiden et al., 2008) and most laminate design guidelines have to be discarded (for instance, the thickness are continuous variables and the ply orientations can take any real value in the interval]-90°; 90°]).

The continuous optimization results in an idealized design defined by a stiffness distribution and a thickness distribution over the structure. A subsequent discrete optimization step is necessary to retrieve the laminates (Herencia et al., 2008; IJsselmuiden et al., 2009; Montemurro et al., 2012). The overall efficiency of this bi-level scheme depends on the way the first level idealized optimum is targeted at the second level. Aiming to match the stiffness distribution of the discrete design to the stiffness distribution of the idealized design is very efficient in terms of computational cost since no structural analysis is required. The main drawback of the method, however, is that without a structural analysis, the feasibility of the design is not guaranteed. As an alternative approach to stiffness matching, performance matching is proposed and implemented in (Francois-Xavier Irisarri et al., 2011; Meddaikar et al., 2015). At the second level, an evolutionary algorithm is applied to a multi-point structural approximation built with a modified Shepard's interpolation method in stiffness space. The method allows a broader exploration of the discrete design space than stiffness-matching and returns feasible designs, while the number of required structural analyses is kept very low.

Chapter I of this thesis presents the development of discrete optimization method for straight fiber composite structures. Indeed, discrete optimization algorithms can be used either to directly solve the composite optimization problem or to retrieve the stacking sequences in the framework of a bi-level approach. The work is based on the evolutionary algorithm proposed in (Irisarri, 2010) for constant stiffness optimization method. Specific encoding and genetic operators are developed to achieve variable-stiffness composite design by allowing thickness variations through adding or terminating plies. The solutions are represented as Stacking Sequence Tables and encoded as integer vectors. A list of design guidelines representative of the industrial practice for the design of composite laminates is drawn up. Specific attention is paid to the handling of the design guidelines at the level of the stochastic optimization algorithm perturbation operators. The algorithm is benchmarked on the 18-panel U-grid test problem (Soremekun et al., 2002) and finally applied to the design of a composite satellite antenna mounting bracket[5].

Chapter I aims at improving the efficiency of the optimizer both in terms of parsimony in finding performing solutions and accuracy in finding the optimal solutions. To achieve this goal, algorithms are investigated that simultaneously carry out the optimization in the space of stacking sequences and lamination or other adhoc auxiliary parameters. Statistics are drawn on simple

[5] http://www.mecano-id.fr/en/space/space-products

analytical composite optimization test problems and used to compare algorithms and their settings. The idea of exploiting a probability density estimator in an auxiliary design space, originating from the Double-Distribution Optimization Algorithm (Grosset et al., 2006), is transposed to the evolutionary algorithm devised in Chapter I. The efficiency of the method is shown on several constant stiffness and variable stiffness test problems and the choice of a relevant auxiliary design space is discussed.

Optimal design of a CROR blade

Another way to reach a better environmental performance is to enhance engine efficiency. As higher bypass ratios may lead to higher propulsive efficiencies, the turbofan technologies have been progressively improved during the last decades. However, a growth in bypass ratio implies an increase of the dimension and the weight of the nacelle. In order to overcome such issue, other engine architectures were suggested. Among alternative engines, the Counter-Rotating Open Rotor (CROR), as illustrated in Figure 8, regained interest within the aerospace community thanks to its low drag and weight penalty, its high bypass ratio and propulsive efficiency (Hager and Vrabel, 1988). Compared to modern conventional turbofan engines, the CROR architecture represents a fuel consumption reduced by 25%. However, the CROR is noisier than turbofans at equivalent thrust since its propellers are not ducted in a nacelle. Additionally, the counter-rotating propellers interfere with each other. Indeed, while the first stage may be exposed to pylon wakes depending on the engine installation, the second stage is systematically exposed to front propeller wakes. Thus, many optimization studies are currently being led to reduce the perceived noise on the ground, either by investigating new blade configurations or optimizing the propellers and blade shape.

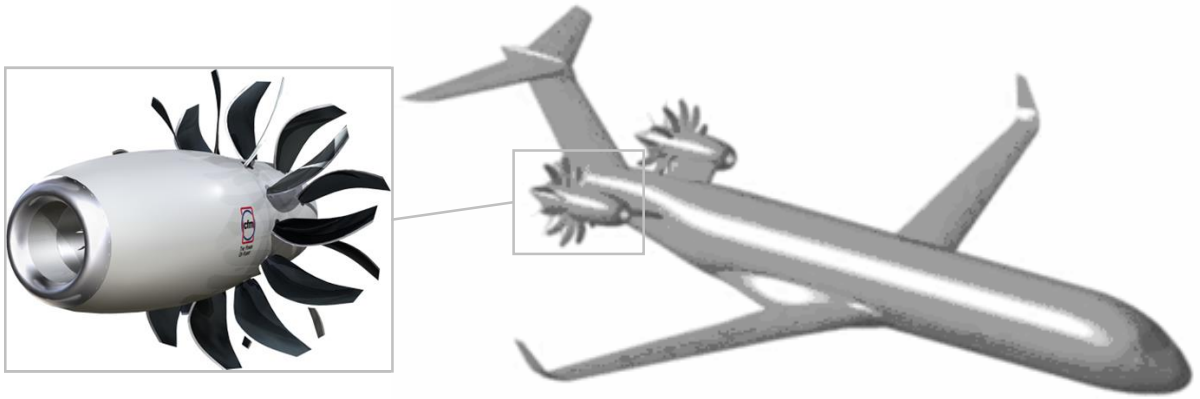

Figure 8. Snecma's CROR (left) and example of CROR integration in a pusher configuration (right) [source: Snecma]

The high bypass ratio of CROR is by definition linked to the size of its propellers, and hence the size of its blades. Considering the high rotational speed necessary to reach the required thrust, metallic blades cannot sustain the centrifugal loading because of their density. Composite blades are currently being developed to overcome this limitation thanks to their higher specific

properties. Furthermore, the use of composites gives an opportunity to tailor the material anisotropy to control the shape of the blade at different flight conditions. New design methods, however, have to be developed to enable using the full potential of the composite structure in the blade design. Indeed, the blades are generally considered as rigid bodies in aerodynamic analyses. The shape of the blade is optimized for given operating conditions in order to maximize their efficiency and minimize the noise emission while reaching a given thrust. The shape of the blade is usually designed to maximize the efficiency of the propeller at cruise flight conditions in order to minimize the fuel consumption. Aerodynamic and aeroacoustic performances at other operating points are assessed based on that shape. Such a design process does not take into account the structure of the blade (Negulescu, 2013) and its radial stiffening under the centrifugal loading and bending / twisting under the aerodynamic loading. Hence, in order to optimize the performances of the blade through its internal composite structure, new design methods are required, able to capture the deformations of the blade in specific flight conditions (i.e. take-off and cruise).

Chapter I presents the development of the "Hot-to-Cold" (H2C) analysis method and its counterpart "Cold-to-Hot" (C2H) analysis. The H2C analysis aims at determining the shape of the unloaded composite blade, starting from its operating shape. The method couples aerodynamic and finite element analyses through a fixed-point method. The blade is supposed to be solicited by centrifugal and aerodynamic loads. While the first ones may be easily computed into CSM, the aerodynamic loads require CFD computation. In order to keep both H2C and C2H processes fast enough, a first strategy consisted in using fast techniques such as lifting line methods, which are widely used for aerodynamic design of CROR blades (Béchet et al., 2011; Saito et al., 1987).

Finally, this chapter discusses the possible leverages on engine performance when tailoring the composite structure of the Onera HTC5 CROR blade shape (Bousquet et al., 1991). A reduced-scale blade designed for wind tunnel testing is considered. The evolutionary algorithm proposed in Chapter I is applied to the maximization of the propulsive efficiency of the CROR at take-off and cruise flight conditions.

CHAPTER I. PARAMETRIC OPTIMIZATION OF BLENDED COMPOSITE STRUCTURES

The work presented in this chapter has been published in a different form in the following references:

- *F.-X. Irisarri, A. Lasseigne, F.-H. Leroy, R. Le Riche, "Optimal design of laminated composite structures with ply drops using stacking sequence tables", Composite Structures, Vol. 107, 559–569, 2014*
- *A. Lasseigne, F.-X. Irisarri, R. Le Riche, "Optimal design of a composite structure relevant to laminate design guidelines", 19th International Conference on Composite Materials, July 28 – August 2, 2013, Montréal, Canada*

I.1 Introduction

Laminated composite materials are widely used for modern aeronautical structures. Over the last decade, the design and manufacturing of large one-shot panels, such as wing-skin panels, have attracted an increasing attention from structural designers. The mass of such panels can be minimized by tailoring the thickness of the panel to the local load distribution. In the case of wing-skin panels, for example, the local loads can vary to a great extend depending on the considered region of the skin, from the wing root to the vertical of the engine nacelle pylon, to the wing tip. Furthermore, strength-critical load introduction zones are generally reinforced with extra material to prevent bearing or tensile failure along fastener rows. Classical engineering practice recommends thick quasi-isotropic laminates in load introduction zones. Minimizing the mass of the panel consists in progressively reducing the thickness away from the load introduction zones while allowing for oriented laminates to obtain locally optimized designs.

Detailed design of large composite structures is usually based on the subdivision of the global problem into local panel design problems. The subdivision results from higher design levels and is not meant to be called into question at lower design levels. For the usual straight-fiber laminates used in aeronautics, thickness variations between panels can only be achieved by adding or terminating plies. Stiffness variations are obtained by modifying the ply orientations and the number of plies. Continuity of the plies has to be preserved to obtain one-shot manufacturable structures and avoid stacking sequence mismatch between adjacent panels. The ply-drops form taper sections between adjacent panels. Ply-drops cause out-of-plane stress concentrations in tapers that can initiate in-plane matrix cracking and delamination.

In their literature survey on tapered composite structures, He *et al.* (He et al., 2000) bring out two major categories of studies. The first category aims at understanding the damage mechanisms at ply-drop locations and studies the propagation of delamination in the structure. The second category aims at identifying and investigating the influent parameters on the strength of the taper section and suggests design guidelines to reduce damage initiation at ply-drops. Since then a third category of related studies has developed that deals with the optimal design of composite structures with ply-drops. Review about the topic can be found in (Ghiasi et al., 2010).

Designing laminated structures with ply-drops is commonly referred to as blending. There are few if any links between laminate blending optimization and the first two categories of studies. In particular, no design guidelines for the taper sections are considered in the optimization. Thus, there is no guarantee for the optimized designs that damages initiated at ply-drops could not propagate and lead to failure under the design loads. The present work intends to bridge this gap and introduces a complete set of relevant design guidelines into the optimization.

Industrial design guidelines for composite structures with ply-drops are summarized in Section I.2. Section I.3 provides background on blending and introduces the concept of stacking sequence tables (SSTs). Next, an evolutionary algorithm (EA) is specialized for SST-blending optimization in Section 0. The results obtained for an analytical benchmark from the literature, consisting of an 18-panel U-grid structure, are compared and discussed in Section I.5. Further testing is depicted in Section I.6 in which a satellite antenna mounting bracket is optimized using finite elements analyses (FEA).

I.2 Design guidelines

Laminate design starts by selecting the set of ply angles relevant to a given application. Due to manufacturing constraints, the allowed ply orientations are reduced to a discrete set of angles such as $\{0°, \pm 15°, \pm 30°, \pm 45°, \pm 60°, \pm 75°, 90°\}$. Once the angles are selected, the total number of plies and proportion of each orientation in the laminate are set and a stacking sequence is chosen. Additionally, when designing structures comprising several zones of different thicknesses, thickness variations are obtained by dropping off plies at specific locations. For both laminate stacking sequence design and ply-drop-off design, numerous guidelines apply, based on return on experience (ROE) of the industry from testing and analysis. A more detailed discussion about design guidelines and their justifications is provided in (MIL-HDBK-17-3F, 2002) and (Bailie et al., 1997).

Six *laminate design guidelines* are considered as a basis for the design of the stacking sequences of most composite structures in aerospace industry.

1. *Symmetry*: whenever possible, stacking sequences should be symmetrical about the mid-plane.
2. *Balance*: whenever possible, stacking sequences should be balanced, with the same number of $+\theta°$ and $-\theta°$ plies ($\theta \neq 0$ and $\theta \neq 90$).
3. *Contiguity*: no more than a given number of plies of the same orientation should be stacked together. The limit is set here to two plies.
4. *Disorientation*: the difference between the orientations of two consecutive plies should not exceed 45°.
5. *Ten percent rule*: a minimum of 10% of plies in each of the $0°$, $\pm 45°$ and $90°$ directions is required. Here to allow for other ply orientations, this rule is transposed in terms of a minimal in-plane stiffness requirement in all directions, as suggested in (Abdalla et al., 2009).
6. *Damage tolerance*: no 0°-ply should be located on the lower and upper surfaces of the laminate.

Symmetry and balance guidelines aim at avoiding respectively shear-extension and membrane-bending coupled behaviors. The other rules are beneficial to the strength of the structure. They aim at avoiding matrix dominated behaviors (10%-rule) and possible strength problem due to unwanted failure modes such as free-edge delamination (disorientation) or propagation of transverse matrix cracking (contiguity). With primary load carrying plies shielded from the exposed surface of the laminates (damage tolerance), the effect on strength of exterior scratches of surface ply delamination is reduced.

The *ply-drop design guidelines* aim first at avoiding delamination at ply-drop location and, secondly, at obtaining ply layouts that can be manufactured with current techniques.

7. *Covering*: covering plies on the lower and upper surfaces of the laminate should not be dropped off.
8. *Maximum taper slope*: the taper angle should not exceed a maximum inclination. Here, the maximum inclination is set to 7°, i.e. the minimal stagger distance (the length of the increment of thickness) is about eight times the thickness of the dropped plies.

9. *Max-stopping*: a maximum number of plies may be stopped at the same increment of thickness. This maximum is set here to two plies.
10. *Internal continuity*: Continuous plies should be kept between consecutive ply-drops. Here are allowed three dropped plies for one continuous ply.
11. *Ply-drop alternation*: as far as possible, ply-drops should be located alternately close and far from the mid-surface of the laminate.
12. *Taper guidelines*: all laminates in the taper section should respect the laminate design guidelines to the maximum possible extend.

The schematic of a 4-ply-drops transition zone is shown in Figure 9. All the above guidelines are local, i.e. they apply to the design of each individual panel of the structure, or each ply-drop. However, the design of a variable-thickness composite structure also has to fulfill two *global requirements*.

13. *Continuity*: the requirement aims at ensuring structural integrity and manufacturability of the structure. All plies from the thinner panel must cover the whole structure. Ply orientation mismatches between adjacent panels are not allowed, i.e. cutting plies between two panels to change their orientation is forbidden.
14. *Δn-rule*: the second requirement specifies a maximum number of ply-drops Δn between adjacent zones. Indeed, constraining the thickness variation between adjacent zones may contribute to smoothing the load distribution over the structure and avoid high stress concentrations at dropped plies, especially interlaminar stresses.

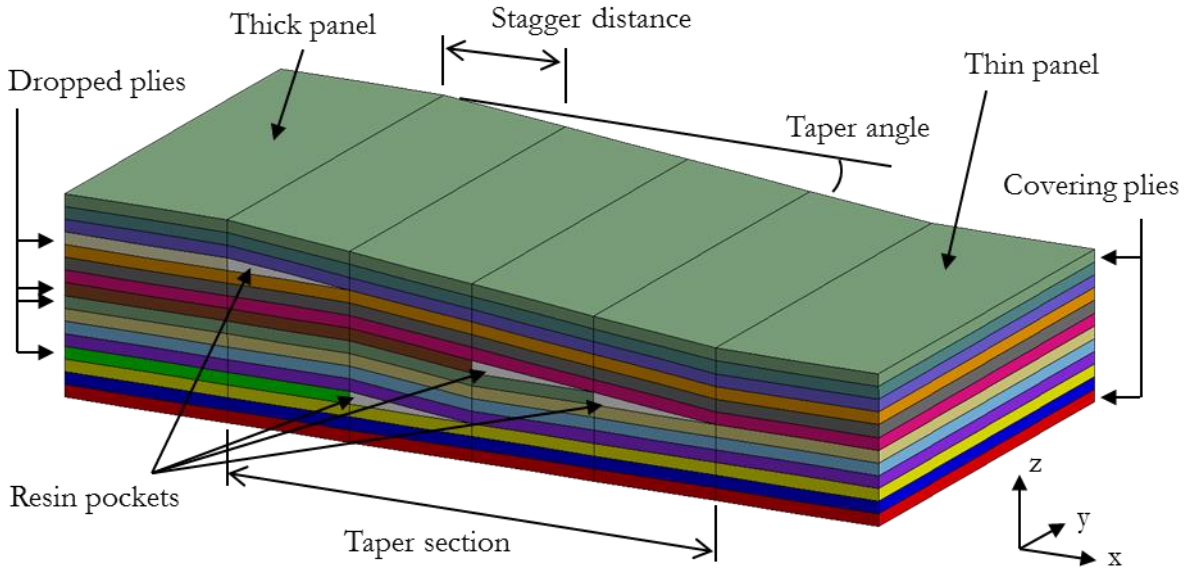

Figure 9. Schematic of a taper section with four internal ply-drops.

I.3 Blending of laminates and stacking sequence tables

I.3.1 Blending definitions

The continuity requirement is commonly referred to as the blending constraint in the composite optimization literature. The term *blending* was first introduced by Kristinsdottir *et al.* in 2001 (Kristinsdottir et al., 2001). In their work, each ply emanates from a key region and may cover any number of adjacent regions. The fiber angle of a ply is held fixed for the entire coverage of the ply. Once a ply is dropped, it is not allowed to be added back in the structure. The authors named this way of consistently dropping plies from the most loaded region the *greater-than-or-equal-to* blending rule. In this approach what is designed is a set of N ply orientations, where N is a fixed maximum number of plies, and a Boolean matrix defining whether or not the ply covers the considered region. Blending is enforced during optimization through a set of inequality constraints, which typically leads to highly constrained problems with many variables. Similarly, Liu and Haftka (Liu and Haftka, 2001) investigated the use of inequality constraints to enforce stacking sequence continuity while minimizing the mass of the structure. Much smaller weight penalty for perfectly blended solutions were obtained by Soremekun *et al.* (Soremekun et al., 2002) using an approach based on sublaminates. Figure 10 illustrates the greater-than-or-equal-to blending rule.

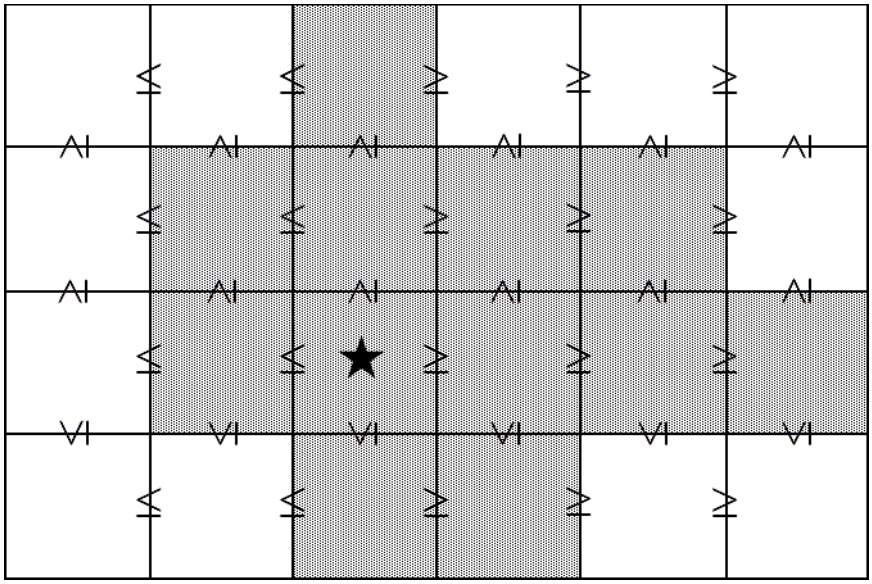

Figure 10. Illustration of the greater-than-or-equal-to blending rule. The key region for the considered ply is indicated by a star. The greater-than-or-equal-to symbols show the direction of the admissible ply-drops. An admissible ply configuration is shown in grey. A key region and the corresponding set of constraints can be defined for each ply in the structure.

The most promising definition up to now originates from (Adams et al., 2004) in which the authors introduce the concept of *guide-based blending*. A guiding stack is defined from which all laminates in the structure are obtained by deleting contiguous series of plies. In case of *inner blending*, the innermost plies are dropped whereas in case of *outer blending*, the outermost ones are

dropped (see Figure 11). The main asset of the method relies on enforcing blending without adding any constraint into the optimization problem while adding only one variable per region of the structure, representing the number of plies dropped from the guide. However, contiguity of the deletions narrows the design space (Seresta et al., 2009; Van Campen et al., 2008). A trade-off still exists between the design freedom and the size of the search space, the last one being likely to increase too high for an efficient search.

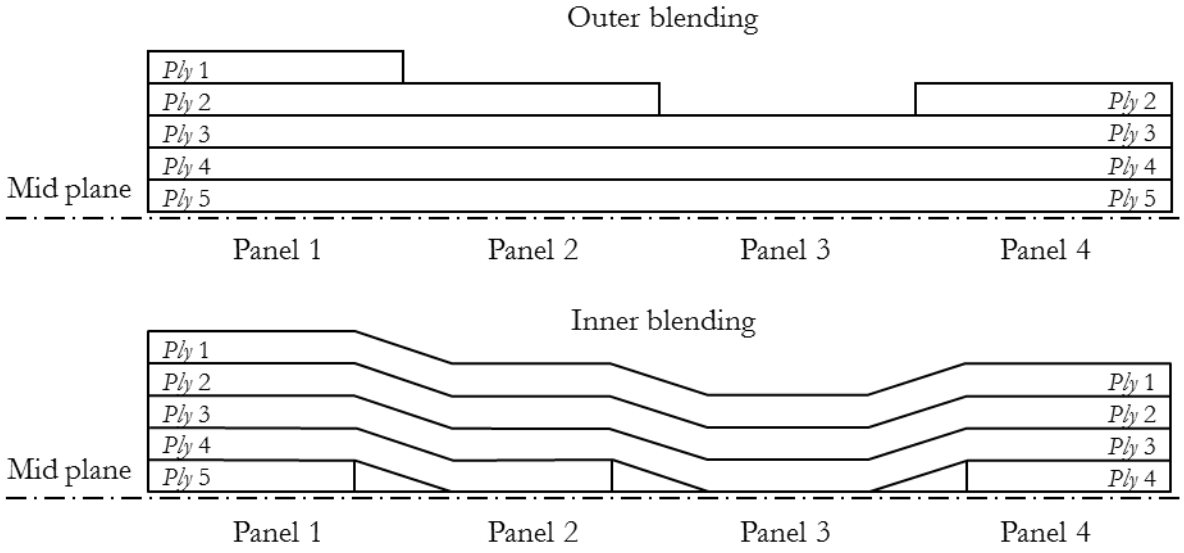

Figure 11. Inner and outer blending for a four-region panel.

Another worth mentioning approach is the *patch concept* suggested by Zehnder and Ermanni (Zehnder and Ermanni, 2006), further used and developed in (Giger et al., 2008) and (Keller, 2010). In this approach, a patch is a layer of arbitrary shape that can be positioned anywhere over the structure. At any point of the structure, the stacking sequence is defined by the order and orientations of the patches. The patch concept hence provides parameters which directly derive from the physical composition of laminated structures and does not narrow the design space. However, the large number of degrees of freedom allowed by the method makes engineering problems difficult to solve. The patch concept is illustrated in Figure 12.

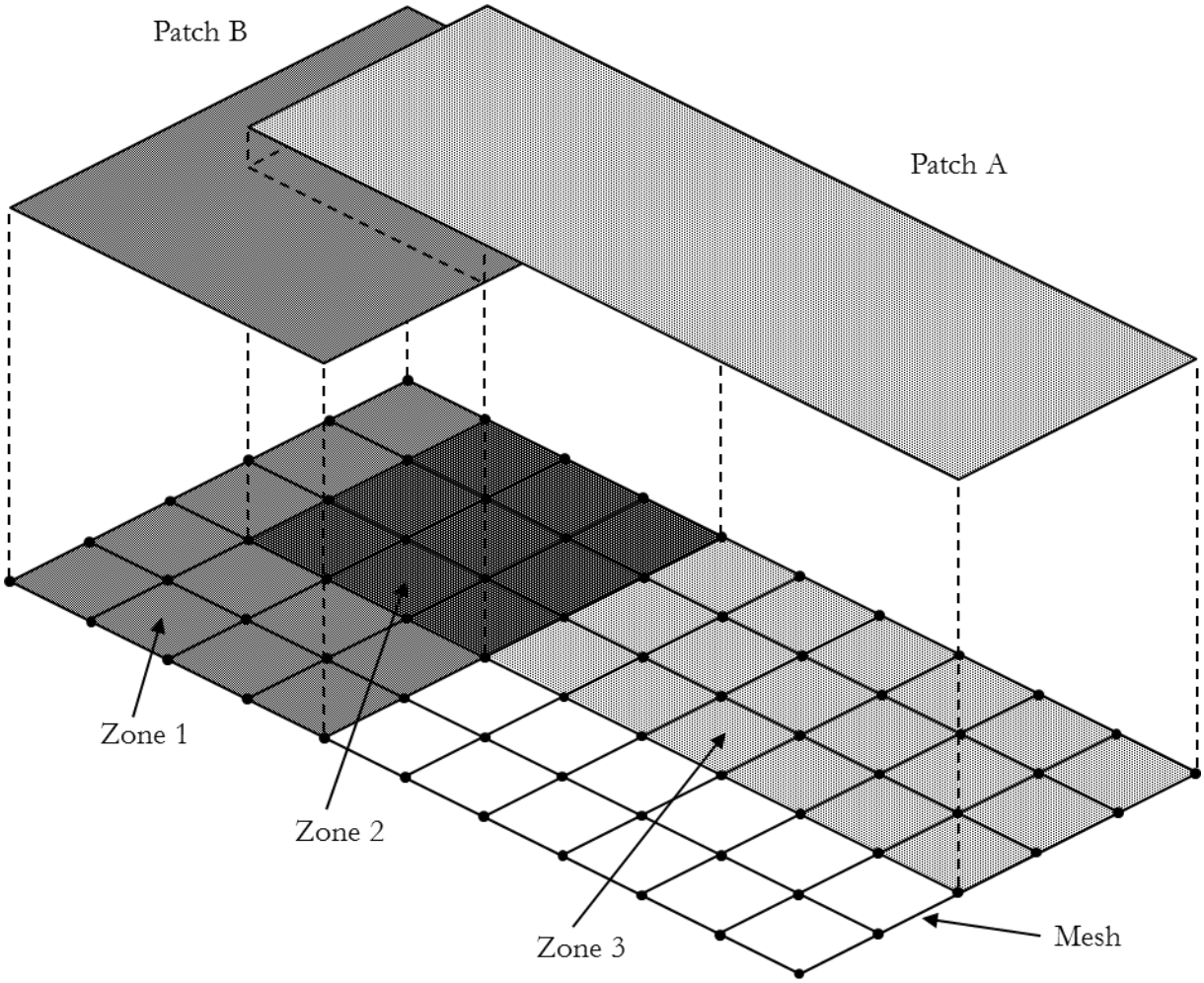

Figure 12. Illustration of the patch concept. A patch covers several adjacent elements of the mesh. The position, size and shape of the patch are defined by the list of connected elements it covers. The patches A and B form three laminate zones. Zone 1 contains one layer form patch B. Zone 2 contains the layer form patch B covered by the layer from patch A and zone 3 contains one layer from patch A.

I.3.2 Stacking sequence tables

In all the studies mentioned above, the set of design guidelines handled is mostly restricted to continuity, symmetry and balance guidelines. This chapter introduces the stacking sequence table (SST) as a convenient tool to handle the full set of guidelines listed in Section I.2. The SST originates in composite panels design and manufacturing practices from aeronautical industry (Carpentier et al., 2006). A SST describes a unique laminate for each number of plies between a lower bound n_{min} and an upper bound n_{max}. A SST ranging from a 12-plies laminate ($n_{min} = 12$) to a 16-plies laminate ($n_{max} = 16$) is illustrated in Figure 14. Plies are added one by one from the thinnest laminate to the thickest one (in the right-hand column of the table). Thus, plies from the thinnest laminate spread over the whole structure and ensure its continuity. For a given structure and a given distribution of numbers of plies over its constitutive regions, the laminate associated to each region can be read in the SST based on its number of plies. The laminates in the transition zone between two regions of different thicknesses are also described in the SST.

The SST describes general thicknesses: once the thickness of a region is fixed, the corresponding laminate is read from the SST which can therefore be read in any order.

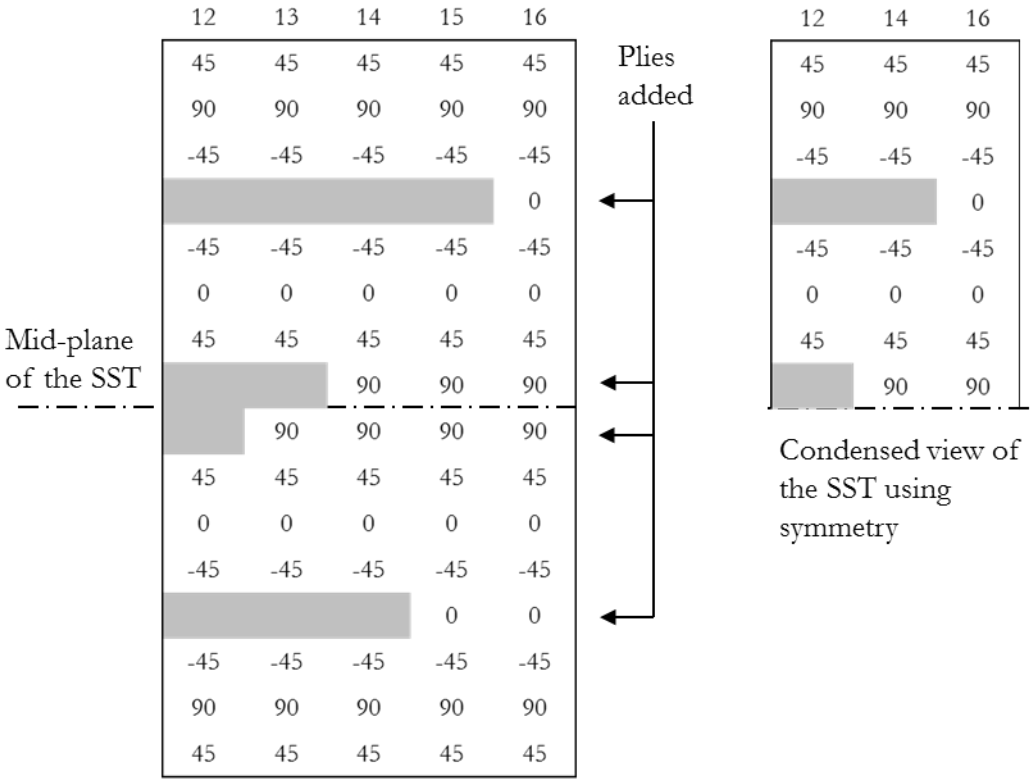

Figure 13. Stacking sequence table with four internal ply drops (n_{min} = 12 and n_{max} = 16). Full view (left) and condensed view using symmetry (right). The numbers of plies of the laminates are indicated over the corresponding columns.

Compared to the guide-based blending method as suggested in (Adams et al., 2004), the SST contains additional information consisting in the order of the ply-drops. Thus, the notion of SST encompasses the classical guide-based blending by providing a more detailed description of the layout of the plies over the structure and affording more freedom to define which plies to drop. Additionally, fulfillment of the ply-drop design guidelines can be assessed based on the SST. The SST in Figure 13 is compatible with the unidirectional taper zone presented in Figure 9. Figure 14 shows a four-region panel with thickness variations compatible with the SST in Figure 13.

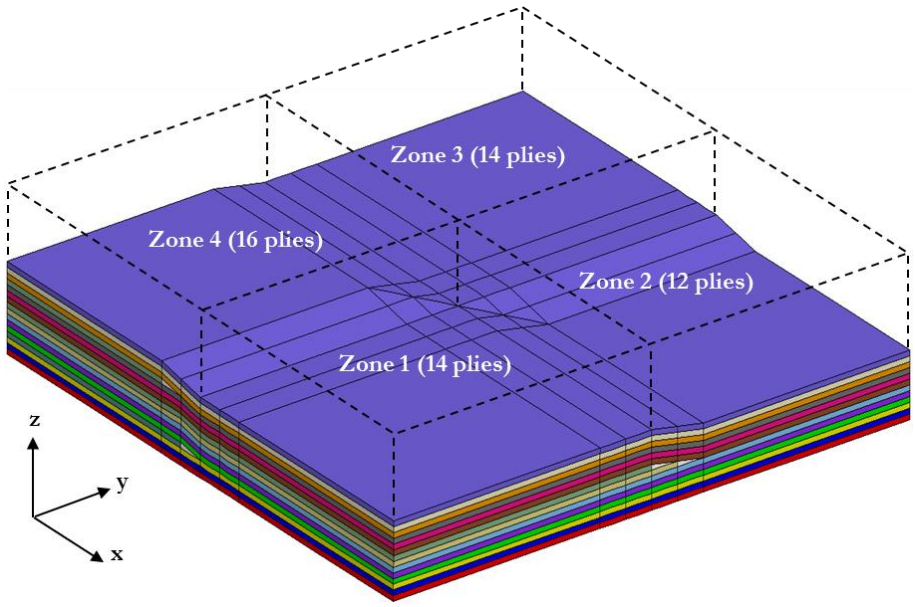

Figure 14. Schematic of a 4-region panel with thickness variations along the x-y directions (n_{min}= 12 and n_{max}= 16).

I.4 Evolutionary optimization of stacking sequence tables

Evolutionary algorithms (EA) are stochastic optimization algorithms that sample the design space by iteratively creating sets (populations) of solution points using stochastic operations. These algorithms are mostly described through the metaphor of evolution in nature to ease their comprehension, so this section will refer to the metaphor while providing its optimization meaning. EA iterations are made of selection and replacement phases, and stochastic variations of the current population of points. The stochastic variations aim at exploring the design space with respect to the current population of points. Mutation and recombination operators are the two main stochastic variations. Mutation locally perturbs solution points while recombination explores subregions of the design space described by two or more solution points. The selection and replacement operators are progressively limiting the population to the best performing ones, where performance is measured by a fitness function f to maximize. The goal of the selection and replacement operators is to focus the search in high performing regions. The encoding of the solution points is specific to the treated application, so it will be detailed in this chapter when required. The variation operators, as well as the initialization, work in the space of the encoding characteristics of the solutions. It may be considered that, through the encoding and variation operators, EAs implicitly define a probability density of sampling a given part of the design space. The selection and replacement phases update this density iteratively. Some versions of EAs, such as CMA-ES in continuous space (Hansen, 2006) or estimation of density algorithms (EDA) (Lozano, 2006), handle the sampling density explicitly in generic optimization cases, but the design of composite structures calls for specific operations. For a particular application, the efficiency of the evolutionary search depends on the coupled choices of encoding and variation operators.

I.4.1 Overview of the algorithm

Reviews about the use of EA for stacking sequence optimization of composite structures can be found in (Ghiasi et al., 2010; Matsuzaki and Todoroki, 2007; Venkataraman and Haftka, 2004). The Pareto multi-objective EA used in the present study is based on previous work by Irisarri *et al.* in (Irisarri, 2010; Irisarri et al., 2009). The algorithm is adapted for *SST-based blending* optimization in the following. The main features of the EA are briefly summarized below, with reference to the flowchart of Figure 15. The specific modules of the algorithm are problem-dependent and are detailed in the following. The generic modules come from (Irisarri, 2010).

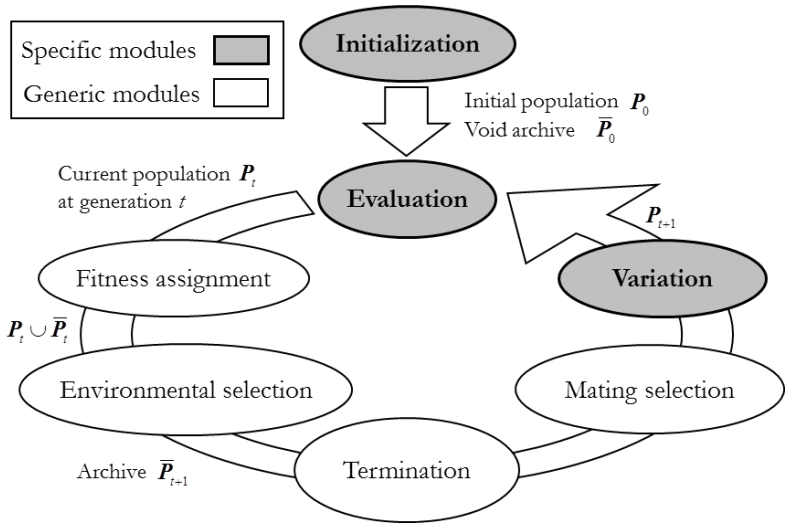

Figure 15. Flow chart of the evolutionary algorithm. Specific modules are problem-dependent. In the present work, specific modules are developed for SST-based blending optimization.

Fitness assignment. The proposed algorithm is a multiobjective optimization algorithm. The Pareto-ranking method (Deb et al., 2002) is used to sort the solutions. Additional density information is incorporated in the fitness function to discriminate between solutions of identical Pareto rank. The density estimation technique used here is an adaptation of the k-th nearest neighbor method, with k equal to the square root of the population size, as it is done in SPEA2 (Zitzler et al., 2001). The Euclidean distance in the objective space is used here.

Environmental selection. The best solutions hitherto encountered are preserved in an archive population and transferred from generation to generation, as proposed in SPEA2. This strategy, called elitism, aims at preventing the loss of portions of the non-dominated front due to random effects.

Mating selection and constraint handling. Binary tournament selection with replacement is performed on the archive to fill the mating pool. The modified binary tournament selection scheme for robust optimization proposed by Deb *et al.* (Deb and Gupta, 2005) is used. The method is simple and can efficiently handle the optimization constraints with no additional parameters required. It mostly relies on checking the feasibility of each solution required to compute the effective function values (i.e. mean of the function values in the vicinity of a

solution), ensuring the feasibility of all solutions in the vicinity of a robust feasible optimal solution.

Variation. Crossover and mutation operators are applied to the mating pool to generate the next population. The operators are detailed in Section I.4.4.

Termination. The algorithm stops once the maximum number of evaluations set by the user is reached.

I.4.2 Encoding

The algorithm is specialized for combined thickness and laminate blending optimization, using an encoding based on stacking sequence tables (SST). Applying the metaphorical terminology of EAs to the laminate blending problem, the *phenotype* is a decoded design which consists of the set or r laminates corresponding to the r regions of the panel which are chosen *a priori*. Additionally, the complete phenotype must also define the ply-drops between zones of different thickness. The phenotype of a blended solution can be conveniently represented by a SST and the distribution of the numbers of plies over the structure. Figure 13 and Figure 14 show a possible phenotype for a 4-region square panel. The thickness of the ply, the number of regions of the panel, their numbering and connectivity are fixed parameters of the problem.

The *genotype* encodes the solution in vectors called *chromosomes*. In this work, a three-chromosome genotype is suggested. Two chromosomes are dedicated to the SST, and one to the thickness distribution over the structure.

I. **Chromosome $\boldsymbol{SST_{lam}}$** represents the stacking sequence of the thickest laminate of the SST. SST_{lam} is an integer vector of length n_{max}.

II. **Chromosome $\boldsymbol{SST_{ins}}$** contains the rank of insertion of the plies from the thinnest laminate to the thickest one. SST_{ins} is an integer vector of length n_{max}. The first ply introduced is given rank 1, the second ply rank 2, etc. Plies from the thinnest laminate are given rank 0. Thus, the vector contains n_{min} zero values.

III. **Chromosome $\boldsymbol{N_{str}}$** represents the distribution of the numbers of plies over the structure. It is an integer vector of length r.

Table 1 shows the genotype of the 4-region square panel illustrated in Figure 13 and Figure 14 for $n_{max} = 16$ and $n_{min} = 12$. The symmetry guideline allows encoding half of the relevant SST only.

Chromosome $\boldsymbol{N_{str}}$	[14 12 14 16]
Chromosome $\boldsymbol{SST_{lam}}$	[45 90 -45 0 -45 0 45 90]
Chromosome $\boldsymbol{SST_{ins}}$	[0 0 0 2 0 0 0 1]

Table 1. Genotype corresponding to the 4-regions panel in Figure 13 ($n_{max} = 16$ and $n_{min} = 12$).

During the optimization process, a solution is generated such that the values contained in N_{str} most likely cover only a part of the interval $[n_{min}, n_{max}]$. For such a solution, part of the

genotype is non-coding. Thus, several genotypes encoding the same phenotype may exist. Non-coding genes are not a common feature for composite structure optimization algorithms. Nevertheless, they have been extensively studied in the field of evolutionary computing, and are not irrelevant to the metaphoric aspect. Wu and Lindsay (Wu and Lindsay, 1995) show that including non-coding segments in a GA can improve its performance and stability. In the present work however, the suggested EA significantly differs from their binary GA so that extension of their conclusions to this work remains questionable. Nonetheless, numerical experiments and the results presented in next section show the efficiency of the method.

I.4.3 Constraint and design guideline handling

Direct and indirect constraints handling

On a conceptual level, Eiben (Eiben, 2001) distinguishes direct from indirect constraints handling strategies. *Indirect constraint handling* consists in circumventing the problem of satisfying the constraints by incorporating them in the fitness function f, generally through penalty functions. This means that the constraints are transformed into optimization objectives, thus creating a new optimization problem such that optimality of the penalized f implies that the constraints are satisfied. With *direct constraint handling*, the EA is modified at the chromosome level to enforce the constraints. Violating the constraints is not reflected in the fitness function. Therefore, the population will not become increasingly feasible as it is expected with indirect constraint handling methods. This means that feasible solutions have to be created and maintained in the population. Specific operators able to preserve feasibility are required. They can be compared to projections into the feasible domain.

In this work, both direct and indirect approaches are used. The constraints handled with an indirect approach are related to the global mechanical performance of the structure (e.g. buckling, cf. Section I.5) and are referred to as *constraints*. The required computational cost to evaluate these constraints is typically the main computational expense. The constraints usually delineate a feasible domain made of one or few clusters. In the following, the modified binary tournament selection scheme suggested by Deb and Gupta (Deb and Gupta, 2005) is used.

The constraints handled with a direct approach are referred to as the *guidelines*. The guidelines are formulated on the stacking sequences of the laminates and, as such, represent negligible computational costs. The guidelines are satisfied in disconnected regions of the decision space organized in a complex pattern. Thus, finding a feasible solution with respect to the guidelines may not help finding another feasible solution. Therefore, penalty methods fail to guide the search toward feasible solutions. All the design guidelines listed in Section I.2 are considered as guidelines in the following, with the notable exception of the ten-percent rule. Indeed the ten-percent rule defines a convex feasible region in the in-plane stiffness space of the laminate (Abdalla et al., 2009)). Hence, the ten-percent rule is handled with an indirect approach. We now explain how a direct approach to design guidelines satisfaction can be implemented in an EA.

Satisfaction of design guidelines by EA – General principle

The evolutionary algorithm is implemented so that, at each of its step, the encoded solutions, i.e. the chromosomes, satisfy the design guidelines. The operations of the EA that affect the design

chromosomes are the initialization of the population and the variation operators. These operators are all devised according to the same general principle. The following steps are repeated, sometimes in a recurrent way, until the initialization or variation is complete.

a) **Selection of a subset of the optimization variables.** For example, it can be a one angle component of SST_{lam}, or more generally it can be any subset of any chromosomes.
b) **Enumeration of guidelines compatible values.** Enumerate and store all possible values of the optimization variables within this subset that satisfy the purpose of the operator and all the guidelines.
c) **Random choice.** Choose at random, with uniform probability, one of the feasible subset of optimization variables values and assign it to the chromosome.

Application specific expertise enters in step a). EA operators are presented in the next section, and the process of choosing the subset of variables within the chromosomes, for each EA operation, is also detailed. A general principle underlying the design of the suggested algorithm is that the stacking sequence table (chromosomes SST_{lam} and SST_{ins}) is handled before the thickness distribution (chromosome N_{str}). In the following, SSTs operations are presented in Section I.4.4 and thickness distribution operations in Section 0.

I.4.4 Evolutionary operations for stacking sequence tables

SST initialization: creation of SB-cycles

Creation of a feasible SST starts from the thinnest laminate. The procedure for the creation of laminates satisfying the laminate design guidelines has already been published in (Ghiasi et al., 2009). The procedure follows the general principle presented in Section I.4.3. It consists of the following steps.

a) **Optimization variables subset order.** Symmetrical laminates are created ply-by-ply from the surface to the mid-plane of the laminate.
b) **Enumeration.** Feasible ply orientations satisfy the following guidelines for the plies chosen so far: symmetry and damage tolerance, contiguity, disorientation, and balance.
c) **Random choice** within the above set of admissible ply orientations.

The balance guideline is handled at the overall level of the laminate, taking into account that any created $\theta°$-ply ($\theta \neq 0$ and $\theta \neq 90$) has to be balanced by a $-\theta°$-ply before the end of the stack.

Once the thinnest laminate is chosen, the SST is built as follows. The method is illustrated in Figure 16.

1) **Variables subset order.** Plies are added one-by-one until the maximum number of plies in the SST n_{max} is reached, thus building the SST column by column from the thinner laminate to the thicker one. First SST_{ins} is considered, then SST_{lam}.
2) **Enumeration.** For each added ply, the set of admissible positions and the set of admissible angles are enumerated. The following guidelines are applied: covering, internal continuity and taper guidelines (i.e. symmetry, balance, contiguity and disorientation, see Section I.2). The covering guideline implies that no ply can be added to the surface of the laminates. The internal continuity guideline requires a continuous ply every three consecutive ply-drops in

the SST. The taper guidelines define the set of admissible angles corresponding to a given position of insertion. If the set is empty, the position is considered unfeasible.

3) **Random choice.** The position of the added ply is drawn in the set of admissible positions. Roulette wheel selection is used to handle the ply-drop alternation guideline. The probability associated to a position is proportional to the distance to the surface of the laminate or to its mid-plane, depending on whether the last position drawn is closer to the mid-plane than to the surface of the laminate or not. The kth ply added is attributed value k in chromosome SST_{ins}. The orientation of the ply is drawn with uniform probability in the set of admissible angles and added to chromosome SST_{lam}.

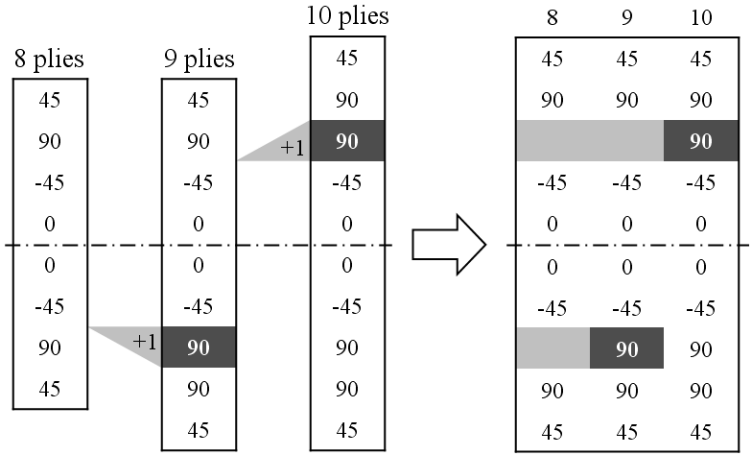

Figure 16. Creation of a SST. Plies are added one by one to create the SST on the right-hand side of the figure. The orientation of the first ply added is chosen in the set $\{\mathbf{0°}, \pm\mathbf{45°}, \mathbf{90°}\}$. $\mathbf{0°}$ and $+\mathbf{45°}$ are forbidden by the disorientation guideline. A $\mathbf{90°}$-ply is drawn in the set of the remaining admissible values. A second $\mathbf{90°}$-ply is then added to recover symmetry.

Eight guidelines are explicitly handled in the process. The remaining guidelines are either satisfied or not relevant at this step. The continuity requirement is satisfied by building the SST. The damage tolerance guideline is enforced for the whole SST through the covering rule. Indeed, the thinnest laminate of the SST satisfies the damage tolerance guideline by construction and the covering rule entails that no plies are added to the surface of the SST. The maximum taper slope rule and the max-stopping one apply to the detailed representation of the solutions rather than the optimization process and are not taken into account here. The Δn-rule applies to chromosome N_{str} and will be handled later with the appropriate operators (see Section 0).

Adding plies one by one in the SST necessarily generates unsymmetrical and/or unbalanced laminates. If a $0°$-ply or a $90°$-ply is added to a symmetrical laminate, the next ply added reestablishes symmetry. If θ is different from 0 and 90, symmetry is restored first, then balance. In the first case, a cycle of length 2 is formed, in the second case, a cycle of length 4. Such cycles are called symmetry and balance cycles, or SB-cycles, and used to modify SSTs as explained in the following.

SST mutation

The mutation operator for SSTs modifies chromosome SST_{lam} or SST_{ins} with equal probability. The mutation operator for SST_{lam} modifies the orientation of a pair of $\pm\theta°$-plies or a couple of plies oriented at $0°$ or $90°$. The new orientation is randomly chosen in a set of feasible orientations depending on the orientations of the neighboring plies in the SST and the contiguity and disorientation guidelines. Figure 17 illustrates an example of mutation of chromosome SST_{lam} and the corresponding variation of the SST.

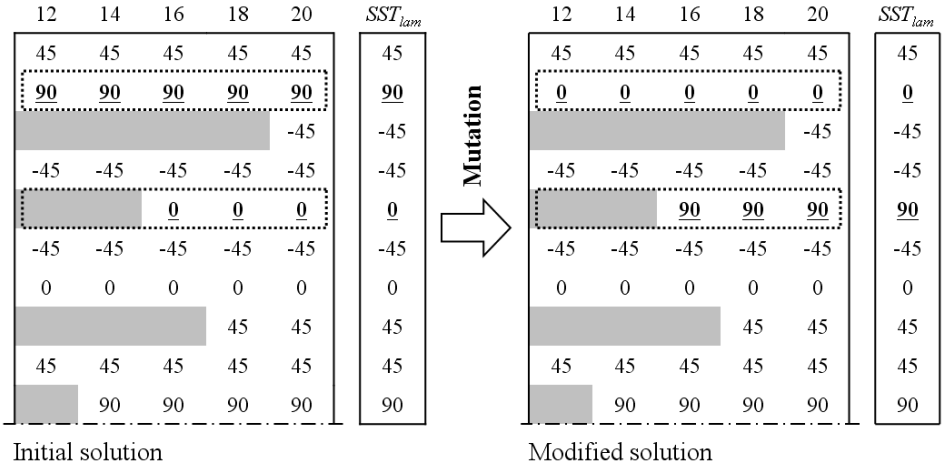

Figure 17. Mutation of chromosome SST_{lam} and corresponding variation of the SST

The mutation operator for chromosome SST_{ins} permutes the order of insertion of two SB-cycles. The permutation is illustrated in Figure 18. In the figure, SB-cycles are identified with Roman numerals. Cycles I and II are permuted to generate a new solution. The corresponding variation of SST_{ins} is shown in the figure. The operator is applied to the same SST example as in Figure 17.

SST recombination

The recombination operator developed in this work consists of a crossover operation followed by a repair operation. The crossover operator exchanges same-length balanced sublaminates between the thinner laminates of the parent solutions. The respective position of the two sublaminates within chromosome SST_{lam} can differ, as shown in Figure 19. Offspring SSTs are scanned from the thinnest laminate to the thickest one for violation of the contiguity and disorientation guidelines. Unfeasible SSTs are cut before their first unfeasible column. The remaining columns are regenerated using the process described in Section I.4.4.

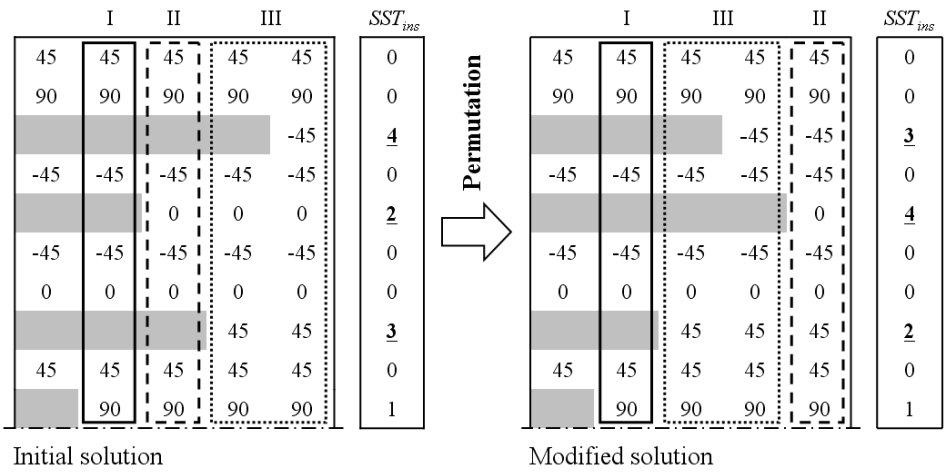

Figure 18. Permutation within chromosome SST_{ins} and corresponding variation of the SST. SB-cycles are numbered with Roman numerals. Cycles I and II are permuted.

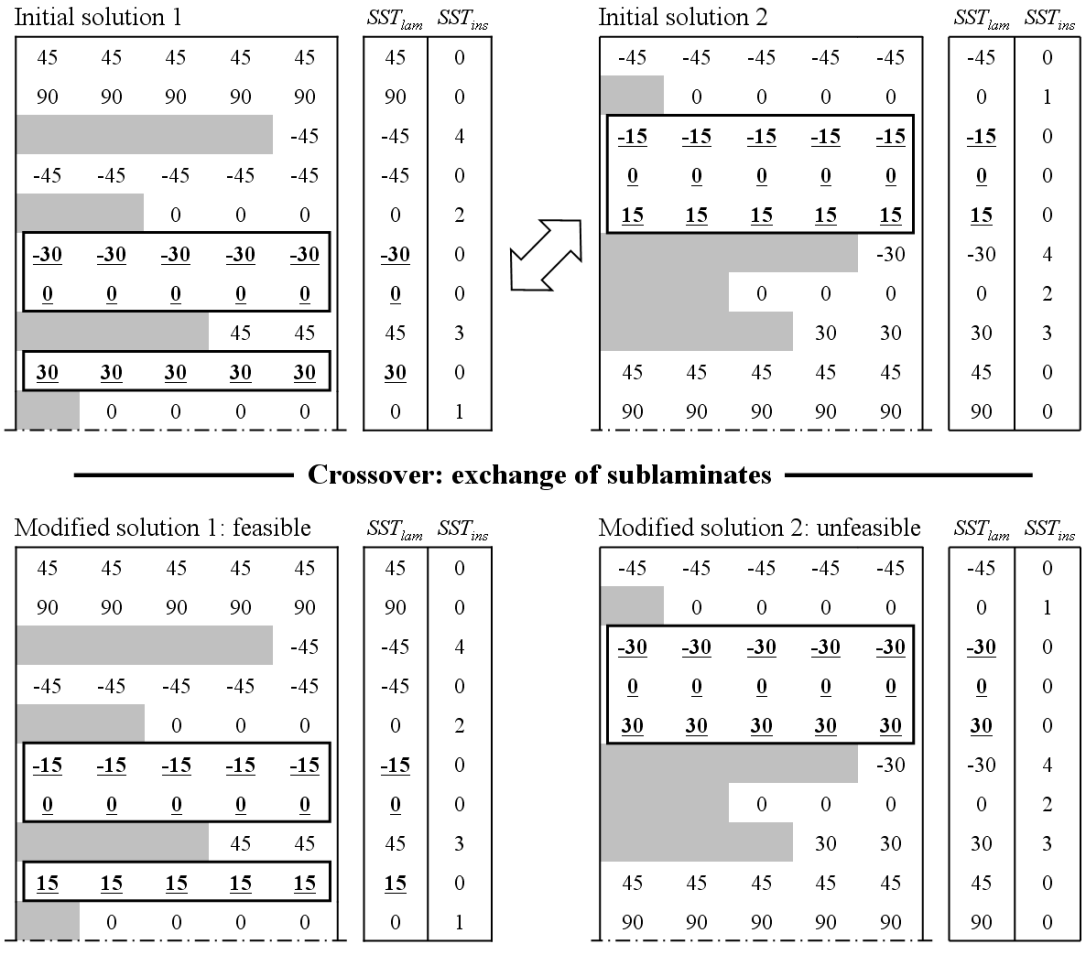

Figure 19. Crossover operator. Same length balanced sublaminates are exchanged between the thinner laminates of the parent solutions. Plies 5 and 6 of modified Solution 2 do not satisfy the disorientation guidelines.

I.4.5 Evolutionary operations for thickness distribution

The only guideline applying to chromosome N_{str} is the Δn-rule which defines a maximum difference Δn between the numbers of plies of contiguous zones. Contiguity between zones is defined by a r-by-r array of connectivity which is a fixed parameter of the problem. Feasible instances of N_{str} are created by random generation of uniform distributions of number of plies over the structure.

The mutation operator modifies the number of plies associated to a region i. The new number of plies in region i is randomly selected in the set of admissible values which are defined by n_{min}, n_{max}, Δn and the number of plies of the regions connected to region i. A 2-points crossover is used to exchange sequences of genes between the two parent chromosomes. A preliminary scan is performed to identify which genes can be exchanged with respect to the Δn-rule. Contiguous sequences formed of these genes are exchanged only.

The suggested encoding and the corresponding operator maintain a complete separation between the thickness distribution and the SST. Nevertheless, the notion of SB-cycles calls for a comment. Allowing the number of plies per panel to take any value in the range $[n_{min}, n_{max}]$ would result in designs composed of unsymmetrical or unbalanced laminates, or both. Forcing the optimizer to drop full SB-cycles restricts the search to designs composed of symmetrical and balanced panels only.

In order to preserve separation between the thickness distribution and the SST, chromosome N_{str} id interpreted and repaired prior to the evaluation of the solution. The chromosome is not altered by this process which does not penalize the overall mass of the population of designs. The method is inspired by the recessive gene-like repair strategy suggested by Todoroki and Haftka (Todoroki and Haftka, 1998). The SST is scanned for symmetrical and balanced laminates resulting in a set of admissible ply numbers. The genes of N_{str} are interpreted to the nearest admissible ply number. In case of violation of the Δn-rule due to the decoding process, the new thickness distribution is repaired by iteratively forcing the number of plies of the thinnest non-feasible region to the upper admissible number of plies until a satisfactory distribution is obtained. The overall process is deterministic so that a chromosome can only be interpreted in a single way.

I.5 Application to the 18-panel benchmark problem

The test problem consists of 18 panels in horseshoe configuration ($r = 18$), as shown in Figure 20. The problem was raised by Soremekun *et al.* (Soremekun et al., 2002) and subsequently examined in (Adams et al., 2004; IJsselmuiden et al., 2009; Irisarri et al., 2014; Seresta et al., 2009; Yang et al., 2016). The dimensions of the panels and the panel loadings are given in the figure. The connectivity between panels is defined by a r-by-r binary array. Row and column numbers correspond to the panel numbers in the structure. In the present work, two panels are considered connected if they share a common edge or vertex. Nevertheless, panels 6, 10 and 13 in Figure 20 are considered disconnected. The array of connectivity χ of the panels is given below ($r = 18$):

$$\chi = \begin{vmatrix} 1 & 1 & 0 & 0 & 0 & 0 & 0 & 0 & 1 & 1 & 0 & 0 & 0 & 0 & 0 & 0 & 0 & 0 \\ 1 & 1 & 1 & 0 & 0 & 1 & 0 & 0 & 1 & 1 & 0 & 0 & 0 & 0 & 0 & 0 & 0 & 0 \\ 0 & 1 & 1 & 1 & 0 & 1 & 1 & 0 & 0 & 0 & 0 & 0 & 0 & 0 & 0 & 0 & 0 & 0 \\ 0 & 0 & 1 & 1 & 1 & 1 & 1 & 1 & 0 & 0 & 0 & 0 & 0 & 0 & 0 & 0 & 0 & 0 \\ 0 & 0 & 0 & 1 & 1 & 0 & 1 & 1 & 0 & 0 & 0 & 0 & 0 & 0 & 0 & 0 & 0 & 0 \\ 0 & 1 & 1 & 1 & 0 & 1 & 1 & 0 & 0 & 0 & 0 & 0 & 0 & 0 & 0 & 0 & 0 & 0 \\ 0 & 0 & 1 & 1 & 1 & 1 & 1 & 1 & 0 & 0 & 0 & 0 & 0 & 0 & 0 & 0 & 0 & 0 \\ 0 & 0 & 0 & 1 & 1 & 0 & 1 & 1 & 0 & 0 & 0 & 0 & 0 & 0 & 0 & 0 & 0 & 0 \\ 1 & 1 & 0 & 0 & 0 & 0 & 0 & 0 & 1 & 1 & 1 & 1 & 0 & 0 & 0 & 0 & 0 & 0 \\ 1 & 1 & 0 & 0 & 0 & 0 & 0 & 0 & 1 & 1 & 1 & 1 & 0 & 0 & 0 & 0 & 0 & 0 \\ 0 & 0 & 0 & 0 & 0 & 0 & 0 & 0 & 1 & 1 & 1 & 1 & 0 & 0 & 0 & 0 & 0 & 0 \\ 0 & 0 & 0 & 0 & 0 & 0 & 0 & 0 & 1 & 1 & 1 & 1 & 1 & 0 & 0 & 1 & 0 & 0 \\ 0 & 0 & 0 & 0 & 0 & 0 & 0 & 0 & 0 & 0 & 0 & 1 & 1 & 1 & 0 & 1 & 1 & 0 \\ 0 & 0 & 0 & 0 & 0 & 0 & 0 & 0 & 0 & 0 & 0 & 0 & 1 & 1 & 1 & 1 & 1 & 1 \\ 0 & 0 & 0 & 0 & 0 & 0 & 0 & 0 & 0 & 0 & 0 & 0 & 0 & 1 & 1 & 0 & 1 & 1 \\ 0 & 0 & 0 & 0 & 0 & 0 & 0 & 0 & 0 & 0 & 0 & 0 & 1 & 1 & 1 & 0 & 1 & 1 & 0 \\ 0 & 0 & 0 & 0 & 0 & 0 & 0 & 0 & 0 & 0 & 0 & 0 & 0 & 1 & 1 & 1 & 1 & 1 & 1 \\ 0 & 0 & 0 & 0 & 0 & 0 & 0 & 0 & 0 & 0 & 0 & 0 & 0 & 1 & 1 & 0 & 1 & 1 \end{vmatrix} \quad \text{I-1}$$

The loads are assumed to be fixed. All panels are assumed to be simply supported on their four edges. As in (Soremekun et al., 2002), n_{min} is set to 14 and n_{max} is set to 48. A graphite/epoxy IM7/8552 material is used with: $E_1 = 141\ GPa$, $E_2 = 9.03\ GPa$, $G_{12} = 4.27\ GPa$ and $\nu_1 = 0.32$. Ply thickness is 0.191 mm. Ply orientations are restricted to the set $\{0°, \pm 15°, \pm 30°, \pm 45°, \pm 60°, \pm 75°, 90°\}$. The objective is to find a fully blended design that minimizes the mass of the structure without individual panel failure under buckling. The minimal buckling factor over the individual panels is called *Reserve factor* and noted RF in the following. Buckling analysis relies on the computation of the buckling factor $\Lambda_{(l_a,l_b)}$ for each buckling mode, defined by the number of half-waves (l_a, l_b) in the longitudinal (x) and transverse (y) directions, is given by:

$$\Lambda_{(l_a,l_b)} = \frac{\pi^2[D_{11}(l_a/a)^4 + 2(D_{12} + 2D_{66})(l_a/a)^2(l_b/b)^2 + D_{22}(l_b/b)^4]}{(l_a/a)^2 N_x + (l_b/b)^2 N_y} \quad \text{I-2}$$

Where N_x and N_y are the stress resultants in the longitudinal and transverse directions respectively. Parameters a and b are the corresponding dimensions of the panel. Parameters l_a

and l_b are the number of half wave-lengths along the x and y directions respectively. D_{11}, D_{12}, D_{22} and D_{66} are bending stiffness terms of the laminate. The critical buckling mode is the mode of minimal buckling factor.

In the following, the problem is first solved for symmetrical and balanced laminates, then with all laminate design guidelines enforced. In each case, the problem is solved first with a single objective (minimize the total mass of the structure), then with two objectives (minimize the total mass of the structure and maximize the reserve factor RF. For both exercises, the constraint that no individual panel fails under buckling ($RF > 1$) is enforced. Ply-drop design guidelines and global design guidelines (cf. Section I.2) are enforced. The parameter settings of the EA are given in Table 2. The crossover operator described in Section I.4.4 may result in significantly altered solutions while mutation generates only small variations of the solutions. Thus, the proposed settings favor mutation. The algorithm is able to solve both single objective optimization problems and multiobjective problems. Indeed, the notion of Pareto dominance with a single objective corresponds to the usual ordering of real numbers. However, the role of the archive population is modified. In the case of single objective optimization, the archive population enforces elitism only. In the case of multiobjective evaluation, the archive contains the non-dominated solutions (elitism), but also controls the regularity of the distribution of the points along the front and maximizes the spread of the front. The size of the archive is a trade-off between the quality of the sampling of the front and the initial convergence speed of the algorithm (Irisarri, 2010). The termination criterion corresponds to a maximum number of generations. The algorithm is implemented in MATLAB. With the proposed settings, a single objective optimization run lasts about 5 minutes while a bi-objective optimization run lasts about 10 minutes.

Parameter	**1 objective**	**2 objectives**
Current population size	30	30
Archive population size	1	60
Probability of crossover (per solution)	0.3	0.3
Probability of mutation (per solution)	0.9	0.9
Number of generations	1000	2000

Table 2. Parameter setting of the EA.

It should be pointed out that, although load redistribution is not taken into account here, the suggested method presents no intrinsic limitations in that regard. FE modeling is required to assess load redistributions in complex structures, which raises the problem of the computation costs. A two-step design method, as in (IJsselmuiden et al., 2009), or a response surface method, as in (Francois-Xavier Irisarri et al., 2011), may be needed to circumvent the difficulty. Nevertheless, direct use of a FE model within the evolutionary optimization is possible for the optimal design of small structures involving a reduced number of design variables. Such an example is provided in Section I.6.

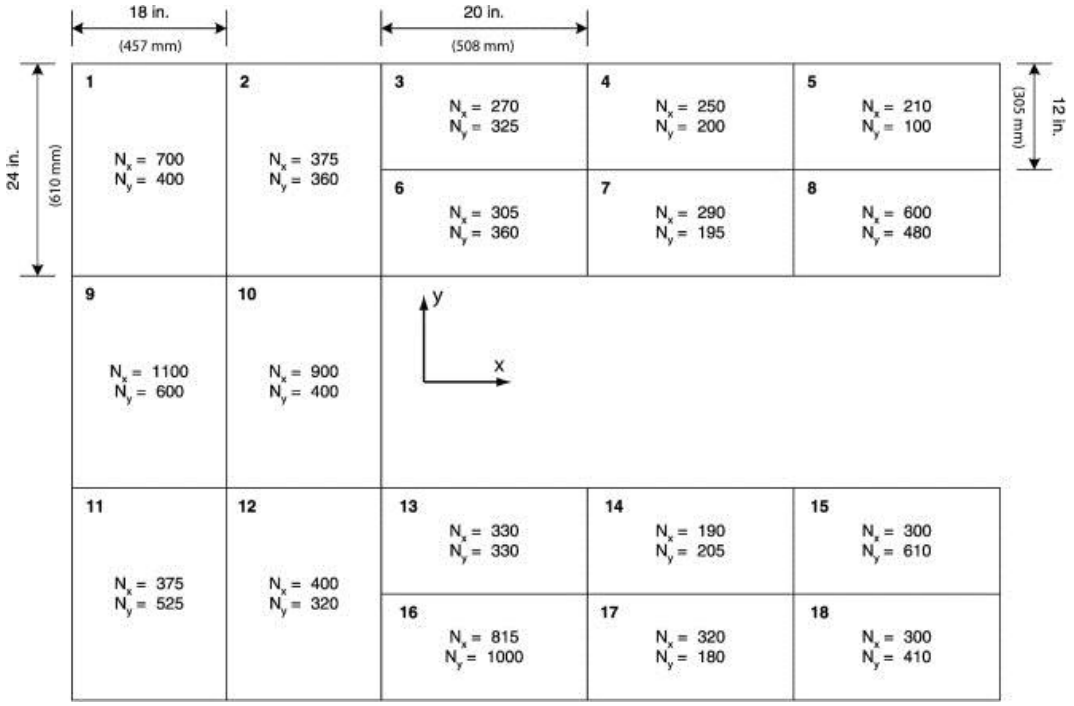

Figure 20. 18-panel U-grid test problem (Soremekun et al., 2002), all loads in lbf/in (×175.1 for N/m)

I.5.1 Symmetrical and balanced laminates

In this section, with respect to the listing of design rules proposed in Section I.2, two laminate design guidelines – *symmetry* (1.) and *balance* (2.) – four ply-drop design guidelines – *covering* (7.), *internal continuity* (10.), *ply-drop alternation* (11.) and *taper guidelines* (12.) – are enforced as well as one global requirement, *continuity* (13.) that is directly enforced through the encoding of the solutions. The *maximum taper slope* (8.) and the *max-stopping* (9.) guidelines are discarded since they are related to the detailed modeling of the geometry of the thickness transition zone, which is irrelevant with respect to the present test-case. The *∠n-rule* (14.) is discarded in order to allow for direct comparison of the present results with published ones. Note that *symmetry* and *balance* and the *continuity* global requirement (i.e. blending) only are considered in published works about the 18-panel U-grid test problem by other authors (Adams et al., 2004; IJsselmuiden et al., 2009; Seresta et al., 2009; Soremekun et al., 2002).

Figure 21 presents a synthesis of the results of 50 optimization runs of single-objective mass minimization. Figure 21.a shows the evolution of the median performance of the best solution found as a function of the number of evaluations of the mechanical model. The normalized performance on the y-axis corresponds to the mass of the lightest published blended symmetrical and balanced solution given by (Yang et al., 2016), 26.82 kg, divided by the mass of the considered design. Note that infeasible solutions, i.e. solutions with $RF \leq 1$, have been attributed null performance in the plot. Thus, the offset on the x-axis before solutions with performance ranging from 0.65 to 0.85 are found corresponds to the number of evaluations required to find a first feasible design. Since all initial populations are random, it took less than 500 evaluations to find a first feasible design in 50% of the runs, an up to 4,500 evaluations in the worst case. After

having found a feasible design, the curve exhibits a first phase of quick convergence towards lighter solutions before a phase of progressive stabilization (after about 10,000 evaluations).

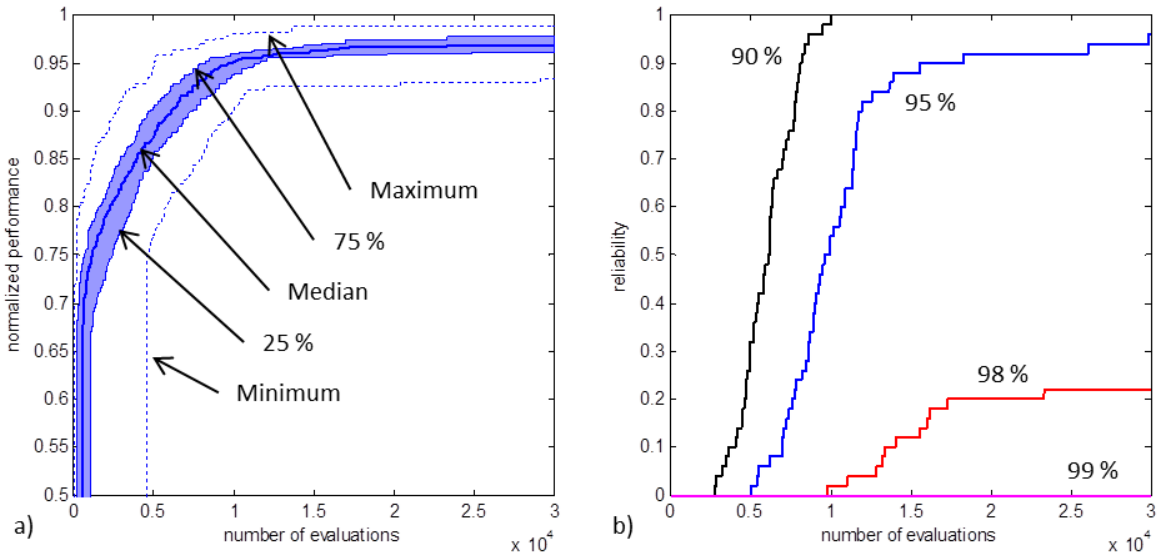

Figure 21. Results obtained after 50 repeated optimizations in the case of symmetrical and balanced laminates. a) Curves of the median performance, 25th and 75th percentiles and extreme values. b) Curves of reliability for different levels of performances.

Figure 21.b shows the curves of reliability of the optimization over the 50 runs for different levels of performances. Reliability is plotted here as function of the number of evaluations. For instance, the 90%-reliability corresponds to the percentage of optimization runs having reached 90% of the best known performance (i.e. a normalized performance of 0.9) after a given number of evaluations. It can be seen in the figure that less than 10,000 evaluations are enough to reach 90% of the best known performance in all runs. For the same calculation cost, 54% of the runs have reached 0.95 of normalized performance. The 95%-reliability curve increases quickly up to about 90% of reliability after 15,000 evaluations before stabilizing. Accurate convergence towards the best solutions is much more difficult, which is typical of EA. The 98%-reliability reaches 20% after approximately 17,500 evaluations and then shows only little improvement. However, in the present case, this lack of accuracy could also be related to the fact that ply-drop design guidelines are enforced in the present work, which was not the case in the work of (Yang et al., 2016). Especially, the surface plies are never dropped in the present work although it is dropped in the reference design, what could have a significant influence on the panel buckling. Thus, there is no evidence that the mass of the reference design can actually be reached while satisfying the additional guidelines handled here. The genotype of the best solution found – Solution 1 – is detailed in Table 3. The performances of the solution are detailed and compared to the reference solution in Table 4. It is worth noticing that although the total numbers of plies are very similar, most of the panels are of different thicknesses.

Chromosome N_{str}	[34 30 22 18 18 22 18 26 40 36 30 30 22 18 26 31 18 22]
Chromosome SST_{lam}	[60 0 30 45 60 45 60 -30 60 -45 -45 -60 -45 0 -60 30 60 -60 -60 -30 45 -60 0 0]
Chromosome SST_{ins}	[0 10 6 4 0 7 1 5 0 3 12 0 8 11 0 15 16 17 0 14 13 2 0 9]

Table 3. Genotype of the lightest symmetrical and balanced solution found (Solution 1).

Panel	**Reference solution** (Yang et al., 2016)			**Solution 1**		
	Number of plies	**Mass [kg]**	**RF [-]**	**Number of plies**	**Mass [kg]**	**RF [-]**
1	33	2.76	1.019	34 (+1)	2.85	1.057
2	29	2.43	1.106	30 (-1)	2.51	1.170
3	23	1.07	1.331	22 (-1)	1.02	1.250
4	19	0.88	1.109	18 (+1)	0.84	1.036
5	16	0.74	1.102	18 (+1)	0.84	1.711
6	23	1.07	1.196	22 (-1)	1.02	1.123
7	19	0.88	1.074	18 (-1)	0.84	1.003
8	25	1.16	1.032	26 (+1)	1.21	1.135
9	39	3.27	1.092	40 (+1)	3.35	1.114
10	35	2.93	1.000	36 (+1)	3.02	1.032
11	30	2.51	1.055	30 (0)	2.51	1.008
12	29	2.43	1.101	30 (-1)	2.51	1.165
13	23	1.07	1.252	22 (-1)	1.02	1.176
14	18	0.84	1.003	18 (0)	0.84	1.099
15	25	1.16	1.000	26 (+1)	1.21	1.100
16	31	1.44	1.035	31 (0)	1.44	1.034
17	19	0.88	1.089	18 (0)	0.84	1.018
18	23	1.07	1.085	22 (+1)	1.02	1.019
Total	459	28.62	-	461	28.90	-
Minimum	-	-	1.000	-	-	1.003

Table 4. Result comparison for symmetrical and balanced laminates. Difference of number of plies per panels is labeled between brackets.

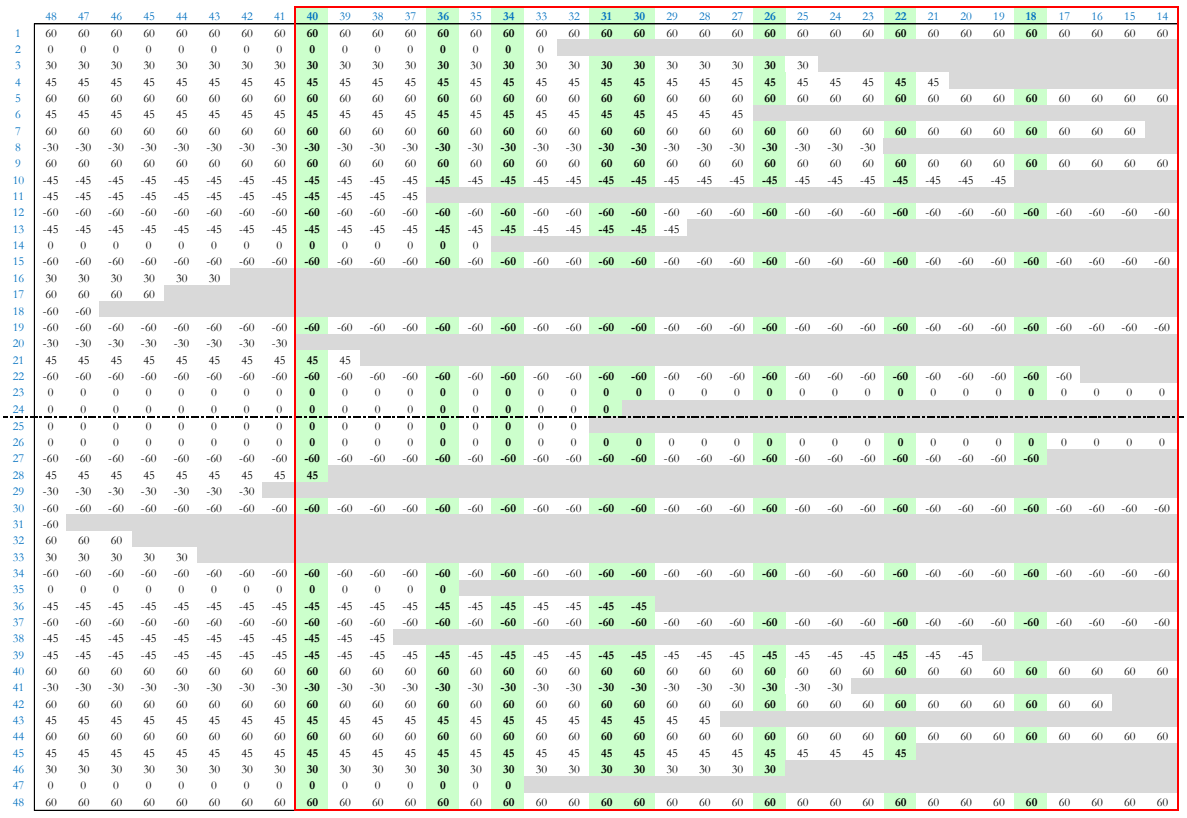

	48	47	46	45	44	43	42	41	40	39	38	37	36	35	34	33	32	31	30	29	28	27	26	25	24	23	22	21	20	19	18	17	16	15	14
1	60	60	60	60	60	60	60	60	**60**	60	60	60	**60**	60	**60**	60	60	**60**	**60**	60	60	60	**60**	60	60	60	**60**	60	60	60	**60**	60	60	60	60
2	0	0	0	0	0	0	0	0	**0**	0	0	0	**0**	0	**0**	0																			
3	30	30	30	30	30	30	30	30	**30**	30	30	30	**30**	30	**30**	30	30	**30**	**30**	30	30	30	**30**	30											
4	45	45	45	45	45	45	45	45	**45**	45	45	45	**45**	45	**45**	45	45	**45**	**45**	45	45	45	**45**	45	45	45	**45**	45							
5	60	60	60	60	60	60	60	60	**60**	60	60	60	**60**	60	**60**	60	60	**60**	**60**	60	60	60	**60**	60	60	60	**60**	60	60	60	**60**	60	60	60	60
6	45	45	45	45	45	45	45	45	**45**	45	45	45	**45**	45	**45**	45	45	**45**	**45**	45	45	45													
7	60	60	60	60	60	60	60	60	**60**	60	60	60	**60**	60	**60**	60	60	**60**	**60**	60	60	60	**60**	60	60	60	**60**	60	60	60	**60**	60	60	60	
8	-30	-30	-30	-30	-30	-30	-30	-30	**-30**	-30	-30	-30	**-30**	-30	**-30**	-30	-30	**-30**	**-30**	-30	-30	-30	**-30**	-30	-30	-30									
9	60	60	60	60	60	60	60	60	**60**	60	60	60	**60**	60	**60**	60	60	**60**	**60**	60	60	60	**60**	60	60	60	**60**	60	60	60	**60**	60	60	60	60
10	-45	-45	-45	-45	-45	-45	-45	-45	**-45**	-45	-45	-45	**-45**	-45	**-45**	-45	-45	**-45**	**-45**	-45	-45	-45	**-45**	-45	-45	-45	**-45**	-45	-45	-45					
11	-45	-45	-45	-45	-45	-45	-45	-45	**-45**	-45	-45	-45																							
12	-60	-60	-60	-60	-60	-60	-60	-60	**-60**	-60	-60	-60	**-60**	-60	**-60**	-60	-60	**-60**	**-60**	-60	-60	-60	**-60**	-60	-60	-60	**-60**	-60	-60	-60	**-60**	-60	-60	-60	-60
13	-45	-45	-45	-45	-45	-45	-45	-45	**-45**	-45	-45	-45	**-45**	-45	**-45**	-45	-45	**-45**	**-45**	-45															
14	0	0	0	0	0	0	0	0	**0**	0	0	0	**0**	0																					
15	-60	-60	-60	-60	-60	-60	-60	-60	**-60**	-60	-60	-60	**-60**	-60	**-60**	-60	-60	**-60**	**-60**	-60	-60	-60	**-60**	-60	-60	-60	**-60**	-60	-60	-60	**-60**	-60	-60	-60	-60
16	30	30	30	30	30	30																													
17	60	60	60	60																															
18	-60	-60																																	
19	-60	-60	-60	-60	-60	-60	-60	-60	**-60**	-60	-60	-60	**-60**	-60	**-60**	-60	-60	**-60**	**-60**	-60	-60	-60	**-60**	-60	-60	-60	**-60**	-60	-60	-60	**-60**	-60	-60	-60	-60
20	-30	-30	-30	-30	-30	-30	-30	-30																											
21	45	45	45	45	45	45	45	45	**45**	45																									
22	-60	-60	-60	-60	-60	-60	-60	-60	**-60**	-60	-60	-60	**-60**	-60	**-60**	-60	-60	**-60**	**-60**	-60	-60	-60	**-60**	-60	-60	-60	**-60**	-60	-60	-60	**-60**	-60			
23	0	0	0	0	0	0	0	0	**0**	0	0	0	**0**	0	**0**	0	0	**0**	**0**	0	0	0	**0**	0	0	0	**0**	0	0	0	**0**	0	0	0	0
24	0	0	0	0	0	0	0	0	**0**	0	0	0	**0**	0	**0**	0	0	**0**																	
25	0	0	0	0	0	0	0	0	**0**	0	0	0	**0**	0	**0**	0	0																		
26	0	0	0	0	0	0	0	0	**0**	0	0	0	**0**	0	**0**	0	0	**0**	**0**	0	0	0	**0**	0	0	0	**0**	0	0	0	**0**	0	0	0	0
27	-60	-60	-60	-60	-60	-60	-60	-60	**-60**	-60	-60	-60	**-60**	-60	**-60**	-60	-60	**-60**	**-60**	-60	-60	-60	**-60**	-60	-60	-60	**-60**	-60	-60	-60	**-60**				
28	45	45	45	45	45	45	45	45	**45**																										
29	-30	-30	-30	-30	-30	-30	-30																												
30	-60	-60	-60	-60	-60	-60	-60	-60	**-60**	-60	-60	-60	**-60**	-60	**-60**	-60	-60	**-60**	**-60**	-60	-60	-60	**-60**	-60	-60	-60	**-60**	-60	-60	-60	**-60**	-60	-60	-60	-60
31	-60																																		
32	60	60	60																																
33	30	30	30	30	30																														
34	-60	-60	-60	-60	-60	-60	-60	-60	**-60**	-60	-60	-60	**-60**	-60	**-60**	-60	-60	**-60**	**-60**	-60	-60	-60	**-60**	-60	-60	-60	**-60**	-60	-60	-60	**-60**	-60	-60	-60	-60
35	0	0	0	0	0	0	0	0	**0**	0	0	0	**0**																						
36	-45	-45	-45	-45	-45	-45	-45	-45	**-45**	-45	-45	-45	**-45**	-45	**-45**	-45	-45	**-45**	**-45**																
37	-60	-60	-60	-60	-60	-60	-60	-60	**-60**	-60	-60	-60	**-60**	-60	**-60**	-60	-60	**-60**	**-60**	-60	-60	-60	**-60**	-60	-60	-60	**-60**	-60	-60	-60	**-60**	-60	-60	-60	-60
38	-45	-45	-45	-45	-45	-45	-45	-45	**-45**	-45	-45																								
39	-45	-45	-45	-45	-45	-45	-45	-45	**-45**	-45	-45	-45	**-45**	-45	**-45**	-45	-45	**-45**	**-45**	-45	-45	-45	**-45**	-45	-45	-45	**-45**	-45	-45						
40	60	60	60	60	60	60	60	60	**60**	60	60	60	**60**	60	**60**	60	60	**60**	**60**	60	60	60	**60**	60	60	60	**60**	60	60	60	**60**	60	60	60	60
41	-30	-30	-30	-30	-30	-30	-30	-30	**-30**	-30	-30	-30	**-30**	-30	**-30**	-30	-30	**-30**	**-30**	-30	-30	-30	**-30**	-30	-30										
42	60	60	60	60	60	60	60	60	**60**	60	60	60	**60**	60	**60**	60	60	**60**	**60**	60	60	60	**60**	60	60	60	**60**	60	60	60	**60**	60	60		
43	45	45	45	45	45	45	45	45	**45**	45	45	45	**45**	45	**45**	45	45	**45**	**45**	45	45														
44	60	60	60	60	60	60	60	60	**60**	60	60	60	**60**	60	**60**	60	60	**60**	**60**	60	60	60	**60**	60	60	60	**60**	60	60	60	**60**	60	60	60	60
45	45	45	45	45	45	45	45	45	**45**	45	45	45	**45**	45	**45**	45	45	**45**	**45**	45	45	45	**45**	45	45	45	**45**								
46	30	30	30	30	30	30	30	30	**30**	30	30	30	**30**	30	**30**	30	30	**30**	**30**	30	30	30	**30**												
47	0	0	0	0	0	0	0	0	**0**	0	0	0	**0**	0	**0**																				
48	60	60	60	60	60	60	60	60	**60**	60	60	60	**60**	60	**60**	60	60	**60**	**60**	60	60	60	**60**	60	60	60	**60**	60	60	60	**60**	60	60	60	60

Figure 22. Decoded SST for Solution 1. The active part of the table is bordered in red. The laminates of the panels of the structure are emphasized in bold type in light green columns.

Figure 23 shows the decoded SST for Solution 1 in a standard view, with plies dropped from the left to the right. Note that the solution is built from right to left within the algorithm, in order to better handle the design guidelines with the proposed specific operators detailed in Section 0. The actual laminates of the panels are emphasized in bold type. The number of plies in the U-grid structure ranges from 18 to 40 plies. All additional ply insertions have no influence on the solution. The active part of the SST corresponds to the part that is taken into account for the evaluation of the solutions.

The optimization has also been repeated 50 times with two objectives: minimization of the total mass of the panel and maximization of the reserve factor. The constraints and guidelines are unchanged with respect to the single objective case. The results are shown in Figure 22. Evaluating the performance of a multiobjective optimizer is not a straightforward task (Zitzler, 1999) and is beyond the scope of the present work. Thus, a simple graphical method is used here to assess the reproducibility and the convergence rate of the search. Figure 22.a shows in gray scale the non-dominated fronts obtained after 3,000 evaluations for the 50 optimization runs. All the solutions plotted are feasible (they satisfy the active guidelines by construction and they verify $RF > 1$). The non-dominated front corresponds to the best trade-offs between the conflicting objectives in the sense of the Pareto dominance (see for instance (Collette and Siarry, 2002) for more details on the topic). In red in the figure is shown the overall non-dominated front consisting of the non-dominated solutions in the union of the 50 fronts shown in gray. The area of the zone of the objective space covered by these 50 fronts gives a qualitative estimate of the

reproducibility of the search, both in terms of proximity to the overall front and spread of each singular front with respect to the global one. After 3,000 evaluations the fronts can be very different from one run to another, in terms of number of design, spread and performance. For some of the runs, no feasible solutions have been found yet, thus no results are plotted. Figure 22.b, Figure 22.c, Figure 22.d and Figure 22.e show the evolution with the number of evaluations of the non-dominated fronts. It can be seen that the overall performance and consistency of the fronts over repeated optimizations quickly improves and stabilizes after about 20,000 evaluations. The less repetitive aspect of the optimization is the spread of the fronts. Some fronts only describe half of the spread of the global front. As a matter of fact, the bi-objective optimization turns out to be less performing in finding the lightest solution than its single objective counterpart. The lightest solution found weights about 29.22 kg and is thus slightly heavier (1.1%) than Solution 1. Figure 22.d presents a synthetic view of the evolution of the global fronts as a function of the number of evaluated designs (which is directly related to the overall calculation cost). The overall behavior of the algorithm in solving the bi-objective problem seems consistent with the behavior observed in the single optimization case. It can be summarized in three distinct phases. i) Searching for feasible designs for which no panel buckles. ii) A second phase of rapid convergence towards increasingly performing solutions. In this phase the results obtained over repeated runs are first rather scattered before gaining in consistency. iii) A third phase of stabilization with slow improvements of the solutions (a single solution in the single objective case and a non-dominated front in the bi-objective case).

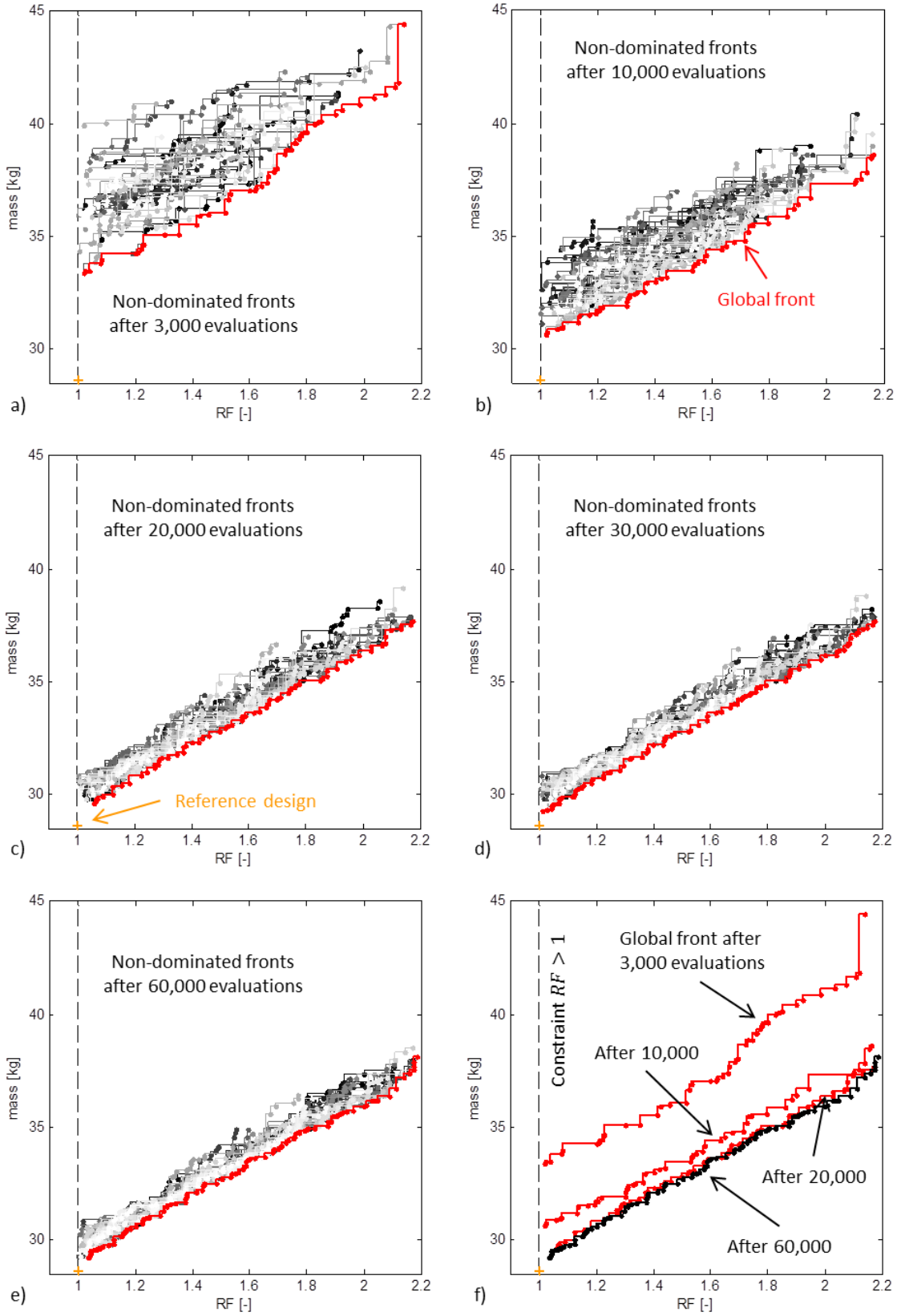

Figure 23. Illustration of the results obtained in the bi-objective case, with 50 repeated optimization runs. a) In gray, the 50 non-dominated fronts obtained and the corresponding global front in red after 3.000 evaluations. b), c), d) and e) Evolution of the global front as a function of the number of evaluations. The reference design is taken from (Yang et al., 2016). f) Evolution of the global front with the number of evaluations.

I.5.2 All laminate design guidelines

In this section, all the six laminate design guidelines listed in Section I.2 are enforced – *symmetry* (1.) *balance* (2.), *contiguity* (3.), *disorientation* (4.), *ten percent rule* (5.) and *damage tolerance* (6.) – as well as the same ply-drop guidelines and global requirement than in the symmetrical and balanced case. The ten percent rule is defined here in membrane stiffness space as proposed by (Abdalla et al., 2009). The ten percent rule and the constraint that no panel should buckle are handled using the modified tournament selection scheme while all other guidelines are handled during the creation and variation of the solutions (see Section 0).

Figure 24 illustrates the behavior of the algorithm over 50 optimization runs in the same manner than Figure 21. The solution considered here as the reference is the best one ever found in the present work (Solution 2). The algorithm exhibits similar behavior with all guidelines enforced than with symmetry and balance only. After finding a first feasible solution, the algorithm first quickly reduces the mass of the design until stabilization after about 15.000 evaluations. However in the present case, final accurate convergence towards the reference solution is better than in the symmetrical and balanced case. After approximately 10.000 evaluations, all runs have reached 90% of the performance of the reference solution. After about 15.000 evaluations, they all reach 95% of the reference performance. 98% and 99% reliability increase rather steadily from about 7.500 evaluations. After 30.000, more than 60% of the runs have reached 98% of the performance of the reference solution and 20% of the runs have reached 99% of the reference performance. This improvement in the final phase of the optimization is probably related to the fact that the reference solution was actually reached, while in the case of symmetrical and balanced designs, the guidelines made the reference performance out of reach by about 1%. It is remarkable in Figure 24.a that the scatter of the results between the 50 optimization runs decreases significantly over the generations and stabilizes after about 15.000 evaluations. Figure 21.a shows similar trend, but less pronounced.

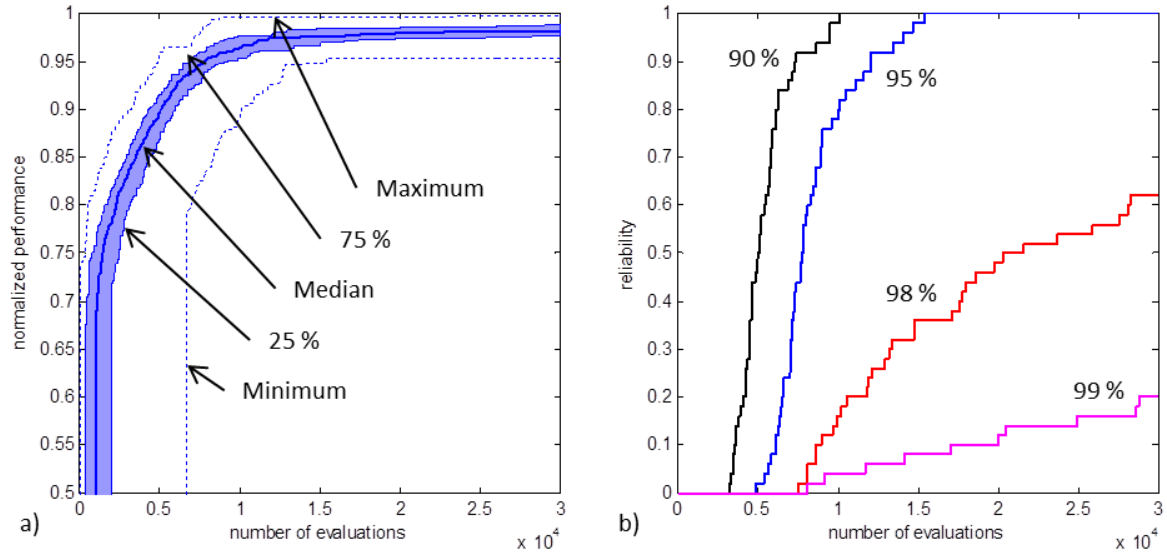

Figure 24. Results obtained over 50 repeated optimizations with all laminate design guidelines enforced. a) Curves of the median performance, 25th and 75th percentiles and extreme values. b) Curves of reliability for different levels of performances.

The genotype of Solution 2 is detailed in Table 5. The performances of Solution1 and Solution 2 are detailed and compared in Table 6. Figure 25 shows the decoded SST of Solution 2. The mass of Solution 2 is 29.29 kg to compare to the 28.90 kg of Solution 1. Thus, satisfying all laminate design guidelines instead of only symmetry and balance causes a weight penalty of 1.3%. Compared to the 28.62 kg of the solution given by (Yang et al., 2016), Solution 2 is only 2.3% heavier. Thus the proposed EA specialized for SST-based blending optimization allows finding performing designs. These results show that enforcing all the strength related design guidelines into the optimization only brings very low weight penalty with respect to a less constrained optimization performed with stiffness related guidelines only (i.e. symmetry and balance).

Chromosome N_{str}	[34 28 24 20 16 24 20 28 38 35 30 28 24 20 28 34 20 24]
Chromosome SST_{lam}	[-45 -30 0 -30 -45 -15 0 -45 90 90 45 0 30 75 45 15 45 30 75 -75 -75 75 -75 90]
Chromosome SST_{ins}	[0 3 8 5 0 9 12 6 0 17 0 1 2 15 0 10 7 4 0 14 16 13 0 11]

Table 5. Genotype of the lightest solution found with all guidelines enforced (Solution 2).

Panel	Symmetrical and balanced (Solution 1)			All laminate design guidelines (Solution 2)		
	Number of plies	Mass [kg]	RF [-]	Number of plies	Mass [kg]	RF [-]
1	34	2.85	1.057	34 (0)	2.85	1.121
2	30	2.51	1.170	28 (-2)	2.35	1.008
3	22	1.02	1.250	24 (+2)	1.12	1.257
4	18	0.84	1.036	20 (+2)	0.93	1.110
5	18	0.84	1.711	16 (-2)	0.74	1.020
6	22	1.02	1.123	24 (+2)	1.12	1.130
7	18	0.84	1.003	20 (+2)	0.93	1.076
8	26	1.21	1.135	28 (+2)	1.30	1.228
9	40	3.35	1.114	38 (-2)	3.18	1.003
10	36	3.02	1.032	35 (-1)	2.93	1.004
11	30	2.51	1.008	30 (0)	2.51	1.061
12	30	2.51	1.165	28 (-2)	2.35	1.004
13	22	1.02	1.176	24 (+2)	1.12	1.183
14	18	0.84	1.099	20 (+2)	0.93	1.178
15	26	1.21	1.100	28 (+2)	1.30	1.190
16	31	1.44	1.034	34 (+3)	1.58	1.016
17	18	0.84	1.018	20 (+2)	0.93	1.091
18	22	1.02	1.019	24 (+2)	1.12	1.025
Total	461	28.90	-	475	29.29	-
Minimum	-	-	1.003	-	-	1.003

Table 6. Comparison between Solution 1 (symmetrical and balanced) and Solution 2 (with all laminate design guidelines enforced). Difference of number of plies per panels is labeled between brackets.

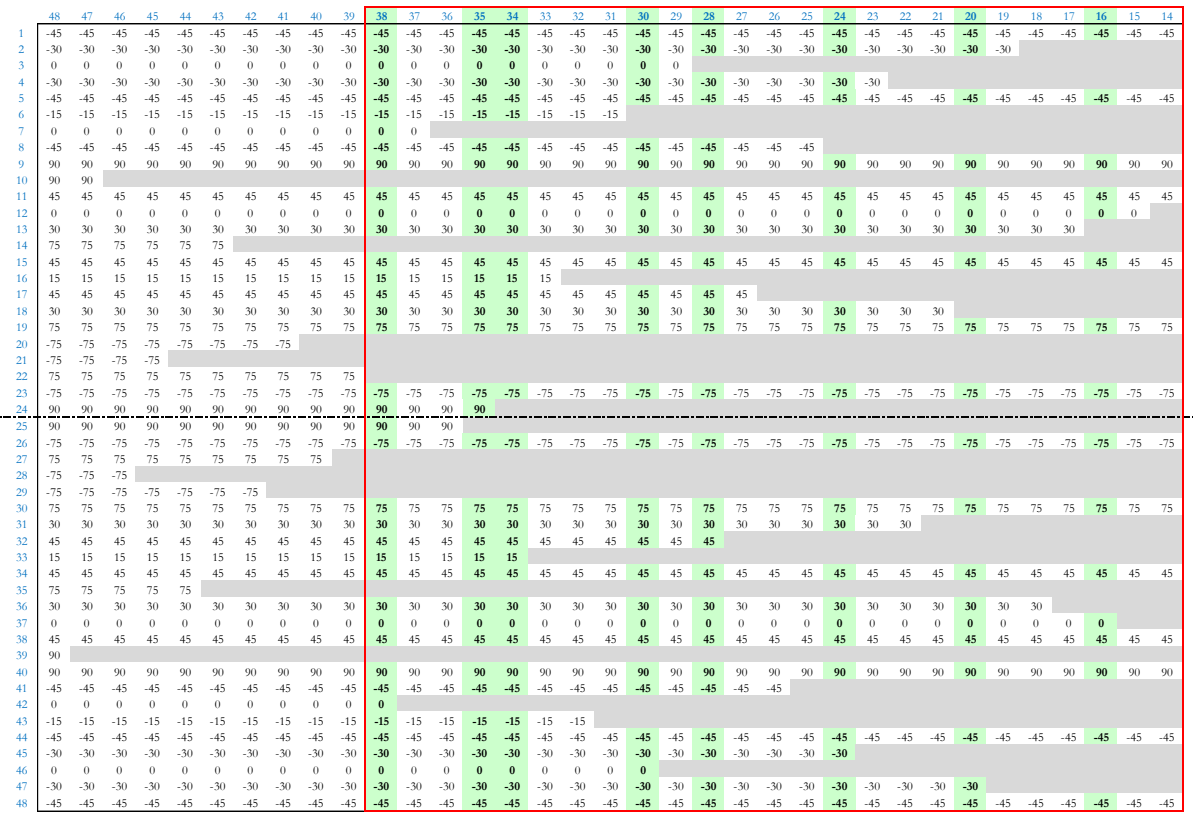

	48	47	46	45	44	43	42	41	40	39	38	37	36	35	34	33	32	31	30	29	28	27	26	25	24	23	22	21	20	19	18	17	16	15	14
1	-45	-45	-45	-45	-45	-45	-45	-45	-45	-45	**-45**	-45	-45	**-45**	**-45**	-45	-45	-45	**-45**	-45	**-45**	-45	-45	-45	**-45**	-45	-45	-45	**-45**	-45	-45	-45	**-45**	-45	-45
2	-30	-30	-30	-30	-30	-30	-30	-30	-30	-30	**-30**	-30	-30	**-30**	**-30**	-30	-30	-30	**-30**	-30	**-30**	-30	-30	-30	**-30**	-30	-30	-30	**-30**	-30					
3	0	0	0	0	0	0	0	0	0	0	**0**	0	0	**0**	**0**	0	0	0	**0**	0															
4	-30	-30	-30	-30	-30	-30	-30	-30	-30	-30	**-30**	-30	-30	**-30**	**-30**	-30	-30	-30	**-30**	-30	**-30**	-30	-30	-30	**-30**	-30									
5	-45	-45	-45	-45	-45	-45	-45	-45	-45	-45	**-45**	-45	-45	**-45**	**-45**	-45	-45	-45	**-45**	-45	**-45**	-45	-45	-45	**-45**	-45	-45	-45	**-45**	-45	-45	-45	**-45**	-45	-45
6	-15	-15	-15	-15	-15	-15	-15	-15	-15	-15	**-15**	-15	-15	**-15**	**-15**	-15	-15	-15																	
7	0	0	0	0	0	0	0	0	0	0	**0**	0																							
8	-45	-45	-45	-45	-45	-45	-45	-45	-45	-45	**-45**	-45	-45	**-45**	**-45**	-45	-45	-45	**-45**	-45	**-45**	-45	-45	-45											
9	90	90	90	90	90	90	90	90	90	90	**90**	90	90	**90**	**90**	90	90	90	**90**	90	**90**	90	90	90	**90**	90	90	90	**90**	90	90	90	**90**	90	90
10	90	90																																	
11	45	45	45	45	45	45	45	45	45	45	**45**	45	45	**45**	**45**	45	45	45	**45**	45	**45**	45	45	45	**45**	45	45	45	**45**	45	45	45	**45**	45	45
12	0	0	0	0	0	0	0	0	0	0	**0**	0	0	**0**	**0**	0	0	0	**0**	0	**0**	0	0	0	**0**	0	0	0	**0**	0	0	0	**0**	0	
13	30	30	30	30	30	30	30	30	30	30	**30**	30	30	**30**	**30**	30	30	30	**30**	30	**30**	30	30	30	**30**	30	30	30	**30**	30	30	30			
14	75	75	75	75	75	75																													
15	45	45	45	45	45	45	45	45	45	45	**45**	45	45	**45**	**45**	45	45	45	**45**	45	**45**	45	45	45	**45**	45	45	45	**45**	45	45	45	**45**	45	45
16	15	15	15	15	15	15	15	15	15	15	**15**	15	15	**15**	**15**	15																			
17	45	45	45	45	45	45	45	45	45	45	**45**	45	45	**45**	**45**	45	45	45	**45**	45	**45**	45													
18	30	30	30	30	30	30	30	30	30	30	**30**	30	30	**30**	**30**	30	30	30	**30**	30	**30**	30	30	30	**30**	30	30	30							
19	75	75	75	75	75	75	75	75	75	75	**75**	75	75	**75**	**75**	75	75	75	**75**	75	**75**	75	75	75	**75**	75	75	75	**75**	75	75	75	**75**	75	75
20	-75	-75	-75	-75	-75	-75	-75	-75																											
21	-75	-75	-75	-75																															
22	75	75	75	75	75	75	75	75	75	75																									
23	-75	-75	-75	-75	-75	-75	-75	-75	-75	-75	**-75**	-75	-75	**-75**	**-75**	-75	-75	-75	**-75**	-75	**-75**	-75	-75	-75	**-75**	-75	-75	-75	**-75**	-75	-75	-75	**-75**	-75	-75
24	90	90	90	90	90	90	90	90	90	90	**90**	90	90	**90**																					
25	90	90	90	90	90	90	90	90	90	90	**90**	90	90																						
26	-75	-75	-75	-75	-75	-75	-75	-75	-75	-75	**-75**	-75	-75	**-75**	**-75**	-75	-75	-75	**-75**	-75	**-75**	-75	-75	-75	**-75**	-75	-75	-75	**-75**	-75	-75	-75	**-75**	-75	-75
27	75	75	75	75	75	75	75	75	75																										
28	-75	-75	-75																																
29	-75	-75	-75	-75	-75	-75	-75																												
30	75	75	75	75	75	75	75	75	75	75	**75**	75	75	**75**	**75**	75	75	75	**75**	75	**75**	75	75	75	**75**	75	75	75	**75**	75	75	75	**75**	75	75
31	30	30	30	30	30	30	30	30	30	30	**30**	30	30	**30**	**30**	30	30	30	**30**	30	**30**	30	30	30	**30**	30	30								
32	45	45	45	45	45	45	45	45	45	45	**45**	45	45	**45**	**45**	45	45	45	**45**	45	**45**														
33	15	15	15	15	15	15	15	15	15	15	**15**	15	15	**15**	**15**																				
34	45	45	45	45	45	45	45	45	45	45	**45**	45	45	**45**	**45**	45	45	45	**45**	45	**45**	45	45	45	**45**	45	45	45	**45**	45	45	45	**45**	45	45
35	75	75	75	75	75																														
36	30	30	30	30	30	30	30	30	30	30	**30**	30	30	**30**	**30**	30	30	30	**30**	30	**30**	30	30	30	**30**	30	30	30	**30**	30	30				
37	0	0	0	0	0	0	0	0	0	0	**0**	0	0	**0**	**0**	0	0	0	**0**	0	**0**	0	0	0	**0**	0	0	0	**0**	0	0	0	**0**		
38	45	45	45	45	45	45	45	45	45	45	**45**	45	45	**45**	**45**	45	45	45	**45**	45	**45**	45	45	45	**45**	45	45	45	**45**	45	45	45	**45**	45	45
39	90																																		
40	90	90	90	90	90	90	90	90	90	90	**90**	90	90	**90**	**90**	90	90	90	**90**	90	**90**	90	90	90	**90**	90	90	90	**90**	90	90	90	**90**	90	90
41	-45	-45	-45	-45	-45	-45	-45	-45	-45	-45	**-45**	-45	-45	**-45**	**-45**	-45	-45	-45	**-45**	-45	**-45**	-45	-45												
42	0	0	0	0	0	0	0	0	0	0	**0**																								
43	-15	-15	-15	-15	-15	-15	-15	-15	-15	-15	**-15**	-15	-15	**-15**	**-15**	-15	-15																		
44	-45	-45	-45	-45	-45	-45	-45	-45	-45	-45	**-45**	-45	-45	**-45**	**-45**	-45	-45	-45	**-45**	-45	**-45**	-45	-45	-45	**-45**	-45	-45	-45	**-45**	-45	-45	-45	**-45**	-45	-45
45	-30	-30	-30	-30	-30	-30	-30	-30	-30	-30	**-30**	-30	-30	**-30**	**-30**	-30	-30	-30	**-30**	-30	**-30**	-30	-30	-30	**-30**										
46	0	0	0	0	0	0	0	0	0	0	**0**	0	0	**0**	**0**	0	0	0	**0**																
47	-30	-30	-30	-30	-30	-30	-30	-30	-30	-30	**-30**	-30	-30	**-30**	**-30**	-30	-30	-30	**-30**	-30	**-30**	-30	-30	-30	**-30**	-30	-30	-30	**-30**						
48	-45	-45	-45	-45	-45	-45	-45	-45	-45	-45	**-45**	-45	-45	**-45**	**-45**	-45	-45	-45	**-45**	-45	**-45**	-45	-45	-45	**-45**	-45	-45	-45	**-45**	-45	-45	-45	**-45**	-45	-45

Figure 25. Decoded SST for Solution 2. The active part of the table is bordered in red. The laminates of the panels of the structure are emphasized in bold type in light green columns.

Figure 18 presents the results obtained over 50 repeated optimization runs in the bi-objective case. The maximum number of generation has been set to 1000 here (i.e. 30,000 evaluations). The overall behavior of the algorithm seems to be consistent with what was observed in the single objective case. It turns out that the increased complexity brought by the additional guidelines considered here makes the scatter of the results more important in the beginning of the optimization. Nevertheless the final results after 30,000 show comparable scatter with respect to the symmetrical end balanced case only. Thus, the variation operators developed to handle the guidelines do not seem to bias significantly the optimization. Similarly, the recessive gene-like repair strategy described in Section 0 proves efficient. The algorithm shows satisfactory behavior in both single and bi-objective optimization and is able to handle efficiently the set of design guidelines listed in Section I.2, which is thought to be representative of the type of constraints that are currently in use in the aeronautical industry. For comparison, a random search should be able to find the optimal solution with a probability inversely proportional to n^A, with n the number of genes and A the number of possible values of each gene.

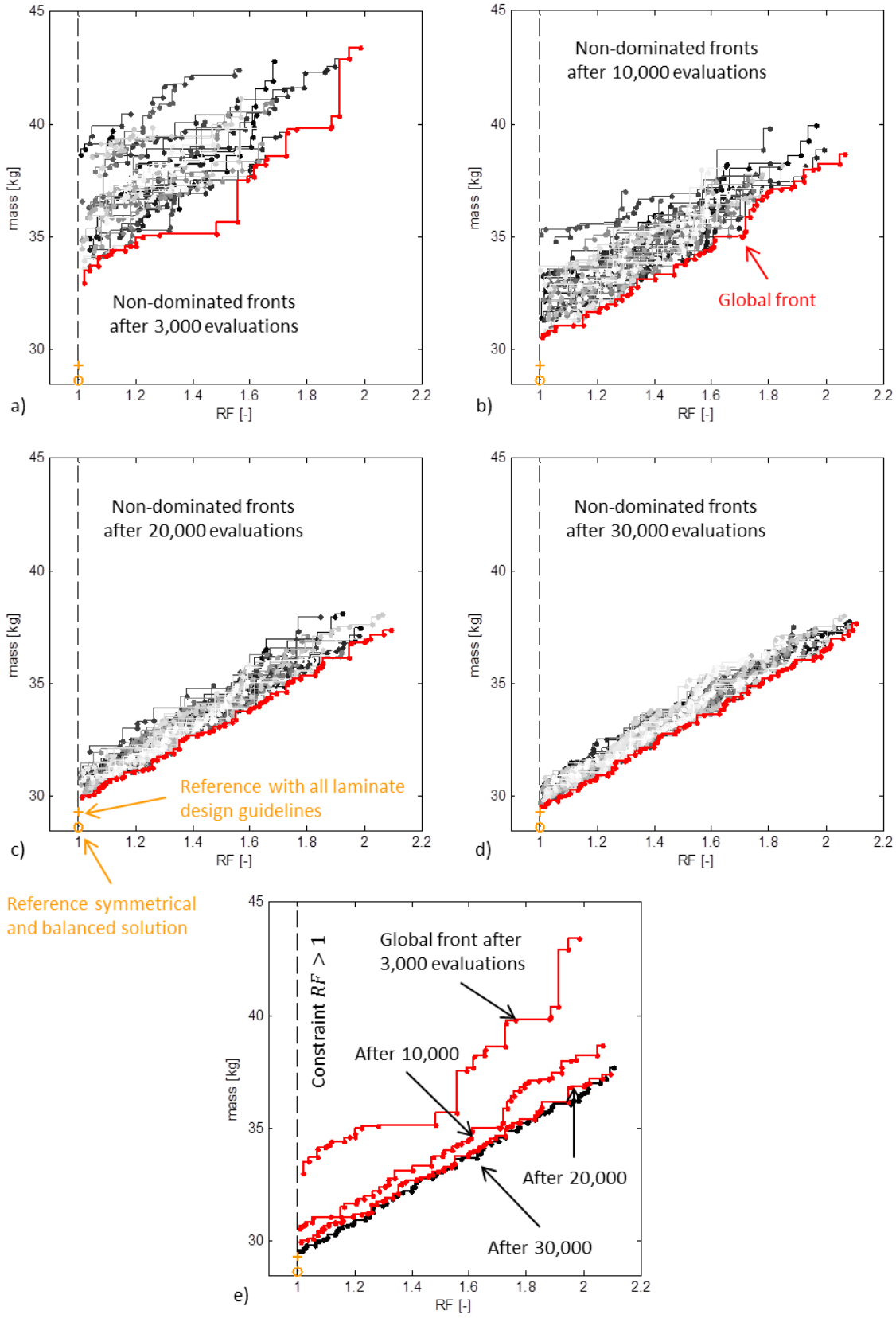

Figure 26. Illustration of the results obtained in the bi-objective case, with 50 repeated optimization runs and all laminate design guidelines enforced. a) In gray, the 50 non-dominated front obtained and the corresponding global front in red after 3.000 evaluations. b), c) and d) Evolution of the global front as a function of the number of evaluations. e) Evolution of the global front with the number of evaluations.

I.6 Application to the design of an industrial part

The method is applied to the design of a satellite antenna mounting bracket developed by the company MECANO I&D (http://www.mecano-id.fr). This section briefly presents the specifications of the structure, its design constraints, as well as the modeling work. The results of the optimization are then discussed. It is shown that it is possible to increase the stiffness and reduce the total mass simultaneously. Significant performance gains are observed when new designs are compared to the reference one provided by classical design approach without optimization. A brief comparison of the possible gains for a laminate made of 2D-woven fabrics and a laminate of UD prepreg plies is also presented to evaluate the potential of an alternative technological solution with respect to the considered specifications.

I.6.1 Optimal design of a satellite antenna mounting bracket

The composite fitting presented in this section is a satellite antenna mounting bracket, as illustrated in Figure 27 (the illustration is generic and does not correspond to the actual antenna). The fitting provides the mechanical connection between the satellite structure and the mounting stand of a telecom antenna, both made of CFRP materials. The bracket is expected to minimize the differential thermal expansion due to large temperature changes throughout the satellite's orbit. The original titanium alloy solution has a very complex geometry intended to minimize the stresses induced by the material dilation. The composite design is expected to allow a much simple geometry as there will be no more material thermal dilation coefficients contrast between the fitting and the attached parts of the satellite. The composite bracket is designed according to the following specifications:

- **Stiffness:** through its first natural frequency in order to keep the antenna aligned with its target.
- **Strength:** resistance to a given critical load case in order to ensure full functionality when mechanical stresses peak.
- **Mass:** overall net mass of the composite bracket must not exceed the mass of the titanium alloy one.

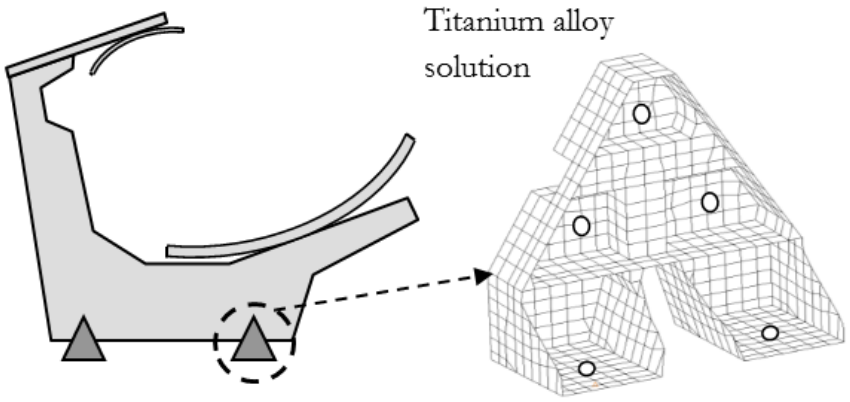

Figure 27. Schematic of the titanium alloy solution of the satellite antenna mounting bracket.

In this context, the company MECANO I&D, in collaboration with ONERA, developed a new solution, illustrated in Figure 28, by replacing the original material by a CFRP made through resin transfer molding (RTM) of a preform of 2D-woven fabrics (see http://www.mecano-id.fr/en/space/space-products). This new solution resulted in reducing the mass by 35%. This result was achieved without numerical optimization. Prototypes of the new bracket have been built and tested to validate the concept and its performance, with satisfactory results. The purpose of the work presented in this section is to explore the opportunities for improvement provided by the parametric optimization of the bracket. The composite solution presented in Figure 28 is considered as the reference design in the following.

Figure 28. Photographs of the CFRP solution made by MECANO I&D (front and rear views).

A constrained multicriteria optimization problem is formulated from the specifications detailed previously. The objectives are to maximize the first natural frequency and minimize the total mass of the bracket. The optimization variables are the stacking sequences, the order of the inserted plies, and the number of plies per zone. These zones represent distinct regions of the structure where its thickness and material properties do not vary. Each zone can be directly identified from the geometry of the composite structure. The minimal first natural frequency is required to be superior or equal to the one of the reference composite design. Additionally, the same set of design guidelines than in Section I.5.2 is enforced (i.e. all six laminate design guidelines, four ply-drop design guidelines and the blending global requirement). These guidelines originate from aeronautical industry design practice, but in the absence of known recommendations for the spatial industry they have considered as an interesting safeguard for the present application.

The rapid sizing FE model consists in a shell model of the composite part mid-surface. The model is developed with ABAQUS. It is illustrated in Figure 29 with shell thickness rendering enabled. The mesh is composed of reduced integration quadrangular shell elements. Thicknesses and composite lay-ups can be assigned to each element or element set. As a consequence, stacking sequences are parameterized within the model without modifying the mesh. Thus, the

parameterization of the model only consists in composite lay-up definitions associated with a set of elements. Text files are used to link the optimizer implemented in MATLAB and the ABAQUS FE model.

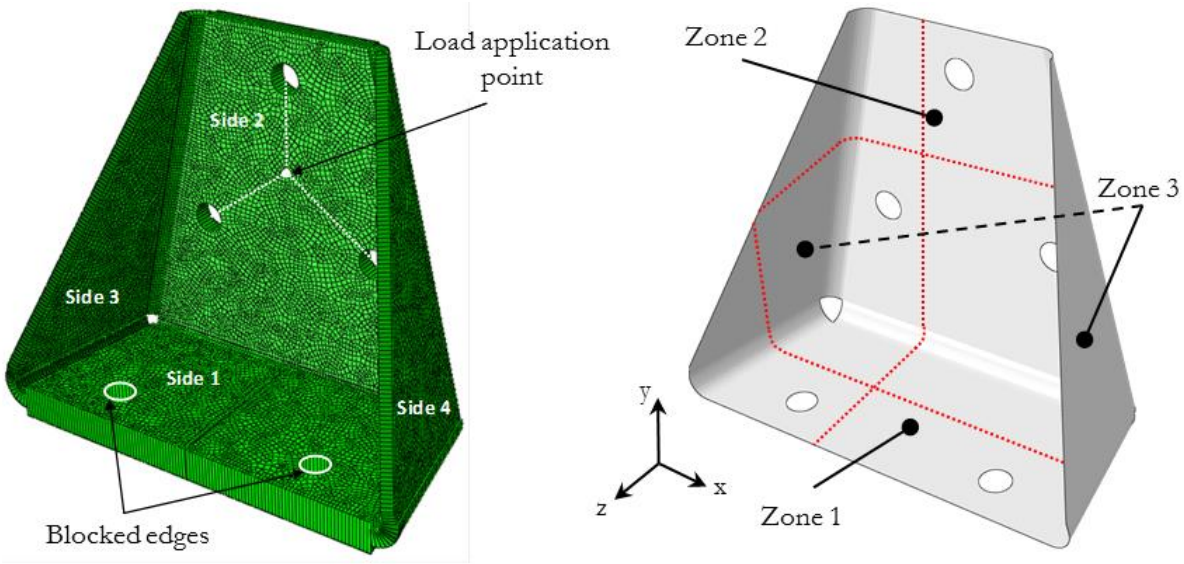

Figure 29. On the left, thickness-rendered view of the reference CFRP satellite antenna mounting bracket. On the right, view of the model of the mid-layer of the bracket with redirection of the orthotropy axes.

The connection from the bracket to the satellite is modeled through blocking all the degrees of freedom of the nodes of the edges of the holes on side 1. For each hole of side 2, the nodes of the circumference are connected through rigid links to a reference point located at the center of the hole. All three reference points, corresponding to the three holes on side 2, are connected to a fourth one located at their iso-barycenter. The efforts are inserted at this reference point. Two different analyses are performed for each evaluation of a solution. A linear elastic static analysis is done in order to evaluate the resistance of the structure to a critical load case indicated in the specifications. A modified Tsai-Hill first ply failure criterion is used for strength analysis in post-processing of the elastic stress analysis. The first natural frequency is computed from a modal analysis with small perturbations performed on the unloaded structure. The mass is estimated through the densities of the materials and the volume estimate provided by ABAQUS.

The reference bracket suggested by MECANO I&D is realized from cut plies of patterns with variable complexity. The plies are successively folded on male or female molding dies and stacked as to form a dry preforms, slightly powdered, to be injected by RTM in a closed mold. The process is not modeled in the present work. However it is necessary to take into account its influence on the fiber orientations in the constitutive zones of the fitting. The shapes of the patterns and the folding angles define the local orientations of the material within each zone of the structure. Indeed, the angle between side 1 and side 3 (or side 4) is an acute angle whereas side 2 and side 3 (or side 4) traces an obtuse angle. These angles imply a redirection of the material orthotropy axes (1,2,3) on the sides of the bracket as shown in red in Figure 29.

I.6.2 Results and discussion

The objectives of the optimization problem are to maximize the stiffness of the antenna bracket through its first natural frequency and to minimize its mass. The MECANO I&D reference solution is made of G803/RTM6, a balanced orthotropic 2D-woven fabric, whose fibers are of type T300. Thus, the problem is first solved for this base ply material. In order to explore the possibilities offered by UD plies compared to 2D plies, the optimal design problem is then solved using a T300/914 unidirectional prepreg ply that shares similar type of fibers. The elastic and strength properties of both materials are shown in Table 7. The number of plies per zone ranges from $n_{min} = 12$ to $n_{max} = 34$ in the case of the G803/RTM6 2D ply, and $n_{min} = 18$ and $n_{max} = 68$ for T300/914 UD ply. Ply orientations are restricted to following set of admissible values $\{0°, \pm 15°, \pm 30°, \pm 45°, \pm 60°, \pm 75°, 90°\}$. With respect to the listing of design rules proposed in Section I.2, two laminate design guidelines – *symmetry* (1.), *balance* (2.), *contiguity* (3.), *disorientation* (4.), *ten percent rule* (5.) and *damage tolerance* (6.) – four ply-drop design guidelines – *covering* (7.), *internal continuity* (10.), *ply-drop alternation* (11.) and *taper guidelines* (12.) – are enforced as well as one global requirement, *continuity* (13.) that is directly enforced through the encoding of the solutions. Other guidelines are discarded here.

Property	**G803/RTM6**	**T300/914**
Longitudinal modulus E_1	61.23 GPa	140 GPa
Transverse modulus E_2	61.23 GPa	10 GPa
In-plane Poisson's ratio υ_{12}	0.32	0.31
In-plane shear modulus G_{12}	3.46 GPa	4.4 GPa
Out-of-plane shear modulus $G_{23} = G_{31}$	2.96 GPa	3.81 GPa
Longitudinal tensile strength X_t	700 MPa	1500 MPa
Longitudinal compressive strength X_c	-468 MPa	-900 MPa
Transverse tensile strength Y_t	690 MPa	27 MPa
Transverse compressive strength Y_c	-438 MPa	-200 MPa
Shear strength S	103 MPa	80 MPa
Ply thickness	0.28 mm	0.158 mm

Table 7. Material properties of the G803/RTM5 2D ply and the T300/914 UD ply.

The settings of the evolutionary algorithm correspond to the one described in Table 2. The optimization was led with a fixed budget of 6,000 solutions. One solution evaluation takes less than 2 min. All evaluations were performed sequentially, in order to minimize the use of ABAQUS licenses. The overall computation time is about 300 hours (about 12 days). Parallel evaluations of the solutions at each generation of the algorithm would reduce the total time of the optimization to about 5 hours only.

The results obtained in the case of the 2D woven ply and the UD ply are presented in Figure 30.a and Figure 30.b respectively. In the figures, the solutions belonging to the initial population are emphasized with green squares. Feasible solutions are shown in blue. Unfeasible solutions shown in black fail either with respect to the 10%-rule or the strength constraint. Non-dominated solutions are shown with red diamonds. The algorithm converges in the bottom right quadrant where the solutions improve both objectives with respect to the reference design. Figure 30.c presents a comparison of the two non-dominated fronts. With both materials, the mass saving is significant for the lightest non-dominated solutions (about 10%). The increase in stiffness is even more important (about 30%) when considering the non-dominated solution that maximizes the first natural frequency. The two fronts are consistent in that they seem to be linear and parallel what gives some confidence in the optimization process and the corresponding results.

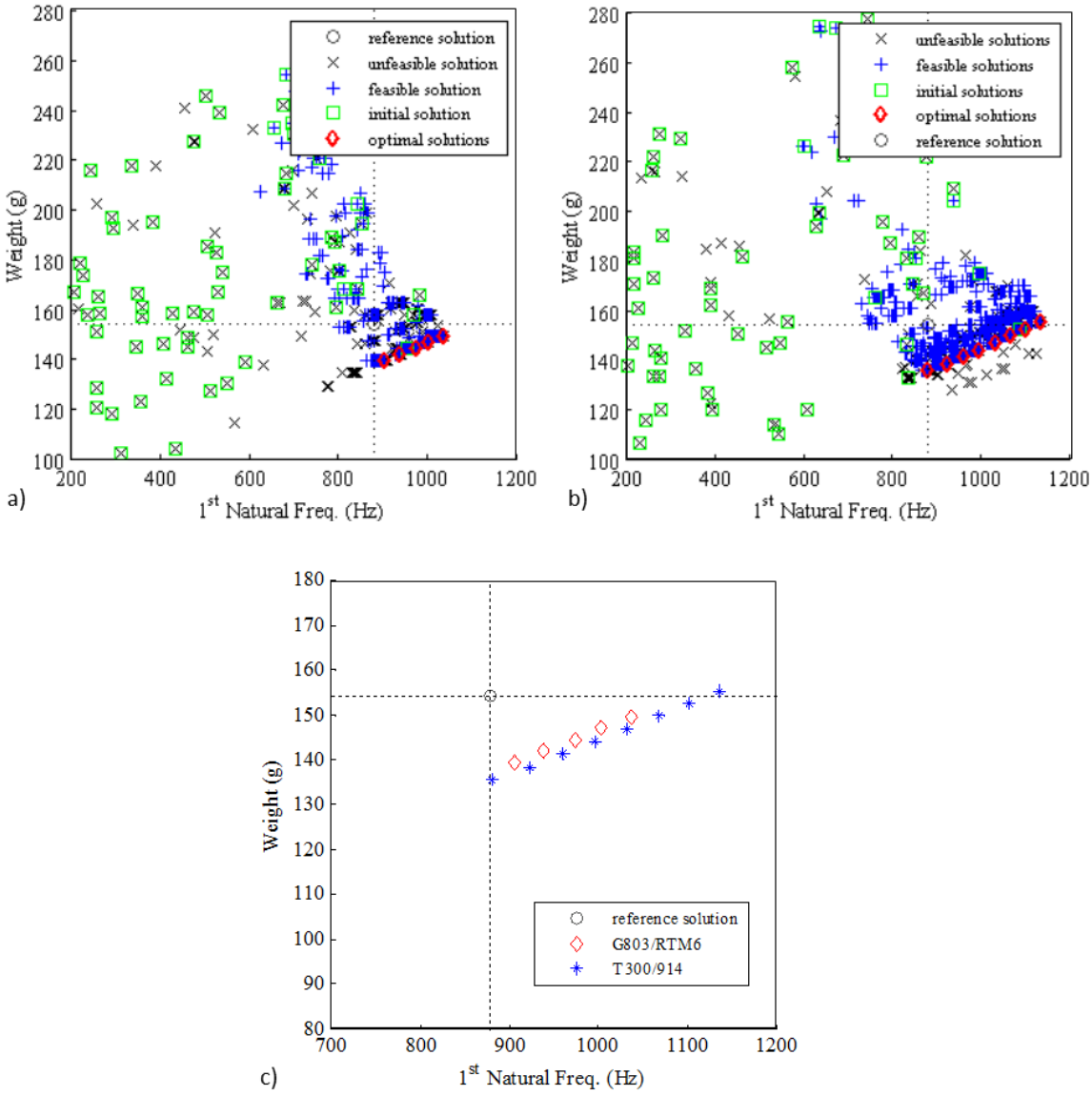

Figure 30. Optimization results of the composite fitting. a) Solutions obtained with the 2D woven ply. b) Solutions obtained with the UD ply. c) Compared non-dominated fronts.

Table 8 details the characteristics and performances of the lightest optimal solutions found with both materials. The G803/RTM6 solution is detailed in Table 9 and Figure 31. The lightest G803/RTM6 solution enables a mass saving of 10% with respect to the reference solution. The lightest T300/914 solution presents a 12% weight savings. It is interesting to note that the added freedom offered to the optimization by using a UD ply does only bring little improvement to the solution. The UD ply is approximately twice thinner than the 2D ply. Thus, the number of design variables is increased. Moreover the UD ply and the 2D ply have different anisotropy. With much higher stiffness and strength in longitudinal direction, the UD ply gives more freedom than the balanced 2D woven ply to tailor the laminate anisotropy.

Criteria		**Reference**	**G803/RTM6**	**T300/914**
Number of plies	Zone 1	33	30	52
	Zone 2	19	12	22
	Zone 3	12	12	18
Total mass (g)		154.3	139.5	135.5
First natural frequency (Hz)		879	905	880
Failure criteria		0.751	0.992	0.997

Table 8. Comparison of the lightest Pareto-optimal solutions found with the 2D woven G80S/RTM6 ply and the T300/914 UD ply.

In the composite fitting proposed by MECANO I&D, ply-drops are located within the fillet radii connecting the faces of the part. Moreover, ply drops are distributed over a very short distance. The representation of fillet radii is therefore very limited in the optimization model. Three-dimensional effects arising around ply-drops and high curvature zones cannot be captured with a simple shell model. The results obtained with the optimization model in the case of the reference solution manufactured and tested by MECANO I&D were satisfactory with respect to the design criteria. Thus the model is considered to give fair trends overs the design space.

Guidelines aiming at limiting the risks of premature failure are enforced in the optimization to overcome the limitations of the model in predicting the strength of the laminated composite structure, especially delamination that requires much more detailed analysis. However, the use of some of the design guidelines, for instance the disorientation guideline, in the case of a balanced 2D woven might be of questionable usefulness. Nevertheless, in the absence of specific guidelines for woven plies, it was chosen here to use the usual set of guidelines whatever the base ply. Additionally, most of the design guidelines have been thought for large structures, thus their relevance may be called into question for this application. They are probably pushed beyond their range of validity in this study. Numerical validation based on a detailed three-dimensional model, and experimental validation, would be necessary to validate the results.

Finally, despite all the limitations discussed previously, the SST-based optimization method proposed in this chapter proves relevant and efficient for a real-life design problem. Three main conclusions can be drawn from this exercise. First, one of the main difficulty in performing structural optimization in an industrial environment might not be the optimization method itself,

but the development of a modeling consistent with the optimization. Indeed, the model has to be of minimal computational cost, parameterized to be linked to the optimizer, automatically post-processed to extract the numerical values of the design criteria, and relevant in an engineering viewpoint. Building the corresponding mesh can be a cumbersome task and the required engineering time should not be neglected when planning an optimization study. Second, directly coupling an EA with a FE model is costly, either in terms of total calculation cost or FE software licenses if many FEA have to be ran simultaneously. Third, up to our knowledge there is no quick and efficient delamination criteria to be used with a shell rapid sizing model. This last point is the main limitation of the presented attempt to improve the MECANO I&D composite fitting since delamination in the fillet radii is of primary importance in the failure of the part.

Chromosome N_{str}	[30 12 12]
Chromosome SST_{lam}	[45 0 30 -15 0 -45 -30 0 45 15 -30 -45 -75 75 -75 75 30]
Chromosome SST_{ins}	[0 7 1 3 0 8 10 0 9 4 2 0 5 6 0 0 11]

Table 9. Genotype of the lightest Pareto optimal solution found with the 2D woven G80S/RTM6 ply.

	34	33	32	31	**30**	29	28	27	26	25	24	23	22	21	20	19	18	17	16	15	14	13	**12**
1	45	45	45	45	**45**	45	45	45	45	45	45	45	45	45	45	45	45	45	45	45	45	45	**45**
2	0	0	0	0	**0**	0	0	0	0	0													
3	30	30	30	30	**30**	30	30	30	30	30	30	30	30	30	30	30	30	30	30	30	30	30	
4	-15	-15	-15	-15	**-15**	-15	-15	-15	-15	-15	-15	-15	-15	-15	-15	-15	-15	-15					
5	0	0	0	0	**0**	0	0	0	0	0	0	0	0	0	0	0	0	0	0	0	0	0	**0**
6	-45	-45	-45	-45	**-45**	-45	-45	-45															
7	-30	-30	-30	-30																			
8	0	0	0	0	**0**	0	0	0	0	0	0	0	0	0	0	0	0	0	0	0	0	0	**0**
9	45	45	45	45	**45**	45																	
10	15	15	15	15	**15**	15	15	15	15	15	15	15	15	15	15	15							
11	-30	-30	-30	-30	**-30**	-30	-30	-30	-30	-30	-30	-30	-30	-30	-30	-30	-30	-30	-30	-30			
12	-45	-45	-45	-45	**-45**	-45	-45	-45	-45	-45	-45	-45	-45	-45	-45	-45	-45	-45	-45	-45	-45	-45	**-45**
13	-75	-75	-75	-75	**-75**	-75	-75	-75	-75	-75	-75	-75	-75	-75									
14	75	75	75	75	**75**	75	75	75	75	75	75	75											
15	-75	-75	-75	-75	**-75**	-75	-75	-75	-75	-75	-75	-75	-75	-75	-75	-75	-75	-75	-75	-75	-75	-75	**-75**
16	75	75	75	75	**75**	75	75	75	75	75	75	75	75	75	75	75	75	75	75	75	75	75	**75**
17	30	30																					
18	30																						
19	75	75	75	75	**75**	75	75	75	75	75	75	75	75	75	75	75	75	75	75	75	75	75	**75**
20	-75	-75	-75	-75	**-75**	-75	-75	-75	-75	-75	-75	-75	-75	-75	-75	-75	-75	-75	-75	-75	-75	-75	**-75**
21	75	75	75	75	**75**	75	75	75	75	75	75												
22	-75	-75	-75	-75	**-75**	-75	-75	-75	-75	-75	-75	-75	-75										
23	-45	-45	-45	-45	**-45**	-45	-45	-45	-45	-45	-45	-45	-45	-45	-45	-45	-45	-45	-45	-45	-45	-45	**-45**
24	-30	-30	-30	-30	**-30**	-30	-30	-30	-30	-30	-30	-30	-30	-30	-30	-30	-30	-30	-30				
25	15	15	15	15	**15**	15	15	15	15	15	15	15	15	15	15								
26	45	45	45	45	**45**																		
27	0	0	0	0	**0**	0	0	0	0	0	0	0	0	0	0	0	0	0	0	0	0	0	**0**
28	-30	-30	-30																				
29	-45	-45	-45	-45	**-45**	-45	-45																
30	0	0	0	0	**0**	0	0	0	0	0	0	0	0	0	0	0	0	0	0	0	0	0	**0**
31	-15	-15	-15	-15	**-15**	-15	-15	-15	-15	-15	-15	-15	-15	-15	-15	-15	-15						
32	30	30	30	30	**30**	30	30	30	30	30	30	30	30	30	30	30	30	30	30	30			
33	0	0	0	0	**0**	0	0	0	0														
34	45	45	45	45	**45**	45	45	45	45	45	45	45	45	45	45	45	45	45	45	45	45	45	**45**

Figure 31. Decoded SST of the lightest Pareto optimal solution found with the 2D woven G80S/RTM6 ply.

I.7 Concluding remarks

This chapter introduces the concept of stacking sequence table (SST) for the optimal design of laminated composite structures with ply drops. The SST describes the sequence of ply-drops ensuring the transition between a thick guide laminate and a thinner one. A blended design is represented by a SST combined with a thickness distribution over the regions of the structure. An evolutionary algorithm is specialized to operate on that representation of the solutions. The algorithm is able to perform single objective optimization as well as multi-objective optimization.

SST-based blending encompasses the classical guide-based blending while affording more freedom to define which ply to drop off. Optimization of the position and order of the ply insertions, rather than the order of ply termination, enables satisfying design guidelines that could only be discarded in previous guide-based blending methods. An extensive set of design guidelines representative of the actual industrial requirements has been introduced. The laminate design guidelines aim at preventing unwanted coupled behaviors, matrix dominated behaviors or premature failure modes in the panels. The ply-drop design guidelines aim at avoiding delamination at ply-drop location and obtaining ply layouts that can actually be manufactured. The global requirements aim at ensuring ply continuity and smooth load redistribution over the structure. Accounting for the guidelines in the optimization is possible by devising specific evolutionary operators. A clear distinction is made between guidelines and other constraints such as buckling. Guidelines are incorporated to the objectives of the optimization through specific evolutionary operators. The method is applied to a benchmark problem from the literature with convincing results. The EA shows satisfactory convergence rate and good reproducibility over successive runs. The lightest designs obtained are only slightly heavier than published solutions while satisfying many more design guidelines. In particular, the present results show that strength-related guidelines can be enforced without significantly penalizing the stiffness behavior and consequently the mass of the structure.

Finally, an industrial demonstration case is tackled, consisting in a satellite composite fitting designed by MECANO I&D, with interesting results. A multi-objective optimization problem is formulated based on the specifications of the part. Evaluations of the solutions are performed through FEA due to the complexity of the geometry of the part. The optimization problem is solved for a carbon/epoxy 2D-woven fabric and a carbon/epoxy UD ply to explore different design spaces and to provide alternatives in improving the reference solution.

The main issue in directly calling for finite element analysis of the structure within an evolutionary optimization is the total computation cost that can become prohibitive. The presented application shows that the method is tractable thanks to the efficient solution encoding proposed in this chapter that enables to represent large stacking sequence tables with a limited number of variables. However, the proposed application is limited in that the considered structure is small and does not require important unit evaluation time. In order to apply the method to more complex structures, it is necessary to improve as much as possible the efficiency of the evolutionary optimizer (i.e. its capacity to find optimal solutions – or, in a more pragmatic viewpoint, performing solutions – in a reduced number of evaluations and with good accuracy). Thus, in the next chapter, a method is proposed to improve the efficiency of the search, and the question of the tuning of the algorithm settings is tackled.

CHAPTER II. DOUBLE DISTRIBUTION EVOLUTIONARY ALGORITHM FOR LAMINATE OPTIMIZATION

II.1 Introduction

In Chapter I, an elitist evolutionary algorithm (EA) is specialized for laminate blending optimization. The emphasis is placed on the enforcement of numerous industrial design guidelines through the use of staking sequence tables (SST) and the development of specialized variation operators. Chapter I is focused on improving the efficiency of the optimization algorithm itself with a double distribution technique.

With direct search techniques such as EA, the number of evaluations required prior to convergence can be very high, typically of the order of thousands of evaluations or more. Induced computational costs can be affordable when the optimization criteria rely on simple closed form solutions but quickly become prohibitive when FEA are required. In the field of composite optimization, two main types of methods can be found to reduce computational costs: response surface methods (RSM) and bi-level design methods. The first kind of methods consists in replacing the costly FEA with inexpensive response surfaces – also called metamodels – in the evolutionary search (F.-X. Irisarri et al., 2011; Lanzi and Giavotto, 2006; Liu and Haftka, 2001; Todoroki and Ishikawa, 2004). Within bi-level decomposition methods, the first level of the decomposition consists in searching for the optimal thickness and homogenized stiffness of the material. The second level consists in searching for the corresponding optimal laminates. Various implementations of the bi-level optimization strategy for composite structures can be found in the literature (Herencia et al., 2008; IJsselmuiden et al., 2009; Francois-Xavier Irisarri et al., 2011; Irisarri et al., 2015; Liu, 2001; Liu et al., 2011, 2006; Liu and Toropov, 2013; Montemurro et al., 2012; Yamazaki, 1996). These implementations mainly differ in the degree of sophistication of the optimization algorithms used for the first level and second level optimizations, and in the way the two steps are chained. Gradient-based methods are used for first level optimization whereas EA are usually used for stiffness matching, targeting the optimal thickness distribution at the second level optimization. In both RSM methods and bi-level methods, EA are used on inexpensive models only, to solve the combinatorial staking sequence optimization problem. Improving the efficiency of the EA itself is not the first concern.

The purpose of this work is to improve the convergence rate of the EA by taking advantage of the nature of the laminate optimization problem itself. The evaluation step within a direct search generally calls for series of calculations where intermediate results are merely exploited. Regarding classical laminate design problems, this is generally the case for stiffness ABD matrix terms and lamination parameters (LP). Laminate optimization can be improved by fully exploiting the richness of the multiscale information related to the CLT. This feature has been investigated by (Grosset, 2004; Grosset et al., 2006), who developed the so-called Double Distribution Optimization Algorithm (DDOA), relying on auxiliary variables (e.g. lamination parameters) to guide the search in the design space. Their study showed that DDOA significantly outperformed the single distribution search as well as standard genetic algorithm (GA) for several laminate optimization test problems.

In this chapter, the algorithms developed in (Grosset, 2004) are first investigated and compared to the specialized evolutionary algorithms introduced in (F.-X. Irisarri et al., 2011; Irisarri, 2010; Irisarri et al., 2009) on which the developments presented in Chapter I are based. Second, a Double Distribution Evolutionary Algorithm (DDEA) is proposed in order to take advantage

from both the specific genetic operators developed for composite optimization and the increased efficiency provided by the use of a double distribution method. Section II.2 introduces the Univariate Marginal Distribution Algorithm (UMDA), from which DDOA is derived. Its efficiency is compared to the specialized evolutionary algorithm presented in Section I.4.1. The trade-off between exploration of the design space and intensification of the search in its most promising regions is discussed in Section II.3 through tuning and improvement attempts for UMDA. DDOA is detailed and implemented in Section II.4to show the interest of guiding the search in the space of auxiliary variables chosen to capture joint actions of the design variables. The guidance scheme is transposed in Section II.5to the EA with the development of DDEA. Finally, in Section II.6, DDEA is benchmarked to the buckling load maximization of a long cylinder, the maximization of the strength of a laminate under in-plane loading, and applied to the SST-based blending optimization of the semi-analytical 18-panel U-gird problem discussed in Chapter I. In the following, all algorithms have been implemented in MATLAB.

II.2 The Univariate Marginal Distribution Algorithm

As shown in Chapter I, evolutionary algorithms are stochastic optimization techniques that can be competitive in solving most of the laminate optimization problems. However, EAs suffer from their metaphoric nature when it comes to tuning the parameters of their complex operators, which require a specific engineering. As concluded in (Grosset, 2004), UMDA constitute an interesting alternative to a generic EA in solving laminates optimization problems. This section explores the advantages and limits of a population-based UMDA for laminate optimization. The parameters of the algorithm are tuned for a simple test case problem and various additional features are suggested and tested on laminated plate buckling maximization problem. UMDA results are compared with the results of the specialized EA developed in this study. Tuning of the parameters of the EA is also discussed.

II.2.1 UMDA for laminate optimization

Algorithm 1 details the UMDA implemented in this study for laminate optimization. The algorithm is written here for the maximization of a function $f(x)$ where x represents a n-ply laminate. Each coordinate $x_{j=1,\dots,n}$ of x corresponds to a ply orientation and takes its values among a discrete set of allowed ply orientations $\{\theta_{j=1,\dots,m}\}$. The corresponding design space is noted $\mathcal{S}$ in the following. UMDA searches for the best designs by sampling the probability distribution $p(x)$ of the best performing points. The optimization starts with a uniform probability distribution. A first population of λ designs is generated by sampling $p(x)$. The designs are evaluated and ordered according to their performance. The distribution $p(x)$ is updated based on the μ best performing solutions of the population and the process is repeated until a given stopping criterion – here a maximum number of iterations – is reached.

$p(x)$ is here a discrete probability distribution, i.e. a probability mass function (PMF). At iteration t, the PMF $p^t(x)$ is learnt from the best solutions of the current population. As the x^i can take m possible discrete values, there should be $n(n-1)/2 \times m^2$ joint probabilities

$P(x^i = \theta^k, x^i = \theta^m)$ to estimate. Since the number of variables n can be important, the PMF is computed with the hypothesis of independency of the variables such as:

$$p^t(x) = \prod_{i=1}^{n} p^t(x^i) \quad \text{II-1}$$

The PMF $p^t(x)$ is thus learnt as the frequency of appearance of the value θ_j for the variable x_i among the selected μ individuals at iteration t. The PMF is subsequently sampled using a classical roulette wheel algorithm.

Algorithm 1. Population-based Univariate Marginal Distribution Algorithm (UMDA).

Set λ, the population size
Set μ, the number of points considered as good in the population

Initialize $p(x)$ as a uniform distribution: $p^0(x) = U(x)$

while not stop **do**
  for $i = 1$ to λ **do**
    Sample $p^t(x) \rightarrow x^i$ by taking randomly $x_j^i = \theta_j$ with probability $p^t(\theta_j^i)$
  end for
  Calculate $f(x)$
  Calculate the ordered indices $i{:}\,\lambda$, such as $f(x^{1:\lambda}) \geq f(x^{2:\lambda}) \geq \cdots \geq f(x^{\lambda:\lambda})$
  Update $p^t(x)$ from $\{x^{1:\lambda}, f(x^{1:\lambda}), \ldots, x^{\mu:\lambda}, f(x^{\mu:\lambda})\}$
  $t \leftarrow t + 1$
end while

According to the literature (Larrañaga and Lozano, 2002), UMDA are EA-like instances. Indeed, for EAs, the variation operators, such as crossover and mutation, generate new points with the characteristics of the best previous points. Thus, the fitness function and the selection operators define an implicit probability mass function over the whole search space, covering the promising regions. Metaphoric algorithms such as EA or other nature-inspired metaheuristics may lead to very efficient implementations but the implicit analysis makes the parameter sets more difficult to choose and justify. Conversely, UMDA has been addressed to exploit explicitly the PMF $p(x)$ of the best performing points, without calling for metaphoric operators. This results in clear tendencies when tuning the parameters of the algorithm, as it is shown in the following.

II.2.2 Plate buckling maximization test problem

In this section, UMDA is tested on a simple plate buckling optimization problem. The problem consists in maximizing the buckling load factor of a square plate with straight edges solicited in uniaxial compression. The four edges are considered simply supported. The following orthotropic material properties are used for the base ply: $E_{11} = 181$ GPa, $E_{22} = 10.3$ GPa,

$G_{12} = 7.17$ GPa and $\nu_1 = 0.28$. The laminate is assumed to be symmetric and balanced and can be written as $[x_{i=1,\dots,n}/-x_{i=1,\dots,n}]_s$. Ply orientations are restricted to the set $\{0°, \pm 15°, \pm 30°, \pm 45°, \pm 60°, \pm 75°, 90°\}$. Buckling is evaluated with the closed form solution given in Equation I-2 and reminded below:

$$\Lambda_{(l_a,l_b)} = \frac{\pi^2[D_{11}(l_a/a)^4 + 2(D_{12} + 2D_{66})(l_a/a)^2(l_b/b)^2 + D_{22}(l_b/b)^4]}{(l_a/a)^2 N_x + (l_b/b)^2 N_y} \qquad \text{II-2}$$

where N_x and N_y are the stress resultants in the longitudinal and transverse directions respectively ($N_y = 0$ in the following). Parameters a and b are the corresponding dimensions of the panel. Parameters l_a and l_b are the number of half wave-lengths along the x and y directions respectively. D_{11}, D_{12}, D_{22} and D_{66} are bending stiffness terms of the laminate. The critical buckling mode is the mode (l_a, l_b) of minimal buckling factor.

In the following the number n of design variables is set to 32. The problem hence allows 7^{32}, or 1.1×10^{27}, different mechanical solutions, while the total number of possible combinations reaches 12^{32}, or 3.4×10^{34}. According to the classical laminate theory (CLT), ply orientations, stacking order and number of plies affect the bending stiffness of the laminate and consequently the buckling factor. Several stacking combinations share the same mechanical behavior since the bending stiffness terms are not sensitive to the signs of the orientations, i.e. unbalanced conditions. The optimal solutions are known and correspond to all ±45° angle-ply laminates. Performances are normalized with respect to the optimal performance.

II.2.3 Influence of the population size and the selection ratio

The influence of the parameters of the algorithm is investigated here for the plate buckling maximization problem in tight-budget conditions. The stopping criterion is set to a maximum number of 3000 evaluations. Parameters are the size λ of the population and the selection ratio $\tau = \mu/\lambda$. The results obtained for 50 optimizations performed for 15 different settings (λ, μ) are shown in Figure 32. The figure shows the convergence curve of the median performances for each setting and the corresponding 95% reliability curves. The 95% reliability is defined as the proportion of runs having reached 95% of the optimal performance. 90% reliability and 99% reliability are similarly defined thereafter. These results call for several comments. First, it can be seen that whatever the setting the median performance never reaches the optimal performance. UMDA converges prematurely. This tendency is due to loss of diversity within the population and premature convergence of the probability distribution $p(x)$. Indeed, without diversity preserving mechanisms, some values of the variables quickly disappear with $p(x)$. This phenomenon has been previously shown in (Grosset, 2004). Second, median performance curves show a rather clear tendency with respect to the population size: the lower is λ, the faster is the convergence at the beginning of the optimization. This could be explained by the fact that a small population size implies more frequent updates of the distribution of probability. However it is for the smallest populations that the algorithm gets trapped into the less performing local optima.

Using population sizes smaller than the number of variables does not allow for sufficient exploration of the design space. Selection ratios that are inferior or equal to $1/3$ seem to be offering the best convergence rates and reliability.

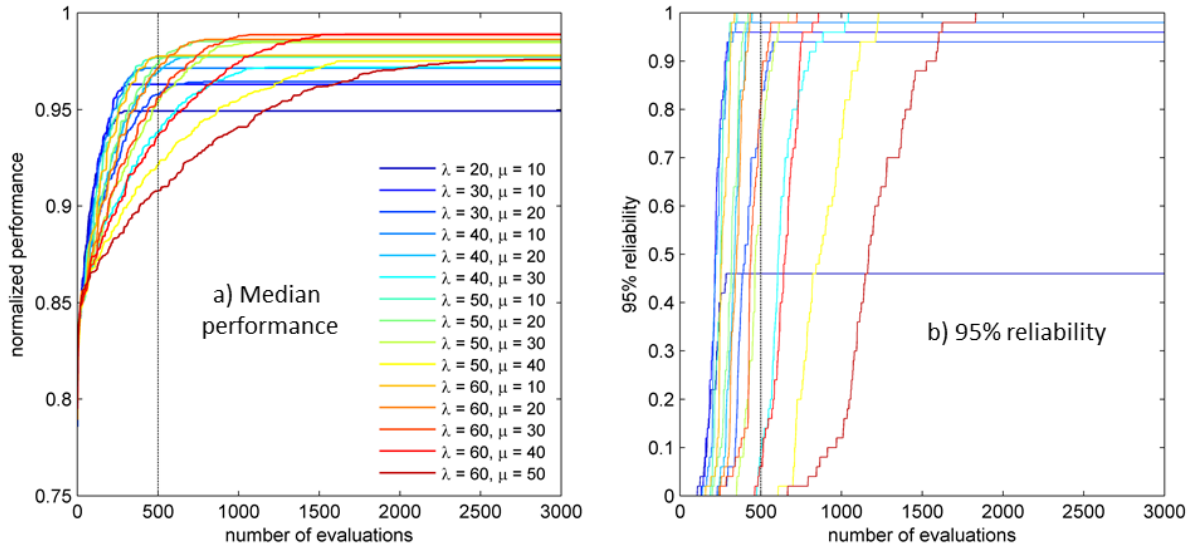

Figure 32. a) Normalized median performance curves. b) 95% reliability curves of UMDA for the plate buckling maximization problem. Optimizations have been repeated 50 times for each setting (λ, μ).

Figure 33 suggests different reading of the same results than Figure 32. Figure 33.a shows the convergence curves for 50 runs with $\lambda = 40$ and $\mu = 10$. This setting is used in the following sections as it seems to offer a reasonable trade-off between intensification of the search around good solutions (the selection ratio is rather low) and exploration with an average population size in the range of the tested values. The trade-off lies here between population size and number of generations within the given total number of evaluations. In Figure 33.b, 2.c and 2.d the results are ordered by increasing selection ratio. Figure 33.b plots the number of evaluations required sp that 90% of the runs reach 95% reliability. The figure shows that this number increases for selection ratios superior to $1/3$. The outlier corresponds to the smallest population size tested, $\lambda = 20$, which result in premature convergence of the algorithm. In that case, the number of samples to learn the distribution $p(x)$ is probably too low. Figure 33.c illustrates the dispersion of the results with boxplots after 500 evaluations. The smallest selections ratios give the smallest scattering. It can also be seen that the selected setting, with $\lambda = 40$ and $\mu = 10$, gave the best run in terms of the best performance reached after 500 evaluations. Finally, Figure 33.d shows the value of 99% reliability after 3000 evaluations. The largest population sizes λ give the best results. However, this figure mostly shows that the algorithm is unable to converge with precision toward the optimal solution. In Section II.3 several features are implemented and tested to overcome this issue.

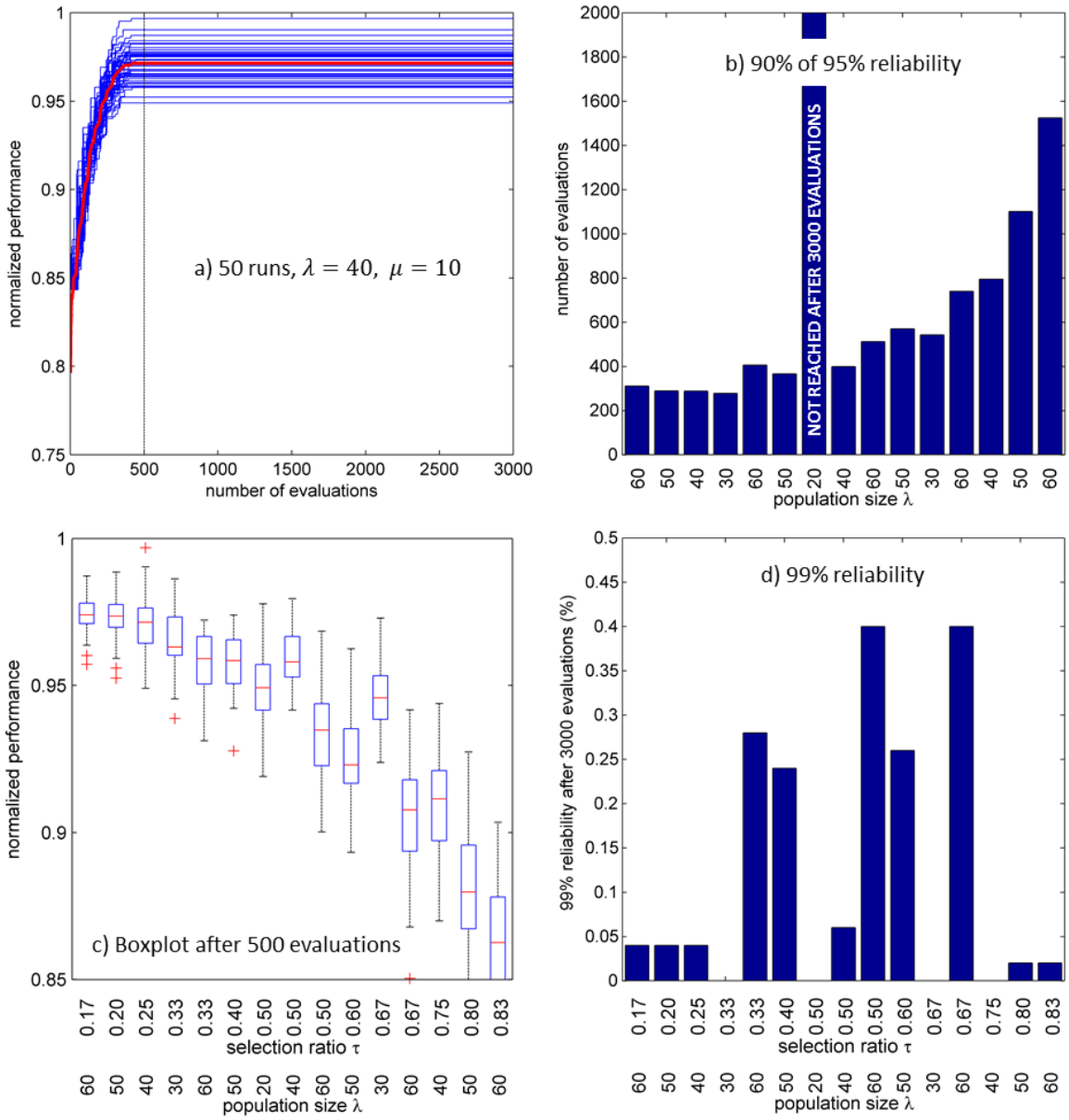

Figure 33. a) Convergence curves for 50 repetitions of the optimization. b) Number of evaluations required to reach 95% of reliability for 90% of the optimization runs. c) Boxplots after 500 evaluations. d) 99% reliability after 3000 evaluations.

II.2.4 Comparing UMDA with EA

The EA used here, and whose core originates from (Irisarri, 2010; Irisarri et al., 2009) and was applied in (F.-X. Irisarri et al., 2011), is specialized for laminate optimization. The EA is presented in Algorithm 2. It shares the same general structure as the algorithm developed in Chapter I. These two algorithms differ from the encoding of the solutions and their initialization and variations operators. The EA that is compared in the following with UMDA is intended for the optimization of a single laminate. The algorithm is able to deal with the usual laminate design guidelines (see Section I.2), a feature that is not implemented in UMDA. Three variation operators are implemented: crossover, mutation and permutation. To handle design guidelines, these operators have been devised according to the general principles presented in Section I.4.3. In the present application however, no design guidelines are handled through the operators. Hence, the operators are described hereafter in their most simple form. The crossover operator consists in exchanging between two parent laminate a sublaminate defined by two cutting points. The mutation operator gives a randomly chosen value in the set of allowed ply orientations to a randomly chosen ply. Finally the permutation executes a random permutation of a randomly chosen 3-ply sublaminate.

Algorithm 2. Evolutionary algorithm (EA).

Set λ, the size of population x
Set N_a size of the archive population
Set P_c, P_m, P_p, the probability of crossover, mutation and permutation respectively

Initialize x_a as an empty population
Initialize x as a random population

while not stop **do**
    Calculate objective $f(x)$
    Calculate fitness $C(x)$ relevant to $f(x)$ as stated in Chapter I
    $x_a \leftarrow$ Update the archive population x_a with the best N_a solutions from $x \cup x_a$
    Fill the mating pool from x_a using modified binary tournament selection
    $x \leftarrow$ Reproduction phase: apply the variation operators to the mating pool
    $t \leftarrow t + 1$
end while

In order to compare EA and UMDA, the parameters of the EA are tuned for the plate buckling maximization problem. While EA has mutation operators available, UMDA does not and may suffer from sampling errors: any deletion of $\pm 45°$ plies cannot be recovered in UMDA. A first attempt is performed with the population size λ arbitrarily set to 30 based on previous experience. Several settings are compared with different values of archive size N_a and probabilities of crossover P_c, mutation P_m and permutation P_p. These four parameters drive the trade-off between exploration and intensification of the search with this algorithm. The results obtained are presented in Figure 34. All optimizations have been repeated 50 times. The stopping criterion is set to a maximum number of 1500 evaluations.

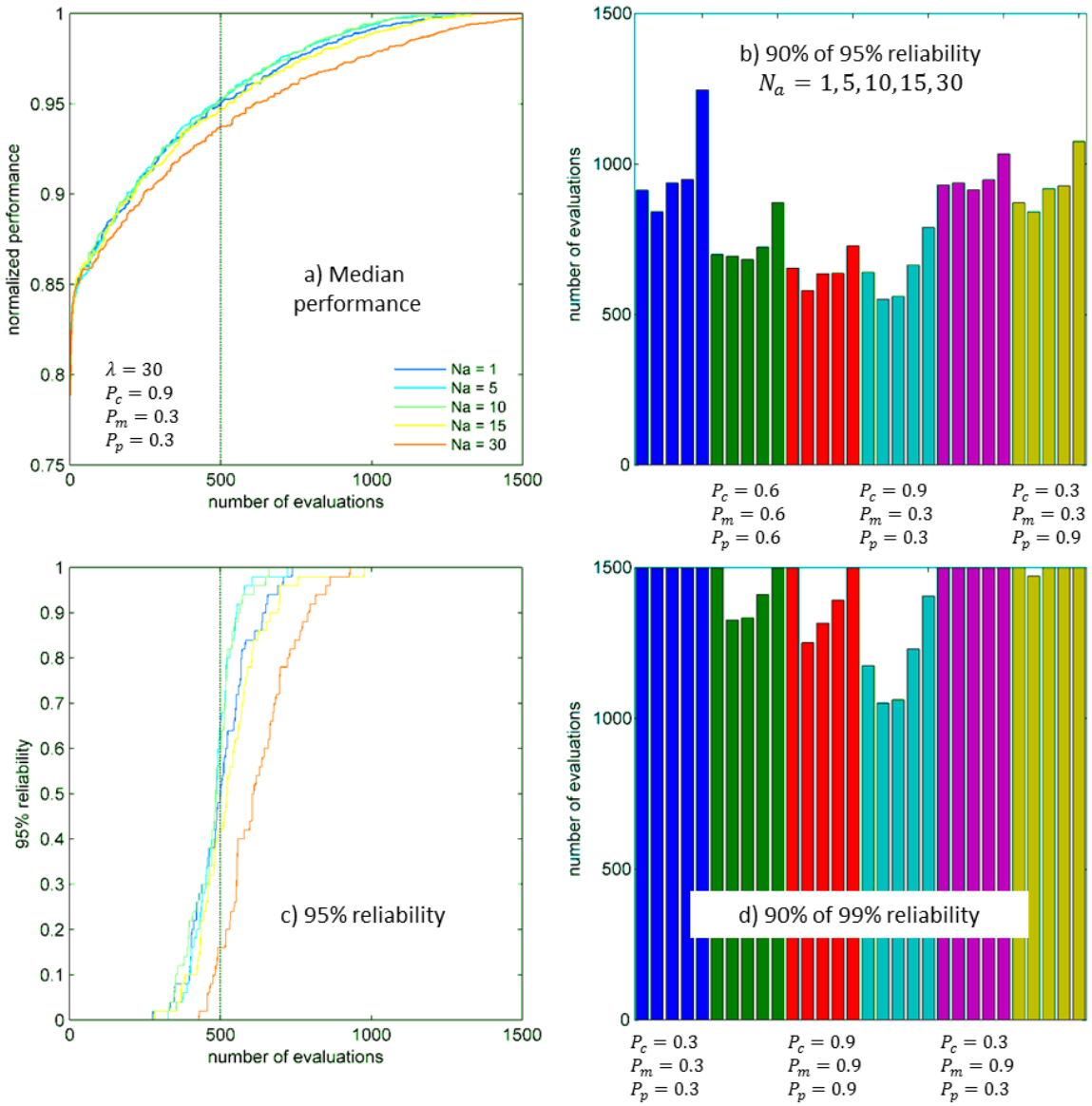

Figure 34. a) Median performance curves for several archive population size, all other parameters fixed. b) Number of evaluations required to reach 95% of reliability for 90% of the optimization runs. c) 95% reliability curves. d) Number of evaluations required to reach 99% of reliability for 90% of the runs. Reliability is considered as not reached if the number of evaluations exceed 1500.

Due to the number of parameters to consider, tuning EA turns out to be much more challenging than tuning UMDA. Nonetheless, Figure 34 exhibits two clear tendencies. First, high crossover probability $(P_c = 0.9)$ with lower mutation and permutation rate $(P_m = P_p = 0.3)$ provides the most efficient and reliable search among the tested settings. This is a non-surprising result for an EA since the crossover operator is used to intensify the search by exchanging sublaminates between two solutions while the mutation and permutation operators are used to explore the design space by generating new sublaminates in the population. This is true only for non-deceptive problems, i.e. problems that are not misleading for the EA. Second, settings with a ratio N_a/λ included between $1/6$ to $1/3$ give the best results. A parallel can be made between

this ratio and the selection ratio in UMDA. Both ratios drive the emphasis that is placed on the best solutions found so far in the generation of the next population.

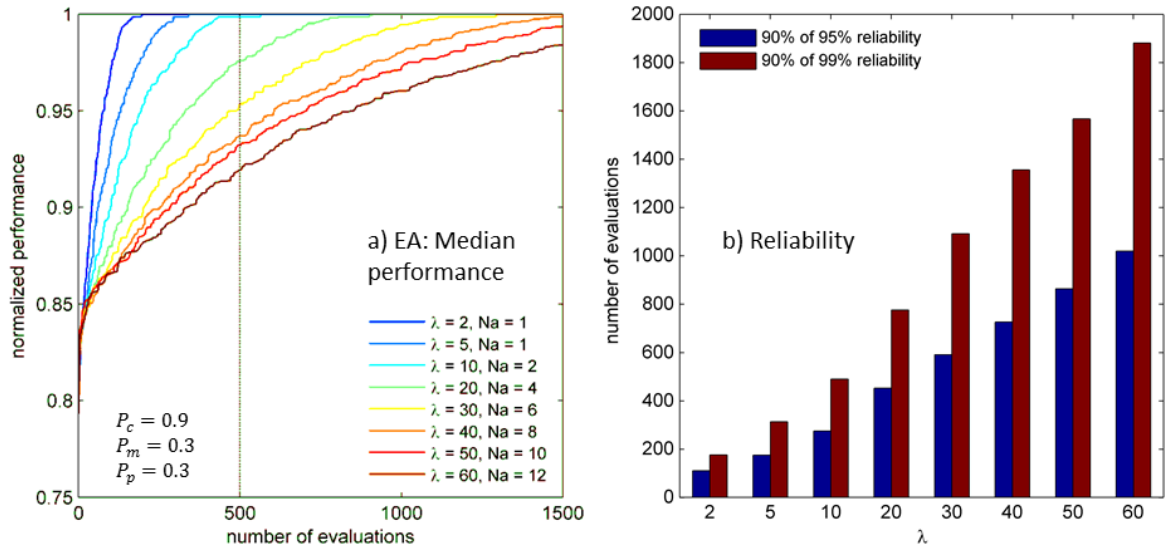

Figure 35. a) Median performance curves for several archive and current population sizes. b) Number of evaluations required to reach 95% and 99% of reliability for 90% of the optimization runs.

Having determined satisfactory settings for the probability of occurrence of the variation operators and the ratio between the size of the archive population and the current population, it is tempting to go back to the tuning of the current population size λ itself. Figure 35 shows the results obtained with varying population size λ and a ratio N_a/λ set to $1/5$ whenever possible. The efficiency of the search varies significantly. The most efficient search is achieved with the smallest population. With $\lambda = 2$ and $N_a = 1$, less than 200 evaluations are required to reach 99% reliability in 90% of the optimization runs. This result gives an insight on both the algorithm and the test problem. With such settings, the EA behaves more or less like a Stochastic Hill-Climbing (SHC) algorithm always trying to improve the best solution found so far by application of the variation operators. The fact that such an algorithm performs so well on the plate buckling maximization problem with $n = 32$ design variables suggests that the problem is much more regular than it seems at first sight. A similar result was obtained in (Grosset, 2004) for the maximization of the first natural frequency of a plate for which the hill-climbing algorithm showed very good performances with respect to UMDA and a generic GA. The buckling maximization and first natural frequency maximization problems are very similar for a plate. However, the number of variables differs from the former study (i.e. 8 or 15 design plies only). The regularity of the plate buckling maximization problem will be analyzed in more details in Section II.4.

The relative efficiency of the settings $\lambda = 2$ and $N_a = 1$ is probably specific to the problem. Thus, both this setting and the more generic one $\lambda = 30$ and $N_a = 6$ are used in the following, based on our past experience of the algorithm.

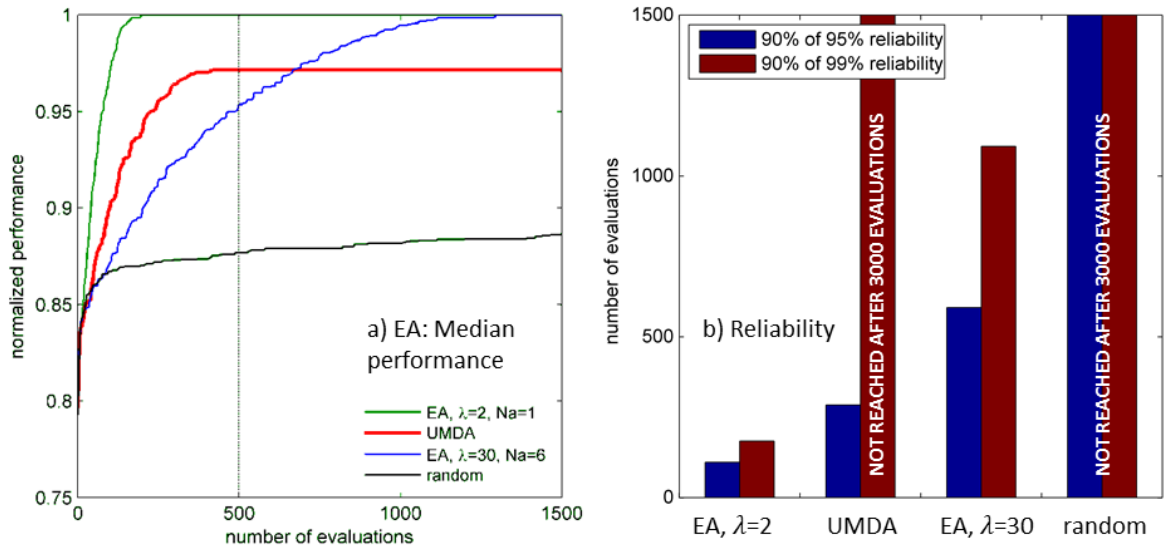

Figure 36. Comparison between UMDA, EA and random search. a) Convergence curves on median performances and b) number of solutions required to reach 95% and 99% of reliability for 90% of the optimization runs.

Figure 36 compares the results obtained with UMDA, the EA and a random search algorithm. UMDA is run here with setting $\lambda = 40$ and $\mu = 10$ determined in subsection II.2.3. The figure shows that with respect to the EA with its generic setting, UMDA achieves a more intensive search around the best points ever reached. However UMDA never reaches 99% reliability, contrary to the EA which proves very efficient here in finding the optimal solution with accuracy although this is not the best quality of evolutionary algorithms in general. Note that the median best performance achieved with the random search is quite high (about 0.88). The lower bound on the normalized performance is achieved for the unidirectional 90° laminate and is about 0.29.

The settings determined in this section are propagated in the next sections of this chapter even if nothing ensures that these parameter settings are the best ones for all the problems. Indeed, some problems require more exploration capabilities (for instance, in case of multiple local optima) while others, such as the plate buckling problem, allow more intensification in the search. In the next section, various features are implemented in UMDA in order to overcome its tendency to premature loss of diversity during the search and gain further insight in the trade-off between exploration and exploitation and how to control it.

II.3 Exploration versus exploitation in UMDA

In this section, three additional features are implemented into UMDA and tested. The purpose is to improve the behavior of the algorithm and overcome its tendency to get trapped into suboptimal solutions because of premature loss of diversity into the current population. Two mechanisms already suggested in (Grosset, 2004) are tested here with different implementations: uniform random mutation and elitism. A third method is proposed, in an attempt to add a second guiding mechanism within the algorithm based on repulsion with respect to the least performing solutions found.

II.3.1 Introducing uniform random mutation into UMDA

Results obtained in Section II.2 show that design variable values tend to disappear prematurely from the probability mass function $p(x)$, resulting in convergence towards suboptimal solutions. To overcome this tendency, the idea is to enforce a minimal probability p_{min} for all possible values of the design variables. The probability density generated by the algorithm can be expressed as:

$$P(x_i = \theta_j) = \frac{p_{min}}{m} + (1 - p_{min}) N_i^j \qquad \text{II-3}$$

where N_i^j is the frequency of appearance of the value θ_j in position x_i among the selected μ best solutions:

$$N_i^j = \frac{\sum_{k=1}^{\mu} \mathbb{I}(x_i^{k:\lambda} = \theta_j)}{\mu} \qquad \text{II-4}$$

with $\mathbb{I}()$ the characteristic functions that is equal to 1 when the condition between brackets is satisfied and 0 otherwise. Algorithm 3 and Algorithm 3.1 present a possible implementation of the uniform random mutation into UMDA. Algorithm 3 details the way the overall UMDA is modified and Algorithm 4 shows how the mutation is performed. Design coordinates are selected with probability p_{min} to be mutated with respect to a random uniform distribution $U[0,1]$.

The parameter p_{min} provides an efficient control parameter on the exploration capabilities of the algorithm. Figure 37shows the results obtained with UMDA for several values of p_{min} ranging from 0 (the classical UMDA tested in Section II.2) to 1 (random search). Population size and selection ratio are set to $\lambda = 40$ and $\tau = 1/4$ respectively. Figure 37.a shows that very fast initial convergence rates are achieved for $p_{min} \in [0.01; 0.10]$. For that range of values, Figure 37.b shows that 95% reliability is achieved within about 300 evaluations. The more restrictive criteria of 99% reliability is reach in about 1000 evaluations for $p_{min} \in [0.02; 0.06]$. The optimum lies around $p_{min} = 0.05$. Larger values may degrade the convergence speed even if the optimum would eventually be reached. These results show that the proposed mutation mechanism is an efficient way to overcome the main defect of the standard UMDA and comfort the conclusions drawn in (Grosset, 2004) with a somewhat less readable "adjacent mutation" algorithm in which

variables can only be mutated to neighboring values (e.g. a 30°-ply can be changed to 15°-ply or 45°-ply only). The 99%-reliability is very sensitive to random mutation. It cannot be reached within 3000 evaluations without mutation since some of the ±45° are lost locally in the laminate, especially near the mid-plane where buckling load factor is less affected by ply orientation.

Algorithm 3. UMDA with uniform random mutation.

Set λ, the population size
Set μ, the number of points considered as good in the population
Set p_{min} the probability of random mutation

Initialize $p(x)$ as a uniform distribution: $p^0(x) = U(x)$

while not stop **do**
  for $i = 1$ to λ **do**
    Sample $p^t(x) \rightarrow x^i$ by taking randomly $x_j^i = \theta_j$ with probability $p^t(\theta_j^i)$
    $x^i \leftarrow$ **Algorithm 3.1. Uniform random mutation**
  end for
  Calculate $f(x)$
  Calculate the ordered indices $i{:}\lambda$, such as $f(x^{1:\lambda}) \geq f(x^{2:\lambda}) \geq \cdots \geq f(x^{\lambda:\lambda})$
  Update $p^t(x)$ from $\{x^{1:\lambda}, f(x^{1:\lambda}), \ldots, x^{\mu:\lambda}, f(x^{\mu:\lambda})\}$
  $t \leftarrow t + 1$
end while

Algorithm 3.1. Uniform random mutation.

Inputs: x^i, p_{min}

for $j = 1$ to n **do**
  $u \sim U[0,1]$
  if $u \leq p_{min}$ **do**
    create x_j^i randomly in $\mathcal{S}$
  end if
end for

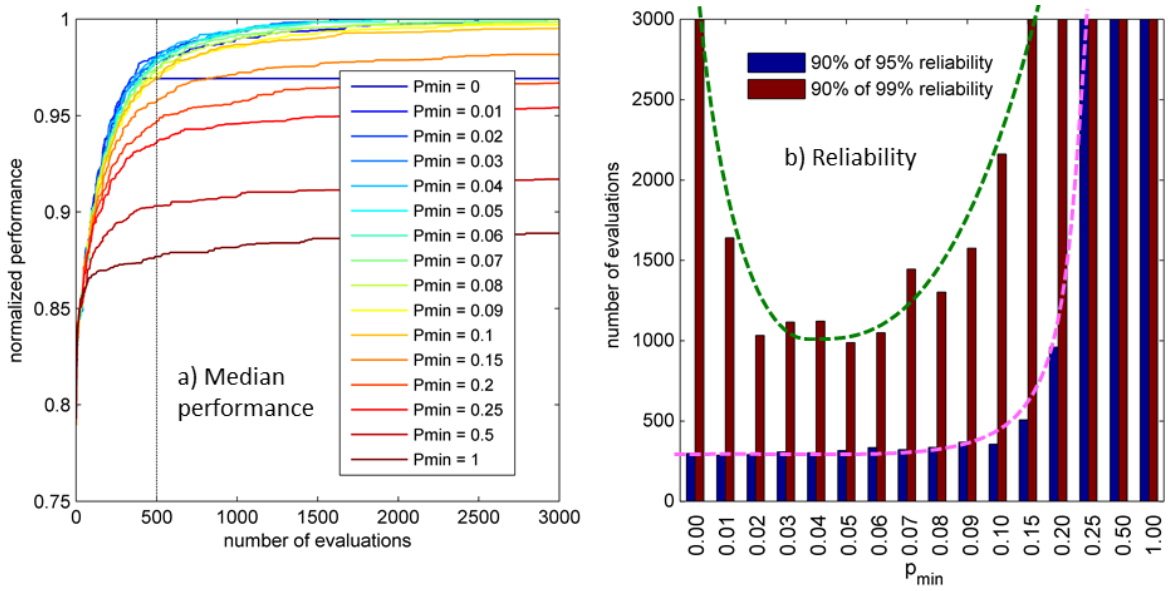

Figure 37. Influence of the mutation probability on a) the convergence and b) the reliability of UMDA.

II.3.2 Introducing elitism into UMDA

With the current mechanisms, intensification of the search in a promising region of the search space relies on the distribution of the previous solutions only. As exploration capabilities were slightly extended in the previous section, attention is now focused on the exploitation capabilities of the algorithm. Elitism is a classical strategy to increase exploitation capabilities of stochastic algorithms around the most promising solutions. The idea is that good solutions should not be lost during the search process. Within the EA used as reference algorithm in this work, elitism is enforced through an archive population constituted of the best solutions found. Generation after generation, the selection for reproduction is applied on the union of the best part of the current population and the archive population. Thus, the implicit probability distribution sampled by the variation operator is biased towards the most promising regions identified in the design space. The method is transposed to UMDA in Algorithm 4 in which the probability mass function is learnt based on the union of the μ best solutions in the current population and the archive population.

Note that all solutions contained in the archive population are unique in the primary design space.

Algorithm 4. Elitist UMDA with uniform random mutation

Set λ, the population size
Set μ, the number of points considered as good in the population
Set p_{min} the probability of random mutation
Set N_a size of the archive population

Initialize $p(x)$ as a uniform distribution: $p^0(x) = U(x)$
Initialize x_a as an empty population

while not stop **do**
  for $i = 1$ to λ **do**
    Sample $p^t(x) \rightarrow x^i$ by taking randomly $x_j^i = \theta_j$ with probability $p^t(\theta_j^i)$
    $x^i \leftarrow$ **Algorithm 3.1. Uniform random mutation**
  end for
  Calculate $f(x)$
  Calculate the ordered indices $i{:}\lambda$, such as $f(x^{1:\lambda}) \geq f(x^{2:\lambda}) \geq \cdots \geq f(x^{\lambda:\lambda})$
  Update the archive population x_a with the best n_a solutions from $x \cup x_a$
  Update $p^t(x)$ from
  $\{x^{1:\lambda}, f(x^{1:\lambda}), \ldots, x^{\mu:\lambda}, f(x^{\mu:\lambda})\} \cup \{x_a^1, f(x_a^1), \ldots, x_a^{n_a}, f(x_a^{n_a})\}$
  $t \leftarrow t + 1$
end while

The influence of the size n_a of the archive population was studied in the present study and showed no significant variation of the influence of n_a on the behavior of the algorithm in the range 1 to μ. Thus, the size of the archive population is set to $n_a = 1$ in the following. The interesting point here is to study the influence of always maintaining the best found design solution within the population on the ability of the algorithm to find the optimum with accuracy, i.e. on the 99% reliability, and on its behavior with respect to the mutation probability p_{min}.

Figure 38.b shows the influence of the mutation probability on the number of evaluations required to reach 90% of 95% reliability and 90% of 99% reliability respectively when an archive population of size 1 is used. The results are compared with the results obtained without archive population presented in Figure 37.b. The comparison is realized by copying the tendency curves drawn in Figure 37.b to Figure 38.b. It is clear from that comparison that elitism, as implemented here, improves the 95% reliability of the algorithm for high values of the mutation probability with p_{min} ranging from 0.15 to 0.25. In parallel, the 99% reliability is improved for p_{min} in between 0.02 and 0.10, the most significant improvement being achieved for a mutation probability greater or equal than 0.07. Thus, elitism has a beneficial influence on the precision of the algorithm. It also somewhat balances the enhanced exploration capability offered by mutation, allowing for higher values of mutation probability.

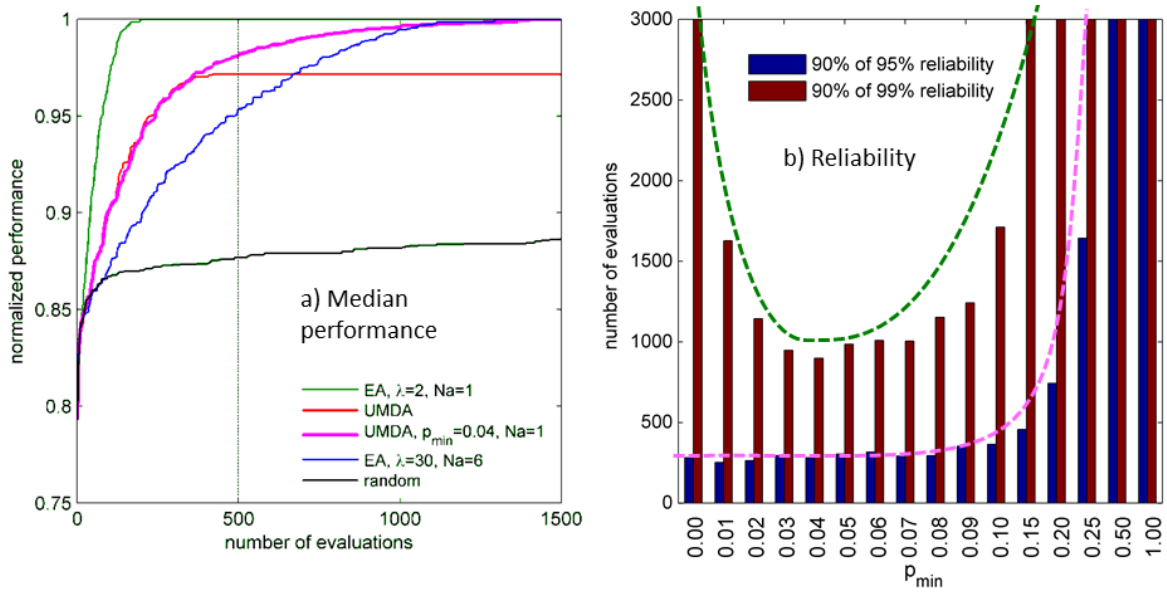

Figure 38. a) Comparison between UMDA, elitist UMDA with mutation, EA and random search: convergence curves of median performances. b) Influence of the mutation probability on the reliability of the elitist UMDA with mutation. Tendency curves correspond to UMDA with mutation (see Figure 37.b).

No influence on convergence rate could be observed. Elitism influences the reliability of the search only. This influence could not be identified in (Grosset, 2004). Figure 38.a compares the curves of convergence of the elitist UMDA with mutation with respect to the standard UMDA, the EA and a random search (see Figure 36.a). All curves are computed over 50 runs. The improvement brought to the standard UMDA is clear. The tendency to premature loss of diversity is corrected thanks to mutation. Elitism slightly improves the precision of the algorithm. By comparison, the EA specialized for laminate optimization offers more freedom in controlling the trade-off between exploration and intensification of the search through its settings. A major difference between EA and UMDA lies in the permutation and the crossover operators that the EA benefits from. Thanks to these operators, the EA can take more diverse paths leading to the best designs. In the present case, a much more efficient search can be achieved with proper setting of the EA than with the enriched UMDA. Nonetheless, the EA has more operators than UMDA, hence more parameters to tune. Setting in this algorithm may be a difficult task when it comes to solve practical engineering problems.

Note that all solutions contained in the archive population are unique in the primary design space.

II.3.3 Guiding UMDA away from low performing designs

In order to further improve the behavior of UMDA and gain insight in the behavior of such probability distribution-based algorithms, an attempt is made to introduce a memory of the worst solutions generated during the whole optimization process. The tested implementation of the method within UMDA is described in Algorithm 5. The idea is to sample a large population of size κ from the density of probability $p(x)$. The population is filtered based on the memory of the worst solutions found in order to eliminate the least promising designs. λ solutions are kept

and evaluated. The μ best performing solution are used to update $p(x)$ and the whole process is repeated. Elitism is not enforced here but mutation is.

Algorithm 5.2 details how memory of the worst performing solutions is built through a density of probability $p_w(x)$ analogous to the density of probability (x) : $p_w(x)$ is the product of the univariate marginal densities of the worst designs However, $p_w(x)$ is not learnt on the current population but on the least performing designs of the complete history of the evaluated solutions during the optimization. This proportion is defined by the quantile q. Algorithm 5.1 details the way the solutions are classified according to $p_w(x)$ and subsequently filtered. Such implementation requires more parameters related to the eviction of the worst solutions. Here the quantile q represents the threshold in the estimation of the probability distribution of the worst solutions. Suppressing solutions implies compensating the loss with larger samples of size κ.

Algorithm 5. UMDA with avoidance of worst performing solutions.

Set κ, the population size
Set λ, the number of evaluated solutions
Set μ, the number of points considered as good in the population
Set p_{min} the probability of random mutation
Set q, the quantile of acceptable solution

Initialize $p(x)$ as a uniform distribution: $p^0(x) = U(x)$
Initialize $p_w(x)$ as a uniform distribution: $p_w^0(x) = U(x)$

while not stop **do**
  for $i = 1$ to κ **do**
    Sample $p^t(x) \rightarrow x^{\mathrm{i}}$ by taking randomly $x_j^i = \theta_j$ with probability $p^t(\theta_j^i)$
    $x^i \leftarrow$ **Algorithm 3.1. Uniform random mutation**
  end for
  $x \leftarrow$ **Algorithm 5.1. Selection based on p_w**
  Calculate $f(x)$
  Calculate the ordered indices $i{:}\,\lambda$, such as $f(x^{1:\lambda}) \geq f(x^{2:\lambda}) \geq \cdots \geq f(x^{\lambda:\lambda})$
  Update $p^t(x)$ from $\{x^1, f(x^1), \ldots, x^\mu, f(x^\mu)\}$
  $p_w^t(x) \leftarrow$ **Algorithm 5.2. Update p_w**
  $t \leftarrow t + 1$
end while

Algorithm 5.1. Selection based on p_w.

Inputs: x, λ, p_w

1: **for** $i = 1$ to κ **do**
2: $g(x^i) = \prod_{j=1}^{n} p_w(x_j^i)$
3: **end for**
4: Calculate the ordered indices $i{:}\kappa$, such as $g(x^{1:\kappa}) \leq g(x^{2:\kappa}) \leq \cdots \leq g(x^{\kappa:\kappa})$
5: $x \leftarrow$ Select the first λ solutions, $1{:}\kappa$ to $\lambda{:}\kappa$

Algorithm 5.2. Update p_w.

Inputs: x, f, q, p_w

1: Update the value f_q of the quantile q based on all evaluated solutions
2: Update $p_w(x)$ from $x \mid f(x) \leq f_q$

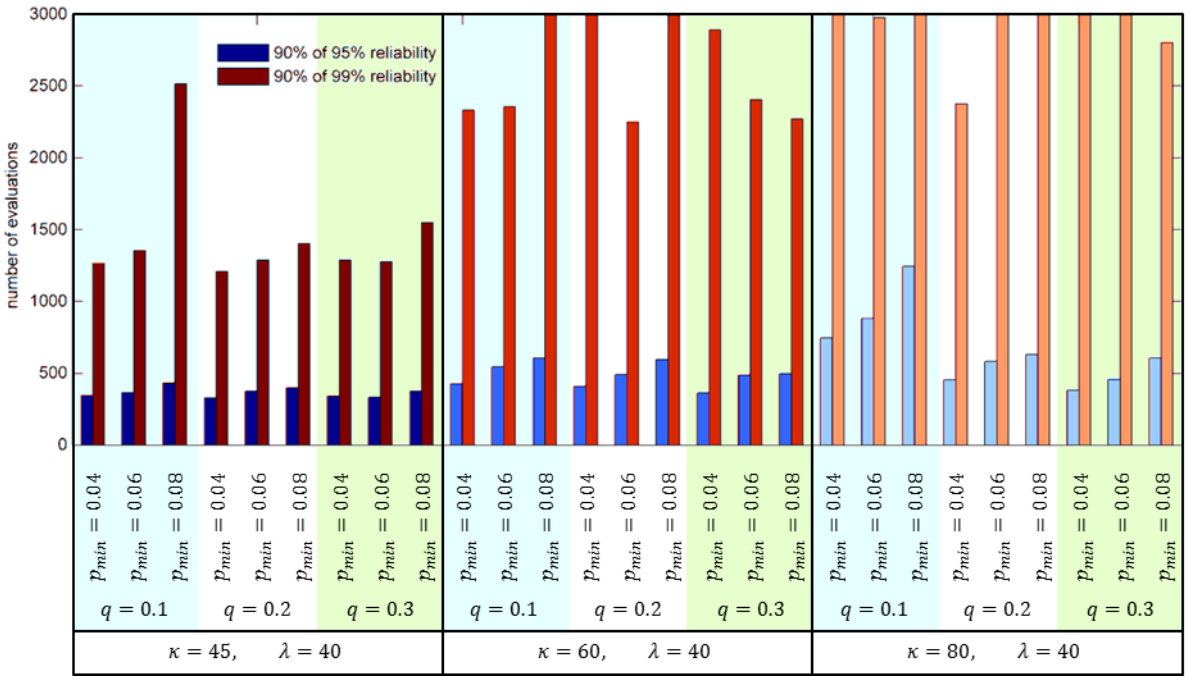

Figure 39. Evolution of the cost of reliability (in number of evaluations of the objective function) of the algorithm for various settings (κ, q, p_{min}).

Figure 39 shows the results obtained for various settings of the algorithm. The results are disappointing. It can be seen that the more filtering is applied, the more the 95% reliability is costly to achieve. Increasing the probability of mutation also degrades the cost to achieve the expected reliability of the algorithm. The influence of the filtering increases with the number of solutions eliminated. It turns out that small values of q are detrimental (for instance when $q = 0.1$, $p_w(x)$ is learnt on 10% of the history of the evaluated solutions). For higher values of q, the influence quickly fades. Results about 99% reliability show no exploitable tendency.

The overall impression is that the method significantly degrades the behavior of the algorithm. It is however difficult to decide whether the method itself fails or the failure is specific to the adaptation of the method to the test case under consideration. As a matter of fact UMDA quickly converges towards good solutions on the plate buckling maximization problem. Thus, it is necessary to impose a very high performance level on the learning of $p_w(x)$ to filter unpromising solutions before their evaluations. Consequently $p_w(x)$ and $p(x)$ can easily become very similar and the overall behavior of the algorithm is degraded. Additionally, even if $p_w(x)$ is correctly learned, filtering the solutions based on $p_w(x)$ is a not a straightforward task. The present study has failed in building a function $g(x)$, based on $p_w(x)$, see Algorithm 5.1 with a sufficient correlation with the cost function $f(x)$ to actually enable efficient filtering of the least promising solutions. This $p_w(x)$ distribution based algorithm may learn a few optimal or near optimal plies because early in the search these positive plies' effects were muted by other plies with negative effect in the laminate. According to the current implementation, the algorithm may not recover from this wrong start as: (i) it rarely generates worst designs so $p_w(x)$ does evolve much over time and (ii) this initial $p_w(x)$ will prevent the algorithm from generating again these positive effect plies because the filter acts before the computation of the objective function. Finally, maintaining two probability distributions of different meaning and use on the same set of variables turns out to be a complex task, if not irrelevant when using products of univariate marginal distributions. In the next section, the use of two distributions to guide the search is addressed based on two different sets of variables.

II.4 The Double Distribution Optimization Algorithm

The use of products of marginal distributions to approximate the actual probability density of an engineering problem is a strong assumption, since coupled effects between variables are neglected. Additionally, the response of a system may often be more regular with respect to some quantities $v_{k=1,\dots,d}$ determined at a more global level of analysis than with respect to design variables $x_{i=1,\dots,n}$. This is especially the case for laminated composite structures with macroscopic stiffness related values, i.e. the laminate stiffness matrices ABD (Berthelot, 1992), the lamination parameters (Gürdal et al., 1999; Tsai and Hahn, 1980) or the polar parameters of the laminate (Vannucci, 2005; Verchery, 1982). Basically, these quantities express some of the joint actions of the optimization variables. They can also be calculated at a negligible computational cost. In an attempt to relax the composite design problem difficulty, we will consider them as continuous (although being functions of discrete variables, they are not continuous): this will allow building kernel-based joined probability densities in the space of auxiliary variables without introducing a large number of additional parameters. Additionally, the number of quantities $v_{k=1,\dots,d}$ is independent of the number of plies of the laminate. Thus, these quantities allow capturing the elastic response of the laminate design problem with a reduced number of variables.

The idea of combining two probability models to guide the search, one for the primary variables x_i and one for the auxiliary variables v_k was first proposed for laminate optimization and implemented in the so-called DDOA in (Grosset, 2004). As stated in (Grosset et al., 2006), exploiting an auxiliary distribution to guide the algorithms in composite optimization problems has mathematical motivation – the need for couplings between variables using independent

distributions – and engineering motivation – the need for expert knowledge in the optimization process. Algorithm 6 presents the version of DDOA implemented in this study. The algorithm is based on the elitist UMDA with mutation described by Algorithm 4. The proposed DDOA follows the conclusions drawn by Grosset concerning (i) the way to model the auxiliary distribution and (ii) the strategy used to create populations of points reflecting the primary distribution $p_x(x)$ and the auxiliary distribution $p_v(v)$.

The two distributions $p_x(x)$ and $p_v(v)$ are learnt on the union of the μ most performing points of the current population and the archive population. The distribution $p_v(v)$ is described here using a very simple multivariate Kernel Density Estimation method (KDE). An isotropic Gaussian kernel is placed at each sample point. Thus, the distribution $p_v(v)$ is obtained as:

$$p_v(v) = \frac{1}{\mu + n_a} \sum_{i=1}^{\mu+n_a} K(v - v_i) \qquad \text{II-5}$$

with the kernels:

$$K(v - v_i) = \frac{1}{\left(\sqrt{2\pi}\,\sigma\right)^d} exp\left(-\frac{(v - v_i)^T (v - v_i)}{2\,\sigma^2}\right) \qquad \text{II-6}$$

where d is the dimension of the auxiliary space $\mathcal{V}$ and σ^2 is the variance of the distribution. Determining a good value for the bandwidth σ is a difficult task that can dramatically affect the quality of the density estimate. In the following the bandwidth is set to $\sigma = 0.15$ since it is shown in (Grosset, 2004) that stable and satisfactory behavior of the algorithm could be obtained in the range 0.1 to 0.2 on similar test problems to the plate buckling maximization problem. The bandwidth determines the smoothness of the density estimate. Small values of σ result in an estimate that quickly falls to nearly null probabilities away from the data points used as kernel centers. On the contrary, large values result in very uniform distributions of probability. Once the bandwidth determined, the only additional parameter of DDOA is the threshold ε.

Algorithm 6. DDOA (with archive population and uniform random mutation)

Set λ, the population size
Set μ, the number of points considered as good in the population
Set p_{min} the probability of random mutation
Set N_a size of the archive population
Set ε, the threeshold distance in auxiliary space

Initialize $p_x(x)$ and $p_v(v)$ as a uniform distributions
Initialize x_a as an empty population
Initialize x by sampling $p_x^0(x)$

1: **while not** stop **do**
2: **for** $i = 1$ to λ **do**
3: $v^{target} \backsim p_v^t(v)$
4: $x^i \leftarrow$ **Algorithm 6.1. Sample** $\boldsymbol{p_x(x^i \mid v(x^i) = v^{target})}$
5: **end for**
6: Calculate $v(x)$
7: Calculate $f(x)$
8: Calculate the ordered indices $i{:}\lambda$, such as $f\left(x^{1:\lambda}\right) \geq f\left(x^{2:\lambda}\right) \geq \cdots \geq f\left(x^{\lambda:\lambda}\right)$
9 Update the archive population x_a with the best n_a solutions from $x \cup x_a$
10: Update $p_x^t(x)$ from $\left\{x^{1:\lambda}, f\left(x^{1:\lambda}\right), \ldots, x^{\mu:\lambda}, f\left(x^{\mu:\lambda}\right)\right\} \cup \left\{x_a^1, f(x_a^1), \ldots, x_a^{n_a}, f\left(x_a^{n_a}\right)\right\}$
11: Update $p_v^t(x)$ from $\left\{x^{1:\lambda}, f\left(v^{1:\lambda}\right), \ldots, v^{\mu:\lambda}, f\left(v^{\mu:\lambda}\right)\right\} \cup \left\{x_a^1, v(x_a^1), \ldots, x_a^{n_a}, v\left(x_a^{n_a}\right)\right\}$
12: $t \leftarrow t + 1$
13: **end while**

The strategy to generate populations reflecting both primary and auxiliary distributions is based on the use of target points in the auxiliary space. Each time a new design has to be sampled in primary space, a target in auxiliary space is first sampled from $p_v(v)$. Candidate points are subsequently sampled in primary space from $p_x(x)$ using a roulette wheel method. The candidate design is then altered by mutation. Distance to the target is computed in the auxiliary space $\mathcal{V}$ and the process is repeated until a design is found located within a distance ε to the target. The method is detailed in Algorithm 6.1.a.

Algorithm 6.1.a. Sample $\boldsymbol{p_x(x^i \mid v(x^i) = v^{target})}$

Inputs: x, v, v^{target}, p_{min}, ε

1: **while not** stop **do**
2: Sample $p_x^t(x) \rightarrow x^{\mathrm{i}}$ by taking randomly $x_j^i = \theta_j$ with probability $p^t\left(\theta_j^i\right)$
3: $x^i \leftarrow$ **Algorithm 3.1. Uniform random mutation**
4: Return x^{i} and Stop if $\left\|v\left(x^i\right) - v^{target}\right\| \leq \varepsilon$
5: **end while**

Algorithm 6.1.a raises two difficulties. First, determining the distance ε is not straightforward. Depending on the nature of the auxiliary variables considered, units and order of magnitude could differ. For instance, lamination parameters have no dimension and take their values within the range -1 to 1 whereas laminate bending stiffness terms are expressed in [N.mm] and vary with the cube of the total thickness of the laminate. Furthermore the auxiliary space is considered as continuously described when generating the target whereas the primary variables are discrete. For laminate optimization, the sampling of the auxiliary space $\mathcal{V}$ depends on the set of allowed ply orientations what will implicitly define a minimal possible distance to the target, depending on its value. Second, introducing such a *while* condition in the algorithm makes computational time quite unpredictable and could result in infinite loops. Both problems are solved by modifying Algorithm 6.1.a into Algorithm 6.1.b at the expense of losing control on the distance between targeted and achieved auxiliary variables. The minimal distance condition is discarded. A candidate population of size η is sampled from $p_x(x)$ and and the closest solution to the target is selected. This operation is repeated λ times. The parameter η is directly related to the overall computational time and its setting has a clear influence on the behavior of the algorithm as will be shown in the following.

Algorithm 6.1.b. Sample $p_x(x \mid v(x) = v^{target})$ – minimal distance to v^{target}

Inputs: $p_x(x),\ v^{target},\ \eta,\ p_{min}$

1: **for** $k = 1$ to η **do**
2: Sample $p_x^t(x) \rightarrow x^k$ by taking randomly $x_j = \theta_j$ with probability $p^t(\theta_j^i)$
3: $x^k \leftarrow$ **Algorithm 3.1. Uniform random mutation**
4: **end for**
5: $x = \arg\min_{k=1,\eta} \| v(x^k) - v^{target} \|$

The choice of the auxiliary space $\mathcal{V}$ can be adapted to the physics of the considered problem. In this section, DDOA is tested on the plate buckling maximization problem described in subsection II.2.2. With the closed form solution given in Equation I-2, with fixed laminate thickness and plate dimensions, the buckling load depends on the bending stiffness matrix D of the laminate only. Equation I-2, is written with the assumption that the laminate can be considered as orthotropic in bending (i.e. $D_{16} = D_{26} = 0$). With such assumption, the bending stiffness matrix can be written as a function of the two lamination parameters V_{1D} and V_{3D} as follows:

$$D = \frac{h^3}{12}(\Gamma_0 + \Gamma_1 V_{1D} + \Gamma_3 V_{3D}) \qquad \text{II-7}$$

where h is the total thickness of the laminate. Γ_0, Γ_1 and Γ_3 are 3×3 matrices fully defined by the material invariants of the base ply. The bending lamination parameters V_{1D} and V_{3D} are written:

$$(V_{1D}, V_{3D}) = 12 \int_{-1/2}^{1/2} \bar{z}^2 (\cos 2\theta\,, \cos 4\theta) d\bar{z} \qquad \text{II-8}$$

with $\bar{z}$ the normalized through-the-thickness dimension. Thus, the bending lamination parameters V_{1D} and V_{3D} form a convenient two dimensional auxiliary space for the plate buckling problem. The dimension of the auxiliary space is independent of the dimension of the primary design space, i.e. the number of ply orientations.

Figure 40.b shows the filled contour plot of the normalized critical buckling value with respect to the ply orientations in the case $n = 2$. Laminates are written $[(\theta_1/\theta_2)/-(\theta_1/\theta_2)]_s$. All ±45° angle-ply laminates are optimal. Thus all local optima in the figure are equal to the global optimum. Maximizing the critical buckling load is thus possible with a simple SHC since successive local improvements of a solution lead to a local optimum. This explains the results shown in Figure 35 (where $n = 32$) and the increasing efficiency of the EA with increasing number of generations rather than increasing size of population. Nonetheless, this performance landscape indicates that any ply in the x-space has 2 optima, +45° and -45°. The main issue when solving such problem relies in sampling errors, i.e. premature loss of some 'genes' in p_x and p_v: such algorithms gain convergence speed by higher risks of losing too early some search location possibilities in accordance with the compromise between speed and robustness. But the adhoc implementation (e.g. EA with relevant operators) strikes very efficient compromises. Figure 40.a shows that the normalized critical buckling value is a convex function of the bending lamination parameters.

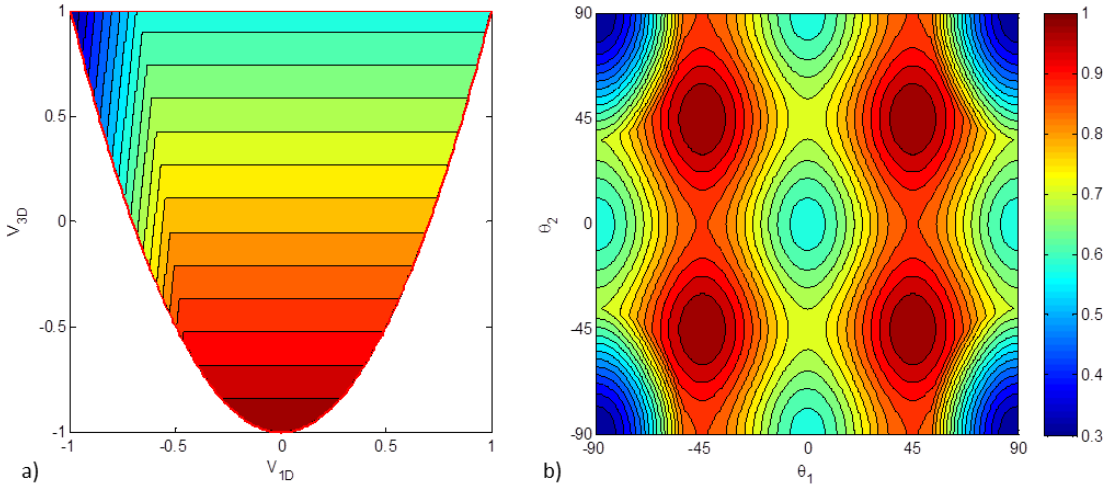

Figure 40. Landscape of the normalized critical buckling factor with respect to a) the bending lamination parameters (for any number of plies), and b) the ply orientations (with $n = 2$ design plies).

Additionally, it is shown in (Grenestedt, 1991) that for any combination of lamination parameters, the feasible region is convex. The equations of the feasible region in the plane (V_{1D}, V_{3D}) are known from (Miki and Sugiyama, 1991):

$$V_{3D} \geq 2V_{1D}^2 - 1 \text{ and } -1 \leq V_{iD} \leq 1 \text{ with } i = 1,3 \qquad \text{II-9}$$

Thus, the plate buckling maximization problem becomes a convex optimization problem in the auxiliary space.

Determining the equations of the feasible domain for any combinations of the 12 lamination parameters in the general case is an open problem. Published work on the topic give further insight into the problem. (Diaconu et al., 2002) proposes a variational method to obtain an implicit approximation of the feasible domain. (Bloomfield et al., 2009) presents a method to compute the convex hull of the feasible region in dimension 12 for any predefined set of angles. (Setoodeh et al., 2006) proposes a numerical method to approximate the convex hull for the combined membrane and bending lamination parameters. (Wu et al., 2013) and (Raju et al., 2014) present new inequality constraints to bound the feasible domain. Another viewpoint on the topic is given by (Vannucci, 2013) who gives the equations of the feasible domain in membrane or bending, without coupling, using the polar method. The point here is that in the general case, the feasible domain in the auxiliary space is difficult to determine. Thus, sampling feasible values only in the feasible domain with a given probability distribution is a complex task. However, with our sampling algorithms, it is not necessary to have feasible auxiliary variables: in the present work no constraints are introduced in the auxiliary space and unfeasible targets can be sampled. Indeed, the Gaussian kernels are of infinite support. A non-feasible target will simply drive the search towards a boundary of the auxiliary space.

Figure 41 shows the evolution of the Euclidean distance from the selected points to their targets in the auxiliary space during the optimization. Figure 41.a presents the results obtained for a single optimization run. Feasible targets and non-feasible targets are differentiated. A significant number of the target points in auxiliary space are unfeasible, what can be explained by the fact the optimal solution lies on the boundary of the feasible region. The figure shows very different distributions of probability depending on whether the target is feasible or not. It is typical that some feasible targets could not be neared. Indeed, since $p_v(v)$ has infinite support, some target points can be sampled in unlikely regions with respect to $p_x(x)$. This illustrates the impossibility to set efficiently a minimal distance ε with Algorithm 6.1.a. Figure 37.1.b illustrates the influence of the parameter η on the probability to fall within a given distance to the target. The higher is η, the most solutions get closer to the target and the higher are the computation costs.

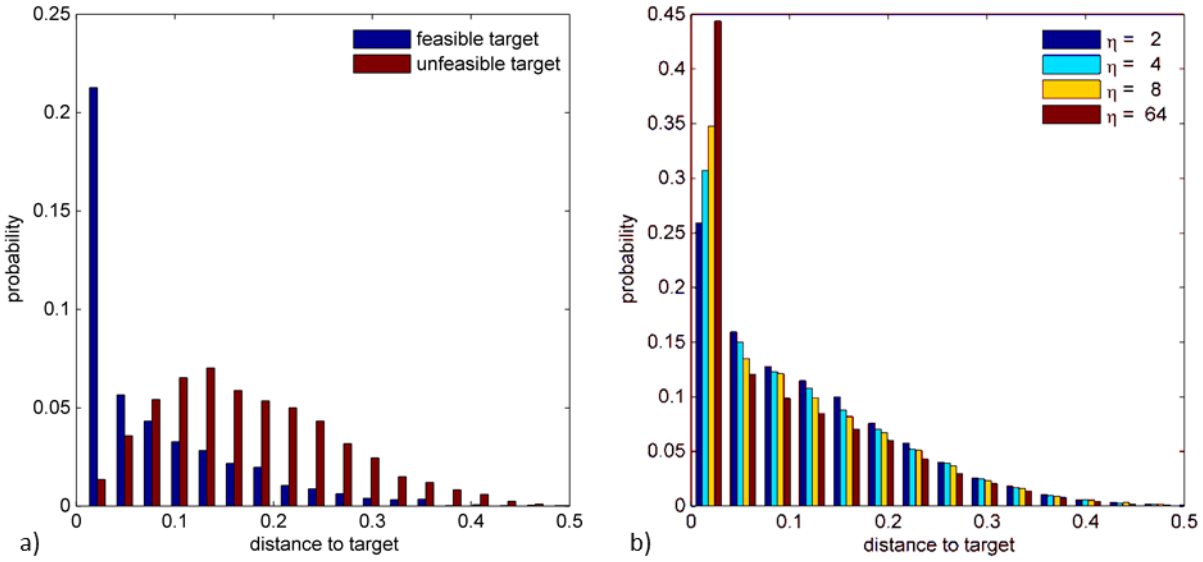

Figure 41. Probability to fall within a given range of distance to the target in auxiliary space: a) depending on the feasibility of the target (one single optimization run, η=2); b) depending on η (50 runs for each value of η).

The efficiency of DDOA with respect to the algorithms previously described is illustrated in Figure 42. Here, η is set to 25, which means that for each evaluation of the critical buckling load of a design, $\lambda \times \mu = 1000$ designs are generated in primary space and evaluated in auxiliary space. The value of η defines a trade-off between the computational cost and how much the newly generated population reflect the auxiliary distribution $p_v(v)$. Nonetheless, in the present case, sampling $p_x(x)$ and computing distances in the two dimensionnal auxiliary space has very low computational costs. Thus, choosing η is rather a matter of efficiency, since Figure 41.b clearly shows that highly increasing η only brings little improvement in terms of distance to the targeted points, especially for the greatest distances. Note that no distinction is made between feasible and unfeasible target points in the figure. Figure 42.a shows that DDOA clearly outperforms the elitist UMDA with mutation, both in terms of convergence rate and accuracy in finding the exact optimum of the problem. In particular, Figure 42.b shows that the reliability of the algorithm is greatly improved. The number of evaluations required to reach 95% of the optimal performance in 90% of the optimization runs is nearly constant over a large range of probability of mutation with p_{min} varying from 0 to 0.25. Nonetheless, the evolution of the number of evaluations required to reach 90% of 99% of reliability shows that enforcing a minimal probability of mutation is still relevant to find the optimum with accuracy. The range of values of p_{min} for which the algorithm shows stable and efficient behavior is still very large, with p_{min} varying from 0.01 to 0.10 approximately.

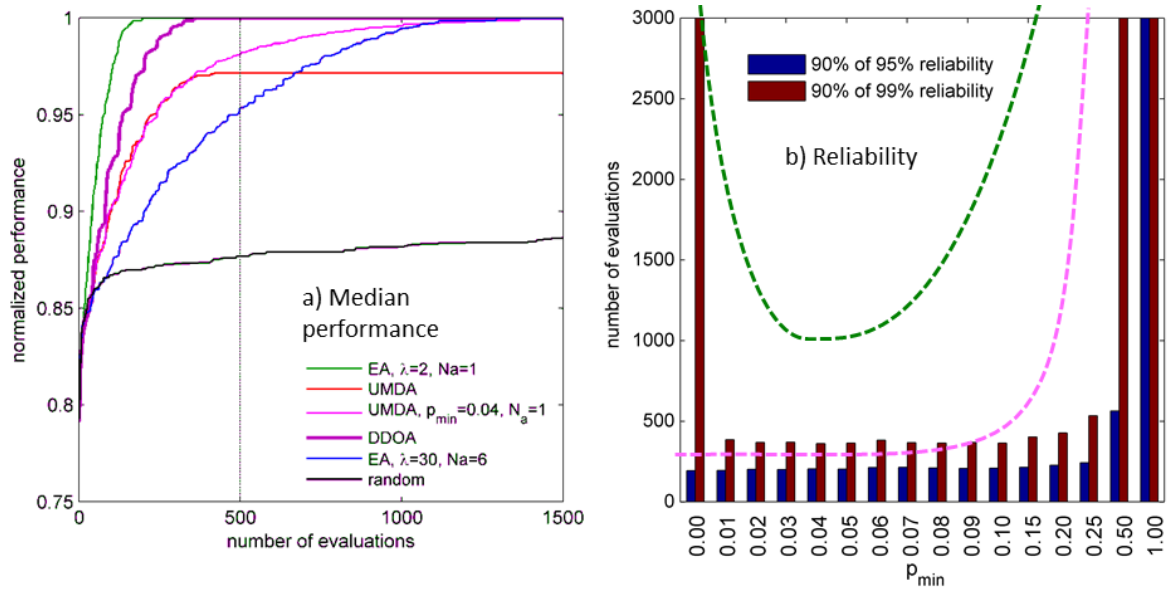

Figure 42. a) Comparison between DDOA and single distribution algorithms: convergence curves of median performances. b) Influence of the mutation probability on the reliability of DDOA. Tendency curves correspond to UMDA with mutation (see Figure 37.b).

Figure 43 shows the evolution of the PMF $p_x(x)$ (without the contribution of the uniform random mutation) and the probability distribution $p_v(v)$ over the first 8 iterations of the algorithm. The distribution $p_v(v)$ is represented over the feasible domain of lamination parameters only. Since the centers of the Gaussian kernels correspond to actual laminate, all the relevant information is contained within the feasible domain. The colorbar ranges from minimal probability in blue to maximal probability in red. Iteration 1 shows a PMF $p_x^1(x)$ close to the initial uniform distribution. The auxiliary distribution $p_v^1(v)$ is learnt on the best solutions of an initial population sampled from a uniform distribution. With 32 plies in the present case, such laminates are close to quasi-isotropic in terms of bending properties. Thus $p_v^1(v)$ is centered on laminates that are close to the central point $V_{1D} = V_{3D} = 0$. The process then converges very quickly towards the optimum that corresponds to ±45° angle-ply laminates in the primary design space, irrespective of the stacking order, and to the point $V_{1D} = 0$ and $V_{3D} = -1$ in the auxiliary space. At iteration 3, the auxiliary distribution is not far from being centered on the optimum. In primary space, convergence is slower, especially for the inner plies (increasing values of j) which have less influence on buckling than the outer plies. Convergence is finally achieved at iteration 8.

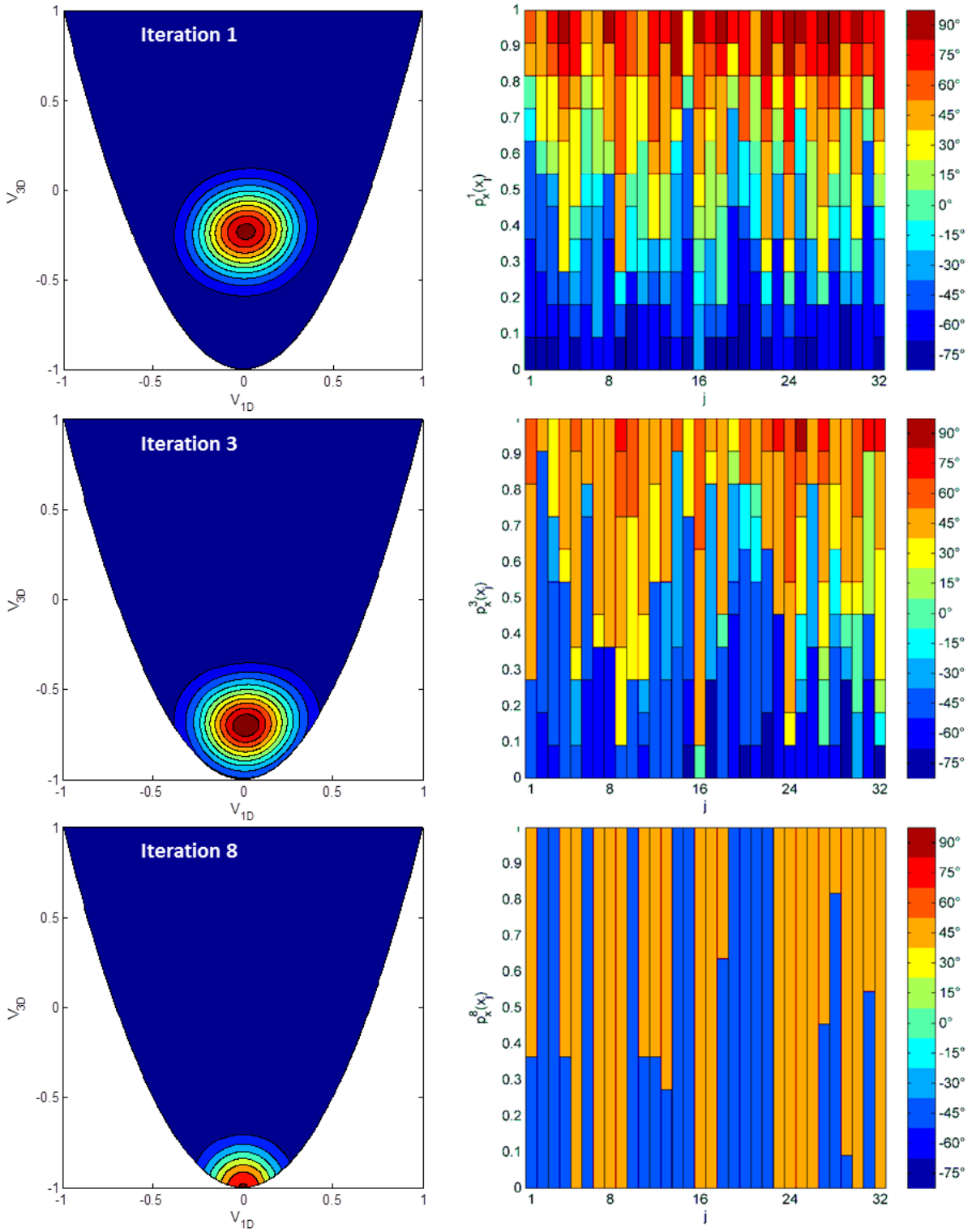

Figure 43. Evolution of $\boldsymbol{p_v(v)}$ (left column) and $\boldsymbol{p_x(x)}$ (right column) towards the optimum during a single run ($\boldsymbol{p_{min} = 0.04,\ \eta = 25}$).

II.5 The Double Distribution Evolutionary Algorithm

Considering (i) the increased efficiency achieved by DDOA with respect to UMDA thanks to the use of the auxiliary distribution, (ii) the satisfactory behavior of the specialized EA and (iii) the amount of effort devoted to devise specific variation operators to handle design guidelines within the EA, in Chapter I and in previous work, the idea of devising a Double Distribution Evolutionary Algorithm (DDEA) analogous to DDOA seems very appealing. Algorithm 7 describes the DDEA implemented in this work. The algorithm is based on Algorithm 2. The auxiliary distribution is learnt on the archive population and described with the same KDE method than previously, with similar settings. Target points in the auxiliary space are used to filter the probability density implicitly defined by the fitness function and the selection operators with respect to the auxiliary distribution (see Algorithm 7.1).

Algorithm 7. DDEA

Set λ, the population size
Set N_a size of the archive population
Set P_c, P_m, P_p, the probability of crossover, mutation and premution respectively
Set η for Algorithm 7.1, with $\eta > 1/\lambda$

Initialize $p_v(v)$ as a uniform distribution: $p_v^0(v) = U(v)$
Initialize x_a as an empty population
Initialize x as a random population

while not stop **do**
    Calculate $v(x)$
    Calculate $f(x)$
    Calculate fitness $C(x)$
    Update the archive population x_a with the best N_a solutions from $x \bigcup x_a$
    Update $p_v^t(x)$ from $\{x_a^1, v(x_a^1), \dots, x_a^{n_a}, v(x_a^{n_a})\}$
    Fill the mating pool from $x \bigcup x_a$ using modified binary tournament selection
    for $i = 1$ to λ **do**
        $v^{target} \backsim p_v^t(v)$
        $x^i \leftarrow$ **Algorithm 7.1. Generate** $x^i \mid v(x^i) = v^{target}$
    end for
    $t \leftarrow t + 1$
end while

Algorithm 7.1. Generate $x^i \mid v(x^i) = v^{target}$

Inputs: v^{target}, η, λ

for $k = 1$ to η **do**
    $x \leftarrow$ Reproduction phase: apply the variation operators to the mating pool
end
$= x = \arg\min_{k=1,\eta} \| v(x^k) - v^{target} \|$

In both Algorithm 6.1.b for DDOA and Algorithm 7.1 for DDEA a population of size $\eta \times \lambda$ is sampled before choosing the closest solution to the target v^{target}. On the one hand, the population size λ is usually set as a function of the number of primary design variables. On the other hand, the parameter η controls the trade-off between generating a population that reflects more the primary distribution (low η values) or the auxiliary distribution (high η values). If $\eta > 1/\lambda$, DDEA degenerates into EA. The influence of η on the precision with which the targets are reached in auxiliary space is provided with Figure 41 in the case of DDOA. Figure 41.b is reproduced here as Figure 44.a to allow for a simple comparison with the analogous data generated with DDEA and presented in Figure 44.b. the comparison shows that it is slightly more difficult to get close to the target in the case of DDEA. Indeed, the average distances to the target are higher. This may be caused by EA since it generates more diverse laminates, through higher mutation and permutation probabilities, than UMDA. The sampled laminates may be far from the laminates used to generate the target. This phenomenon is more visible when calculating the entropy of the distribution. Nevertheless, the frequency of distances greater than or equal to 0.25 is similar. This can be explained by the use of identical models for the auxiliary densities. Thus, the probabilities of generating unfeasible targets are similar.

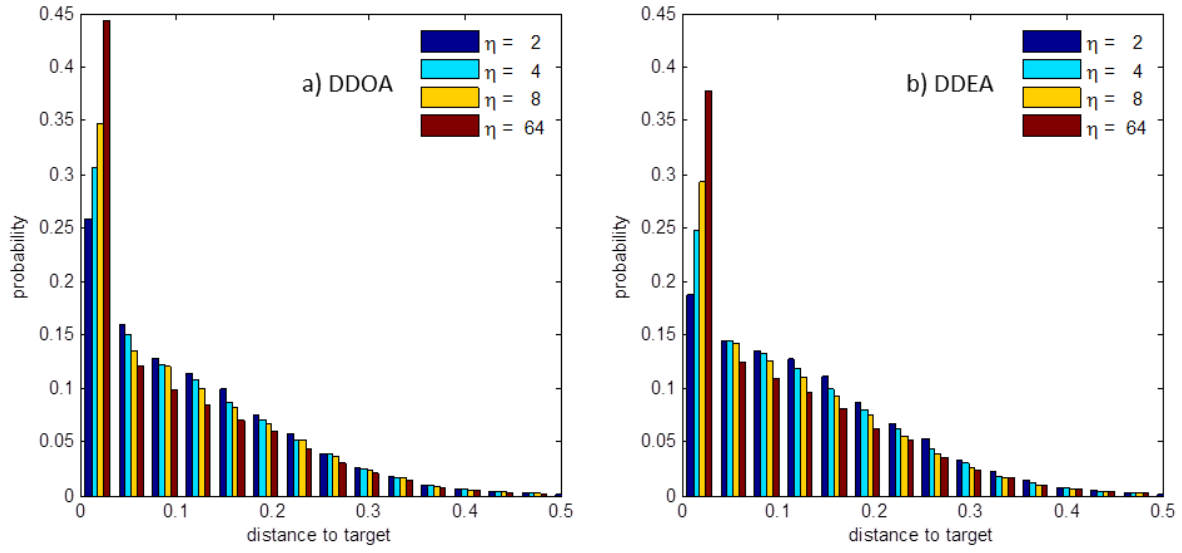

Figure 44. Distribution of the distance to the target points in auxiliary space using a) DDOA and b) DDEA.

Figure 45 compares the influence of the parameter η on the behavior of DDOA and DDEA respectively. DDOA is compared against the elitist UMDA with mutation in Figure 45.a and Figure 45.b. Similar comparison between DDEA and the EA is proposed in Figure 45.c and Figure 45.d. Note that UMDA and the EA correspond to extreme cases of DDOA and DDEA respectively with $\eta = 1/\lambda$. Even if this is not obvious from Figure 44, DDEA turns out to be more sensitive to the value of η than DDOA. Indeed, the reliability and convergence rate of DDOA are stable for $\eta \geq 8$ whereas DDEA requires higher values of η before stabilizing. Although the elitist UMDA with mutation and proper settings proved more efficient than the EA

with the standard settings used in the figure, it is interesting that with increasing values of η DDOA and DDEA tend to very similar performances. Thus the advantage of guiding the search using the auxiliary distribution is even greater with the EA than with UMDA.

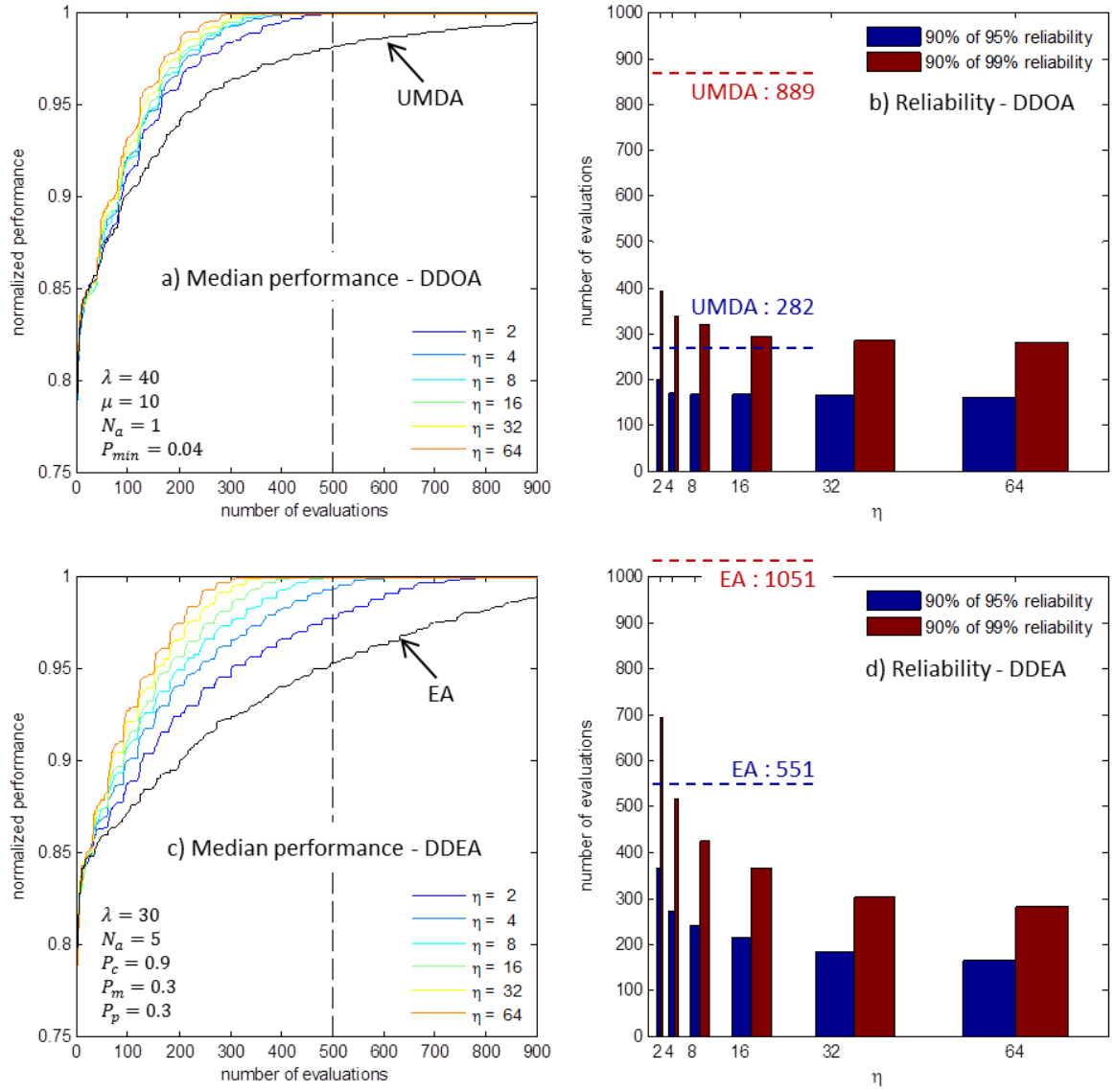

Figure 45. Influence of the parameter η on the convergence and reliability of DDOA and DDEA.

The version of DDOA implemented in this work and the proposed DDEA, although very similar in the way the auxiliary distributions are handled, differ on the choice of the populations that are used to learn $p_v(v)$. In DDOA, the auxiliary distribution is updated from the N_a best designs of the union of the current population and the archive (note that in (Grosset, 2004), there was no archive population). In DDEA, the auxiliary distribution is updated from the archive population only. This choice is related to the fact that the probability density implicitly defined by the fitness function and the selection operator with the EA is much less predictable than the explicitly defined PMF $p_x(x)$ of UMDA. This analysis is also consistent with the results shown in Figure 44 and Figure 45 and explains why a significantly higher computational effort with

DDEA than DDOA has to be placed on generating populations that correctly reflect the auxiliary distribution. The notion of the entropy of a probability distribution is used in the following to illustrate this analysis. The entropy is a simple scalar measure of unpredictability of information content, e.g. a distribution. For instance, the uniform density $U(x)$ has the maximum entropy, while a density related to a fully predictable event (i.e. one of the $p_{x_{ij}} = 1$ and all other are null) has null entropy. Entropy (unit in $nats$) for a discrete random variable with probability density function p_x can be expressed as:

$$H(p_x) = -\sum_{i=1}^{n}\sum_{j=1}^{m} p_{x_{ij}} \ln\left(p_{x_{ij}}\right) \qquad \text{II-10}$$

with n the dimension of x, m the number of possible values. In accordance with $\lim_{p\to 0^+}(p\ln(p)) = 0$, may be stated $p_{x_{ij}} \ln\left(p_{x_{ij}}\right) = 0$, and finally $p_{x_{ij}} = 0$. Summation over variables is related to the independency of the variables x_i.

Generalized to continuous random variable with probability density function p_v, Equation II-10 becomes a differential entropy that can be expressed as:

$$H(p_v) = -\int_{-\infty}^{+\infty} p_v(v) \ln\big(p_v(v)\big) dv_1 \dots dv_d \qquad \text{II-11}$$

In the same manner than discrete random variables, with the hypothesis of independency of the variables v_k, the entropy becomes:

$$H(p_v) = -\sum_{-\infty}^{+\infty} \int_{-\infty}^{+\infty} p_{v_k}(v_k) \ln\left(p_{v_k}(v_k)\right) dv_k \qquad \text{II-12}$$

In order to make the measures of the entropy independent to the number of variables, average entropies, i.e. $H(p_x)$ and $H(p_x)$ divided by n and d respectively, are preferred thereafter. Considering $p_{v_k}(v)$ as a normal distribution with standard deviation σ_k., the average entropy may be expressed as:

$$\bar{H}(p_v) = -\frac{1}{d}\sum_{k=1}^{d} \int_{-\infty}^{+\infty} p_{v_k}(v) \ln\big(p_{v_k}(v)\big) dv = \frac{1}{d}\sum_{k=1}^{d} \ln\big(\sigma_k\sqrt{2\pi e}\big) \qquad \text{II-13}$$

$$\text{With } p_{v_k}(v) = \frac{1}{n_k}\sum_{i}^{n_k} N\big(v^i, \sigma^2\big)$$

However, when it comes to estimate KDE, neither p_v nor p_{v_k} are Gaussian distributions since they result from summation of Gaussian distribution themselves. Therefore, in order to estimate their entropy and eventually its normalization by d, Equation II-11 should be used in the case of estimation by KDE as weighted sum of Gaussian densities, i.e. calculating a d-dimension integral.

Equation II-12 should be used if KDE-based estimation brings the hypothesis of independent variables in each dimension, i.e. calculating d unidimensional integrals.

Figure 46 shows the evolution of the entropy of the internal distributions in the x space handled by the EA and UMDA used as basis for DDEA and DDOA respectively. For each distribution analyzed, the minimal and maximal entropy values as well as the median and 25th and 75th percentile of the entropy over 50 optimization runs are plotted. The results presented for UMDA are generated with the following settings: $\lambda = 50$, $\mu = 23$, $N_a = 1$ and $p_{min} = 0.04$. In the case of the EA, the settings are $\lambda = 60$, $N_a = 12$, $P_c = 0.9$, $P_m = 0.3$ and $P_p = 0.3$. These settings are suboptimal, with respect to the results shown previously, but they allow for populations large enough (at least m designs) to describe uniform distributions. For the plate buckling maximization problem with $m = 12$ and considering uniform density, all ply values are under equiprobability and $p_{x_{ij}} = 1/12$ in Equation II-10. Therefore, the value of the average entropy of p_x becomes:

$$\bar{H}(p_x) = -\frac{1}{n}\sum_{i=1}^{n}\sum_{j=1}^{m} p_{x_{ij}} \ln\left(p_{x_{ij}}\right) = \frac{1}{n}\sum_{i=1}^{n}\frac{\ln(12)}{12} \times 12 = \ln(12) \approx 2.48 \qquad \text{II-14}$$

Figure 46.b shows in the case of UMDA the evolution of the entropy of the PMF described by the union of the current population x and the archive population x_a introduced in subsection II.3.2. The auxiliary distribution in DDOA is based on the selection of the N_a best solutions among this union. It can be seen that the initial distribution is uniform. The entropy quickly decreases in a first phase, and then progressively stabilizes with convergence of the algorithm. The entropy does not fall to 0 because of the uniform random mutation introduced in subsection II.3.1. Figure 46.a shows the evolution of the entropy of the two PMFs corresponding respectively to the union of the current population and the archive population in the EA and the archive alone. Note that EA does not have an explicit PMF but a rough estimation of the effective entropy of the distribution in EA from the population is possible. The difference between the two populations is due to the environmental selection operator (see Figure 15, Chapter I). The entropy related to union of the populations is close to uniform at first generation. It then quickly decreases in a first phase. In a second phase, the decrease is much slower. The global shapes of the curves are similar with the EA and UMDA. Scattering with respect to the repeated optimization run is significantly higher with the EA than with UMDA at the beginning of the optimization but it progressively reduces to similar minimal and maximal values. It is very clear from the figures that the archive population x_a of the EA has much lower entropy than the union $x \cup x_a$. It is also the most similar in terms of entropy to the population shown for UMDA. Overall, the EA has higher entropy than the UMDA. This explains why quickest convergence results – the ones detailed in this section – are obtained with DDEA when learning the auxiliary distribution on the archive population only rather than on the union $x \cup x_a$. All solutions contained in the archive population are unique in the primary design space.

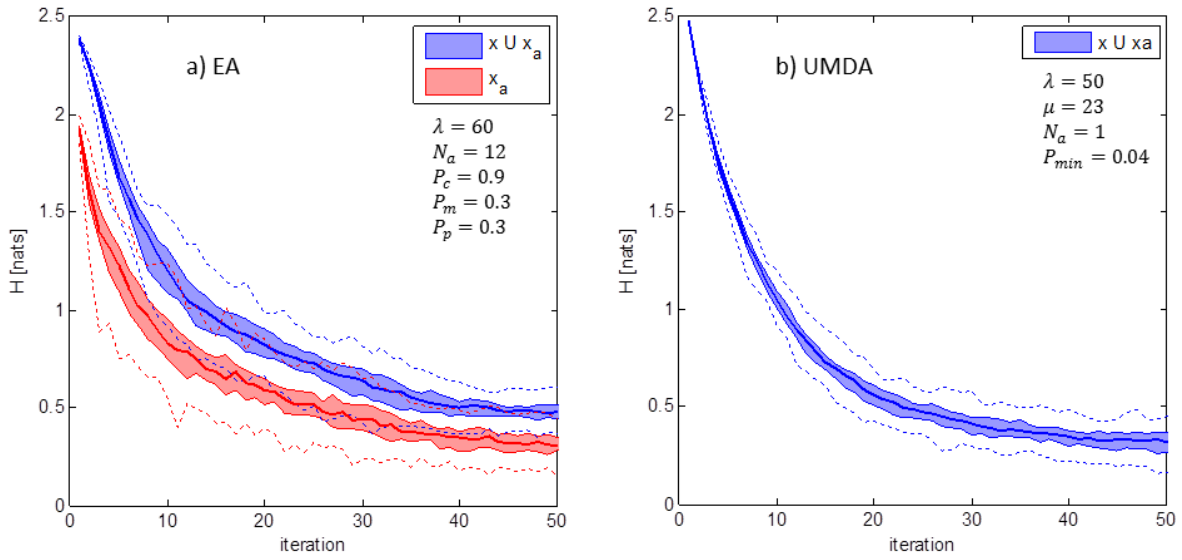

Figure 46. Evolution of the entropy with the iteration of a) the EA and b) UMDA. x stands for the current population and x_a for the archive population. Minimal and maximal entropy values as well as median and 25th and 75th percentile of the entropy over 50 optimization runs.

II.6 Application to other test problems

In the previous sections, the algorithms are compared with regard to their performance at solving the plate buckling problem. The problem is solved with 32 design plies. Figure 40 shows the regularity of the problem and its underlying simplicity. Indeed the closed form solution given in Equation I-2 defines a convex two-dimensional optimization problem when expressed in terms of lamination parameters. The performances of the algorithms presented in Section II.5are compared in this section on more demanding applications.

II.6.1 Cylinder buckling load maximization

The problem consists in the critical buckling load maximization of a long unsymmetrical and unbalanced laminated cylindrical shell solicited in axial compression. The shell is perfect and free of any manufacturing imperfection. Buckling of the cylindrical shell is assessed based on Flügge's theory, as presented in (Cheng and Ho, 1963). External pressure and torsion can also be taken into account with that method. The corresponding equations are expressed in terms of the middle surface displacements of the shell and the full membrane stiffness matrix A, bending stiffness matrix D and coupling stiffness matrix B. The material property of the laminate are: $E_{11}/E_{22} = 20$, $G_{12}/E_{22} = 0.6$ and $\upsilon_{12} = 0.25$. The length-to-radius ratio is $L/R = 125$ and the radius-to-thickness ratio is $R/h = 20$ with $h = 1$ in the following.

This optimization problem has already been solved in (Diaconu and Sekine, 2004; F.-X. Irisarri et al., 2011; Matsuzaki and Todoroki, 2007). The theoretical optimum considering all 12 lamination parameter is known from a continuous optimization performed in (Diaconu and Sekine, 2004). It corresponds to $V_{1A} = V_{3A} = 0$ with all other lamination parameters null. Thus, the optimal laminate is the unidirectional 0°-laminate. Discrete resolution of the problem is proposed for 12-

ply laminates using a fractal branch-an-bound method in (Matsuzaki and Todoroki, 2007) and by combining a response surface method and the EA used in the present work in (Francois-Xavier Irisarri et al., 2011). In the following, 32-ply laminates are considered, i.e. the dimension of the primary design space is $n = 32$. The objective function is the critical buckling load normalized by its optimal value, thus all the designs have a fitness larger or equal to 1, the optimum.

The cylinder buckling problem is similar in nature to the plate buckling problem. The main difference is the dimension of the auxiliary space. Here, $k = 12$ auxiliary variables are required to completely describe the laminate of the shell since no simplifying hypotheses on the laminate are made here. While the algorithm may be functional with partial lamination parameters, incomplete LP could not characterize the whole objective function. Nevertheless the cylinder buckling problem seems to be convex with respect to the lamination parameters. The bandwidth of the KDE in auxiliary space is set to $\sigma = 0.15$, the same value as for the plate buckling problem. This is questionable since the dimension of the auxiliary space has changed. Nevertheless satisfactory results are obtained with this setting. Figure 47 and Figure 48 show the performances of the EA and of DDEA respectively with respect to the sizes of their internal populations. For both algorithms, the best convergence rate and reliability are achieved with the smallest populations. This was already the case for the plate buckling maximization problem and could be related to the underlying regularity of the optimization problem (see discussions about Figure 35 and Figure 40). It is interesting to note that improvement on the efficiency of the search brought by DDEA with respect to the EA increases proportionally with the population size, showing the potential of DDEA for more difficult problems where a larger population size will be needed.

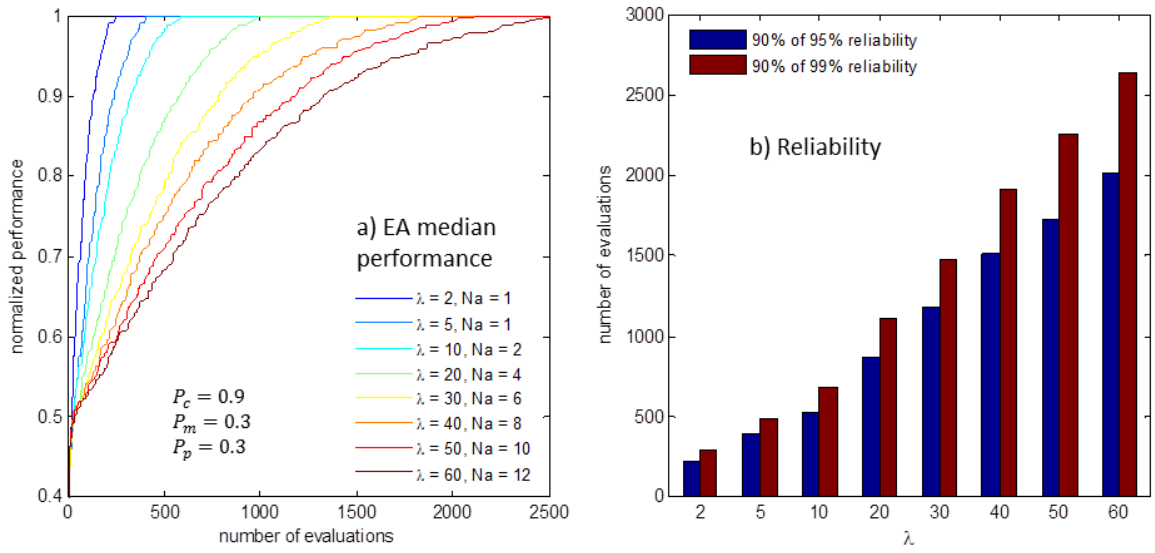

Figure 47. Performance of the EA for the cylinder buckling maximization problem. a) Median performance curves for several archive and current population sizes. b) Number of evaluations required to reach 95% and 99% of reliability for 90% of the optimization runs.

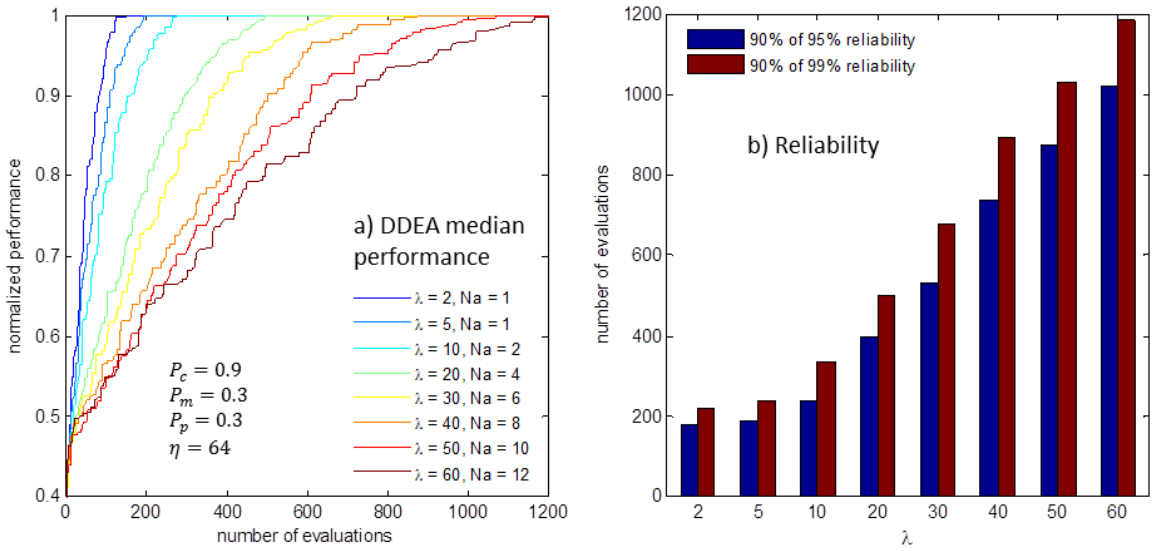

Figure 48. Performance of the DDEA for the cylinder buckling maximization problem. a) Median performance curves for several archive and current population sizes. b) Number of evaluations required to reach 95% and 99% of reliability for 90% of the optimization runs.

The performance of the EA and DDEA for two settings, the best one and a more generic one, are compared in Figure 49 to the random search, the elitist UMDA with mutation and DDOA. The increased difficulty of the cylinder buckling maximization problem with respect to plate buckling maximization problem is traduced by the much lower median performance achieved by the random search. The population sizes for UMDA and DDOA have been set arbitrarily to $\lambda = 40$ and $\mu = 10$, as these values proved efficient on the plate problem. A parametric study has been led to determine the optimal value for the mutation probability p_{min}. As previously, DDOA shows very stable behavior with respect to 95% reliability over a large range of p_{min}. Nevertheless, concerning 99%-reliability, a pattern emerges with an optimal value p_{min}=0.08. DDEA, even with generic settings outperforms its competitors. Note that UMDA behaves rather poorly in that it exhibits very slow final convergence towards the optimum.

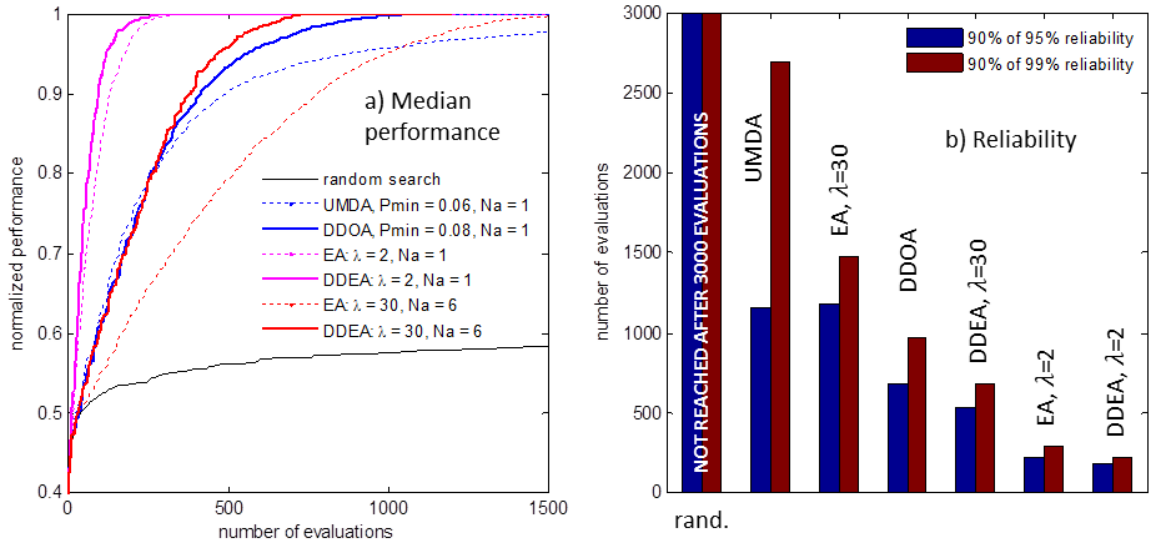

Figure 49. Comparison between double distribution algorithms and single distribution algorithms for the cylinder buckling maximization problem. a) Convergence curves of median performances. b) Number of evaluations required to reach 95% and 99% of reliability for 90% of the optimization runs.

II.6.2 Plate strength maximization

The problem consists in maximizing the reserve factor (RF) of a balanced and symmetrical laminate subjected to the in-plane loading $N_x = -1000$ N/mm, $N_y = 200$ N/mm, and $N_x = 400$ N/mm. The total laminate thickness is 4 mm, irrespective of the number of plies. The stress analysis is based on the classical plate lamination theory (CPLT). The maximum strain first ply failure criterion is used. The optimization problem can be written as follows:

$$\max_x RF \text{ with } RF = 1/\max_{i=1,\dots,n}\left(\max\left(\frac{\varepsilon_{11}}{X_\varepsilon}, \frac{\varepsilon_{22}}{Y_\varepsilon}, \frac{\varepsilon_{12}}{S_\varepsilon}\right)\right) \qquad \text{II-15}$$

where $\varepsilon_{11} \geq 0 \Rightarrow X_\varepsilon = X_{\varepsilon t}$ else $X = X_{\varepsilon c}$ and $\varepsilon_{22} \geq 0 \Rightarrow Y = Y_{\varepsilon t}$ else $Y = Y_{\varepsilon c}$. The material properties of the base glass/epoxy ply are defined in Table 10. The ply is assumed elastic and transverse isotropic. Thus, the maximum longitudinal tensile strain $X_{\varepsilon t}$ is evaluated as $X_{\varepsilon t} = X_t/E_{11}$. Other maximal strains are computed similarly. The plate strength problem is addressed in (Grosset, 2004) using $n = 8$ design variables and $m = 8$ possible ply orientations. Even with such a reduced design space, the problem proved difficult to solve with accuracy and reliability. In the present work $m = 12$ and the problem is solved for $n = 8, 16$ and 32 plies. The laminate is written $[x_{i=1,\dots,n}/-x_{i=1,\dots,n}]_s$.

Property	Value
Longitudinal modulus E_1	65 GPa
Transverse modulus E_2	10 GPa
In-plane Poisson's ratio υ_{12}	0.31
In-plane shear modulus G_{12}	4.5 GPa
Longitudinal tensile strength X_t	500 MPa
Longitudinal compressive strength X_c	-410 MPa
Transverse tensile strength Y_t	35 MPa
Transverse compressive strength Y_c	-110 MPa
Shear strength S	70 MPa

Table 10. Material properties of a glass/epoxy ply.

This simplistic engineering problem makes a difficult optimization problem because of the successive maximizations. Based on engineering judgment, the analysis of the problem shows that the RF is influenced by the proportions of ply orientations only. The RF does not depend on the stacking order for an in-plane loading. Thus, for a number n of design plies and a number m of allowed ply orientations, the number of unique solutions is:

$$\Gamma_m^n = \frac{m^n}{n!} \qquad \text{II-16}$$

Additionally, by construction of the laminates and since the stacking order has not influence on the RF, it is possible to reduce the set of allowed ply orientations to the positive angles only. Table 11 shows the optimal solutions obtained for $n = 2, 3, 4, 8, 16$ and 32 design plies. The optimal solutions have been evaluated by enumeration for $n \leq 8$. The optimal solutions for $n = 16$ have been directly deduced from the solution with $n = 8$ and checked by enumeration. The solution for $n = 32$ is a variation around the solution with $n = 16$. It is worth noticing that the thinner is the ply (the total thickness of the laminate is unchanged), the higher is the RF. In fact, by increasing the number of plies, the discrete optimum gets closer to the continuous optimum of the problem.

The information corresponding to the proportions of the ply orientations, which are the true design variables for this problem, is contained (but not detailed) in the lamination parameters V_{1A} and V_{3A}. These two values are not sufficient to capture the regularity of the objective function with $m = 12$ allowed ply orientations. Bending lamination parameters do not help since the RF for an in-plane loading does not depend on the stacking order of the plies. Additionally the proportions of the ply orientations cannot be conveniently used as auxiliary variables (in their KDE with Gaussian representation) since they form a partition of unity: a KDE with Gaussian kernels cannot be used to sample relevant targets in such an auxiliary design space. Thus, defining a customized auxiliary space for this problem is not a straightforward generalization of the technique presented earlier (with the lamination parameters).

Number of design plies n	Total number of solutions	Number of unique solutions	Optimal $x_{i=1,\dots,n}$	Optimal RF
2	144	28	[0 70]	0.915
3	1,728	84	[0 0 60]	0.847
4	20,736	210	[0 0 60 90]	0.930
8	429,981,696	3003	$[0_5\ 60_2\ 90]$	1.031
16	$\approx 10^{17}$	74,613	$[0_{10}\ 60_4\ 90_2]$	1.031
32	$\approx 10^{34}$	2,760,681	$[0_{19}\ 60_9\ 90_4]$	1.038

Table 11. Cardinality of the design space and optimal solutions of the plate strength maximization problem for different number of design variables. By considering only positive orientations value, $m = 7$ here.

The idea is here to introduce engineering knowledge into the search through the auxiliary design variables. First, since the sign of the design variable is irrelevant, temporary variables y_i are built based on the absolute value of the design ply orientations: $y_i = |x_i|,\ i = 1, \dots, n$. Second, because the stacking order has no influence, the temporary variables are sorted in ascending order: $y_1 \leq y_2 \leq \cdots \leq y_n$. Finally, since the optimal solution for a given number of plies can be deduced from the optimum with a lower number of plies, the temporary variables are averaged by groups of 2 (resp. 4) in the case of $n = 8$ (resp. $n = 16$ or 32) to form the auxiliary variables:

$$\begin{gathered} v_1 = \frac{y_1 + y_2}{2}; \dots; v_4 = \frac{y_7 + y_8}{2} \quad if\ n = 8 \\ v_1 = \frac{y_1 + y_2 + y_3 + y_4}{4}; \dots; v_d = \frac{y_{n-3} + y_{n-2} + y_{n-1} + y_n}{4} \quad if\ n = 16\ or\ 32 \end{gathered} \qquad \text{II-17}$$

The auxiliary variables have here the dimension of an angle. The bandwidth of the KDE is arbitrarily set to 15°, since this value corresponds to the ply orientation discretization.

The results obtained are shown in Figure 50. For each value of n and each algorithm only one curve is presented that corresponds to 50 repeated runs. The curve presented corresponds to the best observed behavior – or to a representative behavior – of the algorithm among several settings. UMDA and DDOA have been tested with the following settings: $\lambda = 40$, $\mu = 10$, $N_a = 1$ and $p_{min} = 0, 0.05, 0.10, 0.15, 0.20, 0.25, 0.50, 1.00$. The EA and DDEA have been tested with $P_c = 0.9$ and $P_c = P_p = 0.3$. The following $(\lambda; N_a)$ couples have been tested $(32; 1), (32; 6),\ (64; 1), (64; 12), (128; 1), (128; 24), (256; 1), (256; 48)$. It is interesting to note that the shapes of the curves of median performances are much more irregular than in the previous buckling maximization test problems, what reflects the difficulty of the strength problem. Figure 50 shows that all algorithms, except random search, share similar performances for $n = 8$. If the advantage of using DDEA over the EA is clear, UMDA shows surprisingly good behavior with respect to DDOA. Note that the probability of mutation is high (0.15) for UMDA to achieve good results. With $n = 16$, the EA and UMDA lose much of their efficiency. Increasing the probability of mutation in UMDA deteriorates its performances. DDOA achieves comparable performances with respect to DDEA, but with very high probability of mutation (0.25). With $n = 32$, only DDEA achieves better performances than the random search.

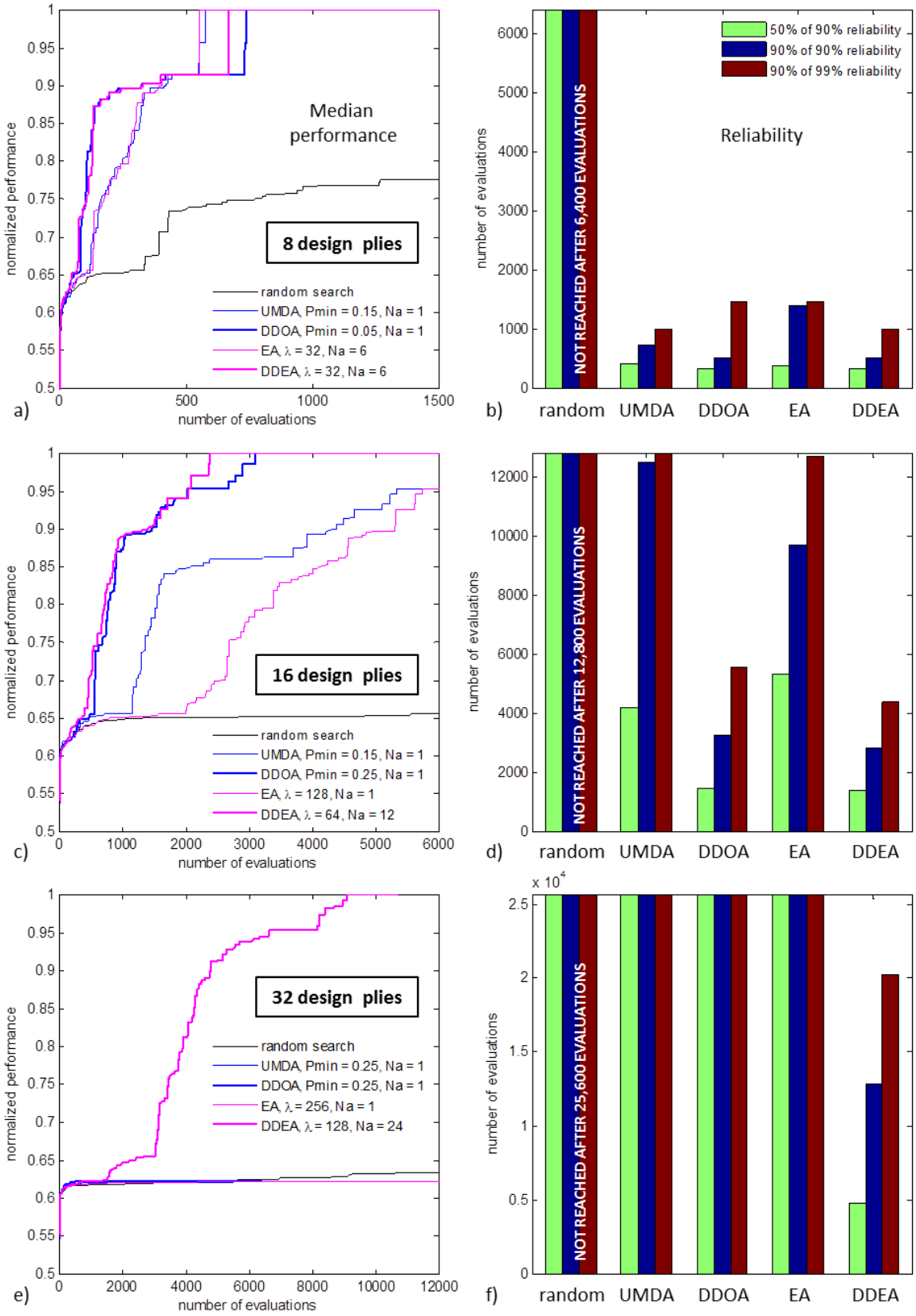

Figure 50. Comparison between EA and UMDA, DDEA and DDOA and random search: convergence curves of median performances and reliability. a) and b) with 8 design plies. c) and d) with 16 design plies. e) and f) with 32 design plies.

II.6.3 Application of DDEA to the 18-panels benchmark problem

One of the main motivations of introducing the double distribution guidance into the specialized EA proposed in Chapter I, rather than simply switching to DDOA, is to take advantage of the flexibility of the EA in handling design guidelines. Thus, DDEA is applied to 18-panel U-grid benchmark already solved and discussed in Section I.5. UMDA and DDOA cannot be applied to the benchmark since the guidelines cannot be handled in their present implementation. Moreover, the encoding proposed in Section I.4.2 for the SST is not compatible with these two algorithms without modifications. Indeed, the ply insertion rank chromosome is a mere combinatorial variable. Sampling such a variable from univariate distributions might not be relevant or even possible. This requires a specific treatment, different from more general strategies suggested previously, since order-based statistics exist. On the contrary, specific operators have been developed in Chapter I for the EA that efficiently create and maintain feasible populations with respect to the design guidelines. The operators are used in DDEA without any modification. Thus, the design guidelines – as well as all other optimization constraints – are handled in the primary design space.

In this benchmark, the mass of the structure is directly influenced by the thickness distribution, while panel buckling is influenced by the laminate bending stiffness. In the single objective formulation of the problem, the mass is the objective and the panel buckling the constraint. Both quantities, i.e. thickness and bending stiffness, have to be integrated in the auxiliary design space for it to be relevant. A first possible auxiliary design space can be assembled from the bending stiffness matrices of the panels of the structure. Since the closed form solution given in Equation II-1 is written under the assumption of orthotropic bending behavior, the design space can be reduced to the quadruplets $(D_{11};\ D_{22};\ D_{66};\ D_{12})$ for each of the 18 panels.

Using bending stiffness terms to form the auxiliary design space has two main advantages. First, the bending stiffness terms reflect both the anisotropy and the thickness of the laminate. Second, a distance in stiffness space is defined in (Francois-Xavier Irisarri et al., 2011):

$$d(D_1, D_2) = D_1^{-1} : D_2 + D_1 : D_2^{-1} - 6 \qquad \text{II-18}$$

where D_1 and D_2 are two bending stiffness matrices and the operator : stands for the trace of the product of the two square matrices. This stiffness-based distance is convenient to work with in Algorithm 7.1 since the different orders of magnitude of the bending stiffness terms as well as the variation of order of magnitude related to thickness variations are handled on a physical basis. Indeed, the distance $d(D_1, D_2)$ is related to the extreme values of the ratio of the bending stiffness of the two laminates over all possible curvature states. For multiple panels, the distance is defined as the weighted sums of the panel-to-panel distance, where the weights correspond to the panel area divided by the total area of the structure.

Setting the bandwidth of the KDE however is not straightforward when working with bending stiffness. Indeed, the order of magnitude of the stiffness varies approximately with the cube of the thickness of the laminate. Thus, for each panel of the structure, it has been chosen to link the bandwidth to the total thickness, instead of resorting to maximum likelihood like in general

methods. This choice is made here to simplify and speed up the algorithm since mechanical knowledge may be brought in. The bandwidth is set to 10% of the stiffness of the homogeneous "black metal" solution that can be computed from Equation II-7 with $V_{1D} = V_{3D} = 0$. Thus, the bandwidth is defined as a function of the thickness of the laminate. In practice, the thickness of the design used as center of the kernel from which the target is sampled is used. The targets sampled in the auxiliary design space $(D_{11};\ D_{22};\ D_{66};\ D_{12})$ are used to assemble a real and symmetric target matrix D^{target} per panel, so the panels are handled independently. No constraints are enforced in the auxiliary space. Nonetheless, the matrix has to be definite positive for the target to be meaningful. Otherwise, negative distance values could arise in Equation II-18. Thus, targets are sampled until definite positive target matrices are found for all panels. The corresponding calculation cost is negligible. The choice of the kernel center and bandwidth are consistent and make the probability of sampling non-definite positive matrices quite low. Note that the double distribution guidance is activated once a first feasible solution is found with respect to the design constraints. The auxiliary distribution is learnt on feasible solutions only.

The results obtained with DDEA in the case of symmetrical and balanced laminates are presented in Figure 51 and compared to the results obtained with the EA and already presented and discussed in Section I.5.1. The solutions are blended and satisfy ply-drop design guidelines. The settings of both algorithms are almost identical (see Chapter I, Table 2) except for the size of the archive population. For single objective optimization, N_a is set to 1 for the EA. For DDEA, since the auxiliary distribution is learnt on the archive, N_a is set to 5 to maintain a minimal diversity. The parameter η is set to 10 to save computational time. The computational time for one optimization run with DDEA is about 1 hour. Figure 51.a shows the evolution of the median performance over 50 repeated optimization runs. DDEA shows much faster initial convergence rate than the EA. Latter during the search, both algorithm stabilize on equivalent median performance. Figure 51.b compares the evolution of four levels of reliability. In about 90% of the runs DDEA reaches 90% of the best known performance before 5.000 evaluations. In comparison, with the same optimization budget, only 30% of the EA runs have reached that level of performance. The curves of 95% reliability and 99% reliability follow similar trends. The fact that the final 95% reliability of the EA is higher than DDEA one, while the opposite is observed for the 99% reliability, is due to a slightly more important scatter of DDEA results.

Figure 52 shows the results obtained with all laminate design guidelines obtained. In that case, the sampling of the primary design space is more constrained, thus it might be more difficult to near the targets in auxiliary space. The results however are consistent with those obtained in the less constrained case presented in Figure 51, even if the gains are less important. After about 7.500 evaluations, Figure 52.b shows that all DDEA runs have reached 90% of the best known performance and about 25% have reached 98% of it. Comparatively, in the case of the EA, about 90% of the runs have reached 90% of the reference performance and 98% of it has never been reached.

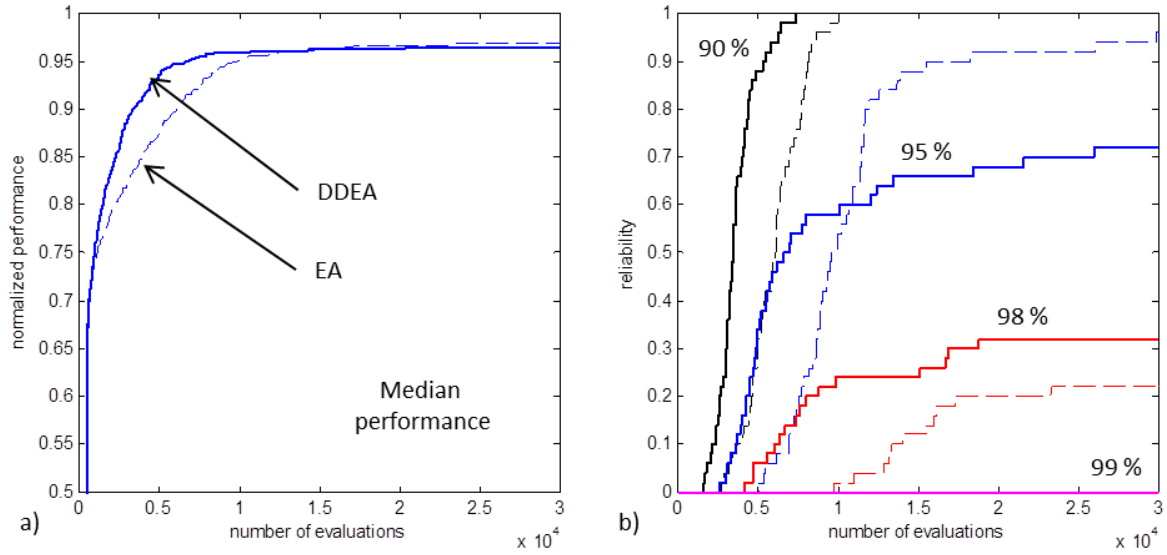

Figure 51. Comparison of the EA and DDEA on the 18-panel U-grid benchmark with symmetrical and balanced laminates. a) Median performance curves. b) Reliability curves.

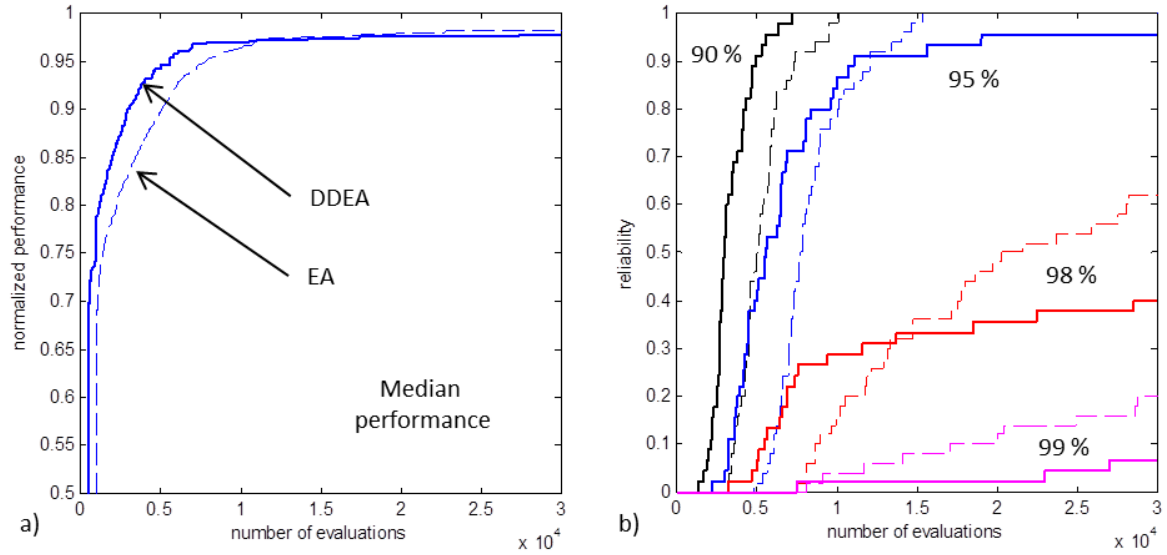

Figure 52. Comparison of the EA and DDEA on the 18-panel U-grid benchmark. All laminate design guidelines enforced. a) Median performance curves. b) Reliability curves.

II.7 Concluding remarks

This chapter has highlighted the potential benefits to draw from the exploitation of an auxiliary distribution to guide the algorithms in composite optimization problems. Such a process has mathematical and numerical motivations, respectively the need for couplings between variables described by independent univariate distributions and the need for expert knowledge in the optimization process. The double distribution method comes from previous work by (Grosset, 2004). The algorithms proposed by Grosset – the Univariate Marginal Distribution Algorithm (UMDA) and the Double Distribution Optimization algorithm (DDOA) – are implemented and compared with the EA described in Chapter I in order to solve mono-objective composite optimization problems. Special attention is paid to the settings of the algorithm and the influence of the setting on the convergence speed and reliability of the algorithm. Finding the optimal setting of the algorithm is a real difficulty. In the case of UMDA, the influence of each parameter is rather clear which make the algorithm simple to use. DDOA partly inherits this simplicity. Nevertheless, the introduction of a KDE in the auxiliary space and choice of the auxiliary space itself requires a thorough knowledge of both the problem and the algorithm. Here, kernels have been set according to known variation domains of lamination parameters. In the case of the EA, and consequently DDEA, it is much more difficult to find the optimal settings for a new optimization problem. Nonetheless, the results presented in this chapter suggest that there exist generic settings for which the optimizer shows satisfactory behavior on a large range of problems.

The guiding scheme of DDOA has been adapted to the EA in a new algorithm, the Double Distribution Evolutionary Algorithm (DDEA), in order to solve mono-objective composite optimization problem. DDEA combines the advantage of the EA and of DDOA. On the one hand, DDEA shares with the EA its elitist structure and the variation operators specialized for design guidelines handling. The development of specialized operators enables to adapt the algorithm to the design variable of considered problem. On the other hand, DDEA inherits from DDOA the guidance scheme through an additional probability distribution explicitly defined in an auxiliary design space. The flexibility in the choice of the auxiliary design space is a strong asset since it allows introducing expert knowledge in the optimization and thus adapting the algorithm to the criteria of the considered problem. Hence with respect to the EA, DDEA achieves one further step towards the specialization of the optimization algorithm to the optimization problem, which is considered in the present work as a key for the development of efficient optimization methods. DDEA is applied with promising results on four benchmark problems of increasing complexity: plate buckling maximization, cylinder buckling maximization, plate strength maximization and the 18-panel U-grid problem used as benchmark for the SST-based blending optimization in Chapter I. Compared to the EA, DDEA achieves better initial convergence speed and is thus better-suited for tight budget optimization.

CHAPTER III. SIMPLIFIED METHOD FOR AERO-STRUCTURAL ANALYSIS OF CROR BLADES

III.1 Introduction

This chapter aims at predicting, under given specific flight conditions, the mechanical behavior and aerodynamic performances of a blade of a Counter-Rotating Open Rotor (CROR). The Onera HTC5 blade shape (Bousquet et al., 1991) is used here. For certification purpose, a reduced scale model of the blade is required to validate its aerodynamic performance through wind tunnel testing. The present study is focused on the analysis of the reduced scale HTC5 blade. Modern blades are sized with interlock woven fabrics to resist to foreign object damage and bird impact. Problems of representativeness related to the scale factor may hence occur, not only from an aerodynamic perspective, but most of all from a material perspective especially around the thinnest regions. Indeed the mesoscopic structure of woven composites cannot be scaled. Consequently, a laminated composite structure is considered in the following for the reduced scale blade.

A classical design process starts with optimizing the shape of the blade at a given operating point – the so-called "hot-shape", e.g. take-off for which maximal thrust is required. Another operating point, e.g. cruise flight conditions for which the efficiency of the propeller is of outmost importance, results in a different blade shape. However the structure of the blade is not considered at this point (Negulescu, 2013). Thus, there is no guarantee that a structure, matching the optimal shapes at both operating points, exists. Additionally the unloaded shape of the blade – the "cold shape" – is unknown. The purpose of the present work is to combine the computation of the aerodynamic loading and the analysis of the mechanical deformations of the blade to explore the design space offered by laminates to simultaneously optimize the aerodynamic performances of the blade at both take-off and cruise operating points.

Section III.2 gives a quick overview of some existing methods used to compute propeller blades performances. The HTC5 blade is detailed in Section III.3. Section III.4 presents the Onera LPC2 aerodynamic code devoted to the simulation of the performance of isolated counter-rotating propeller (Gardarein, 2013). Section III.5 details a monolithic laminated composite structure for the reduced scale blade and the corresponding geometric non-linear FE structural modeling. Section III.6 details the simplified "Hot-to-Cold" (H2C) analysis method developed in the present work. The inverse analysis known as "Cold-to-Hot" (C2H) is presented in Section III.7. The H2C analysis enables determining the cold shape of the blade starting from a hot shape at a given operating point. The developed method is based on fixed-point iteration and successively executes LPC2 computations and FE analyses in order to determine the aerodynamic loads and the induced deflection. Section III.8 presents some results about the optimization of a monolithic composite blade. The results obtained suggest considering lighter and more compliant structures, thus a hollow blade with a balsa wood core and thin composite skins is studied in Section III.9.

III.2 About propeller blade analysis

The aero-mechanical optimization strategy proposed in this chapter relies on different solvers chained through MATLAB. While ABAQUS performs the structural FEA in line with the previous chapters, two codes may be called to solve either the Lifting –Line Theory (LPC2) or the Reynolds-averaged Navier-Stokes equations of the aerodynamic problem (elsA).

LPC2 is a low computational cost method which relies on the blade-element theory (Guermond and Sellier, 1991) and the reading of a 2D airfoil database (Gardarein, 2013). For each known airfoil, the database provides a table of lift and drag coefficients and the corresponding effects of the angle of attack. These are computed with 2D assumptions for different blade sections and for various Mach numbers. The sweep of the blade is corrected on Mach number and angle of attack to assess the aerodynamic effects on the third dimension of the blade. The velocity induced by the propeller on each blade section is computed through a singularity method. For this method the wake is described as a lattice of vortex filaments with a prescribed motion, and the blade itself is described as a vortex filament joining the quarter-chord of the sections. LPC2 remains a pre-design method at Onera to quickly estimate the performance of various open-rotor configurations (Gardarein, 1991).

elsA is the 3D CFD solver developed by Onera and intended to complex flow simulations and multidisciplinary applications implying aerodynamics (Cambier and Veuillot, 2008). Figure 53 shows the result of the simulation of the flow field around the open-rotor test rig developed by the TsAGI within the European FP7 program DREAM. elsA is also used to solve CROR applications with more reasonable computation costs through two mono-channel methods (i.e. only one blade is modeled). The first method is the mixing plane approach, a steady RANS method which relies on the average flow field between the downstream and upstream propellers as well as the hypothesis of space periodicity between the blade channels. The second method is the chorochronic (phase-lag) approach, an unsteady RANS method relying on the hypothesis of space-time periodicity (Castillon, 2012; Gerolymos et al., 2002; Li and He, 2002). Usually, complex computations are using the mixing plane approach to initialize the chorochronic simulation as explained in (VION et al., 2011).

Since the aerodynamic solver is expected here to communicate with ABAQUS within iterative H2C and C2H processes, the computation costs related to elsA simulations may increase drastically. Additionally, the C2H process will be linked to an evolutionary optimizer dedicated to composite design. Hence, LPC2 is privileged in a first instance to assess the aerodynamic behavior of the blade, as coupling advanced solvers is a complex operation that is beyond the scope of this thesis.

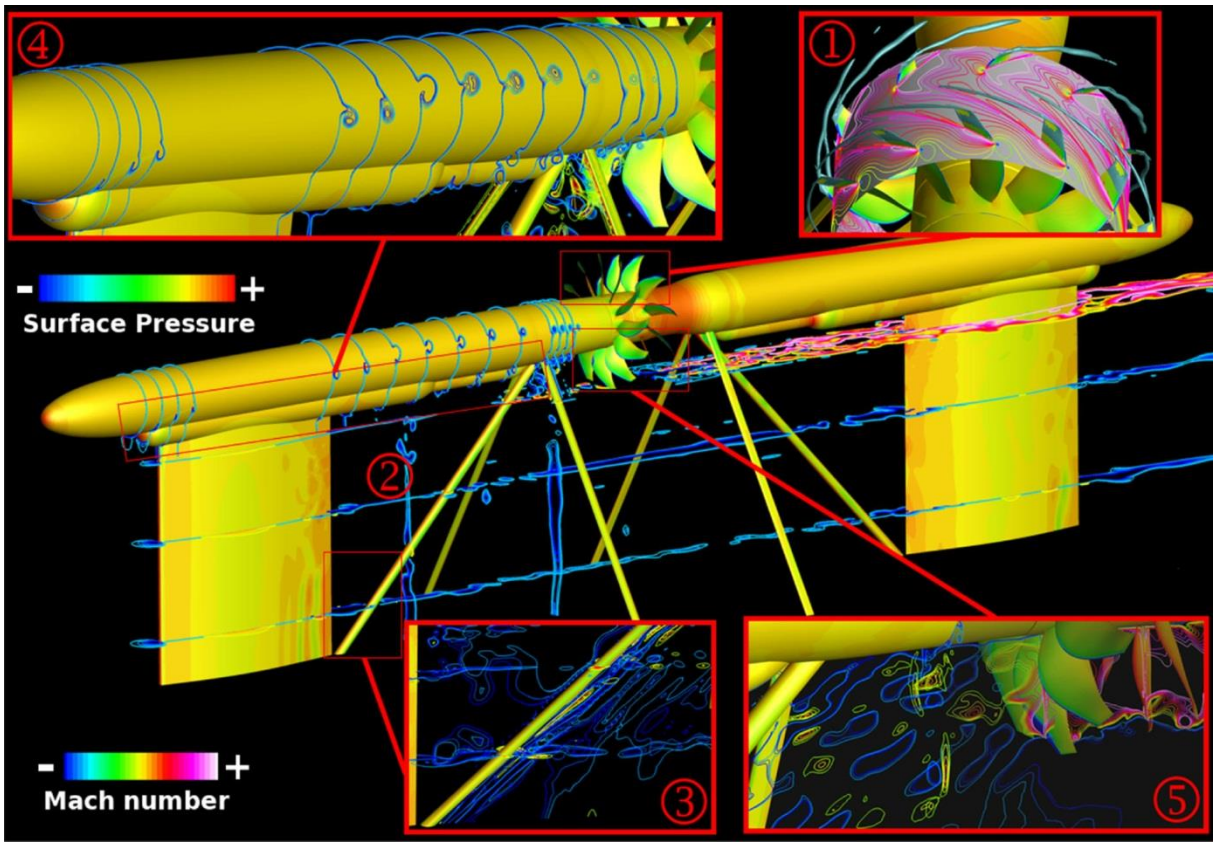

Figure 53. Aerodynamic flow field around the test rig of a reduced scale CROR model computed with elsA (Boisard et al., 2014). 1) Undisturbed flowfield around propellers. 2) Steady wake at upstream structural pylon. 3) Unsteady wake and vortices at upstream central beam. 4) Vortices at pylon trailing edge, fairing enlargement and strut-to-fairing intersection. 5) Vortices shedding at the front propeller blade.

III.2.1 Hot-to-Cold analysis

Aerodynamic design processes provide propeller blade geometries according to the given flight conditions. The resulting hot shapes are therefore already stressed by aerodynamic and centrifugal loadings. They are mostly useful for preliminary analyses, as mentioned in (Ernst, 1992). On the contrary, the geometry of the blade before aerodynamic and centrifugal loads are applied is referred to as 'cold shape'.

The cold shape may be determined through Hot-to-Cold analysis in order to manufacture the blade. This method has been first published in 1992 by NASA researchers (Ernst, 1992) to design and analyze the blades of counter-rotating open-rotors, or propfans, intended to be set on long range cruise missiles. Aeroelastic analyses of classical linear aerodynamic models were conducted, mostly with NASTRAN solvers, in order to predict flutter. Propfan blades were suspected to induce aeroelastic instability because of their slenderness ratio. Indeed, since the propfan blades are relatively thin and therefore more flexible than conventional fan blades, deflections under centrifugal and aerodynamic loading are significantly larger. According to (Reddy et al., 1993), such problems required to be simulated with a geometric non-linear theory of elasticity. At this time, all the propfan blade analyses were performed for isolated blade rows and single-rotation propfans. From these developments was suggested an iterative multidisciplinary method to

achieve hot-to-cold processing with respect to aerodynamics, elastic and thermal considerations (Mahajan and Stefko, 1993).

More recently, in (Yang et al., 2014), a fluid-structure coupling method has been suggested to predict the cold shape of conventional fan blade and hollow fan blade geometries. Non-linear geometric structural analyses are performed by ANSYS within the fluid-structure coupling solver HGAE. The hot-to-cold scheme stays similar to the methods found in the literature. Starting with a hot shape designed through aerodynamic methods, its deflection under centrifugal loads is determined through static FEA. A hypothetic cold shape is provided by subtracting the static deflection due to centrifugal loads only from the hot shape. Another static FEA is performed for this cold shape with the same aerodynamic and centrifugal loads in order to match the input hot shape. Any gap between the deformed cold shape and the input hot shape is added to correct the hypothetic cold shape. The operation is repeated until matching the hot shape with acceptable error. The successive iterations allow providing a converged cold shape.

A few commercial methods exist to perform hot-to-cold analyses, like NASTRAN Hot-to-Cold[6] procedure or Sculptor Hot-to-Cold method[7].

III.2.2 Cold-to-Hot analysis

In 1991, NASA sponsored studies about the effect of the structural flexibility of the propfan blades on the performance of the propeller (Srivastava et al., 1991). They concluded that structural deflection due to centrifugal and aerodynamic loads should be taken into account to improve the accuracy of the analysis, and that rigid-body rotation hypothesis should be evicted to determine a correct shape.

Such an assumption implies that any deflection of the structure due to the modification of the blade incidence should be determined for every considered design point. The aerodynamic performance of the blade may vary as blade deflection induces different design parameters (i.e. sweep, twist or dihedral distributions). Starting from either the cold shape found through the Hot-to-Cold analysis or from a blade FEM eventually tuned by dedicated laboratory tests (static and dynamic) (Stürmer and Akkermans, 2014), the steady state of the blade at a given design point may be approximated by iterative processes (Mauffrey, 2015). This process is referred to as Cold-to-Hot processing, static coupling, or simply aeroelastic computation.

[6] NASTRAN 2014.1 Quick Reference Guide, see page 268 or page 274.
[7] http://gosculptor.com/HottoColdTurbineBlade.html retrieved 11 November 2015.

III.3 Description of the HTC5 front blade geometry

The CROR is here considered as fitted with HTC5 blades. Blades are usually designed (Delattre and Falissard, 2013) and sized (Vion, 2013) for maximal efficiency at the cruise (CR) condition. However, the take-off (T/O) condition implies higher stresses since it requires a higher thrust and, for modern designs, a greater rotational speed with respect to cruise condition. The HTC5 front blade depicted here is the optimal shape obtained for cruise. In the following, the analysis is focused on one blade of the front propeller. Special attention is paid to the definition of the geometric parameters that will be used to compare the hot shapes obtained for different structures.

III.3.1 Blade shape

Figure 53 shows the shape of the blade and the global coordinate system used for the definition and analysis of the HTC5 blade. The x-axis, in front-rear propeller direction, defines the thrust direction and corresponds to the axis of rotation of the propeller. The z-axis, in span-wise or radial direction, defines the propeller pitch axis. The (y,z) plane is the plane of rotation of the propeller. The shape presented here is the optimal shape at cruise conditions. The full scale blade tip radius is 2134 mm. The required tip radius for the reduced scale model is R_{tip} = 336 mm (Boisard et al., 2014), thus a scale factor of about 1:6.35 applies. The hub radius is R_{hub} = 141 mm. The airfoil chord lengths vary from about 97.1 mm at the root to 69.8 mm at the tip of the blade.

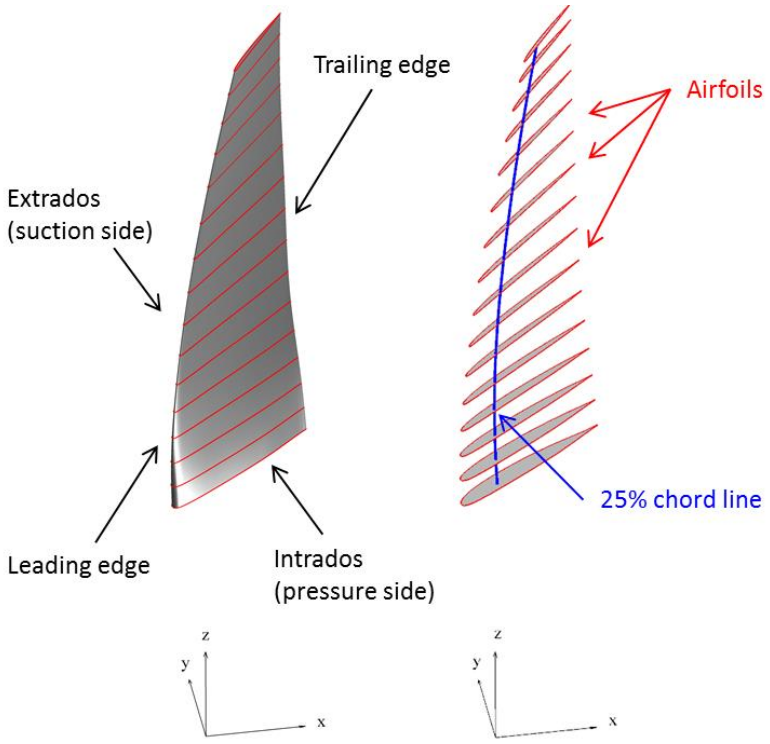

Figure 54. The HTC5 blade.

III.3.1 Design parameters

The shape of the HTC5 blade is defined by the stacking of a set of predefined airfoils evolving from the root to the tip of the blade. Thus, the blade design parameters directly inherits of the characteristics of the airfoils, as illustrated in Figure 55, including:

- The airfoil reference point (i.e. 25%-chord point).
- The airfoil chord length.

The HTC5 geometry is given with no dihedral distribution, i.e. all its airfoil reference points lay within a plane, the reference plane, as illustrated in Figure 56. In the following, for blades with non-zero dihedral, the reference plane is defined by the 25% chord point and the direction chord of the root airfoil and the z-axis. The design of the blade is defined through:

- The radial locations of the airfoils sections, defining the 25% chord line.
- The dihedral distribution $d(z)$, defined as the distance between the 25% chord line and the reference plane.
- The sweep distribution $a(z)$, defined as the distance between the projection of the 25% chord line onto the reference plane and the z-axis.

The dihedral and sweep distributions are illustrated in Figure 57. Angular adjustment is required locally at each airfoil section to adapt the incidence of the section airfoil to the helical Mach number. Finally, in order to trigger the thrust performance of the entire propeller, angular adjustment of the entire blade may be required (with respect to the reference plane, for a blade without dihedral distribution). The blade design parameters therefore include:

- The twist angle distribution $\varphi(z)$ (i.e. the angle between the chord and the reference plane);
- The blade incidence β (i.e. the angle between the reference and the rotation planes).

The airfoil twist angle and the incidence of the blade are defined in Figure 56.

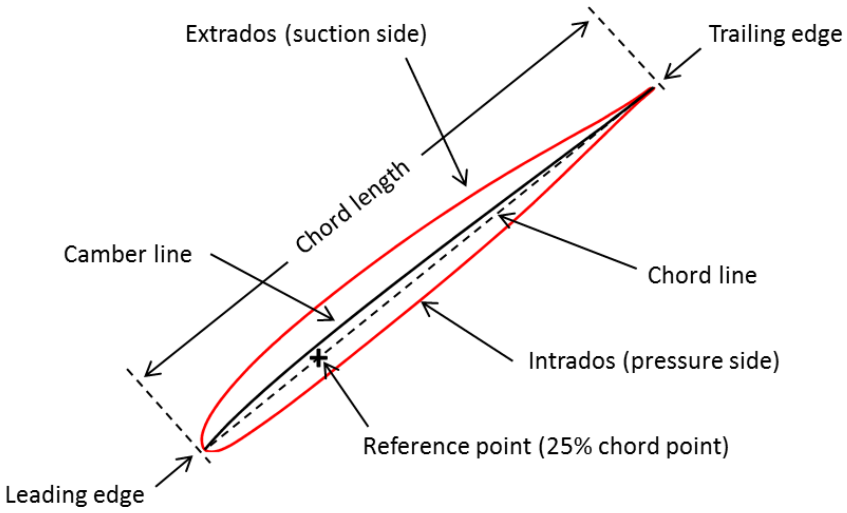

Figure 55. Airfoil characteristics.

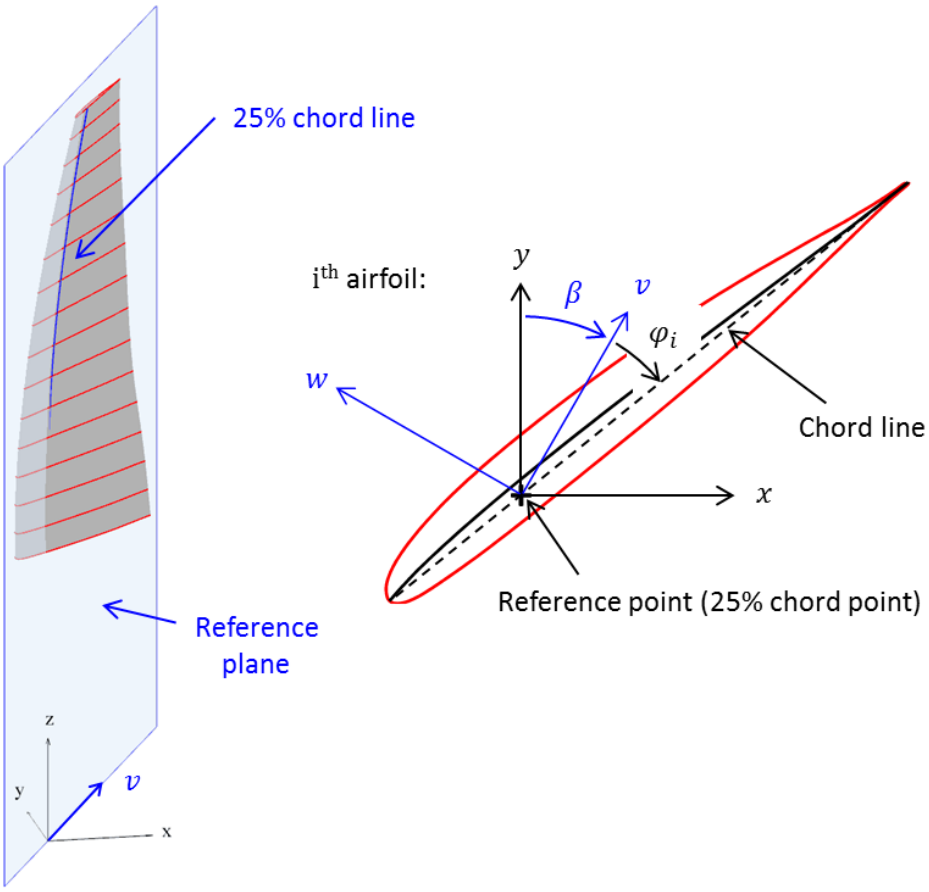

Figure 56. Incidence of the reference plane of HTC5 front blade and airfoil twist angle.

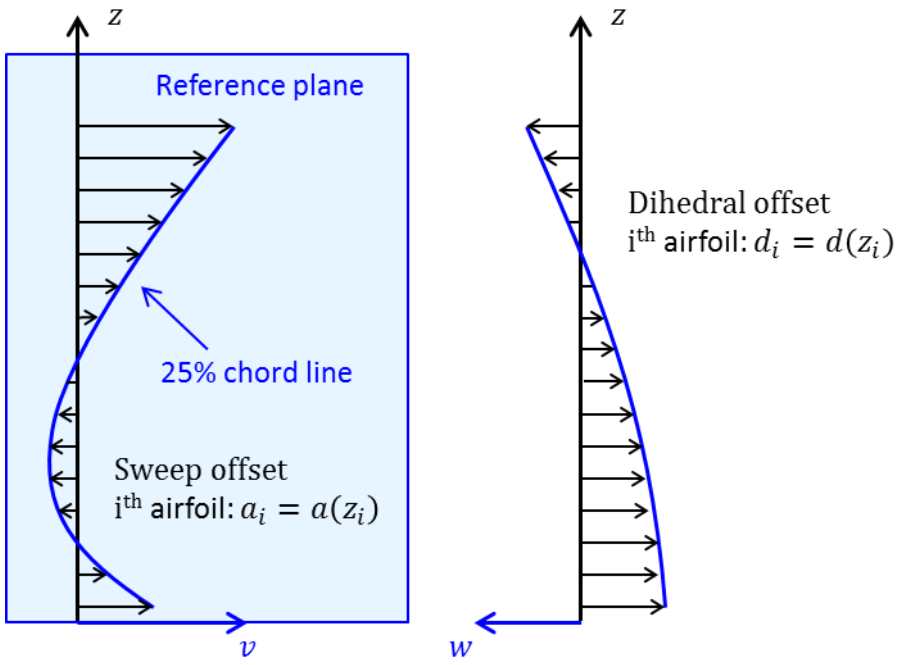

Figure 57. Sweep and dihedral distributions along the blade.

III.4 Aerodynamic modeling

In order to keep computational costs low, the aerodynamic analyses are performed with LPC2, a code developed at the Onera, and dedicated to the parametric studies of the performance of propellers. LPC2 performs lifting-line computation from a method based on the blade element theory (BET). The influence of the compressibility as well as the viscidous effects are taken into account in this method, initially inviscid (Gardarein, 1991). The code computes resultant forces of the aerodynamic loading at the reference points of the considered airfoils. The code can also optimize the blade incidence angle to match a target thrust. Since blade element momentum theory (BEMT) is not provided here by LPC2, any output moments are generated through misalignment of output resultant forces application points with the inertia center of the corresponding airfoil section. They hence result from a geometrical approximation and are not intended to be accounted for.

III.4.1 Flight condition inputs

The aerodynamic performances of the CROR blade are analyzed at either take-off (T/O) or cruise (CR) conditions since acoustic emissions and propulsive efficiency specifications are critical at these design points respectively. The corresponding flight conditions are summarized in Table 12. The use of non-dimensional coefficients enables to compare the performance of a propeller whatever its scale for high Reynolds number. This allows the use of scaled models in wind tunnels to assess the prediction of full scale propeller performance. The infinite upstream Mach number as well as the advance ratio are kept constant. Thus the rotational speed is adapted to the scale so as to keep the value $R_{tip} \times \omega$ constant. The power coefficient χ is evaluated for a target thrust coefficient τ, enabling the estimation of the propeller efficiency η.

$$\chi = \frac{P}{\rho . n^3 . D^5}$$
$$\tau = \frac{T}{\rho . n^2 . D^4} \qquad \text{III-1}$$
$$\eta = \frac{V_0 . T}{P} = \frac{\tau . \gamma}{\chi}$$

where ρ stands for the air density, n the rotation frequency, D the propeller diameter, T the thrust, P the power and V_0 the advancing speed of the propeller. The ratio $\gamma = V_0/n.D$ is the advance coefficient. For a CROR, the thrust target is usually the overall thrust of the CROR and the thrust ratio may vary. The use of a gearbox between the two propellers of the CROR imposes a torque ratio. For HTC5, another technical solution has been addressed to impose a neutral torque ratio through direct drive system. The performance of the HTC5 design computed with LPC2 for T/O and CR conditions are presented in Table 13. In Table 12 and Table 13, index 1 refers to the front propeller and index 2 refers to the rear propeller. The thrust target is about 3300 N for T/O and 950 N for CR condition. The front propeller is fitted with 10 blades and the rear propeller is fitted with 8 blades. As it is shown in Table 12, the HTC5 is designed for the

same rotation speed at all design points. For the reduced scale model, the shaft power is about 45 kW at T/O and 28 kW at CR for the whole engine (the full scale shaft power is about 12 MW at T/O). The corresponding torque on the front propeller is about 32.5 N.m at T/O and 20.8 N.m at CR.

Design point	Take-Off (T/O)	Cruise (CR)
Mach number	$M = 0.20$	$M = 0.78$
Rotation speed	$\omega_1 = \omega_2 = 6413.55\ RPM$	$\omega_1 = \omega_2 = 6413.55\ RPM$
Air density	$\rho_\infty = 1.138\ kg/m3$	$\rho_\infty = 0.458\ kg/m3$
Air temperature	$T_\infty = 297.6\ K$	$T_\infty = 228.7\ K$
Advance coefficient	$\gamma_1 = \gamma_2 = 0.963$	$\gamma_1 = \gamma_2 = 3.292$

Table 12. Onera HTC5 CROR propeller mission profile design points characteristics.

Design point	Take-Off (T/O)	Cruise (CR)
Power coefficient	$\chi_1 = 1.19$ $\chi_2 = 1.19$ $\chi_{total} = 2.37$	$\chi_1 = 1.85$ $\chi_2 = 1.85$ $\chi_{total} = 3.69$
Thrust coefficient	$\tau_1 = 0.598$ $\tau_2 = 0.647$ $\tau_{total} = 1.24$	$\tau_1 = 0.422$ $\tau_2 = 0.468$ $\tau_{total} = 0.890$
Efficiency	$\eta_1 = 0.485$ $\eta_2 = 0.524$ $\eta_{total} = 0.505$	$\eta_1 = 0.752$ $\eta_2 = 0.835$ $\eta_{total} = 0.793$

Table 13. HTC5 CROR predicted performance (LPC2) at design points.

III.4.2 LPC2 inputs and outputs

All the detailed input parameters are defined by the user within a standard input file, as well as the specifications and eventual options related to calculations. From these inputs, LPC2 computes several aerodynamic and acoustic performances of the propellers and their blades, including the induced forces (axial and tangential) and the total efficiency. The inputs and outputs of LPC2 that will be used to link the aerodynamic analysis to the structural analysis in this chapter are summarized in Table 14. A more exhaustive list of LPC2 inputs and outputs is available in (Gardarein, 2013).

Inputs	Outputs
Blade incidence β_1	Axial force density dF_X/dr
Airfoil twist angles Φ_i	Tangential force density dF_T/dr
Airfoil sweep offsets a_i	Optimal blade incidence $\beta_1^{opt} = \beta_1 + d\beta_1$
Airfoil span-wise location z_i	Total efficiency η_{total}

Table 14. Aerodynamic modeling I/O. Index 1 refers to the front propeller.

Aerodynamic analysis inputs

The blades of the propellers are defined by stacking a fixed set of airfoil sections. For each airfoil detailed, LPC2 reads the look-up table corresponding to the relevant airfoil type (for interpolation in the polar values). According to the given flight condition, LPC2 can compute the performance of the blade from the characteristics of this stack. In the present study, the HPC5 blade is defined by a stack of 15 airfoils. In order to assess the influence of the deformations of the blade on the aerodynamic loads, only the following parameters are triggered:

- The blade tip radius R_{tip} and hub radius R_{hub}.
- The geometric incidence of the reference plane with respect to the plane of rotation (y, z), denoted here as the blade incidence β_1.
- The span-wise location $z_{i=1,\dots,15}$ for each section i between R_{tip} and R_{hub}.
- The sweep offset a_i with respect to pitch axis for each of the i^{th} section.
- The airfoils twist angle Φ_i [deg] with respect to the reference plane of the blade.

Aerodynamic analysis outputs

The blade incidence offset $d\Phi_1$ is optimized by LPC2 to reach the target total thrust for the given propeller shape, and therefore corrects the incidence of the blades, as illustrated in Figure 56. In order to perform the structural analysis of the blade, the following LPC2 outputs are taken into account:

- The optimal blade incidence angle $\beta_1^{opt} = \beta_1 + d\beta_1$.
- The axial force density dF_x^i/dz from steady load distribution for each section i, to be integrated over the finite intervals $[(z_i + z_{i-1})/2, (z_{i+1} + z_i)/2]$. The total axial force after summation on all blades of the front and rear propeller gives the total thrust of the CROR engine.
- The tangential force density dF_y^i/dz from steady load distribution each section i, to be integrated over the finite intervals $[(z_i + z_{i-1})/2, (z_{i+1} + z_i)/2]$. The total tangential force after summation on all blades of a propeller gives the engine torque.
- The total propeller efficiency η_{total} that will be used as an objective function.

III.5 Structural modeling

While operating, the blade undergoes bending moments due to aerodynamic loads and stiffening due to centrifugal loads. The resulting deformation may modify the dihedral and sweep distributions of the blade. These loads also create twisting moments modifying the twist angle distribution of the blade. This can significantly affect the aerodynamic loading – and therefore the performances of the blade (e.g. thrust and efficiency) – since the twist distribution impacts the pressure distribution over the suction and pressure sides. The deformation of the blade is driven by its mechanical structure. In this section, the structural modeling used to compute the deformation of the blade for a fixed aerodynamic loading is described. Firstly, a simple composite structure is assessed for the blade. The construction of a structural mesh of the blade from the CFD mesh is then detailed. Finally the structural modeling is detailed. In particular, the model is parameterized to be linked with LPC2 to allow for iterative mechanical and aerodynamic analyses in the next sections. The structural analysis is performed here using ABAQUS. The model is parameterized to enable modifications of the design parameters of the blade and aerodynamic efforts regarding flight condition.

III.5.1 A monolithic laminated composite blade

In this study, a simple monolithic laminated structure is assumed for the reduced scale blade. Indeed, the length of the blade is 195 mm which does not allow for a very complex internal structure. Assuming that manufacturing a twisted plate whose midplane follows the camber surface of the blade, the blade could be machined from such a laminate, resulting in an outer blended composite monolith, as illustrated in Figure 58. In an outer blended solution, the plies are dropped from the surface of the blade in accordance with the thickness variations along the blade. More design freedom can be obtained by allowing other ply drop orders, which can be achieved using stacking sequence tables (SST). In the following, the structure of the blade is defined using two variable thickness sublaminates: for the intrados and for the extrados of the blade. Thus, two SSTs are used. The stacking direction is defined in Figure 58.

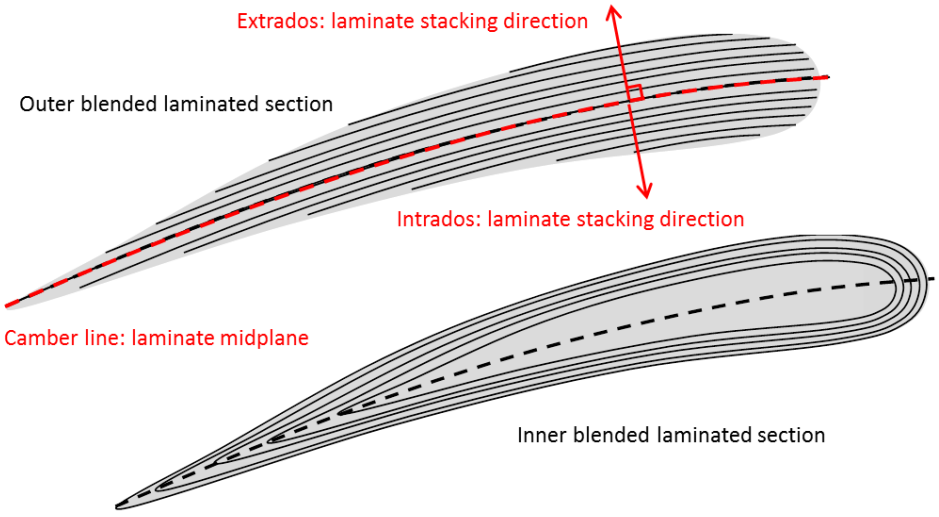

Figure 58. Cross-sections of monolithic (top) and hollowed (bottom) composite blades.

Figure 59 describes the thickness distribution defined by the shape of the HTC5 blade. In the present work, the input shape is defined by the CFD structured mesh of the blade. Figure 59 shows the contour lines of the number of plies in the CFD mesh and the corresponding pixelated distribution in the structural mesh. In the structural model, each element is attributed a laminate in accordance with the intrados SST and the extrados SST and the local number of plies (defined at the center of the element). The ply thickness is 0.126 mm.

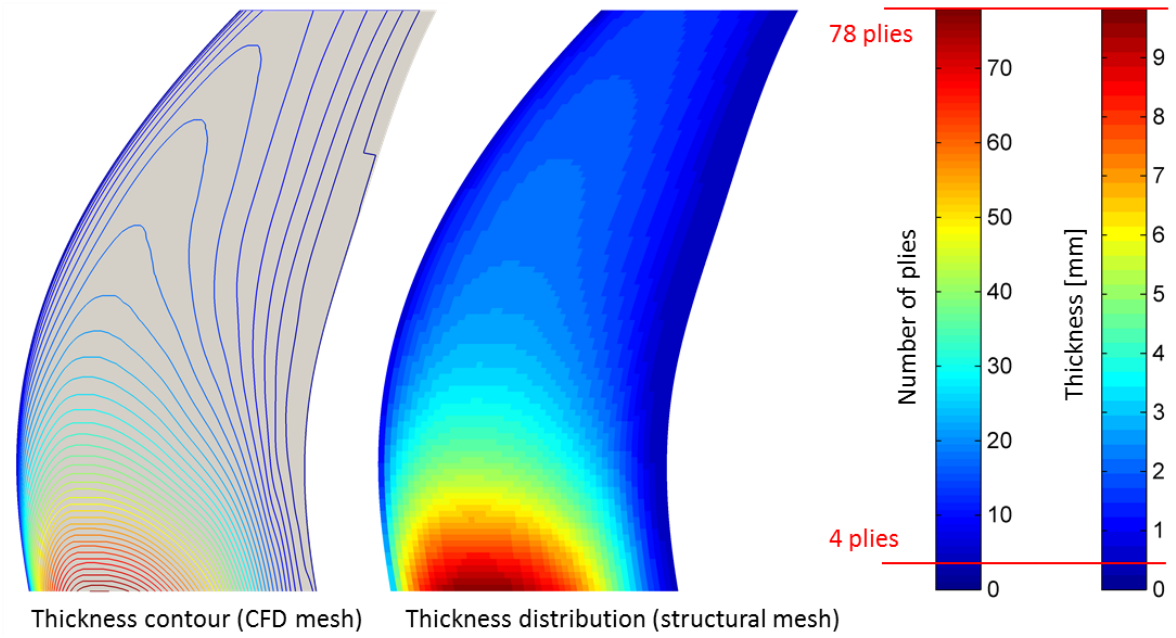

Figure 59. Thickness distribution along the blade (CFD stands here for Computational Fluid Dynamics).

III.5.2 From CFM mesh to structural mesh

In order to perform the finite element analysis of the blade structure, modifications are mandatory to obtain an acceptable structural mesh. Indeed, the original structured CFD mesh describes the surface of the blade through 318 airfoils each one discretized using 250 nodes. The span-wise distribution of the airfoils is regular, but the mesh of the airfoils is highly refined around the leading edge (LE) and trailing edge (TE) to accurately describe these high curvature zones and capture the important gradients of pressure and velocity in the vicinity of the blade surface. Most of the resulting quadrangular elements are highly distorted, as can be seen in Figure 60. In order to resample the surface, the points clouds of the suction and pressure sides of the front blade are extracted from the CFD mesh and assembled after deleting redundant nodes. The first curve corresponds to the leading edge so that the rest of the mesh is generated by sweeping the LE curve along the suction and pressure sides respectively, both ending to the trailing edge. The mesh is scaled in accordance with the chosen scale factor. The camber surface of the blade, passing by the camber lines of the airfoil sections, is computed as the surface equidistant to the intrados and extrados surfaces. A regular structured mesh of the camber surface is generated. Both intrados and extrados surfaces are subsequently resampled by orthogonal projection of the

camber surface mesh. The resulting mesh, shown in Figure 60, is composed of two layers of 8-nodes brick elements, from either side of the camber surface.

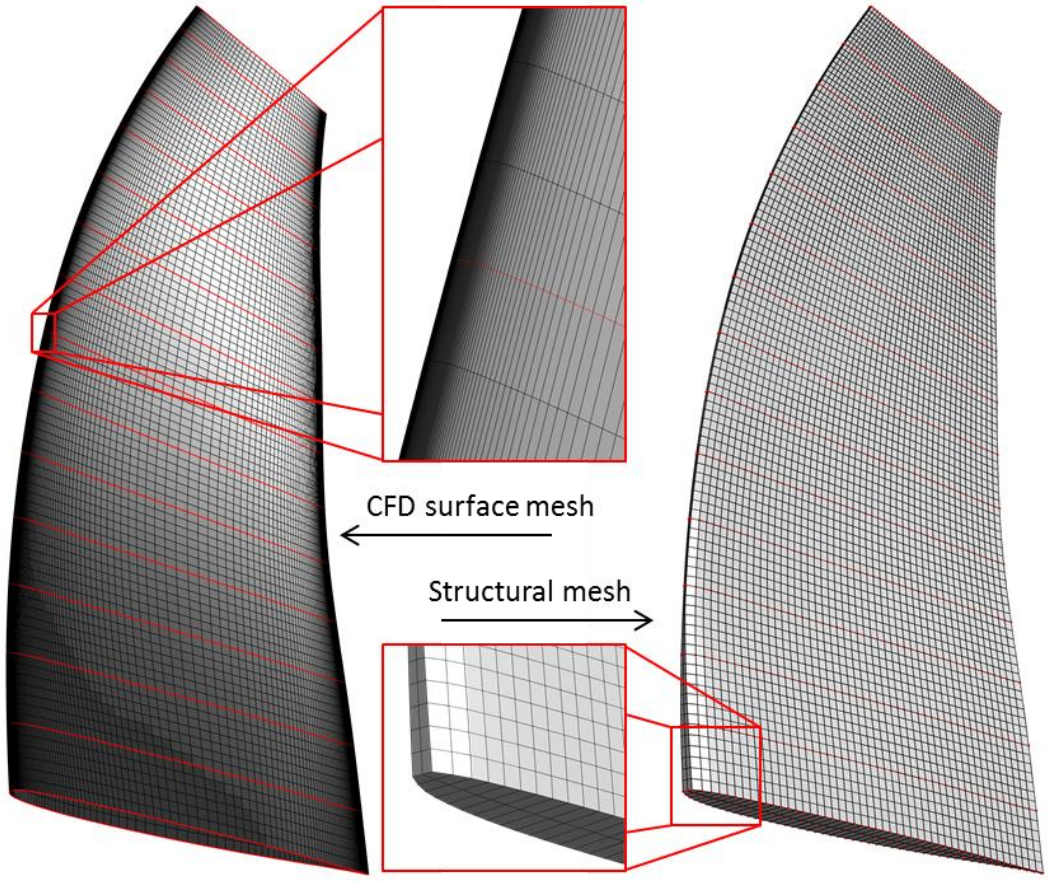

Figure 60. CFD mesh and corresponding CSM mesh.

For the sake of simplicity, the geometry of the blade is approximated around the trailing and leading edges. The LE is split to replace the prismatic definition of the edge by an octahedral one, as illustrated in Figure 61, allowing generating the mesh fully defined with octahedral elements shown in Figure 60. This operation is performed to limit the maximum thickness variation over one element at leading edge, and to enforce a minimal thickness of four plies at trailing edge, i.e. two plies from either side of the camber surface. Sets of nodes are created for each of the airfoil sections, as well as TE and LE, suction and pressure sides, and camber surface. Sets of elements are created according to areas of equivalent thickness distribution along the blade. An element is attributed to a set according to the distance between the center of the face on the camber surface and center of the face on the intrados or extrados surface. In order to enable a layer-wise description of the laminates, ABAQUS 8-nodes continuum shell elements (e.g. SC8) are used. The stacking directions for the intrados and extrados sides are shown in Figure 58. The out-of-plane material direction is orthogonal to the camber surface. The longitudinal axis (i.e. the 0°-direction of the lay-up) is defined by projection of the z-axis of the global coordinate system onto the camber surface. The transverse direction (i.e. the 90°-direction of the lay-up) is tangent to the camber surface and defined so that the local coordinate system is orthonormal.

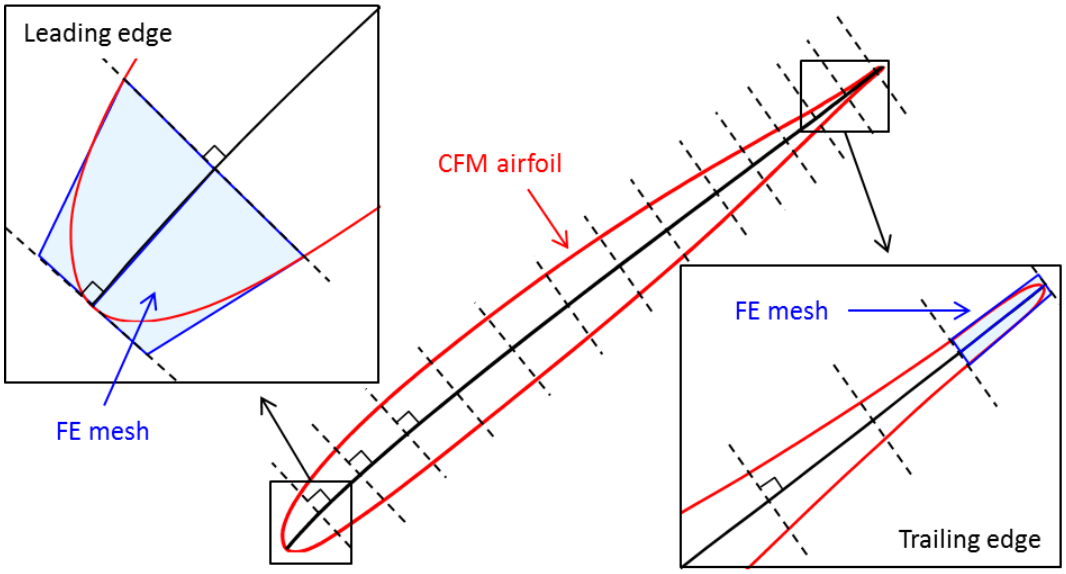

Figure 61. Edge approximation at leading and trailing edges.

III.5.3 Boundary conditions and loadings

With respect to the assembly envisaged to fix the blade to a pitch control system, the blade may be considered as fully embedded to the dovetail root at hub radius. The boundary conditions applied are essentially consisting in fixing constraint on all displacements (U) at the whole node set of the blade root section.

The optimal aerodynamic shape of the blade is a steady-state obtained at specific flight condition when the blade is operating. For now, the cold shape of the blade is unknown but centrifugal loads are easily estimated from rotation speed. The centrifugal loading is represented within ABAQUS using a distributed loading condition of type "Rotational body force".

The induced aerodynamic loads are available for the hot shape via LPC2. LPC2 returns the axial and tangential force density resultants at the 25%-chord points (see Table 13) of the 15 sections highlighted in red in Figure 60. The question is how to introduce this loading into the structural model since the 25%-chord points do not correspond to nodes of the structural mesh (some are even located out of the volume of the blade). Two solutions have been implemented in the present work.

The first solution consists in defining, in the model, the reference points corresponding to the 25%-chord point of each section considered in LPC2. The reference points are linked through rigid body constraints to the nodes of their respective airfoil section, ensuring the motion of the whole section in accordance with the motion of its reference point. Load resultants are integrated from LPC2 load density resultants and applied as concentrated loads at the corresponding reference points. The approximation made on the geometry around the TE and LE does not have an impact on such an aerodynamic loading.

The second solution consists in interpolating and parameterizing a template pressure distribution. For each operating point, a pressure distribution is computed using elsA. The pressure distributions are subsequently interpolated at the center of the faces of the structural mesh, on both suction side and pressure side. The load resultants are computed at the 25%-chord point of each section considered in LPC2. The pressure distribution is normalized with respect to these resultants to obtain parameterized template pressure distributions compatible with LPC2 outputs. Of course, this normalization results in a non-physical loading but is an efficient manner of obtaining a pressure distribution coherent with the LPC2 loading. The pressure distribution can finally be applied on the faces of the continuum shell elements located on the intrados and extrados surfaces. Shell elements do not allow for pressure to be applied on the side of the element, orthogonally to the stacking direction so that leading edge and trailing edge are not loaded in the proposed model, which is a strong approximation. The pressure distributions computed with elsA for T/O and CR are shown in Figure 62 and Figure 62 respectively. These figures show the important pressure gradient located at the leading edge of the blade. In this case, the shape simplification at the LE and TE will have an important impact on the aerodynamic loading. A refined CSM mesh would be necessary to accurately interpolate the aerodynamic loading from a CFD computation. However although the normalized pressure distribution is not as physical as an interpolation from a CFD computation would be, it is much more representative of the real aerodynamic loading than the linear distribution of the first solution.

III.5.4 Structural analysis inputs and outputs

The input parameters are defined within a standard input file parameterized using MATLAB. From these inputs, ABAQUS computes the mechanical behavior of the blade, including stress and strain required to check the integrity of the blade toward failure and feedback the design parameters of the deflected blade. The model is used to return the nodal displacements and the in-plane stresses per elements per plies. The model is implemented within a MATLAB routine that enables to link the structural modeling to the aerodynamic analysis. The corresponding inputs and outputs are summarized in Table 15.

Inputs	Outputs
Blade incidence angle β_{opt}	Airfoil twist angles Φ_{i}
Airfoil twist angles Φ_{i}	Airfoil sweep offsets a_{i}
Airfoil sweep offsets a_{i}	Airfoil span-wise location z_{i}
Airfoil span-wise location z_{i}	Airfoil dihedral offsets d_{i}
Axial force density dF_{X}/dr	Failure criterion
Tangential force density dF_{T}/dr	
Rotation speed Ω [rad/s]	

Table 15. Structural modeling I/O

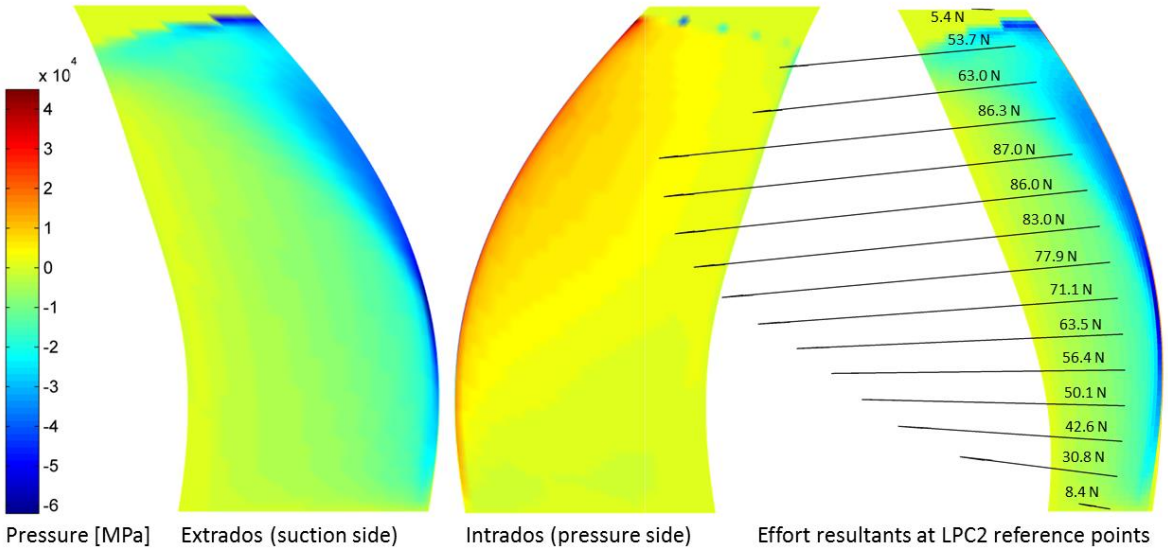

Figure 62. Pressure field and resultant forces on the blade at T/O conditions.

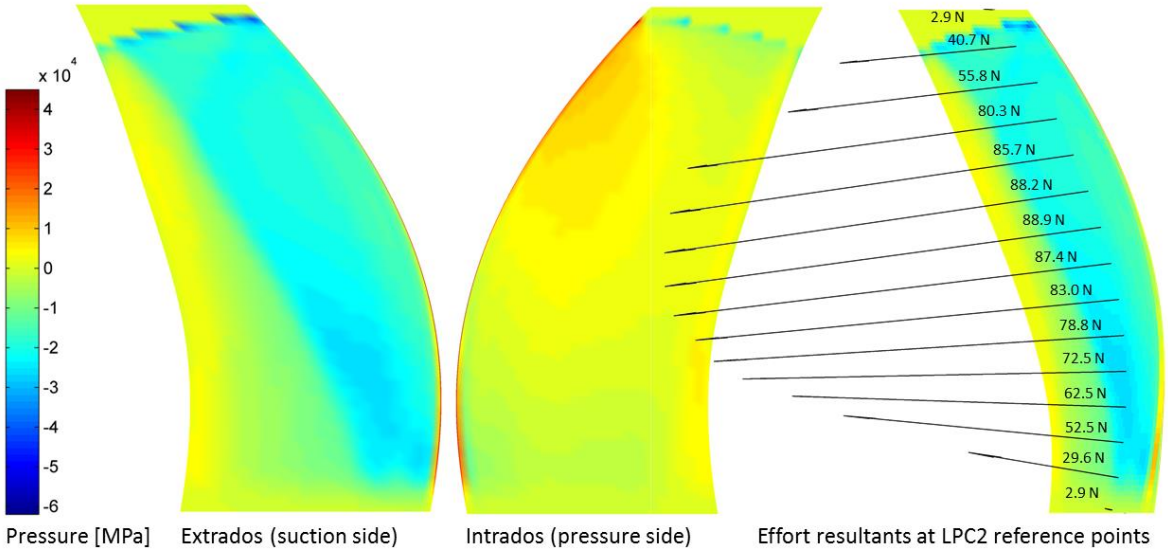

Figure 63. Pressure field and resultant forces on the blade at CR conditions.

Structural analysis inputs

The inputs β_{opt}, Φ_{i}, a_{i} and z_{i} are used to morph the mesh of the blade to take into account a given deformation state. These inputs result from a previous structural analysis. The corresponding aerodynamic load density distributions assessed using LPC2 are introduced in the model either as concentrated loads on the reference points of the rigid body sections or through the template pressure distributions. Due to the design philosophy of the HTC5 blade, the rotation speed is a fixed parameter in this study, whatever the operating point (see Table 12).

Structural analysis outputs

The stress fields resulting from the structural analysis of the blade enable computing the first ply failure criterion of the structure, while the displacement field allows updating the blade design parameters to be passed to LPC2. The deformed mesh is analyzed to compute the new blade geometric parameters values based on the definitions given in Section III.3.1. The modified Tsaï-Hill first ply failure criterion is computed based on the in-plane stresses returned by the model at the section points of the shells, according to the following equation:

$$f_{TH} = \frac{\sigma_{11}^2}{X^2} - \frac{\sigma_{11}\sigma_{22}}{X^2} + \frac{\sigma_{22}^2}{Y^2} + \frac{\sigma_{12}^2}{S^2} \qquad \text{III-2}$$

where $\sigma_{11} \geq 0 \Rightarrow X = X_t$, else $X = X_c$ and $\sigma_{22} \geq 0 \Rightarrow Y = Y_t$, else $Y = Y_c$. The material properties of the base ply are defined in Table 16. Local failure is reached for $f_{TH} \geq 1$. In the following, the notion of reserve factor (RF) is used to assess the ability of the structure to sustain larger loads without failure:

$$RF = \frac{1}{\sqrt{f_{TH}}} \qquad \text{III-3}$$

Property	Value
Longitudinal modulus E_1	115 GPa
Transverse modulus E_2	8.5 GPa
In-plane Poisson's ratio υ_{12}	0.32
In-plane shear modulus G_{12}	4.5 GPa
Out-of-plane shear modulus G_{23}	3 GPa
Longitudinal tensile strength X_t	2000 MPa
Longitudinal compressive strength X_c	-1300 MPa
Transverse tensile strength Y_t	76 MPa
Transverse compressive strength Y_c	-260 MPa
Shear strength S	81 MPa
Density d	1.618
Ply thickness t_{ply}	0.126 mm

Table 16. Material properties of the T700/M21 ply. The ply is assumed transverse isotropic.

III.6 Hot-to-Cold process

Aerodynamic optimization of a propeller blade returns an optimal shape at a given operating point, i.e. flight conditions inducing specific loading conditions for the blade. Thus, the optimal shape is the shape of a deformed structure under both centrifugal and aerodynamic loading. The purpose of the Cold-to-Hot process is to find the shape of the unloaded blade.

III.6.1 Method

Figure 64 describes the H2C analysis method devised in the present work. Starting from the optimal hot shape at given flight conditions, the aerodynamic loads and thrust-optimal blade incidence are computed through LPC2. The optimal hot shape itself is considered solicited by these aerodynamic loads, in addition of the centrifugal loads related to the flight conditions. A FEA is performed to determine an 'overheated' shape. The displacements of the nodes induced by the solicitation are subtracted to the optimal hot shape, in order to assess a first hypothetical cold shape. This intermediate cold shape is hence submitted to FEA with the same load cases and then corrected iteratively until its deflected shape matches the optimal hot shape.

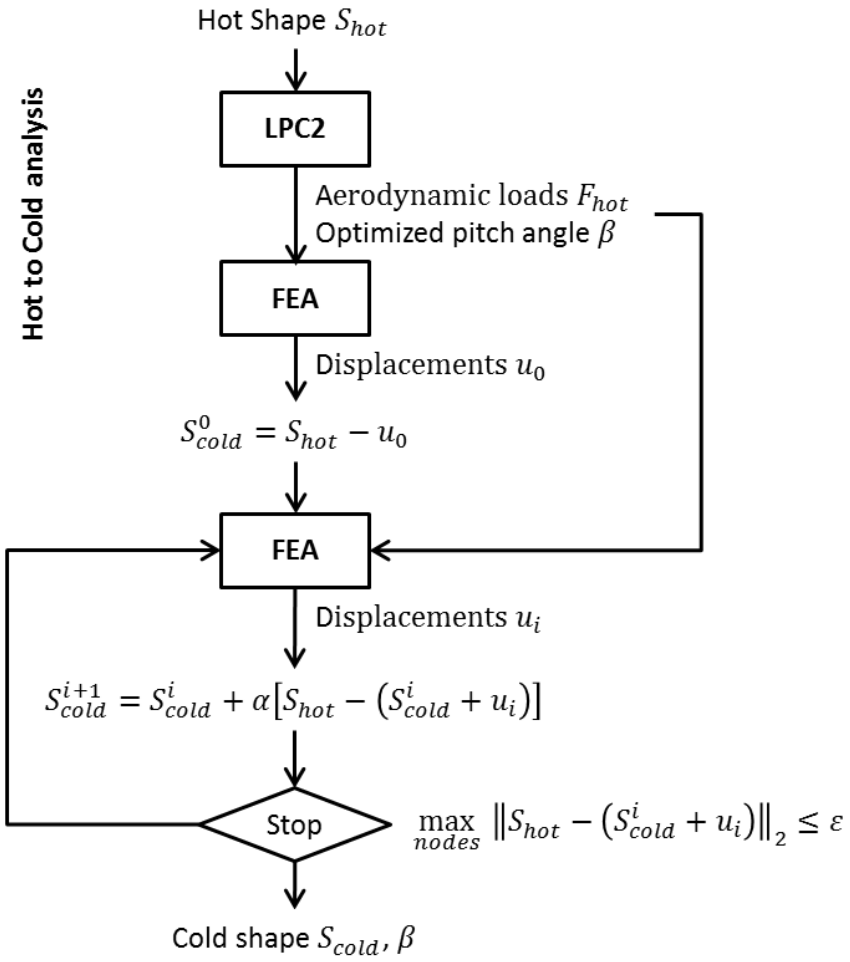

Figure 64. Hot-to-Cold (H2C) iterative process.

Initialization of the Hot-to-Cold process

The Hot-to-Cold process shown in Figure 64 is programmed with MATLAB. It calls iteratively the aerodynamic modeling and the structural modeling previously presented in Section III.4 and Section III.5 respectively. The H2C analysis starts form a hot shape at a given operating point.

First, the initial radial positions z_{i} of the airfoil sections of the blade, the offsets a_{i} of the 25% chord line with respect to pitch axis, and the twist angles Φ_{i} are evaluated on the hot shape. These geometric design parameters and the flight conditions are used as inputs for LPC2, enabling computing the aerodynamic loads and the optimal incidence angle to use for the whole H2C process. Additionally, the efficiency and thrust coefficient of the two propellers are computed. The LPC2 optimization process is sensitive to the initial value of β: calculation may not converge if the initial value is ill-chosen and the further the initial point from the optimal solution, the longer to converge the LPC2 computation. In this work, the initial value of β is set to 45°, which is shown to be a good trade-off value between all tested configurations.

The optimal incidence angle β^{opt} and the aerodynamic loads are passed as inputs of a first structural analysis to compute an "overheated" shape S_{over}. The "overheated" shape corresponds to the deformed shape obtained by applying to the initial hot shape S_{hot} the centrifugal loading corresponding to the considered operating point and the aerodynamic loadings computed by LPC2. A first assumption of the cold shape is built by subtracting the nodal displacements u_0 resulting from the FEA from the initial hot shape:

$$S_{cold}^{0} = S_{hot} - u_0 \quad \text{with } u_0 = S_{over} - S_{hot} \qquad \text{III-4}$$

The iterative process of the Cold-to-Hot analysis starts from here, correcting the predicted cold shape until its deformed shape matches the hot shape with an acceptable precision ε.

Subsequent iterations

At iteration i, a FEA is performed to compute the displacement u_i of the cold shape S_{cold}^{i} under the aerodynamic and centrifugal loads obtained for the targeted hot shape S_{hot}. The difference δ_i between the deformed cold shape and the optimal hot shape S_{hot} is expressed as:

$$\delta_i = S_{hot} - \left(S_{cold}^{i} + u_i\right) \qquad \text{III-5}$$

The cold shape S_{cold}^{i} is corrected as follows:

$$S_{cold}^{i+1} = S_{cold}^{i} + \alpha\delta_i \qquad \text{III-6}$$

where α is a relaxation factor used to ease convergence. In the present work, α is defined as a linear function of the radius of the blade. Convergence of the whole H2C process is assessed on

the maximal distance between nodes on the target hot shape S_{hot} and the hot shape computed at iteration i. Criterion ϵ is set to 0.05 mm in the following.

$$\max_{nodes} \left\| S_{hot} - \left(S_{cold}^{i} + u_i \right) \right\|_2 \leq \varepsilon \qquad \text{III-7}$$

III.6.2 Determination of the cold shape of an aluminum HTC5 blade

Here, the H2C process is applied to determine the cold shape of a HTC5 blade made of aluminum ($E = 75$ GPa, $\upsilon = 0.3$ and $d = 2$). Twist, dihedral and sweep distributions of the cold shape are discussed as well as the Von Mises stress distribution in the blade. Two cases are compared here depending on how the aerodynamics loadings are introduced within the structural analyses. The hot shape considered is the HTC5 shape optimized for CR condition but used up to now for every operating point without deformation. In this section, we consider the HTC5 design to be the hot shape of the blade at CR condition.

Through concentrated forces on reference points

Figure 65 shows, on the left, the final cold shape obtained after H2C analysis together with the initial hot shape. The HTC5 blade undergoes a significant deflection between the cold shape and the hot shape. The H2C process converged within 8 iterations. Using concentrated axial and tangential forces on reference points of fixed airfoil sections requires enforcing rigid-body constraints at each of the sections of the structural model corresponding to the 15 sections considered in LPC2. The rigid body constraints raise artificial stress concentration in the blade, as can be seen from Figure 13, which could provide locally inconsistent results about failure.

Through pressure fields

The idea of using template pressure distributions in this work (as explained in Section III.5.3) was mostly driven by the necessity of obtaining smooth stress distributions to assess the failure of the blade, what rigid body constraints do not enable. With respect to Figure 65, Figure 66 shows very similar deflection between the cold shape and the hot shape. The H2C process also converged within the same number of iterations than previously. However, introducing the aerodynamic loads through a pressure distribution results in much more physical stress distribution within the blade. Consequently, the use of pressure distribution will be preferred from now on.

Figure 67 shows the evolutions of the radial location of the blade tip over the different iteration of H2C (top left), the variations of the dihedral distribution of the blade (top right) and the distributions (left) and variations of the sweep (middle row) and twist angle (bottom row). All structural computations here have been performed using non-linear displacement analysis (ABAQUS NLGEOM = YES). The figure shows that the cold shape of the blade presents a significant dihedral, with a pronounced curvature at the mid-span of the blade, which corresponds to the zone where the blade gets thinner (see Figure 59) and thus loses most of its local bending stiffness. The variation of the tip section radius is a combined effect of the dihedral of the cold shape and lengthening of the blade due to centrifugal loading. The sweep variation is the highest at the tip of the blade where the local thickness and stiffness are the lowest. The twist

variation is rather low, but it is interesting to notice that the main variations are mostly located at about mid-span of the blade, where the chord lengths are the most important which gives more lever to the bending moments to twist the blade.

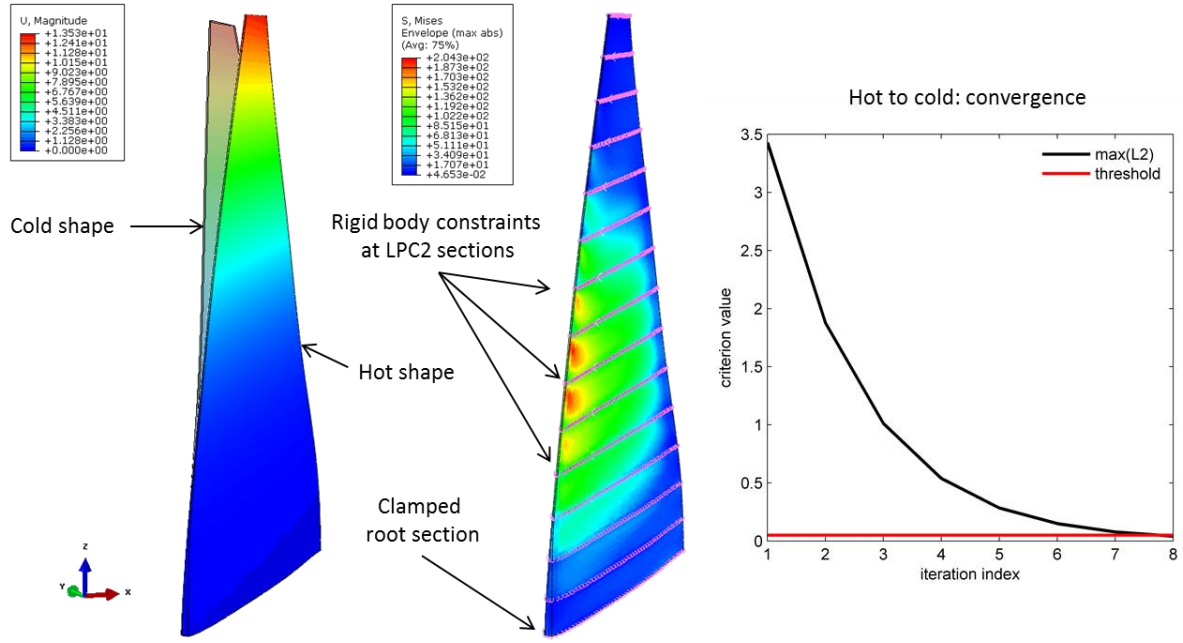

Figure 65. Cold shape versus hot shape of the aluminum HTC5 blade (left). Rigid body constraints and Von Mises stress distribution on the pressure side of the blade (center). Convergence curve of the H2C process (right).

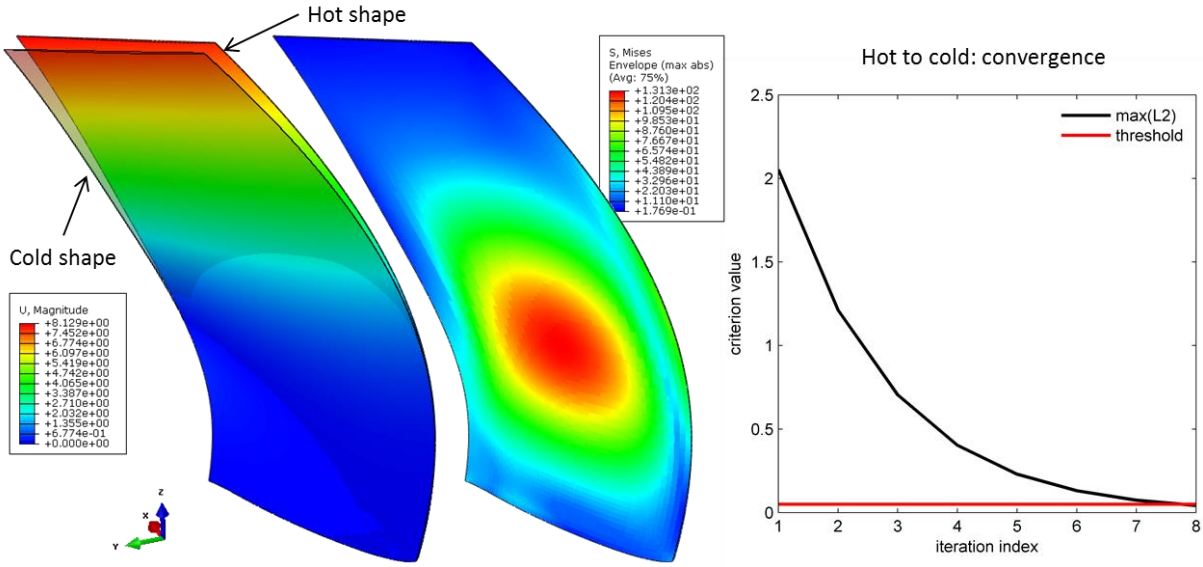

Figure 66. Cold shape versus hot shape of the aluminum HTC5 blade (left). Von Mises stress distribution on the suction side of the blade (center). Convergence of curve of the H2C process (right).

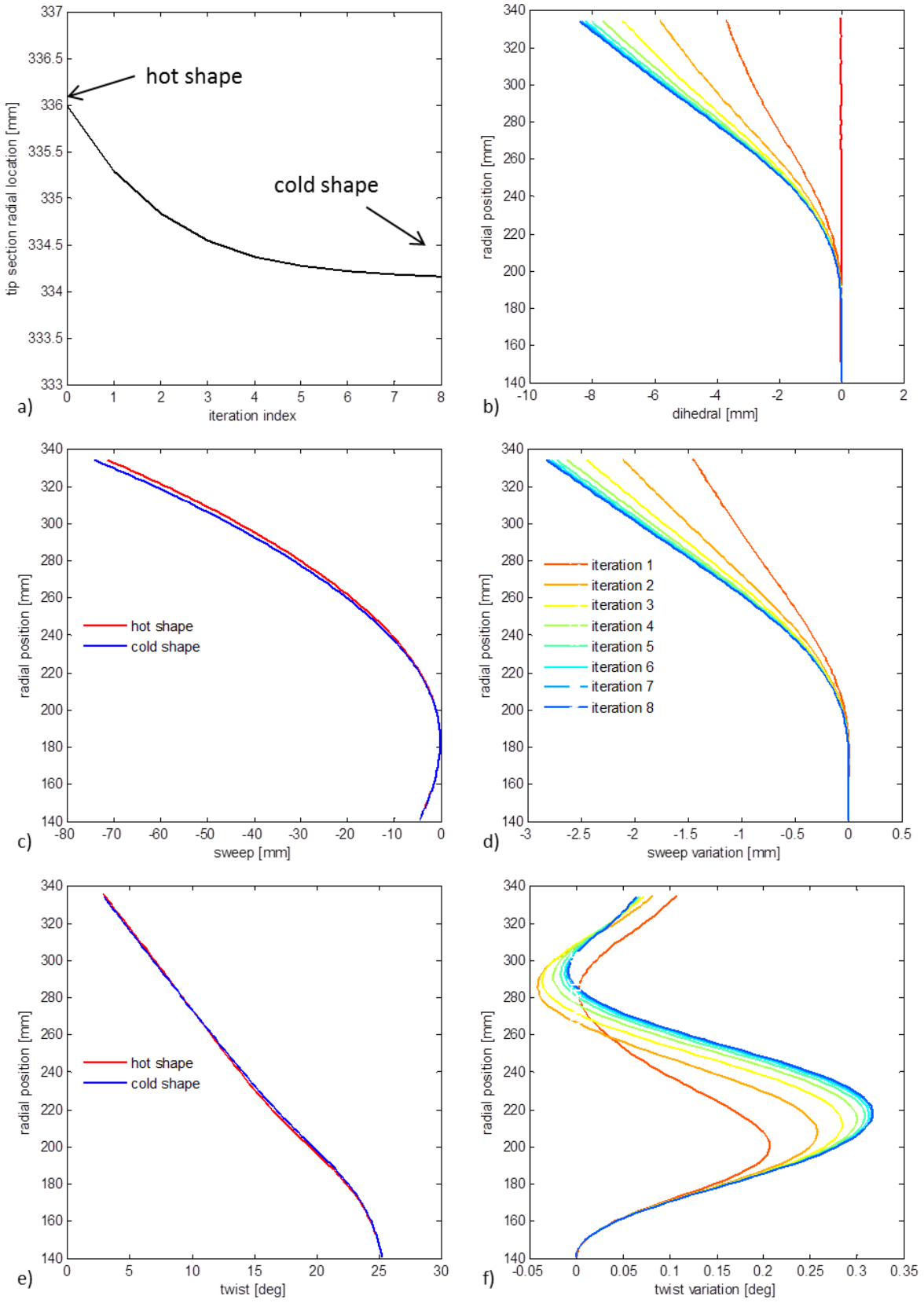

Figure 67. a) Length of the aluminum HTC5 cold shape (computation with non-linear geometry). b) Dihedral variations with respect to the hot shape for the iterations of the H2C process at CR condition. c) Sweep of the initial hot shape and final cold shape and d) sweep variations. e) Twist law and f) twist angle variations.

Figure 68 compares the contributions of the aerodynamic and centrifugal loads to the variations of the design parameters of the cold shape of an aluminum HTC5 blade. The computations are performed with either linear (LGEOM) or non-linear displacement analysis (NLGEOM) in ABAQUS. The figure corresponds to the initialization of the H2C process with the computation of the "overheated shape". These results show that the aerodynamic loads have a very small influence on the design. On the contrary, centrifugal loads have the largest contribution in the modification of the design parameters. This is to be put into perspective with the very high rotation speed of the blade (see Table 12) that induces a very high centrifugal loading. It can be noticed that aerodynamic and centrifugal effects seems to be opposite. The effects of centrifugal loads are significantly overestimated when a linear displacement analysis is performed. Additionally convergence of the C2H process is difficult with linear FEA. A relaxation factor varying from 0.8 at R_{hub} to 0.5 at R_{tip} is necessary to stabilize the convergence whereas, with non-linear FEA, relaxation is not necessary. This difficulty can be explained by the reorientation of the material axes with bending of the blade which can only be taken into account with a non-linear displacement analysis. Thus, non-linear displacement analysis is necessary and used in the following sections.

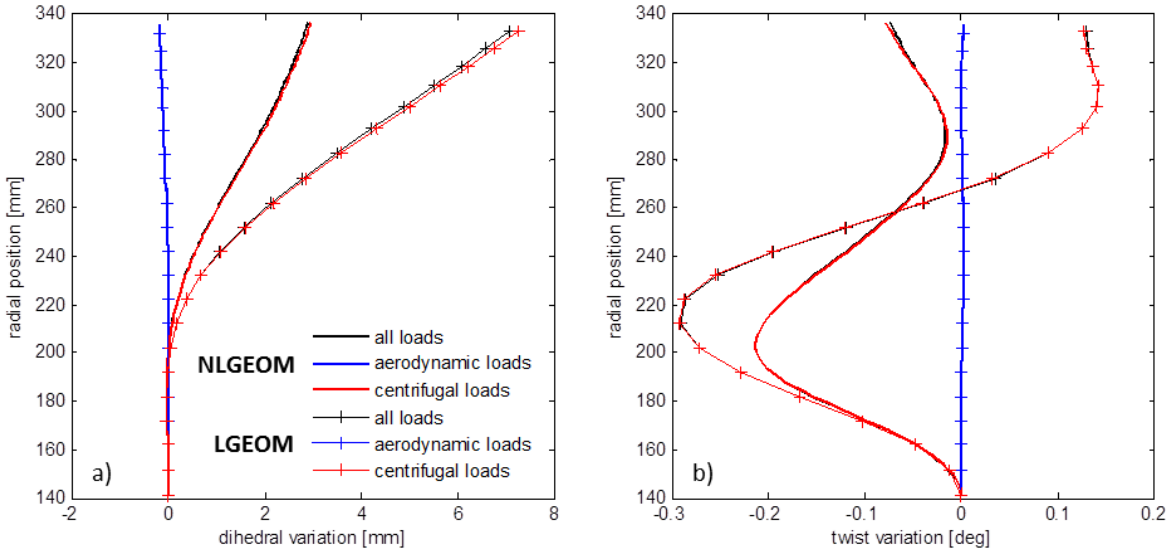

Figure 68. Contribution of the aerodynamic and centrifugal loads to the variations of dihedral (a) and twist (b) of the HTC5 aluminum cold shape. Computation of the "overheated shape". Computations are performed with linear (LGEOM) and non-linear (NLGEOM) displacement analysis.

III.7 Cold-to-Hot analysis

Starting from a known cold shape, the purpose of the cold-to-hot analysis is to compute the deformed shape of the blade, taking into account the interactions between the deformation of the blade and the aerodynamic loading.

III.7.1 Method

The C2H process devised in this work is illustrated in Figure 69. The iterations to reach a stabilized hot shape and aerodynamic loading of the blade all require both LPC2 and FEA computation. Starting from the cold shape S_{cold}, the corresponding aerodynamic loads F_0 and the optimal blade incidence β_0 are computed using LPC2. They complete the structural model which is used to compute a first hot shape S_{hot}^0 using a non-linear analysis. The deformed shape nodes positions may be expressed as:

$$S_{hot}^0 = S_{cold} - u_0 \qquad \text{III-8}$$

The process subsequently iterates on both LPC2 and FEA to reach stabilization of both the hot shape and the aerodynamic loading. At iteration i the deformed shape nodes positions is expressed as:

$$S_{hot}^i = S_{cold} - \alpha . u_i \qquad \text{III-9}$$

where α is the relaxation factor used to ease convergence. In practice, in the following, no relaxation was necessary and α is set to 0. The process iterates until convergence. The convergence criterion is based on a maximal Euclidian distance and maximal concentrated forces variations between two successive iterations:

$$\max_{nodes} \left\| S_{hot}^i - S_{hot}^{i-1} \right\|_2 \leq \varepsilon_1 \qquad \text{III-10}$$

$$\max_{RP} |F_i - F_{i-1}| / |F_i| \leq \varepsilon_2 \qquad \text{III-11}$$

This way, a steady-state shape at any design point may be approximated while monitoring the main characteristics of the geometry of the blade during the process. Criterion ϵ_1 is set to 0.05 mm and criterion ϵ_2 is set to 0.1 % in the following.

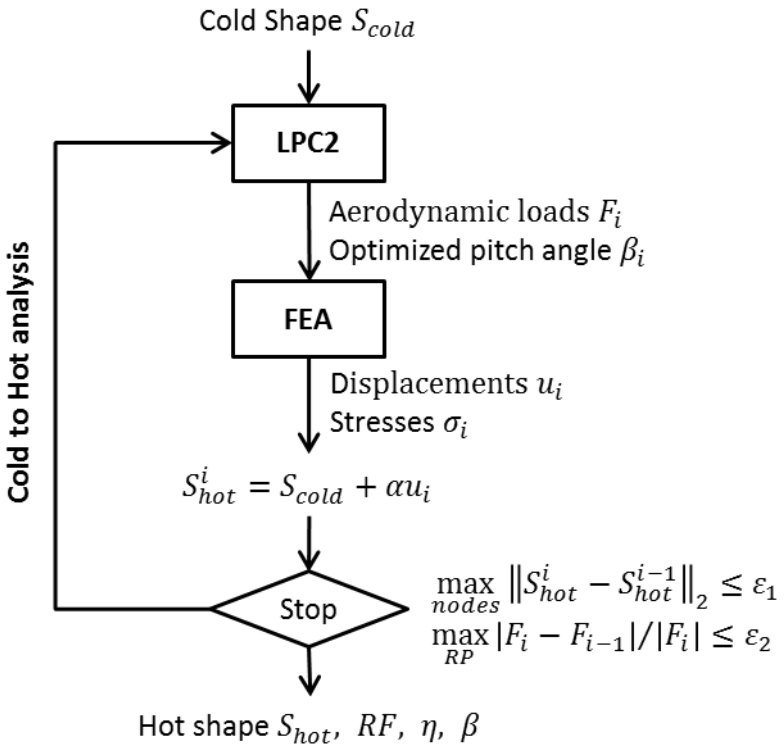

Figure 69. Cold-to-Hot (C2H) iterative process

III.7.2 Influence of the material selection on the blade deformation

The cold shape obtained in Section III.6 for the aluminum HTC5 blade is used as starting point for all C2H analyses, whatever the design point. The C2H process is performed for T/O condition with 10 different materials:

- Two metallic isotropic materials, aluminum ($E = 75$ GPa, $\upsilon = 0.3$, $d = 2$ and $R = 500$ MPa) and titanium ($E = 110$ GPa, $\upsilon = 0.3$, $d = 4.5$ and $R = 1200$ MPa).
- Four laminates are symmetrical and balanced T700/M21 laminates (see Table 15 for material properties): the unidirectional $[0_{40}]_s$ laminate and $[90_{40}]_s$ laminate, the angle-ply $[(45/-45)_{20}]_s$ laminate and the quasi-isotropic $[(45/0/-45/90)_{10}]_s$ laminate. All these laminates have very different membrane and bending stiffness but no membrane-bending coupling or tension-shear coupling.
- Two unbalanced laminates with strong tension-shear coupling: the $[(45/0/45/90)_{10}]_s$ laminate and the $[(-45/0/-45/90)_{10}]_s$ laminate.
- Two unsymmetrical laminates with strong membrane-bending coupling: the $[(-45)_{40}/45)_{40}]$ laminate and the $[(45)_{40}/-45_{40}]$ laminate.

Note that the structure of the blade is here defined using 80-ply laminates for commodity. The first 40 plies define the stacking of the intrados of the blade; the next 40 plies define the extrados of the blade. The mid-plane of the laminate is the camber surface of the blade. The blades considered here are outer-blended (see Figure 58), i.e. plies are dropped from the outer surface of

blade. The actual blade has only 78 plies in its thickest zone (see Figure 59), so that ply 1 and 80 have to be discarded.

Figure 70 shows the influence of the material on the design parameters of the hot shape (i.e. twist angle distribution, sweep distribution, dihedral and radial location of the tip of the blade). Isotropic materials and the quasi-isotropic laminate tend to minimize the dihedral and twist variation. The 0°-laminate gives the stiffest blade in the longitudinal direction and the 90°-laminate the highest lengthening. On the contrary, solutions with high in-plane tensile-shear coupling such as the $[(-45)_{40}/45)_{40}]_s$ laminate and the $[(45)_{40}/-45)_{40}$ laminate tend to maximize the twist variation. Even with such a simple structure as a monolithic composite, these results show that tailoring the laminate offers interesting possibilities to tailor the deformation of the blade in operating conditions.

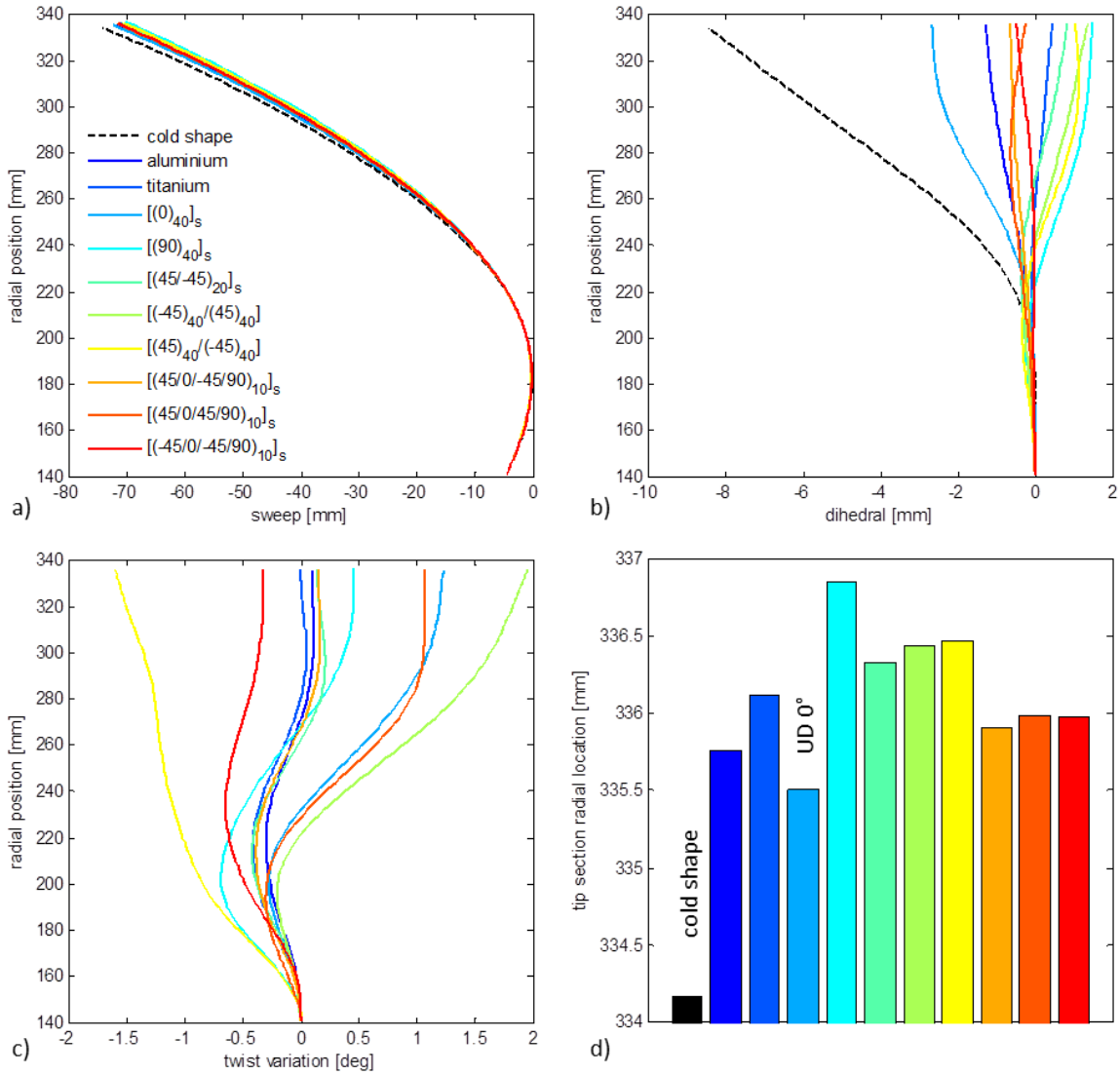

Figure 70. Influence of material selection on the design parameters of the HTC5 blade geometry. The cold shape corresponds to the result of the Hot-to-Cold analysis of the aluminum blade with CR conditions (see Figure 67). The Cold-to-Hot analysis is performed at T/0 condition.

Table 17 shows the performances computed after Cold-to-Hot analysis of the blades detailed in Figure 70. The composite blades are 20 % lighter than the aluminum blade and 64 % lighter than the titanium solution. Significant variation of the reserve factor is observed. The lowest strength is achieved with the 90° unidirectional laminate while the highest strength is obtained with the 0° laminate. This is consistent with the predominance of the centrifugal loading observed in Figure 68. However, the variation of efficiency is low. The lowest efficiency (50.43 %) is obtained with the aluminum blade.

It is interesting to compare the efficiency of the hot shape at CR condition evaluated at T/O condition (50.46 %, see Table 13) and the efficiency computed for the aluminum blade after Hot-to-Cold analysis from CR conditions and Cold-to-Hot analysis at T/O conditions (50.43 %). The variation is very low which suggest that the whole H2C and C2H processes are unnecessary in that case. This result is disappointing but higher variations are expected for other materials (see Section III.9). The results shown in Table 17 suggest that massive monolithic blades are too stiff to observe, between different operating conditions, variations of the twist law of the blade important enough to modify significantly the total efficiency of the propeller. Note that for all the results presented, the rear propeller is still unchanged.

It is also interesting to note that the lowest efficiency is matched by the $[(45)_{40}/\text{-}45_{40}]$ composite solution while the best efficiency (50.82 %) is obtained with the opposite laminate $[(\text{-}45)_{40}/45)_{40}]$. These two laminates are orthotropic in membrane and bending and present pure in-plane-shear/twisting couplings, B_{16} and B_{26} with $B_{16} = B_{26}$, and opposite signs. This results shows that coupled behaviors are interesting to optimize the blade for various operating conditions.

Material	Mass (g)	Efficiency η (%)	Reserve Factor
Aluminum	98	50.43	3.85*
Titanium	221	50.50	4.74*
UD 0°	79	50.51	5.31
UD 90°	79	50.77	1.63
$[(45/\text{-}45)_{20}]_s$	79	50.56	2.74
$[(\text{-}45)_{40}/45)_{40}]$	79	50.82	2.36
$[(45)_{40}/\text{-}45_{40}]$	79	50.43	2.71
$[(45/0/\text{-}45/90)_{10}]_s$	79	50.48	4.15
$[(45/0/45/90)_{10}]_s$	79	50.58	3.64
$[(\text{-}45/0/\text{-}45/90)_{10}]_s$	79	50.47	3.63

Table 17. Mass and performances of the blades after Cold-to-Hot analysis (see Figure 70) at T/O condition. All designs share the same cold shape. The cold shape corresponds to the result of the Hot-to-Cold analysis of the aluminum blade with CR conditions (see Figure 67).
***For metallic materials, the reserve factor is computed as the ratio between the elastic limit R and the maximum Von Mises stress.**

III.8 Optimization of a monolithic blade

In order to gain some insight in the design of the blade structure, a bi-objective optimization problem is formulated for a given operating condition. The first objective is to maximize the total efficiency η of the propeller. The second objective is to maximize the reserve factor related to the modified Tsaï-Hill first ply failure criterion. The design variables are the SST on the extrados and intrados of the blade (see Figure 58). For both SSTs, the number of plies ranges from $n_{min} = 2$ to $n_{max} = 40$. Thus, each SST is described by a signed integer vector SST_{lam} of length 40 and a permutation vector SST_{ins} of length 40. The distribution of ply numbers is defined by the cold shape of the blade. The designs are evaluated using the Cold-to-Hot process described in Section III.7. The cold shape was obtained after Hot-to-Cold analysis at T/O conditions for an aluminum blade.

The optimization is performed using a slightly modified version of the EA presented in Chapter I. (i) First, since the thickness distribution is fixed, all variation operators devised for chromosome N_{str} are deactivated. In the EA described in Chapter I, for a solution selected for mutation with probability P_m, the mutation operates with equal probability on one of the three chromosomes of the solution. In the present implementation, the mutation operates with equal probability on either chromosome SST_{lam} or chromosome SST_{ins}. Similarly, in the present implementation, the crossover operates on the SST only. Thus, the chromosome N_{str} is kept unchanged. (ii) Second, the EA is able to handle multiple SSTs. Instead of being defined by a single skin determined by the triplet $(SST_{lam}, SST_{ins}, N_{str})$, a solution can now be defined by several skins corresponding to a partition of the structure to be optimized. Each skin is defined by the three chromosomes $(SST_{lam}, SST_{ins}, N_{str})$. This enriched encoding of the solutions affects the creation of the solutions, the variation operators and the evaluation of the designs. The code is adapted to this new encoding in a very simple way. Instead of applying the creation and variation operators once per solution as it is the case in Chapter I, the operators are applied independently to each constitutive skin of each solution.

With respect to the design guidelines listed in Section I.2, no laminate design guidelines are enforced here. The idea is to explore the possibilities offered by coupled laminates (non-balanced, non-symmetrical, etc.) to tailor the hot shape and performances of the blade. Non-symmetrical laminates are obtained by stacking two different SSTs in the thickness of the blade. Three ply-drop design guidelines – *covering* (7.), *internal continuity* (10.) and *ply-drop alternation* – are enforced. The blending global requirement is enforced through the use of SSTs.

The covering guideline imposes that the plies on the surface of the laminates are never dropped in the SST. The internal continuity guideline states that a continuous ply should be kept every three consecutive dropped plies. Within chromosome SST_{ins}, a continuous ply is given rank $rk = rk_{min} = 0$. Strictly positive integer values in SST_{ins} correspond to the insertion rank of the ply within the SST. The internal continuity guideline implies a dependency of the maximal number of plies n_{max} to the minimal number of plies n_{min} of the SST: $n_{max} < 3 \times n_{min} - 2$. When reached, the limitation is relaxed by incrementing the value of rk_{min}. Thus, the relaxed internal continuity guideline states that a ply of rank $rk \leq rk_{min}$ has to be kept every three

consecutive ply drops. By doing so, the dependency between n_{max} and n_{min} disappears. New plies can be inserted in the SST, as long as they are surrounded by plies inserted long before.

The optimization budget was fixed to 3000 design evaluations. The current population size is set to $\lambda = 30$, the archive population size is $N_a = 30$. The probability of crossover per solution is set to $P_c = 0.3$ and $P_m = 0.9$. The optimization was repeated twice. The first optimization was performed for T/O conditions. The second optimization was performed at CR conditions. The results are presented in Figure 71.a and Figure 71.b respectively. Each point in the figures corresponds to a design. However, there is no correspondence between the points in the two figures. The optimizations have been performed simultaneously and independently. One optimization lasted about two weeks, with all FE analysis performed sequentially. The C2H process converged in 3 to 4 iterations. The figures show that for both operating conditions, the propeller efficiency and the reserve factor are conflicting objectives. On the one hand, the range of the reserve factor values is important. Nevertheless the minimal RF is about 2. None of the evaluated laminates fails under the combined centrifugal and aerodynamic loading. On the other hand, the range of variation of the propeller efficiency is about 0.5 % in both cases. One could have expected greater variations. Both optimizations performed at CR and T/O conditions confirm what was inferred from Table 6 in the sole case of CR condition and for a limited set of laminates. The monolithic blade turns out to be a far too resistant and stiff structure to observe the effects of aeroelastical deformations with respect to the applied loading for the reduced scale blade.

The most efficient structures obtained for CR condition and T/O condition are detailed in Table 18 and Figure 72 and Table 19 and Figure 73 respectively.

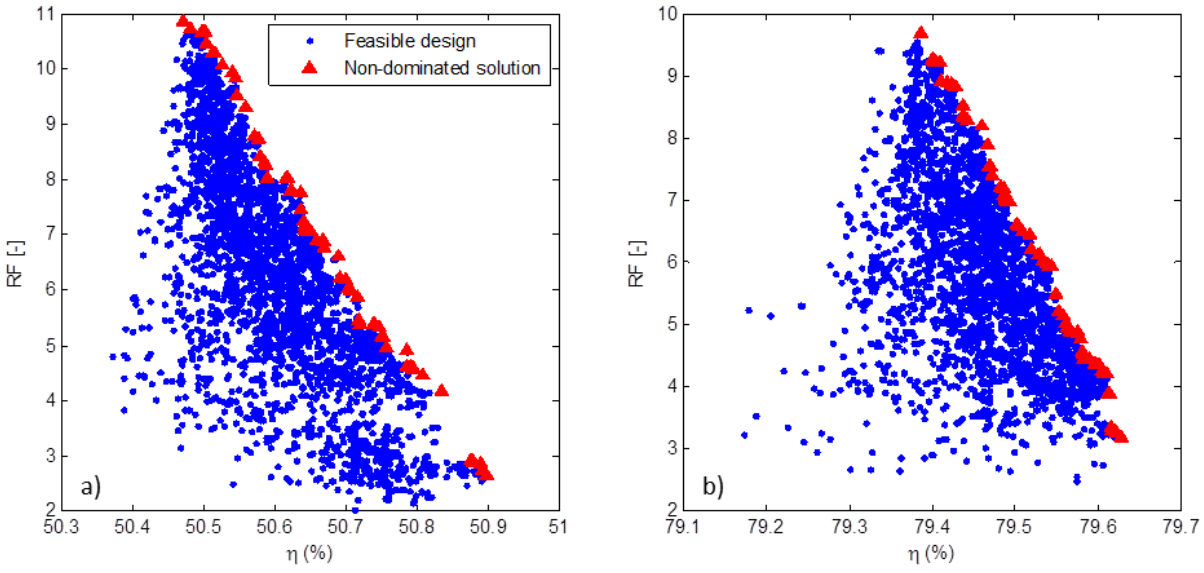

Figure 71. Optimization results. a) TO conditions. b) CR conditions.

Solution 1. CR performances: $\eta = 79.63$ %, $RF = 3.19$, $\beta = 46.0°$	
Intrados (SST to read form camber surface to intrados surface)	
SST_{lam}	[45 0 -45 75 -45 -45 -30 30 -15 -60 -15 -75 75 60 -45 -60 75 45 75 30 30 -75 30 -60 -60 -30 60 30 -75 -60 30 45 -60 90 -60 -45 75 60 45 45]
SST_{ins}	[0 38 37 9 10 11 36 2 13 14 15 3 34 32 35 8 12 19 33 1 20 24 22 5 18 27 25 6 17 29 26 4 30 16 31 7 23 21 28 0]
Extrados (SST to read form camber surface to extrados surface)	
SST_{lam}	[15 15 60 75 30 15 -60 -15 45 -45 0 60 30 30 -75 75 -15 60 -30 15 15 60 -15 75 15 -45 -15 30 -30 0 -45 45 -15 -60 15 45 -75 60 15 15]
SST_{ins}	[0 16 11 10 4 19 17 18 2 36 31 37 9 20 25 3 24 35 34 8 13 32 15 1 27 33 26 6 38 21 12 5 30 23 22 7 28 29 14 0]

Table 18. Details of the most efficient design found for CR flight condition.

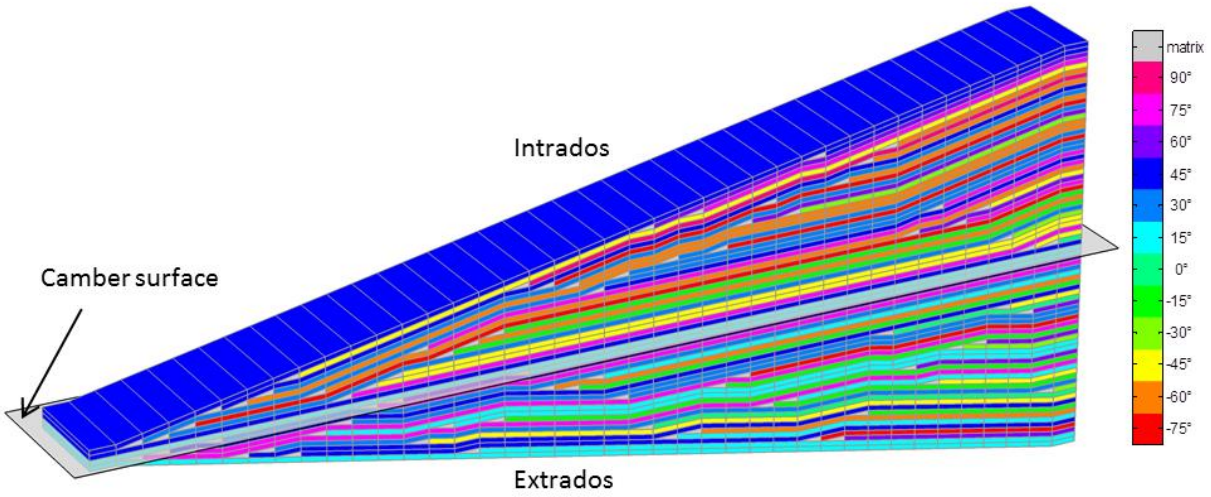

Figure 72. Illustration of the SST of Solution 1 (see Table 18).

Solution 2. T/O performances: $\eta = 50.90$ %, $RF = 2.64$, $\beta = 28.5°$	
Intrados (SST to read form camber surface to intrados surface)	
SST_{lam}	[90 -30 60 15 90 75 15 -60 -45 90 15 90 30 0 15 -60 -60 -15 75 -30 15 75 -60 -45 -30 -30 0 -45 -45 -45 90 -30 75 0 30 90 60 -30 -60 90]
SST_{ins}	[0 36 10 11 9 37 38 6 13 21 15 3 19 20 18 4 33 35 12 8 16 32 34 1 23 24 25 2 27 22 26 5 31 29 30 7 28 17 14 0]
Extrados (SST to read form camber surface to extrados surface)	
SST_{lam}	[60 75 -75 30 75 -60 0 30 -75 90 -45 -60 75 45 75 0 75 15 90 -45 45 75 15 60 75 -45 -45 45 75 -45 -15 30 30 60 30 45 30 -75 75 60]
SST_{ins}	[0 35 21 26 2 20 22 19 6 31 24 30 7 29 23 17 1 27 10 28 4 25 33 34 8 38 37 9 16 32 36 5 11 15 12 3 14 13 18 0]

Table 19. Details of the most efficient design found for T/O flight condition.

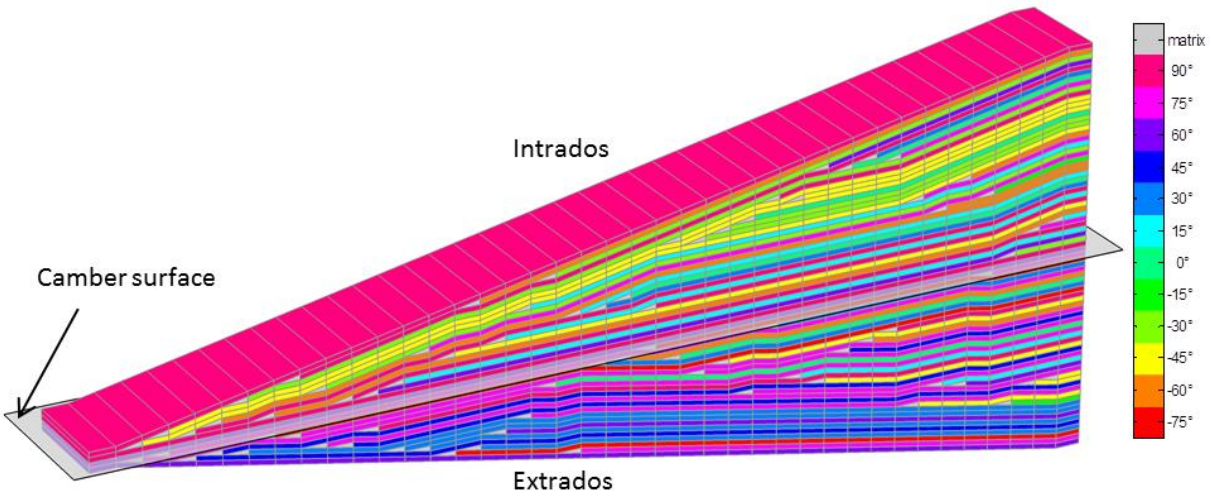

Figure 73. Illustration of the SST of Solution 2 (see Table 19).

III.9 Design of a sandwich blade with balsa wood core

In order to obtain more compliant blades and greater variations of the twist of the blade, a sandwich composite structure is investigated. The sandwich blade is composed of a balsa wood ($E = 4$ GPa, $\nu = 0.3$ and $d = 0.15$) core and 8-ply laminates on the surface of the blade. For the sake of simplicity, the structural mesh is kept unchanged. The main difference with the model of the monolithic blade lies in the declaration of the lay-ups per elements. For the sandwich structure, the 8 outer plies, on the intrados or extrados surfaces of the blade, are declared as composite plies. All other plies are declared as made of the isotropic balsa material. With such definition of the monolithic and sandwich solutions, the designs can be easily compared. The results obtained are presented in Table 20 and Table 21 for the monolithic and sandwich designs respectively. In both tables, two categories of results are presented. First, the results of C2H analyses at T/O condition only are presented, starting from the same reference cold shape for all designs (the cold shape of the monolithic aluminum blade detailed in Figure 67). Second, the results of the successive H2C analyses at CR condition and C2H analyses at T/O condition are given, starting from the HTC5 reference hot shape at CR condition. In Table 21, only the materials of the skins are described. If the two skins are different, the intrados is first described, then the extrados. Both laminates are given from the inside to the outside of the blade.

On the one hand, with thin laminates on the surface of the blade and a light balsa wood core, lighter, less resistant and more flexible blades would be expected. However, the blades are mostly subject to bending and twisting loading, thus the outer plies bring the main contribution to the stiffness of the blade. Removing inner plies might not lead to significant variations of the hot shape of the blades. On the other hand, the centrifugal loading is reduced proportionally to the mass of the blade. Indeed, the centrifugal force can be computed as $F_c = m\omega^2 R$. On the contrary, the aerodynamic loading is not affected by the mass of the structure. It is not intuitive to understand *a priori* how these effects compensate each other. Comparison between Table 20 and Table 21, show that the maximal absolute difference of efficiency obtained with monolithic blades and sandwich blades is very low (0.04 % with C2H analyses only and 0.02 % with chained H2C and C2H analyses). Variations of RF are more significant (up to 50 % in the case of the design with +45° intrados skin and -45° extrados skin). Due to the reduced centrifugal loading, metallic blades and blades with 0° reinforcements (i.e. span-wise reinforcements) with sandwich structure exhibit slightly higher RF than their monolithic counterparts.

The efficiency computed after H2C analysis of the HTC5 blade at CR condition followed by C2H analysis at T/O condition can be compared with the efficiency directly computed on the initial HTC5 shape (50.46 %, see Table 13). The range of variation around the efficiency of the non-deformable blade is [-0.05 %; 0.21 %] which is very low, but represents about half of the variation observed after optimization (see Figure 71.a). Starting from a common cold shape or a common hot shape at another design point leads to solutions that present no major difference of overall efficiency but significant variations of RF. Note that for sandwich blade, failure of the core material is not evaluated in Table 21.

Monolithic blade		**C2H (see** Table 17**)**		**H2C and C2H**	
Material	**Mass (g)**	**η (%)**	**RF**	**η (%)**	**RF**
Aluminum	98	50.43	3.85*	50.43	3.85*
Titanium	221	50.50	4.74*	50.44	3.82*
UD 0°	79	50.51	5.31	50.43	6.39
UD 90°	79	50.77	1.63	H2C divergence	
$[(45/-45)_{20}]_s$	79	50.56	2.74	50.60	2.12
$[(-45)_{40}/45)_{40}]$	79	50.82	2.36	50.58	1.65
$[(45)_{40}/-45_{40}]$	79	50.43	2.71	50.69	1.29
$[(45/0/-45/90)_{10}]_s$	79	50.48	4.15	50.43	3.52
$[(45/0/45/90)_{10}]_s$	79	50.58	3.64	50.41	2.88
$[(-45/0/-45/90)_{10}]_s$	79	50.47	3.63	50.44	2.90

Table 20. Mass and performances of the monolithic blades at T/O condition. In the central columns, all designs share the cold shape of the monolithic aluminum blade with CR conditions. In the right columns, all designs share the same hot shape at CR conditions.
***For metallic materials, the reserve factor is computed as the ratio between the elastic limit *R* and the maximum Von Mises stress.**

Sandwich blade		**C2H**		**H2C and C2H**	
Material	**Mass (g)**	**η (%)**	**RF**	**η (%)**	**RF**
Aluminum	63	50.46	3.96*	50.43	3.59*
Titanium	139	50.53	4.82*	50.44	3.40*
UD 0°	52	50.54	5.74	50.43	6.29
UD 90°	52	50.78	1.61	H2C divergence	
$[(45/-45)_4]$	52	50.57	2.40	50.61	1.97
$[-45_8]$ and $[45_8]$	52	50.86	1.87	50.58	1.36
$[45_8]$ and $[-45_8]$	52	50.43	1.87	50.69	1.02
$[(45/0/-45/90)_2]$	52	50.48	4.40	50.42	3.21
$[(45/0/45/90)_2]$	52	50.57	3.86	50.43	2.73
$[(-45/0/-45/90)_2]$	52	50.48	4.03	50.43	2.78

Table 21. Mass and performances of the sandwich blades at T/O condition. In the central columns, all designs share the cold shape of the monolithic aluminum blade with CR conditions. In the right columns, all designs share the same hot shape at CR conditions.
***For metallic materials, the reserve factor is computed as the ratio between the elastic limit *R* and the maximum Von Mises stress. Failure is not considered in the core material.**

These results lead to the following conclusions about the HTC5 blade and the proposed Hot-to-Cold and Cold-to-Hot analyses.

1. Due to the predominance of the centrifugal loading, there is no significant variation of the hot shape of the blade for different operating points and internal structures. As a matter of fact, the resultant of the centrifugal at the root of the aluminum blade is about 9200 kN at T/O and CR (since the rotation speed is unchanged, see Table 12). The aerodynamic loading, integrated on the whole CROR (with 10 blades for the front propeller and 8 blades for the rear propeller), results in a thrust of 3300 N at T/O and 950 N at CR. The transverse components of the aerodynamic loading correspond to the engine torque which is about 32.5 N.m for the front propeller. These integrated values show that the centrifugal loading and aerodynamic loading are of different order of magnitude. The deformation of the blade is driven by the centrifugal loading.
2. The aerodynamic model and the structural mesh are coarse. The load transfer is also questionable, thus part of the twisting effects on the blade may be underestimated.
3. The Hot-to-Cold analysis is necessary to determine the cold shape (i.e. the shape to manufacture), which can be significantly different from the hot shape.
4. The Cold-to-Hot analysis is required to assess the failure of the blade. Note that both centrifugal and aerodynamic loadings are proportional to the square of the scale factor, thus strength at full scale could be an issue. Light hollow or sandwich structures have to be designed to minimize the mass of the blade and the centrifugal loading.

III.10 Concluding remarks

This chapter successively presents the main geometrical parameters of the Onera HT5 blade for CROR propellers, a simplified aerodynamic modeling dedicated to CROR propellers – the LPC2 code – and the construction of an ABAQUS FE modeling of the HTC5 blade. The two models are implemented within MATLAB routines. In the present study, the blade is described with a reduced set of geometrical parameters (i.e. incidence angle, twist angle distribution, sweep distribution, dihedral distribution and span-wise location of the constitutive airfoils of the blade) that are used to parameterize and chain the models. A Hot-to-Cold (H2C) analysis method and a Cold-to-Hot (C2H) analysis method are proposed based on these two models. The H2C analysis aims at finding the unloaded shape of the blade – the so-called "cold shape" – from its "hot shape" defined at a given operating point (e.g. take-off or cruise flight conditions). The C2H process refers to the opposite process.

A major difficulty in chaining the models lies in the transfer of the aerodynamic loading. Indeed, LPC2 only returns a very coarse description of the aerodynamic loading, reduced to load density resultants expressed at the 25% chord points of a few airfoils distributed along the span of the blade. Two methods have been implemented and compared to apply the aerodynamic load to the FE model of the blade. The first method is the most consistent with LPC2 hypothesis: aerodynamic load resultants are introduced at reference points corresponding to the 25% chord point of the corresponding rigid body airfoils. This method however results in poor description of the stress distribution within the blade and cannot be used to assess the blade failure. The second method is based on template pressure distributions (originating from elsA computations) that are interpolated on the structural mesh and parameterized as functions of the LPC2 outputs. This method results in a much better description of the internal stress state of the blade and is thus favored in this study. Moreover describing the aerodynamic loading through a pressure field could allow replacing in the future the LPC2 module by a more accurate aerodynamic analysis, possibly using elsA.

The H2C process is applied to an aluminum blade to find a reference cold shape. It is shown that due to the significant bending of the blade during loading, non-linear displacement FE analysis is necessary to capture the reorientation of the local material axes. Additionally convergence of the H2C process is improved with non-linear displacement analysis.

Starting from the cold shape obtained for the aluminum blade, the C2H process is applied to blades composed of different materials. The results show that the material of the blade can be used to tailor its hot shape. However, the variation of the propeller efficiency computed using LPC2 is inferior to 1 % for take-off, which is less than expected. Two bi-objective optimizations are performed to maximize both the reserve factor with respect to material failure and the total efficiency of the propeller, one for take-off conditions and one for cruise conditions. Both optimizations confirm that the variations of efficiency obtained by modifying the structure of the blade are very low. Two kinds of composite structures are considered, with similar conclusions: monolithic blades and sandwich blades.

A first explanation for this result could be related to the way the aerodynamic efforts are computed and transferred to the structural model. Indeed, the evaluation of the aerodynamic loading is very coarse. The way the loads are transferred to the structural model is also

questionable. Thus, the twisting moments due to the aerodynamic loads – which have a major influence on the efficiency of the blade and propeller – could be underestimated. The finite element model itself is coarse and could be too stiff due to poor mesh density. These approximations however are not the main reason why the structure does not allow modifying significantly the efficiency of the blade. Indeed, it turns out with the HTC5 propeller that the centrifugal effects are predominant with respect to the aerodynamic loading. Since the rotation speed is the same for all design points, all hot shapes are very similar, irrespective of the internal composite structure. Other propeller designs, with lower and variable rotation speeds depending on the design points would result in different contributions of the centrifugal and aerodynamic loadings that could bring other conclusions. In the present work, however, it turns out that modifying the structure of the blade (with total mass unchanged) does not allow modifying significantly its efficiency at a given design point. Only small variations of the hot shapes are achieved. Nevertheless, the structure drives both the cold shape of the blade – which is shown to be very different from the hot shape – and the strength of the blade. In the present work, important margins with respect to failure are achieved for the reduced scale blades. However, since the loadings vary with the square of the scale factor, strength would be an issue at full scale. Additionally, scaling the composite structure is still an open problem.

H2C and C2H processes are tools that, although operational, are fixed-point methods accounting for centrifugal and aerodynamical considerations only. They should be compared to other available methods (i.e. NASTRAN Hot-to-Cold procedure, or Sculptor Hot-to-Cold model). A particular attention should be paid to the fact that the operating points are far from involving ultimate loads to be withstood by a structure, implying that the FE blade model should be supplied with the relevant load cases. In this chapter, translating the blade surface pressure from a CFD RANS computation to a CSM mesh was made possible through the development of several automated scripts.

Finally, a complete aeroelastic analysis of the blade should also consider the stability of the blade under periodic excitation, especially for counter-rotating propellers, which have not been studied in the present work. Finally, both Hot-to-Cold and Cold-to-Hot processes should be completed by thermal analyses since the CROR blades are expected to be assembled directly to the rotor. If the CROR in pusher configuration has a direct drive transmission, the blades may be located near the high-pressure stages of the engine. Thus, the blades may be exposed to severe temperature gradient due to the heat of the primary flux, emitted from the combustion chamber. Finally, manufacturing of the highly coupled composite solutions evaluated in this chapter also requires thermal analysis to assess the thermal residual stresses and strains in the blade in its cold configuration.

CONCLUSIONS AND PERSPECTIVES

In order to reach the current ACARE[8] objectives for the reduction of CO_2 emissions, NO_X emissions and noise, aeronautics industries search for lighter structures and more efficient aircrafts through the widespread introduction of composite materials in their most recent structural designs, and through new engine concepts. Despite high stiffness-to-weight and strength-to-weight ratios, composites face competition from advanced metallic materials in saving structural mass since they benefit from a longer history of use. In the same time, new thermo-structural composites dedicated to high temperatures have enabled improving engine efficiency, and composite blades are now replacing metallic ones into conventional turbofans. On top of that, composite materials have gained further interest thanks to optimization techniques that allow the aeromechanical tailoring of aerostructures.

From a mechanical perspective, the present study was first set out to develop composite laminate optimization for variable-thickness composite laminates. This study was also set out to assess, from aerodynamics perspectives, the potential of composite laminates in tailoring the aerodynamic performances of a counter-rotating open rotor (CROR) blade model dedicated to wind tunnel testing.

I.1 Summary of the work

Large laminated structures, such as wing or fuselage floor panels, are now usually designed in the industry as blended structures whose thickness vary, either by ply drops or ply insertions. The distribution of material in these structures can hence be described by a layup table, or stacking sequence table (SST). The complexity of such tables dramatically increases with thick structures, since there are as many columns as the structure has thicknesses and as many rows as plies within the laminates. The representation of the SST may be simplified by encoding it as a laminate and by recording the insertion order of the concerned plies. Hence the combination of such representation with the thickness distribution over the different regions of the structure is sufficient to represent the whole blended structure.

The extension of an existing evolutionary algorithm (EA) to SST is the first contribution of this work. It aims at enhancing the capabilities of conventional EA to deal with the optimization of entire structures involving ply-drops. While existing blending optimization methods mostly elude damage mechanism around ply-drops and the propagation of delamination, the present work enables implementing design guidelines that guarantee strength levels at the tapered sections of the structure. Such representation of the layup tables allows taking into account the usual layup practices, or guidelines, when creating the whole table. These guidelines are categorized as:

- Different laminated design guidelines ensuring the mechanical integrity of the structure and avoiding non-desired mechanical behaviors. These guidelines include *Symmetry* (favoring symmetrical stacking sequences about the mid-plane), *Balance* (favoring balanced stacking sequence regarding the plies orientations), *Contiguity* (limiting the number of plies

[8] ACARE: Advisory Council for Aviation Research in Europe

with the same orientation within a stack), *Disorientation* (limiting the angle of the fiber path between two consecutive plies), ten percent rule (preserving at least 10% of each authorized orientation within the laminate), and *Damage tolerance* (avoiding fibers on surface layers to be coaxial with stress path).

- Different ply-drop design guidelines aiming at avoiding unfeasible layup and delamination into ply-drops. These rules include *Covering* (avoiding dropping off the surface layers), *Maximum taper slope* (smoothing the taper angle of ply drop-off regarding the function of the structure), *Max-stopping* (limiting the number of plies to be simultaneously stopped), *Internal continuity* (limiting consecutive ply-drops), *Ply-drop alternation* (favoring even cross-sectional distribution of ply drops), and *Taper guidelines* (imposing laminate design guidelines to taper sections).
- Different global requirements ensuring the feasibility of the whole structure as well as the fair distribution of the load all over the structure and limiting stress concentration at ply-drops. These guidelines encompass *Continuity* (favoring continuous fibers between adjacent panels), and *⊿n-rule* (limiting ply-drops between adjacent zones).

The optimization method suggested in this work is based on the introduction of composite plies into the stacking sequence table instead of ply drops to ease the optimization process of the whole SST. The extension has been realized while developing specific operators for the EA in order to enforce the different guidelines when creating a potential solution. Indeed, enforcing guidelines when adding plies to a thin laminate is much easier than respecting the guidelines when removing plies from a thick laminate. Thus, the choice of encoding the ply insertion order rather than the ply termination order is important. The EA is therefore modified and specialized at the level of the initialization of the population and the variation operators. In this work, the EA has been upgraded to perform single and multi-objective optimization of laminated composite structures requiring blended design, such as large aerostructures. The whole method had been benchmarked against results from the literature on a semi-analytical problem consisting of an 18-panel U grid. In order to provide relevant comparisons, mono and bi-objective versions of this problem have been solved and the corresponding results analyzed to assess the statistical reliability of the method. Then an industrial problem has been submitted to the method in order to assess performance in solving complex problems that require finite element analyses. The method provided relevant solutions when optimizing the industrial part, a satellite antenna composite mounting bracket. Calling directly for numerous FEA induces important computation costs. Nevertheless, the method returned interesting results within acceptable time. Based on this experience, the work was orientated towards the improvement of the capability of the method in finding optimal solutions with fewer evaluations without ceding accuracy.

A first solution is to use the EA in the second step of a bi-level optimization approach. In that case, the structural analyses are performed at the first optimization level and combined with gradient-based optimization using software such as MSC NASTRAN or ALTAIR OPTISTRUCT or other specific method like in (IJsselmuiden, 2011) to find an idealized solution defined by a thickness distribution and a stiffness distribution. At the second optimization level, the EA is used to retrieve the laminates that best match the idealized solution, with negligible computational cost. Such exercise was performed in parallel of this study in (Irisarri et al., 2015). Unfortunately, the first level optimization is not always readily applicable. For instance, commercial codes are limited when it comes to solving coupled optimization problems involving

several physics or significantly non-linear problems. In these cases, the EA has to call directly for the detailed model which raises the issue of computation costs due to the number of structural analyses required to reach convergence. Another drawback of the two levels approach is that it is not guaranteed that the stiffness distribution proposed at the first level can be achieved by realistic laminates at the second level. In this work, in order to improve the efficiency of the EA, a guidance mechanism in an auxiliary design space is introduced within the EA. The method derives from the Double Distribution Optimization Algorithm proposed in the literature by Grosset (Grosset, 2004). This approach enables taking into consideration expert knowledge through additional search space and couplings between variables accordingly. It can be seen as simultaneously performing the optimization at the macro (stiffness) and laminate levels.

Optimally setting the parameters of the EA and the different algorithms studied here may be a difficult task for new optimization problems (from information-theoretic aspects, this is a common issue in optimization, which has been addressed in the No Free Lunch Theorems in (Wolpert and Macready, 1997)). But our study shows that generic algorithms and settings exist which yield optimizers with high-performance behavior for laminate design problems, including plate buckling problems. The EA proposed in the first part has been extended to a new algorithm, DDEA, which further inherits from the guiding scheme of DDOA. Again, its principle is based on an additional, simultaneous, search in an auxiliary space of lamination parameters. DDEA enables solving a large scope of composite optimization problems with the same parameter settings. Auxiliary variables participate to the specialization by exploiting unused information in conventional direct search. It is shown that such implementation improves the efficiency of the whole method in solving benchmark problems (such as the 18-panels U-grid problem). The addition of the custom auxiliary design space to the method is a further specialization of the algorithm to the considered optimization problem, since the auxiliary variable may be adapted to the nature of the problem. This enables DDEA to reach better convergence speed than the original EA and is therefore relevant to solve tight budget optimization problems.

The final aspect of the present work covered the aeromechanical optimization of CROR blades with different materials and composite designs. Since the geometry of the blades and its flight condition are fixed here, the only degrees of freedom rely on the internal structure of the blade. The optimization aims at maximizing the efficiency of the propeller at take-off and cruise conditions. The EA developed in Chapter I is used here. A Cold-to-Hot (C2H) method has been developed in order to assess the deformed shape of the blade in flight conditions knowing its unloaded shape. Conversely, a Hot-to-Cold (H2C) method has been developed to find the unloaded shape knowing the loaded shape. Transferring aerodynamic loadings form the aerodynamic model to the structural model is a difficult task. Two solutions have been explored.

The first one consisted in transferring the load resultants applied at the 25% chord points of predefined airfoils, yielding a poor description of the stress distribution within the blade. The second method consisted in exploiting elsA computation to assess a template pressure distribution over the blade model, then interpolating it for LPC2 This allowed a better description of the internal stress state. Bi-objective optimizations have been performed to maximize both reserve factor with respect to material failure and total efficiency of the propeller for different conditions. Unfortunately, it seems that modifying the inner structure of the blade

does not impact significantly the efficiency of the propeller at a given design point. This result could be caused by multiple factors including the quality of the different models, the computation and transfer of the aerodynamic forces.

I.2 Limitations and perspectives of the work

Concerning the optimization of laminated composite structures, evolutionary strategies find their effectiveness in specialization, as stated in the blending-based design and double distribution schemes investigated in the present study. Eventually, solving complex industrial problems with EAs is still limited by computation capabilities, since they require higher numbers of simulations (from about 10^4 to 10^6 for 3 to 100 unknowns) to achieve sufficient accuracy. Several perspectives may be called upon to tackle the computational budget issue. Firstly, from a pure computing perspective, parallel or even massively parallel computing architectures would be useful. Secondly, the number of calls to the simulation may be reduced by replacing some of the simulations by statistical approximations (also known as metamodels, or surrogates, or response surfaces, see (Forrester and Keane, 2009)). Thirdly, the optimization algorithm itself may be a source of computation savings by using more "exploitation-focused" methods, instead of exploratory ones. However, this increases the risk for premature convergence. Therefore optimization method need both faster methods and adapted computation architectures to solve realistic industrial problems.

The modeling part of our work, in particular that related to mesh quality, would benefit from further improvements: The quality of the mesh used has been kept relatively low to minimize the computation costs. This was not of critical concern since the optimization methods developed in this study were based on ranking the solutions instead of processing fine quantitative analyses. Plus, this study has been focused on parametric problems with discrete variables and several constraints, representative of industrial problem. The coarse finite element models optimized may have resulted in artificial over-stiff behavior. Therefore, establishing a mesh convergence study on the proposed designs and, furthermore, checking that the order of design performances is not sensitive to the mesh, is still essential.

Outside the computational cost difficulties inherent to FEA and optimization, this work also faced difficulties related to current aerodynamics and mechanical numerical practices. We have proposed and applied iterative methods, in the form of Hot-to-Cold and Cold-to-Hot processes used by blade manufacturers, to determine the shape of the composite blade at different flight conditions. Both processes required the translation of the blade surface pressure from a mesh for Computational Fluid Dynamics to a mesh for Computational Structural Mechanics, but we did not explore the implementation of a fully-automated Finite Element Method for this purpose. Although the whole aerostructural optimization has been developed and made operational to deal with different blade inner architectures, the resolution of the design problem did not result in significant improvement of propeller efficiency. The relatively high rotation speed of the propeller at the different considered design points induces predominant centrifugal forces compared to aerodynamical loads. At last, only the external plies of the blade seem important to support stresses. The application of the LPC2 software in this work where the aerodynamic forces are estimated coarsely, and then transferred to a simple structural model; The twisting

moments generated through the aerodynamic loads and influencing the propeller efficiency seem too inaccurate for the final design to be really significant. This illustrates the difficulty to interact between two disciplines in multiphysics problem. Similar difficulties in multiphysics interaction modeling, specifically fluid-structure interaction are discussed in (Roussouly et al., 2013) through model coupling strategies in the framework of the OSYCAF project. Instead of the simplified models used in the present study, the OpenPALM[9] coupler software allowed using two advanced solvers for CFM and CFD simultaneously.

From a technical point of view, the implementation of a fully automated FEM for FSI is laborious, but remains an interesting perspective for a deployment of the optimization method in an industrial context. It mostly relies on automating the creation of the mesh and the application of the load cases, then keeping the mesh consistent for the fluid during the displacement and deformation of the structure. Aside from the construction of the geometrical models, the representativeness of the physics embedded in the simulation is an important source of improvement. The estimation of aerodynamic loads through template pressure field generated by steady RANS computations (see mixing plane technique of elsA in (L. Cambier and M. Gazaix, 2002)), instead of resultant forces computed with lifting line methods (see blade element theory of LPC2 in (Saito et al., 1987)), is a solution to perform more accurate analyses. Indeed, the model presented in this work has shown a better description of the stress state while using template pressure distributions generated from this advanced CFD solver. In order to be coherent with aeromechanics, a complete aeroelastic analysis of the blade requires computing the stability of the blade under periodic excitation. As well, H2C and C2H processes may be enhanced with thermal analysis since CROR blades are expected to be mounted near the high-pressure stages if the CROR is installed in pusher configuration. This requires further modifications in the model of the blade and enough implementation efforts with the models suggested in this thesis.

Finally, the work presented in this thesis could also benefit from experimental testing of the optimal solutions found for the academic and industrial problems in order to assess the accuracy and the relevancy of the whole method.

[9] CERFACS OpenPALM siteweb: http://www.cerfacs.fr/globc/PALM_WEB/index.html

REFERENCES

Abdalla, M.M., Kassapoglou, C., Gürdal, Z., 2009. Formulation of composite laminate robustness constraint in lamination parameters space, in: Proceedings of 50th AIAA/ASME/ASCE/AHS/ASC Structures, Structural Dynamics, and Materials Conference. Palm Springs, California.

Adams, D.B., Watson, L.T., Gürdal, Z., Anderson-Cook, C.M., 2004. Genetic algorithm optimization and blending of composite laminates by locally reducing laminate thickness. Advances in Engineering Software 35, 35–43. doi:10.1016/j.advengsoft.2003.09.001

Aymerich, F., Serra, M., 2008. Optimization of laminate stacking sequence for maximum buckling load using the ant colony optimization (ACO) metaheuristic. Composites Part A: Applied Science and Manufacturing 39, 262–272. doi:10.1016/j.compositesa.2007.10.011

Bailie, J.A., Ley, R.P., Pasricha, A., 1997. A summary and review of composite laminate design guidelines (Technical report NASA No. NAS1-19347).

Béchet, S., Negulescu, C., Chapin, V., Simon, F., 2011. Integration of CFD tools in aerodynamic design of contra-rotating propellers blades.

Berthelot, J.-M., 1992. Matériaux composites : comportement mécanique et analyse des structures, Masson. ed. Paris.

Bettebghor, D., Bartoli, N., Grihon, S., Morlier, J., Samuelides, M., 2011. Surrogate Modeling Approximation Using a Mixture of Experts Based on EM Joint Estimation. Struct. Multidiscip. Optim. 43, 243–259. doi:10.1007/s00158-010-0554-2

Bettebghor, D., Leroy, F.-H., 2014. Overlapping radial basis function interpolants for spectrally accurate approximation of functions of eigenvalues with application to buckling of composite plates. Computers & Mathematics with Applications 67, 1816–1836. doi:10.1016/j.camwa.2014.03.020

Bishop, C.M., 2006. Pattern recognition and machine learning, Information science and statistics. Springer, New York.

Bloomfield, M.W., Diaconu, C.G., Weaver, P.M., 2009. On feasible regions of lamination parameters for lay-up optimization of laminated composites. Proceedings of the Royal Society A: Mathematical, Physical and Engineering Sciences 465, 1123–1143. doi:10.1098/rspa.2008.0380

Bloomfield, M.W., Herencia, J.E., Weaver, P.M., 2010. Analysis and benchmarking of meta-heuristic techniques for lay-up optimization. Computers & Structures 88, 272–282. doi:10.1016/j.compstruc.2009.10.007

Boisard, R., Delattre, G., Falissard, F., 2014. Computational Fluid Dynamics as a Support to Counter-Rotating Open-Rotor Wind-Tunnel Test Analysis. Journal of Aircraft 51, 614–628. doi:10.2514/1.C032348

Bousquet, J.., Gardarein, P., Gouyon, B., Tichtinsky, J.C., 1991. Définition aérodynamique de l'hélice contrarotative HTC5. Etude et réalisation d'une balance de paroi pour essais d'hélices dans la soufflerie S3Ch. Onera.

Cambier, L., Veuillot, J.P., 2008. Status of the elsA CFD software for flow simulation and multidisciplinary applications. AIAA paper 664, 2008.

Carpentier, A., Michel, L., Grihon, S., Barrau, J.-J., 2006. Optimization methodology of composite panels, in: 12th European Conference on Composite Materials (ECCM 12). Biarritz, France, pp. pp. 1–8.

Castillon, L., 2012. Evaluation of a multiple frequency phase lagged method for unsteady numerical simulations of multistage turbomachinery, in: 28th International Congress of the Aeronautic Science.

Catapano, A., Montemurro, M., 2014. A multi-scale approach for the optimum design of sandwich plates with honeycomb core. Part I: homogenisation of core properties. Composite Structures.

doi:10.1016/j.compstruct.2014.07.057

Chang, W., 2010. A Novel Particle Swarm Optimization for Optimal Scheduling of Hydrothermal System. Energy and Power Engineering 02, 223–229. doi:10.4236/epe.2010.24033

Cheng, S., Ho, B.P.C., 1963. Stability of Heterogeneous Aeolotropic Cylindrical Shells Under Combined Loads. AIAA Journal 1, 892–898. doi:10.2514/3.1660

Collette, Y., Siarry, P., 2002. Optimisation multiobjectif. Eyrolles, Paris.

Deb, K., Gupta, H., 2005. A constraint handling strategy for robust multi-criterion optimization (No. 2005001). Indian Institute of Technology Kanpur, Kanpur, India.

Deb, K., Pratap, A., Agarwal, S., Meyarivan, T., 2002. A fast and elitist multiobjective genetic algorithm: NSGA-II. Evolutionary Computation, IEEE Transactions on 6, 182–197. doi:10.1109/4235.996017

Delattre, G., Falissard, F., 2013. Aerodynamic and acoustic impacts of a single protuberance placed on the leading edge of the front blades of an open rotor. Presented at the 48th international Symposium of Applied Aerodynamics of Small Bodies and Details, Saint Louis, France.

Diaconu, C.G., Sato, M., Sekine, H., 2002. Feasible Region in General Design Space of Lamination Parameters for Laminated Composites. AIAA Journal 40, 559–565. doi:10.2514/2.1683

Diaconu, C.G., Sekine, H., 2004. Layup Optimization for Buckling of Laminated Composite Shells with Restricted Layer Angles. AIAA Journal 42, 2153–2163. doi:10.2514/1.931

Eiben, A.E., 2001. Evolutionary Algorithms and Constraint Satisfaction: Definitions, Survey, Methodology, and Research Directions, in: Kallel, L., Naudts, B., Rogers, A. (Eds.), Theoretical Aspects of Evolutionary Computing. Springer Berlin Heidelberg, Berlin, Heidelberg, pp. 13–30.

Erdal, O., Sonmez, F.O., 2005. Optimum design of composite laminates for maximum buckling load capacity using simulated annealing. Composite Structures 71, 45–52. doi:10.1016/j.compstruct.2004.09.008

Ernst, M.A., 1992. Structural analysis of low-speed composite propfan blades for the LRCSW wind tunnel model.

Forrester, A.I.J., Keane, A.J., 2009. Recent advances in surrogate-based optimization. Progress in Aerospace Sciences 45, 50–79.

Gardarein, P., 2013. LPC2 V11a user's manual.

Gardarein, P., 1991. Calculs Aérodynamiques Des Hélices Rapides Transsoniques. Presented at the 28ème Colloque d'Aérodynamique Appliquée, Saint Louis, France.

Gerolymos, G.A., Michon, G.J., Neubauer, J., 2002. Analysis and Application of Chorochronic Periodicity in Turbomachinery Rotor/Stator Interaction Computations. Journal of Propulsion and Power 18, 1139–1152. doi:10.2514/2.6065

Ghiasi, H., Fayazbakhsh, K., Pasini, D., Lessard, L., 2010. Optimum stacking sequence design of composite materials Part II: Variable stiffness design. Composite Structures 93, 1–13. doi:10.1016/j.compstruct.2010.06.001

Ghiasi, H., Pasini, D., Lessard, L., 2009. Optimum stacking sequence design of composite materials Part I: Constant stiffness design. Composite Structures 90, 1–11. doi:10.1016/j.compstruct.2009.01.006

Giger, M., Keller, D., Ermanni, P., 2008. A graph-based parameterization concept for global laminate optimization. Structural and Multidisciplinary Optimization 36, 289–305. doi:10.1007/s00158-007-0165-8

Grenestedt, J.L., 1991. Layup optimization against buckling of shear panels. Structural optimization 3, 115–120.

Grosset, L., 2004. Optimization of Composite Structures by Estimation of Distribution Algorithms. University of Florida.

Grosset, L., LeRiche, R., Haftka, R.T., 2006. A double-distribution statistical algorithm for composite

laminate optimization. Structural and Multidisciplinary Optimization 31, 49–59. doi:10.1007/s00158-005-0551-z

Guermond, J.-L., Sellier, A., 1991. A unified unsteady lifting-line theory. Journal of Fluid Mechanics 229, 427–451. doi:10.1017/S0022112091003099

Gürdal, Z., Haftka, R.T., Hajela, P., 1999. Design and optimization of laminated composite materials, A Wiley-Interscience Publication. Wiley, New York, NY.

Hager, R.D., Vrabel, D., 1988. Advanced turboprop project.

Hansen, N., 2006. The CMA evolution strategy: a comparing review, in: Towards a New Evolutionary Computation. Springer, pp. 75–102.

He, K., Hoa, S.., Ganesan, R., 2000. The study of tapered laminated composite structures: a review. Composites Science and Technology 60, 2643–2657. doi:10.1016/S0266-3538(00)00138-X

Herencia, J.E., Haftka, R.T., Weaver, P.M., Friswell, M.I., 2008. Lay-Up Optimization of Composite Stiffened Panels Using Linear Approximations in Lamination Space. AIAA Journal 46, 2387–2391. doi:10.2514/1.36189

IJsselmuiden, S.T., 2011. Optimal design of variable stiffness composite structures using lamination parameters. TU Delft, Delft.

IJsselmuiden, S.T., Abdalla, M.M., Gürdal, Z., 2010. Optimization of variable-stiffness panels for maximum buckling load using lamination parameters. AIAA journal 48, 134–143.

IJsselmuiden, S.T., Abdalla, M.M., Gürdal, Z., 2008. Implementation of strength-based failure criteria in the lamination parameter design space. AIAA journal 46, 1826–1834.

IJsselmuiden, S.T., Abdalla, M.M., Seresta, O., Gürdal, Z., 2009. Multi-step blended stacking sequence design of panel assemblies with buckling constraints. Composites Part B: Engineering 40, 329–336. doi:10.1016/j.compositesb.2008.12.002

Irisarri, F.-X., 2010. Stratégies de calcul pour l'optimisation multiobjectif des structures composites. ISAT, TU Delft.

Irisarri, F.-X., Abdalla, M.M., Gürdal, Z., 2011. Improved Shepard's Method for the Optimization of Composite Structures. AIAA Journal 49, 2726–2736. doi:10.2514/1.J051109

Irisarri, F.-X., Bassir, D.H., Carrere, N., Maire, J.-F., 2009. Multiobjective stacking sequence optimization for laminated composite structures. Composites Science and Technology 69, 983–990. doi:10.1016/j.compscitech.2009.01.011

Irisarri, F.-X., Julien, C., Espinassou, D., Bettebghor, D., 2015. Optimal design of variable thickness composite structures made by patches using stacking sequence tables. Presented at the 20th International Conference on Composite Materials, Copenhagen, Denmark.

Irisarri, F.-X., Lasseigne, A., Leroy, F.-H., Le Riche, R., 2014. Optimal design of laminated composite structures with ply drops using stacking sequence tables. Composite Structures 107, 559–569. doi:10.1016/j.compstruct.2013.08.030

Irisarri, F.-X., Laurin, F., Leroy, F.-H., Maire, J.-F., 2011. Computational strategy for multiobjective optimization of composite stiffened panels. Composite Structures 93, 1158–1167. doi:10.1016/j.compstruct.2010.10.005

Jibawy, A., Julien, C., Desmorat, B., Vincenti, A., Léné, F., 2011. Hierarchical structural optimization of laminated plates using polar representation. International Journal of Solids and Structures 48, 2576–2584. doi:10.1016/j.ijsolstr.2011.05.015

Keller, D., 2010. Optimization of ply angles in laminated composite structures by a hybrid, asynchronous, parallel evolutionary algorithm. Composite Structures 92, 2781–2790. doi:10.1016/j.compstruct.2010.04.003

Koide, R.M., FranÃ\Sa, G. von Z. de, Luersen, M.A., 2013. An ant colony algorithm applied to lay-up

optimization of laminated composite plates. Latin American Journal of Solids and Structures 10, 491 – 504.

Kristinsdottir, B.P., Zabinsky, Z.B., Tuttle, M.E., Neogi, S., 2001. Optimal design of large composite panels with varying loads. Composite Structures 51, 93–102.

Lanzi, L., Giavotto, V., 2006. Post-buckling optimization of composite stiffened panels: Computations and experiments. Composite Structures 73, 208–220. doi:10.1016/j.compstruct.2005.11.047

Larrañaga, P., Lozano, J.A. (Eds.), 2002. Estimation of Distribution Algorithms, Genetic Algorithms and Evolutionary Computation. Springer US, Boston, MA.

L. Cambier, M. Gazaix, 2002. elsA - An efficient object-oriented solution to CFD complexity, in: Aerospace Sciences Meetings. Presented at the 40th AIAA Aerospace Sciences Meeting & Exhibit, American Institute of Aeronautics and Astronautics.

Le Riche, R., Haftka, R.T., 1993. Optimization of laminate stacking sequence for buckling load maximization by genetic algorithm. AIAA Journal 31, 951–956. doi:10.2514/3.11710

Leroy, F.-H., Irisarri, F.-X., Christophe, B., 2013. Métamodélisation de problèmes multimodaux - application au flambement de panneaux raidis composites dans un processus MDO. Presented at the 11e Colloque National en Calcul des Structures, Giens, France.

Li, H.D., He, L., 2002. Single-Passage Analysis of Unsteady Flows Around Vibrating Blades of a Transonic Fan Under Inlet Distortion. Journal of Turbomachinery 124, 285–292. doi:10.1115/1.1450567

Liu, B., 2001. Two-level optimization of composite wing structures based on panel genetic optimization. University of Florida.

Liu, B., Haftka, R.T., 2001. Composite wing structural design optimization with continuity constraints, in: Fluid Dynamics and Co-Located Conferences. Presented at the 19th AIAA Applied Aerodynamics Conference, American Institute of Aeronautics and Astronautics.

Liu, D., Toropov, V.V., 2013. A lamination parameter-based strategy for solving an integer-continuous problem arising in composite optimization. Computers & Structures 128, 170–174. doi:10.1016/j.compstruc.2013.06.003

Liu, D., Toropov, V.V., Querin, O.M., Barton, D.C., 2011. Bilevel Optimization of Blended Composite Wing Panels. Journal of Aircraft 48, 107–118. doi:10.2514/1.C000261

Liu, W., Butler, R., Mileham, A.R., Green, A.J., 2006. Bilevel Optimization and Postbuckling of Highly Strained Composite Stiffened Panels. AIAA Journal 44, 2562–2570. doi:10.2514/1.22206

Lozano, J.A., 2006. Towards a New Evolutionary Computation: Advances on Estimation of Distribution Algorithms, Studies in Fuzziness and Soft Computing. Springer.

Mahajan, A., Stefko, G., 1993. An iterative multidisciplinary analysis for rotor blade shape determination, in: 29th Joint Propulsion Conference and Exhibit. American Institute of Aeronautics and Astronautics.

Matsuzaki, R., Todoroki, A., 2007. Stacking-sequence optimization using fractal branch-and-bound method for unsymmetrical laminates. Composite Structures 78, 537–550. doi:10.1016/j.compstruct.2005.11.015

Mauffrey, Y., 2015. CROR Blade Deformation, Part 2: Aeroelastic Computations and Comparison with Experiments. Presented at the International Forum on Aeroelasticity and Structural Dynamics, Saint Petersbourg, Russia.

Meddaikar, Y.M., Irisarri, F.-X., Abdalla, M.M., 2015. Blended Composite Optimization combining Stacking Sequence Tables and a Modified Shepard's Method.

Miki, M., 1985. Design of Laminated Fibrous Composite Plates with Required Flexural Stiffness 387–400. doi:10.1520/STP32802S

Miki, M., Sugiyama, Y., 1991. Optimum design of laminated composite plates using lamination parameters. American Institute of Aeronautics and Astronautics. doi:10.2514/6.1991-971

MIL-HDBK-17-3F, 2002. Composite Materials Handbook - Volume 3, Polymer Matrix Composites, Materials Usage, Design, and Analysis.

Montemurro, M., Vincenti, A., Vannucci, P., 2012. A Two-Level Procedure for the Global Optimum Design of Composite Modular Structures—Application to the Design of an Aircraft Wing: Part 1: Theoretical Formulation. Journal of Optimization Theory and Applications 155, 1–23. doi:10.1007/s10957-012-0067-9

Negulescu, C.A., 2013. Airbus AI-PX7 CROR Design Features and Aerodynamics. SAE Int. J. Aerosp. 6(2):626-642.

Pai, N., Kaw, A., Weng, M., 2003. Optimization of laminate stacking sequence for failure load maximization using Tabu search. Composites Part B 34, 405–413. doi:10.1016/S1359-8368(02)00135-X

Park, C.H., Lee, W.I., Han, W.S., Vautrin, A., 2003. Weight minimization of composite laminated plates with multiple constraints. Composites Science and Technology 63, 1015–1026. doi:10.1016/S0266-3538(03)00014-9

Queipo, N.V., Haftka, R.T., Shyy, W., Goel, T., Vaidyanathan, R., Kevin Tucker, P., 2005. Surrogate-based analysis and optimization. Progress in Aerospace Sciences 41, 1–28. doi:10.1016/j.paerosci.2005.02.001

Raju, G., Wu, Z., Weaver, P., 2014. On Further Developments of Feasible Region of Lamination Parameters for Symmetric Composite Laminates. American Institute of Aeronautics and Astronautics. doi:10.2514/6.2014-1374

Reddy, T.S.R., Bakhle, M.A., Srivastava, R., Mehmed, O., Stefko, G.L., 1993. A review of recent aeroelastic analysis methods for propulsion at NASA Lewis research center (Technical Paper No. 3406). NASA.

Roussouly, N., Morlier, J., Charlotte, M., Salaün, M., 2013. Approche fiabiliste pour l'optimisation locale d'un problème couplé fluide-structure.

Saito, S., Kobayashi, H., Nasu, K., 1987. Performance calculation of counter rotation propeller, in: Joint Propulsion Conferences. Presented at the 23rd Joint Propulsion Conference, American Institute of Aeronautics and Astronautics.

Sebaey, T.A., Lopes, C.S., Blanco, N., Costa, J., 2011. Ant Colony Optimization for dispersed laminated composite panels under biaxial loading. Composite Structures 94, 31–36. doi:10.1016/j.compstruct.2011.07.021

Seresta, O., Abdalla, M.M., Gürdal, Z., 2009. A genetic algorithm based blending scheme for design of multiple composite laminates, in: Proceedings of 50th AIAA/ASME/ASCE/AHS/ASC Conference.

Setoodeh, S., Abdalla, M., Gurdal, Z., 2006. Approximate Feasible Regions for Lamination Parameters. American Institute of Aeronautics and Astronautics. doi:10.2514/6.2006-6973

Soremekun, G., Gürdal, Z., Kassapoglou, C., Toni, D., 2002. Stacking sequence blending of multiple composite laminates using genetic algorithms. Composite Structures 56, 53–62.

Srivastava, R., Huff, D.L., Sankar, L.N., Reddy, T.S.R., 1991. Application of an efficient hybrid scheme for aeroelastic analysis of advanced propellers. Journal of Propulsion and Power 7, 767–775. doi:10.2514/3.23390

Stürmer, A., Akkermans, R.A.D., 2014. Multidisciplinary analysis of CROR propulsion systems: DLR activities in the JTI SFWA project. CEAS Aeronautical Journal 5, 265–277. doi:10.1007/s13272-014-0105-4

Svanberg, K., 1987. The method of moving asymptotes—a new method for structural optimization. International Journal for Numerical Methods in Engineering 24, 359–373. doi:10.1002/nme.1620240207

Timothy Simpson, Vasilli Toropov, Vladimir Balabanov, Felipe Viana, 2008. Design and Analysis of Computer Experiments in Multidisciplinary Design Optimization: A Review of How Far We Have Come - Or Not. Presented at the 12th AIAA/ISSMO Multidisciplinary Analysis and Optimization Conference,

American Institute of Aeronautics and Astronautics.

Todoroki, A., Haftka, R.T., 1998. Stacking sequence optimization by a genetic algorithm with a new recessive gene like repair strategy. Composites Part B: Engineering 29, 277–285. doi:10.1016/S1359-8368(97)00030-9

Todoroki, A., Ishikawa, T., 2004. Design of experiments for stacking sequence optimizations with genetic algorithm using response surface approximation. Composite Structures 64, 349–357. doi:10.1016/j.compstruct.2003.09.004

Tsai, S.W., Hahn, H.T., 1980. Introduction to composite materials. Technomic Pub, Westport, Conn.

Van Campen, J., Seresta, O., Abdalla, M., Gürdal, Z., 2008. General Blending Definitions for Stacking Sequence Design of Composite Laminate Structures. Presented at the 49th AIAA/ASME/ASCE/AHS/ASC Structures, Structural Dynamics, and Materials Conference, 16th AIAA/ASME/AHS Adaptive Structures Conference,10th AIAA Non-Deterministic Approaches Conference, 9th AIAA Gossamer Spacecraft Forum, 4th AIAA Multidisciplinary Design Optimization Specialists Conference, American Institute of Aeronautics and Astronautics.

Vannucci, P., 2013. A Note on the Elastic and Geometric Bounds for Composite Laminates. Journal of Elasticity 112, 199–215. doi:10.1007/s10659-012-9406-1

Vannucci, P., 2005. Plane Anisotropy by the Polar Method. Meccanica 40, 437–454. doi:10.1007/s11012-005-2132-z

Venkataraman, S., Haftka, R.T., 2004. Structural optimization complexity: what has Moore?s law done for us? Structural and Multidisciplinary Optimization 28, 375–387. doi:10.1007/s00158-004-0415-y

Verchery, G., 1982. Les Invariants des Tenseurs d'Ordre 4 du Type de l'Élasticité, in: Boehler, J.-P. (Ed.), Mechanical Behavior of Anisotropic Solids / Comportment Méchanique Des Solides Anisotropes: Proceedings of the Euromech Colloquium 115 Villard-de-Lans, June 19–22, 1979 / Colloque Euromech 115 Villard-de-Lans, 19–22 Juin 1979. Springer Netherlands, Dordrecht, pp. 93–104.

Vion, L., 2013. Modifications des tourbillons d'extrémité d'hélices contra-rotatives en vue d'une réduction des nuisances sonores. Ecole Polytechnique X.

Vion, L., Delattre, G., Falissard, F., Jacquin, L., 2011. Counter-Rotating Open Rotor (CROR): flow physics and simulation. 20ème Congrès Français de Mécanique, 28 août/2 sept. 2011-25044 Besançon, France (FR).

Wang, W., Guo, S., Chang, N., Yang, W., 2010. Optimum buckling design of composite stiffened panels using ant colony algorithm. Composite Structures 92, 712–719. doi:10.1016/j.compstruct.2009.09.018

Wolpert, D.H., Macready, W.G., 1997. No free lunch theorems for optimization. Evolutionary Computation, IEEE Transactions on 1, 67–82.

Wu, A.S., Lindsay, R.K., 1995. Empirical Studies of the Genetic Algorithm with Noncoding Segments. Evolutionary Computation 3, 121–147. doi:10.1162/evco.1995.3.2.121

Wu, Z., Raju, G., Weaver, P., 2013. Feasible Region of Lamination Parameters for optimization of Variable Angle Tow (VAT) Composite Plates. American Institute of Aeronautics and Astronautics. doi:10.2514/6.2013-1481

Wu, Z., Raju, G., Weaver, P.M., 2015. Framework for the Buckling Optimization of Variable-Angle Tow Composite Plates. AIAA Journal 53, 3788–3804. doi:10.2514/1.J054029

Yamazaki, K., 1996. Two-level optimization technique of composite laminate panels by genetic algorithms. American Institute of Aeronautics and Astronautics. doi:10.2514/6.1996-1539

Yang, H., Wang, B., Shen, Z., Zheng, Y., 2014. Comparative analysis of numerical methods for rotor blade unrunning design, in: Fluid Machinery and Fluid Engineering, 2014 ISFMFE - 6th International Symposium on. pp. 1–8. doi:10.1049/cp.2014.1221

Yang, J., Song, B., Zhong, X., Jin, P., 2016. Optimal design of blended composite laminate structures

using ply drop sequence. Composite Structures 135, 30–37. doi:10.1016/j.compstruct.2015.08.101

Zehnder, N., Ermanni, P., 2006. A methodology for the global optimization of laminated composite structures. Composite Structures 72, 311–320. doi:10.1016/j.compstruct.2005.01.021

Zitzler, E., 1999. Evolutionary Algorithms for Multiobjective Optimization: Methods and Applications.

Zitzler, E., Laumanns, M., Thiele, L., 2001. SPEA2: Improving the Strength Pareto Evolutionary Algorithm.

École Nationale Supérieure des Mines
de Saint-Étienne

NNT : *2016LYSEM006*

Alexis LASSEIGNE

OPTIMIZATION OF VARIABLE-THICKNESS COMPOSITE STRUCTURES. APPLICATION TO A CROR BLADE.

Speciality : Mechanical Engineering

Keywords : Composite optimization, Variable-thickness, Layup tables, Evolutionary algorithm, Auxiliary space, Open-rotor

Abstract :
This thesis deals with the optimal design of variable-thickness laminated composite structures. The stacking variables define a combinatorial optimization problem and large decision spaces which are potentially multimodal. Stochastic optimization algorithms allow solving this type of problem and allow taking advantage from the performance and the anisotropic nature of unidirectional composite plies to lighten laminated composite structures.
The purpose of this study is twofold: (i) developing an optimization algorithm dedicated to variable-thickness laminated composites and (ii) assessing the potential of laminated composites in influencing the aerodynamic performances of a composite CROR blade.

Firstly, an evolutionary algorithm is specialized in order to optimize layup tables and handle a set of design guidelines which is representative of industrial practices. In this purpose, a specific encoding of the solutions is suggested and specialized variation operators are developed.
Secondly, the algorithm is enriched with a guiding technique based on the exploitation of an auxiliary space in order to improve its efficiency and to include further composites-related knowledge for the resolution of the problem.
Finally, the method is applied for the design of a reduced-scale composite CROR blade intended for wind-tunnel testing. Beforehand, iterative processes are implemented to estimate the shape of the non-operating blade and the stress state within the operating blade.

Onera – The French Aerospace Lab
BP 72 – 29 Avenue de la Division Leclerc
92322 CHATILLON CEDEX
Tél. : +33 (0)1 46 73 40 40 – Fax. : +33 (0)1 46 73 41 41
http://www.onera.fr

École Nationale Supérieure des Mines
de Saint-Étienne

NNT : *2016LYSEM006*

Alexis LASSEIGNE

OPTIMISATION DE STRUCTURES COMPOSITES D'EPAISSEUR VARIABLE. APPLICATION A LA PALE DE CROR.

Spécialité: Mécanique et Ingénierie

Mots clefs : Optimisation composite, Epaisseur variable, Table de drapage, Algorithme évolutionnaire, Espace auxiliaire, Open-rotor

Résumé :
Cette thèse aborde la problématique de la conception optimale de structures composites stratifiées d'épaisseur variable. Les variables d'empilement définissent un problème d'optimisation combinatoire et des espaces de décisions de grande taille et potentiellement multimodaux. Les algorithmes d'optimisation stochastiques permettent de traiter ce type de problème et de tirer profit des performances et de l'anisotropie des plis composites pour l'allègement des structures composites stratifiées. Le but de cette étude est double : (i) développer un algorithme d'optimisation dédié aux composites stratifiés d'épaisseur variable et (ii) estimer le potentiel des composites stratifiés pour la maîtrise des performances aérodynamiques d'une pale de CROR composite.

Dans la première partie de cette thèse, un algorithme évolutionnaire est spécialisé pour l'optimisation de tables de drapage et la gestion d'un ensemble de règles de conception représentatif des pratiques de l'industrie. Pour se faire, un encodage spécifique des solutions est proposé et des opérateurs de variations spécialisés sont développés.
Dans la deuxième partie, l'algorithme est enrichi d'une technique de guidage basée sur l'exploitation d'un espace auxiliaire afin d'accroître son efficacité et d'intégrer davantage de connaissances des composites dans la résolution du problème.
Finalement, la méthode est appliquée pour la conception d'une pale de CROR composite à l'échelle de la maquette de soufflerie. Au préalable, des processus itératifs de mise à froid et mise à chaud de la pale sont mis en place afin d'estimer la forme de la pale au repos et l'état de contraintes dans la pale en fonctionnement.

Office National d'Etudes et de Recherches Aérospatiales
BP 72 – 29 Avenue de la Division Leclerc
92322 CHATILLON CEDEX
Tél. : +33 (0)1 46 73 40 40 – Fax. : +33 (0)1 46 73 41 41
http://www.onera.fr